UNIVERSITEIT ANTWERPEN
UNIVERSITAIRE INSTELLING ANTWERPEN
Departement Scheikunde

TRANSFORMATION, CONCENTRATIONS AND DEPOSITION OF NORTH SEA AEROSOLS

Proefschrift ingediend met het oog op het examen voor de graad van Doctor in de Wetenschappen aan de Universitaire Instelling Antwerpen te verdedigen door Philippe OTTEN.

Promotor: Prof. Dr. R. Van Grieken

Antwerpen, 1991

I Z W O
Instituut voor Zeewetenschappelijk Onderzoek (vzw)
Institute for Marine Scientific Research
Prinses Elisabethlaan 69
B - 8450 BREDENE BELGIUM
Tel. + 32 - (0) 59 - 32 37 15 Fax. + 32 - (0) 59 - 32 06 96

UNIVERSITEIT ANTWERPEN
UNIVERSITAIRE INSTELLING ANTWERPEN
Departement Scheikunde

TRANSFORMATION, CONCENTRATIONS AND DEPOSITION OF NORTH SEA AEROSOLS

Proefschrift ingediend met het oog op het examen voor de graad van Doctor in de Wetenschappen aan de Universitaire Instelling Antwerpen te verdedigen door Philippe OTTEN.

Promotor: Prof. Dr. R. Van Grieken

Antwerpen, 1991

Dankwoord

Het is voor mij overduidelijk dat ik sinds begin 1985, toen ik met experimenteel werk voor mijn licentiaatsverhandeling aanving, enorme mogelijkheden heb gekregen om mezelf als wetenschapper en als mens te ontwikkelen. Het voltooien van dit doctoraal proefschrift is in eerste instantie een verwezenlijking van Prof. Dr. R. Van Grieken waarvoor ik hem bijzonder erkentelijk ben. In de loop der jaren is bij mij het besef gegroeid dat Prof. Dr. R. Van Grieken grote inspanningen heeft geleverd om een zo ideaal mogelijk kader te scheppen waarbinnen een doctoraat kan voorbereid worden. Het hoeft geen betoog dat, in een periode waarin het universitaire onderwijs en het wetenschappelijke onderzoek het met steeds minder middelen moet doen, dit geen sinecure is.

Mia Kerkhoff en Remi Laane (Ministerie van Verkeer en Rijkswaterstaat, Dienst Getijdewateren, Nederland) ben ik bijzonder erkentelijk voor hun positieve inbreng tijdens de voorbije jaren. Hun raadgevingen en opmerkingen hebben in belangrijke mate bijgedragen tot het realiseren van dit werk.

Cmdt Cops, Cmdt Simpelaere, Cmdt Krott, de Officieren, de Onderofficieren en de ganse bemanning van de A962 Belgica ben ik bijzonder erkentelijk voor de vlotte samenwerking en hun inzet om zelfs in uiterst slechte weersomstandigheden de vooropgestelde bemonsteringscampagnes zo volledig mogelijk uit te voeren.

De Heer Blommers en het voltallige team van Geosens B.V. zijn steeds een enorme steun en stimulans voor mij geweest om dit onderzoek verder uit te diepen. In Rotterdam mocht ik meermaals ervaren hoe een gemotiveerde groep van gespecialiseerde mensen in staat is om voor complexe problemen een doordachte oplossing te vinden via een unieke manier van samenwerken.

Het Instituut tot Aanmoediging van het Wetenschappelijk Onderzoek in Nijverheid en Landbouw (IWONL), het Ministerie van Wetenschapsbeleid en het Ministerie van Verkeer en Rijkswaterstaat (Nederland) dank ik voor de financiele steun.

Hierbij wens ik ook alle collega's van het Departement Scheikunde en ook van andere departementen te bedanken voor de aangename werksfeer en de talloze verrijkende discussie's.

Het spreekt vanzelf dat men op professioneel gebied niet voluit kan gaan zonder de ruggesteun van zovelen in de prive-sfeer. Af en toe dient men uit de wolken te worden geplukt om terug te komen tot op een veilige vlieghoogte. In andere gevallen moet een te laag aangehouden hoogte gecorrigeerd worden in positieve zin. Mijn familieleden en in het bijzonder mijn echtgenote, Kristina, ben ik zeer dankbaar voor de onuitputtelijke steun.

Philippe Otten

Table of Contents

INTRODUCTION

History of air pollution

In the period before the 13th century, wood was the most important source of energy. With the discovery of the energetic value of coal and the resulting replacement of wood by coal for heating purposes, man-made air pollution was borne. In an early stage, the noxious effects of air pollution were recognized. Maionedes (Goodhill, 1971; Finlayson-Pitts and Pitts, 1986) stated as early as the 12th century:

"If the air is altered ever so slightly, the state of the physical spirit will be altered perceptibly. Therefore you find many men in whom you can notice defects in the actions of the psyche with the spoilage of the air, namely, that they develop dulness of understanding, failure of intelligence and defect of memory."

At the same time, action was undertaken against the air pollution because of protest reactions. King Edward I of England banned the use of so-called "sea coal" in 1272 in an attempt to clear the polluted sky over London. During the reign of Edward II, the British Parliament ordered the torturing and the hanging of a man who sold and burned the forbidden coal. Further actions against air pollution were undertaken by Richard III through taxation on coal and by Henry V through the installation of a commission for the control of the transport of coal into the city of London (Stern, 1986; Wark and Warner, 1976).

The air pollution problem in London was fully recognized in all its factors by the scientist John Evelyn in his treatise "Fumifugium, or the inconvenience of the air and smoke of London dissipated; together with some remedies humbly proposed".

Since the beginning of the Industrial Revolution, air pollution has

become an increasingly important problem. In the last decades, air pollution episodes have occurred with dramatic consequences. In December 1930, accumulated pollutants, trapped under a low inversion layer in the valley of the Meuse (Belgium), resulted in 600 people taken ill and 63 that died (Bach, 1972).

Marine pollution through air pollution

The growth of industrial activity and the increase in the global population during the recent decades have a significant influence on the marine environment. The world's oceans have been considered to be inexhaustible in all their resources, including the uptake of pollutants. However, man-made pollution occurs mainly in estuaries and coastal areas where the capacity of the marine environment to neutralize the ecotoxic effects of anthropogenic pollutants is limited. Indeed, mixing rates between the surface waters and the deep waters of the oceans are very slow.

The effects of different contaminants such as pesticides, halogenated aromatic hydrocarbons, heavy metals and radioactive species are not understood at full extent. There are however clear indications that some of the pollutants can significantly change the marine environment as a biological environment and its usefulness to mankind (Hood, 1971).

Chemicals, both natural and man-made reach the marine environment through a number of different routes. They are transported by rivers and canals, both in solution and as suspended material. Direct discharges at the coast of industrial waste and sewage is a second input source of contaminants. Dumping of toxic materials by ships is another cause of marine pollution. Furthermore, operational discharges at the coast and at the sea by ships and offshore oil and gas industry have to be taken into account.

Finally, various compounds such as nutrients, metals and organic

micropollutants reach the oceans from the atmosphere. After emission from different sources on land, pollutants are dispersed and transported into the atmosphere. During this transport they can undergo several chemical and physical transformation processes. In the end, atmospheric pollutants will be removed from the atmosphere by wet and dry deposition processes.

The North Sea

According to the definition of the International Hydrographical Bureau, the North Sea is bordered in the south by the Channel between Leathercote Point in England and Walde in France. The northwestern border goes from Dunnet Head in Scotland to the Orcade and the Shetland Islands, and then along the 00°53' W meridian to 61°00' N and finally eastward to the Norwegian coast. In the east, the North Sea is bordered by the Skagerrak through a line between Lindesnes in Norway and Hantsholm in Denmark. The North Sea has a total area of 575000 km^2 and an average depth of 94 m.

A number of different human activities affect the North Sea significantly. Fishing was probably the first activity that led to an important change in the North Sea environment. Through the use of high power vessels and technically improved fishing equipment, the natural fish abundance has decreased dramatically.

The exploitation of the mineral resources is the most valuable use of the North Sea at the moment. Important reserves of gas and oil exist in the British and the Norwegian sectors of the North Sea. In the southern part, commercially valuable quantities of sand and gravel are present.

It is clear that the North Sea is one of the most intensively used traffic routes for international transport. This has led to the growth and development of harbours with important industrial expansion.

The different coastal zones of the North Sea are used for a variety

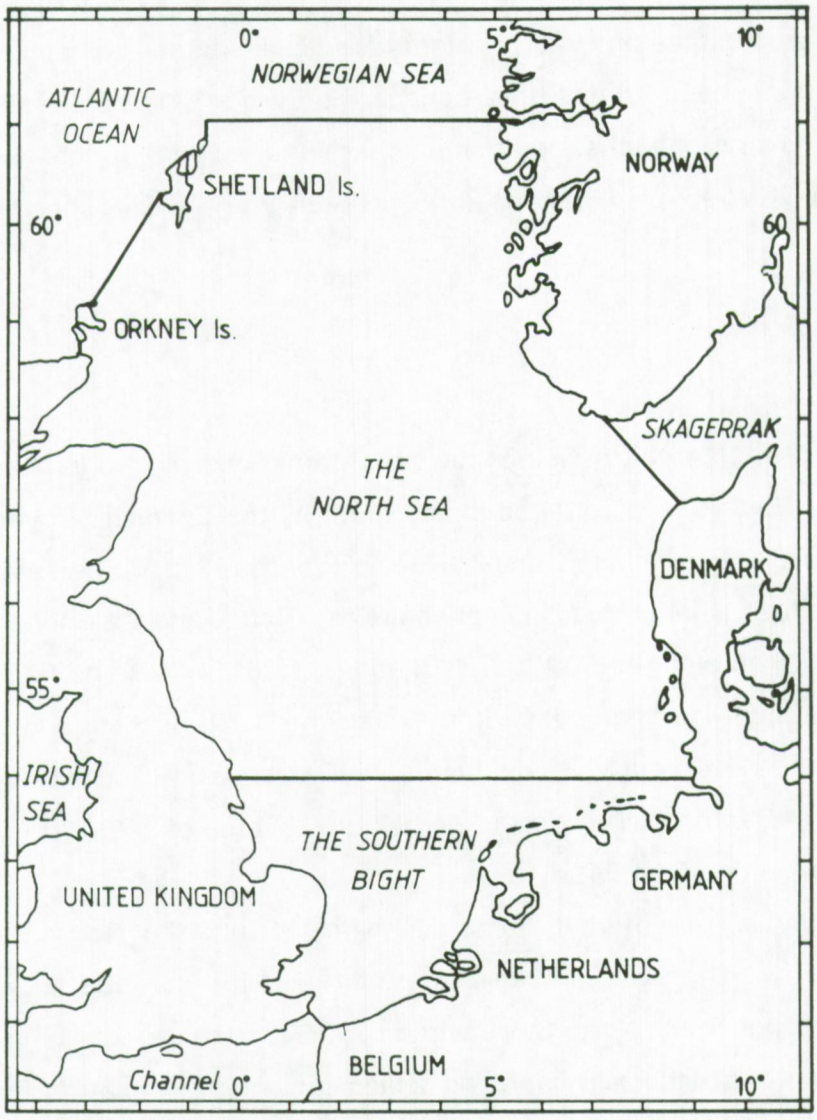

Figure I.1: The North Sea as described by the International Hydrographic Bureau (Cuyvers, 1981).

of activities: residential housing, recreation, expansion of agricultural areas and many other.

As mentioned above, the North Sea is also used as a final dumping site for pollutants through direct and indirect transport routes. The input of pollutants into the North Sea environment will vary from year to year because of natural variations in river flows, economic variations such as industrial expansion and reorganization, changing legislation such as dumping and emission restrictions, atmospheric conditions (wind flow patterns and rain fall intensities) and unforeseen circumstances (accidents).

For many years, research on pollution of the North Sea marine environment has been focused on the most obvious inputs: those borne by rivers and direct discharges of wastes. In the work of Cambray et al. (1975), a first indication can be found that the atmospheric input of trace metals to the North Sea might be a significant input route.

Context of this work

Micro- and Trace Analysis Centre

Since the establishment of the University of Antwerp (UIA) in 1973, the three research groups forming the Analytical Chemistry Laboratory, have made up approximately 50% of the Department of Chemistry. Special attention has been paid from the beginning to multi-element inorganic trace analysis. In 1980, the Micro- and Trace Analysis Centre (MiTAC) was created at the occasion of the start of the Concerted Research Action 'Micro- and Trace Analysis', funded by the Belgian Ministry of Science Policy. On the average, some 50 full-time researchers are active in MiTAC. MiTAC is also one of the corner stones of IMS, the Institute for Material Sciences of the University of Antwerp.

A variety of analytical techniques is available in the MiTAC laboratories: spark source mass spectrometry, laser microprobe mass

analysis, secondary ion mass spectrometry- ion microscopy, electron microprobe x-ray analysis, x-ray fluorescence analysis, glow discharge mass spectrometry, atomic absorption spectrometry, ion chromatography and anodic stripping voltammetry (MiTAC, 1989).

Research projects

The subjects discussed in Chapter 1 on particle-gas interaction and in Chapter 2 on the inorganic composition of North Sea aerosols originated from the Concerted Research Action 'Chemistry of the North Sea'(1984-1989), funded by the Belgian Ministry of Science Policy. Within this project, attention was focused on the study of individual particles in air and water and on the distribution of heavy metals in the marine environment of the North Sea (Van Grieken, 1990).

The research results presented in Chapter 3 on aircraft measurements of heavy metals in the North Sea atmosphere, in Chapter 4 on heavy metal deposition to the North Sea and in Chapter 5 on sulphur dioxide and ozone concentrations above the North Sea were obtained within the framework of the project 'Atmospheric deposition of heavy metals (Cd, Cu, Pb and Zn) into the North Sea' (1987-1990), funded by the Dutch Ministry of Rijkswaterstaat (Injuk et al., 1990).

A more detailed outline of each chapter can be found in the introduction at the beginning of each chapter.

References

Bach W. (1972): *Atmospheric Pollution.* McGraw-Hill Book Company, New York.

Cambray R.S., Jefferies D.F. and Topping G. (1975): *An estimate of the input of atmospheric trace elements into the North Sea and the Clyde Sea (1972-1973).* AERE Report R 7733.

Cuyvers L. (1981): *Het beheer van onze zeeën.* De Nederlandse Boekhandel, Antwerp.

Finlayson-Pitts B.J. and Pitts J.N. (1986): *Atmospheric chemistry: fundamentals and experimental techniques.* John Wiley and Sons, New York.

Goodhill V. (1971): *Maimonides-Modern medical relevance.* XXVI Wherry Memorial Lecture, Transactions of the American Academy of Ophtalmology and Otolaryngology.

Hood D.W. (1971): *Impingement of man on the oceans.* Wiley Interscience, New York.

Injuk J., Otten Ph., Rojas C., Wouters L. and Van Grieken R. (1990): *Atmospheric deposition of heavy metals (Cd, Cu, Pb and Zn) into the North Sea.* Final Report, University of Antwerp, UIA.

MiTAC (1989): *MiTAC, Micro- and Trace Analysis Centre.* Report over 1985- 1989, University of Antwerp, UIA.

Stern A.C. (1968): *Air Pollution. Vol I: Air Pollution and its effects.* Academic Press, New York.

Van Grieken R. (1990): *Geconcerteerde onderzoeksactie 'Chemie van de Noordzee'. Conventie 84-89/69.* Samenvattend eindverslag, University of Antwerp, UIA.

Wark K. and Warner C.F. (1976): *Air Pollution. Its origin and control.* Harper and Row Publishers, New York.

Chapter 1

Particle-gas interaction during sampling of atmospheric aerosols with a cascade impactor

1.1 Introduction

Marine aerosol particles, consisting mainly of NaCl, are often found to be enriched in nitrate and sulphate relatively to the seawater composition (Junge, 1956, Cadle, 1973, Savoie and Prospero, 1982, Harrison and Pio, 1983 and Bruynseels and Van Grieken, 1985). The observed enrichments were attributed, at least partly, to sampling artifacts (Appel et al., 1979). Appel et al. (1981), Forrest et al. (1980) and Okita et al. (1976) even used NaCl impregnated filters to collect gaseous HNO_3. It is therefore quite evident that NaCl particles collected on a filter medium can be subject to artifact nitrate formation when sampled in a HNO_3 containing atmosphere.

Sampling aerosol particles with a cascade impactor offers the obvious advantage of dividing the aerosol in different particle size classes during the collection itself. The possible interaction between particles already collected on the impaction surface and reactive gases still present in the atmosphere could lead to redistribution of gaseous and particulate material during sampling. Single particle analysis of aerosols collected at a coastal site in Belgium (Bruynseels and Van Grieken, 1985) resulted in the observation of a $NaNO_3$-Na_2SO_4 layer around a central NaCl cube. The main objective is to find where this enrichment is coming from. The interaction of NaCl particles on an impaction surface and HNO_3 vapour was studied with laboratory simulations using both bulk analysis methods and single particle techniques. Special attention was paid to the possible quantification of laser microprobe mass spectrometry (LMMS) for measurements of chloride to nitrate ratios in single aerosol particles. A method using denuders for removal of reactive nitric acid during particulate matter sampling was tested and a new method using NaCl aerosol loaded extra-stages for the impactor was proposed.

Analogous interaction between sulphuric acid aerosols and

ammonia vapour will be studied. The possibility of analysis of thermally unstable compounds such as inorganic ammonium salts was thoroughly investigated. The relative sensitivity of LMMS for different major cations in marine aerosol particles was studied.

Finally results are presented of single particle measurements on inorganic ammonium and nitrate compounds collected at the vicinity of the UIA campus.

1.2 Analytical techniques

1.2.1 Laser microprobe mass spectrometry (LMMS)

1.2.1.1 The LAMMA-500 instrument

Within the LAMMA-500 (Leybold-Hereaus, Koln, FRG) instrument, a microvolume of a sample is vaporized and ionized by a short time (15 ns) laser pulse from a Q-switched, frequency quadrupled Nd-YAG laser with a power density of 10^{10}-10^{11} W.cm^{-2}. The laser energy can be attenuated in 25 discrete steps to 2% of the initial value by a two-fold filter system. The laser beam is focused with the aid of a collinear visible He-Ne laser by a binocular light microscope with UV transparent objectives.

The ions formed during the interaction with the laser pulse, are extracted by an Einzel type ion lens into a 1.8 m drift tube of a time-of-flight mass spectrometer with a high extraction and transmission efficiency (up to 50% of the originally formed ions). An energy focusing reflector is installed in the drift tube in order to compensate for the initial spread on the kinetic energy of the ions. Both positive and negative ions can be analyzed by switching polarities of the different electrodes in the drift tube.

The mass dispersion in a time-of-flight mass spectrometer is the

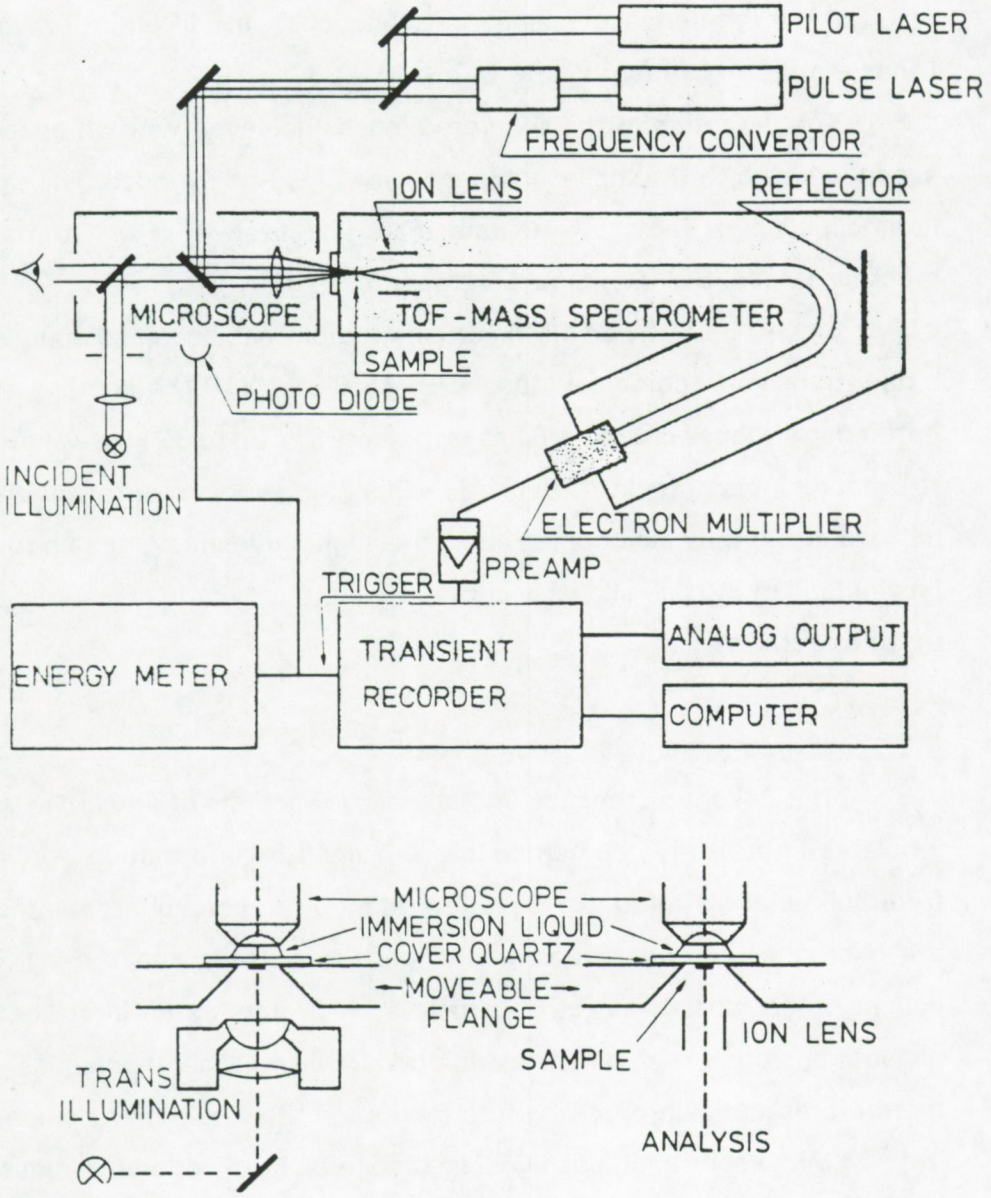

Figure 1.1: The LAMMA-500 instrument: schematic view.

result of the difference in velocity between ions with different m/z ratio. It has a mass resolution of 850 at m/z = 208.

The detection of the separated ions is achieved with an open secondary electron multiplier equipped with 17 Cu-Be dynodes. The signal is amplified by a factor of 10^6 and then digitalized by a fast transient recorder (Model B-8100, Gould-Biomation).

Since 1987, the LAMMA-500 instrument has been equipped with a new transient recorder, a Model TR 818 B-MM 8103/8 (Lecroy), with better performance characteristics: a memory size up to 32 kbyte allowing to record mass spectra over a wider range of masses without compromising the resolution. In addition a higher dynamic range up to 5.6 bits instead of 3.2 bits allows accurate peak intensity ratio measurements up to a factor of 50.

1.2.1.2 LMMS in aerosol research

Physical characteristics and chemical reactions of an aerosol as a whole can not always be completely explained by information obtained from bulk analysis methods. Several effects of an aerosol are related to the microchemical conditions of the particle surface and the particle volume. More specifically, the particle surface acts as an interface for phase transitions and chemical reactions. Microprobe techniques are therefore essential in providing information on the single particle level.

LMM spectra of positive and negative ions contain a massive amount of information on the different chemical compounds in a single particle. The high sensitivity offers the possibility of detecting trace elements down to the ppm range. On the other hand, data treatment is fast enough to analyze a statistically significant number of single particles to obtain relevant information about the total aerosol population.

The light microscope of the LAMMA-500 instrument allows visualisation of particles with a minimum diameter of 0.2 μm. An

important part of both natural and anthropogenic aerosol particles can therefore be analyzed with LMMS.

In some selected cases it is possible to analyze particles both at full laser energy, obtaining a spectrum of the average composition of the total particle, and with attenuated laser energy, resulting in information on the composition of the outer surface of the particle.

Although the LMMS technique uses a high power laser and a vacuum of 10^{-4} Pa is needed, there are limited possibilities of analyzing thermally unstable compounds. This will be discussed later in section 1.5 with regard to the analysis of inorganic ammonium salts.

1.2.2 Ion chromatography

1.2.2.1 General

Small et al. (1975) used a combination of ion-exchange techniques and conductivity measurements to separate and determine quantitatively different anions. This constituted the start of a real revolution in routine analysis of anions and cations.

The IC-1000 (Biotronik, FRG) consists of an injection valve, a dual piston pump, a separation column, a suppressor column and a flow-through cell with conductivity detector (Figure 1.2). A Shimadzu CR3A integrator is connected for data analysis, calibration and results presentation.

1.2.2.2 Anion analysis

50 μl of the test portion is injected and the anions are separated on a Bio-Gel TSK IC-Anion PW (Biorad) column using as the eluent a 0.8 mM $NaHCO_3$/0.9 mM Na_2CO_3 mixture. At the end of the separation column, the anions are detected with a conductivity detector. Because of the high background signal due to the large concentration in eluent

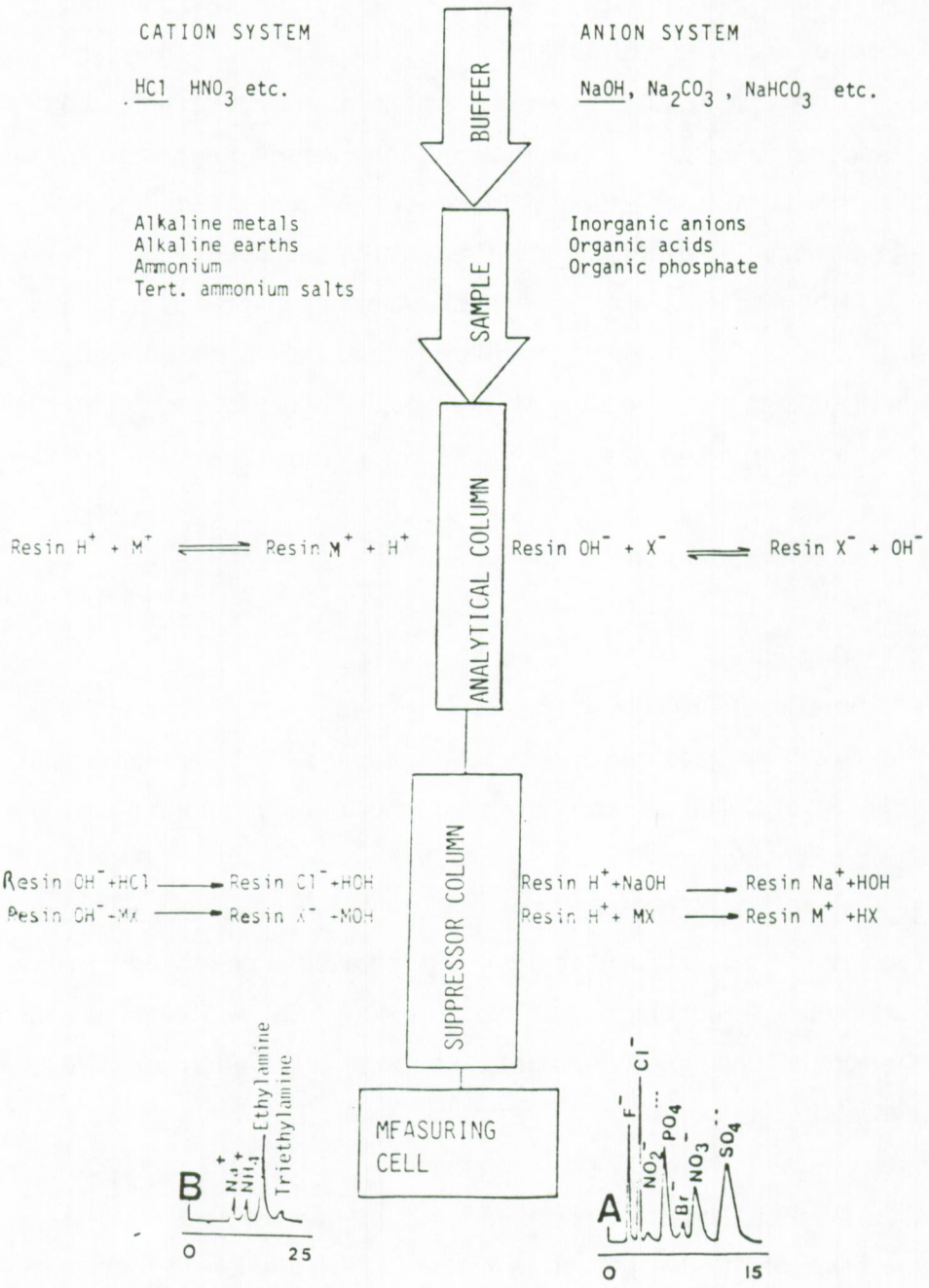

Figure 1.2: Schematic view of the IC-1000 setup.

ions, the eluent has to be transformed into a much less conductive species. This makes it possible to measure low concentrations with a high sensitivity.

The eluent flows on the inner side of a capillary membrane. At the outside of this membrane a solution of dodecylbenzene sulfonic acid is flowing resulting in a continuous exchange of sample cations by hydrogen ions and thus replacing the $NaHCO_3$ and the Na_2CO_3 by H_2CO_3 which dissociates much less and is thus much less conductive.

1.2.3 Ammonia sensitive electrode

An Orion model 95-10 ammonia gas sensing electrode was used in all experiments concerning determination of ammonia or ammonium. The ammonia electrode usus a hydrophobic gas-permeable membrane to separate the sample solution from the internal solution. Dissolved ammonia in the sample solution diffuses through the membrane until the partial pressure of ammonia is the same on both sides of the membrane. Ammonia diffusing through the membrane dissolves in the internal filling solution and reacts reversibly with water:

$$NH_3 + H_2O \rightleftharpoons NH_4^+ + OH^- \qquad (1.1)$$

The internal filling solution contains ammonium chloride at a sufficiently high level so that the ammonium concentration can be considered fixed. Thus the ammonia concentration can be directly related to the OH^- concentration and the Nernst equation can be written as:

$$E = E_0 - 2.303 \left(\frac{RT}{F}\right) \log [NH_3] \qquad (1.2)$$

The partial pressure of ammonia and the concentration of ammonia are related by a proportionality constant that varies with the amount of dissolved species.

This method offers a rapid and sensitive technique for measurement of ammonia concentrations between 0.0085 and 17000 ppm. It has already been applied successfully in the determination of the ammonium ion in airborne particulates (Eagan and Dubois, 1973).

After ultrasonic extraction of the filter samples, NaOH is added in order to adjust the pH to 11-12. A typical low concentration calibration curve is shown in Figure 1.3. Volatile amines may interfere. Also, some metallic ions complex ammonia, causing low results in direct measurements.

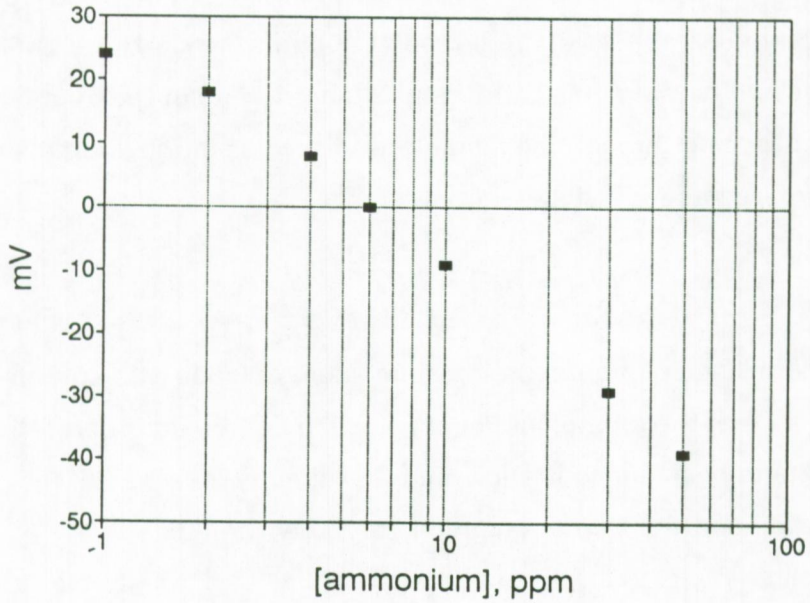

Figure 1.3: Calibration curve for ammonia measurements.

1.3 NaCl - HNO_3 interaction

1.3.1 Marine aerosols: formation, concentration and distribution

In 1819, Beck (Blanchard, 1983) suggested that a significant part of the marine aerosol is produced by the sea. Today it is generally believed that air bubbles bursting at the sea surface are the major source of the marine aerosol.

Those air bubbles are produced by falling raindrops and snowflakes, by supersaturation of seawater as a function of temperature and by whitecaps. The last source is certainly the major one for bubble production. The braking of a wave entrains large amounts of air into the sea. Upon bursting some of the surface free energy of the air bubble is converted into kinetic energy of a jet of water (Figure 1.4)

The jet becomes unstable and breaks into 1 to 10 jet drops, depending on the bubble size. In addition to jet drops, film drops are also produced by bubble bursting. They arise from the bursting of a thin film of water that separates the air in the bubble from the atmosphere. The number of film drops rapidly increases with bubble size.

Woodcock (1953) measured salt concentrations as a function of wind speed. For wind speeds ranging from 5 to 35 $m.s^{-1}$, the salt concentration increases exponentially with the wind speed (5 $\mu g.m^{-3}$ at 5 $m.s^{-1}$ and 500 $\mu g.m^{-3}$ at 35 $m.s^{-1}$). For a wind speed <3 $m.s^{-1}$, the salt concentration decreases rapidly.

Since the mean sea salt particle residence time is in the order of a few days, the salt concentration is correlated with the integrated wind over a period of a few days. Thus variations in sea salt concentrations with local winds can be observed.

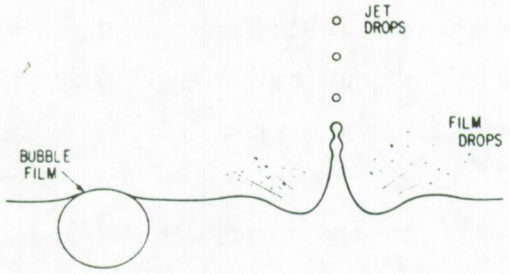

Figure 1.4: Bubble bursting and aerosol formation at the sea surface.

1.3.2 HNO_3 in the atmosphere

Nitric acid is formed by the oxidation of NO_2 with OH radicals. This, relatively rapid oxidation implies that nitric acid formation should occur close to the source. Hydrolysis of N_2O_5 is also a potential source for nitric acid (Platt et al., 1980).

In polluted air, in the prescence of NO_2 and ozone, the nitrate radical is formed in equilibrium with N_2O_5. The nitrate radical reacts rapidly with a variety of organics. In the case of alkanes and aldehydes, this reaction is believed to proceed to hydrogen abstraction to form nitric acid.

Nitric acid is removed from the atmosphere by a number of different mechanisms. Homogeneous condensation of nitric acid is rather unprobable in ambient atmospheric conditions (Kiang et al., 1973). Condensation will mainly take place on existing aerosol particles that act as nuclei for phase transition reactions. The interaction of sea salt particles (NaCl) with nitric acid vapour is a good example, that will be discussed more in detail in this chapter, of heterogeneous condensation

of nitric acid.

Nitric acid can react with bases present in the atmosphere to form salts. One such base frequently present in substantial concentrations is ammonia. The reaction of nitric acid with ammonia is an equilibrium reaction.

Finally, nitric acid can be removed from the atmosphere by wet deposition after absorption into cloud and fog droplets and by dry deposition to the earth's surface trough turbulence and diffusion.

A large number of research groups have measured gaseous nitric acid in the ambient atmosphere, using a variety of sampling techniques.

Atmospheric trace element concentrations are often expressed in different units: ppb (or ppm), $neq.m^{-3}$ and $ng.m^{-3}$ (or $\mu g.m^{-3}$)
For nitric acid measurements, the relations between the different units are:

1 ppb HNO_3 = 39 $ng.m^{-3}$ HNO_3

1 $neq.m^{-3}$ HNO_3 = 63 $ng.m^{-3}$ HNO_3

1 $neq.m^{-3}$ HNO_3 = 1.62 ppb HNO_3

Ruprecht and Sigg (1990) measured HNO_3 using the denuder technique, developed by Niessner and Klockow (1983). Samples were collected in the urban region of Dübendorf, Switzerland. HNO_3 concentrations ranged from 0.04 to 6.8 $\mu g.m^{-3}$.

During a field experiment concerning the validation of the choice of the best coating for HNO_3 and HNO_2 collecting denuders, Perrino et al. (1990) measured 24 h average nitric acid concentrations of 1.4 to 5.0 $\mu g.m^{-3}$. The sampling site was located 30 km northeast of Rome, Italy.

Harrison and Allen (1990) measured gaseous HNO_3 using a filter

pack technique. Between February 1987 and January 1988, an average HNO_3 concentration of 1.01 $\mu g.m^{-3}$ was observed for five locations in eastern England.

Sickells et al. (1990) compared different sampling techniques, a filter pack, an annular denuder and a transition flow reactor, for the determination of gaseous and particulate nitrogen and sulphur compounds. Average nitric acid levels at the Research Triangle Park, North-Carolina, USA, ranged from 1.5 to 2.7 $\mu g.m^{-3}$ for daily samples taken between September 29 and October 12, 1986.

Dasch et al. (1989) compared annular denuder techniques and filter packs for sampling of atmospheric nitric acid. The average, winter-time HNO_3 concentration of a set of 46 samples was 1.24 $\mu g.m^{-3}$ which compares very well with previously measured winter time concentrations of 1.1 $\mu g.m^{-3}$ (Dasch and Cadle, 1986) and 1.8 $\mu g.m^{-3}$ (Cadle, 1985). All samples were collected in Warren, Michigan, USA, a suburb of Detroit.

Tanner et al. (1989) reported on an intercomparison experiment for nitric acid determinations in ambient air. Filter pack, denuder and real-time chemiluminescence techniques were used for nitric acid determination in a coastal site environment, 100 km ENE from New York, USA. The average HNO_3 concentrations were generally in the range of 0.5 to 3 ppbv.

Continuous measurements of nitric acid between January 20 and February 24, 1984 in Powassen, Ontario, Canada yielded and average concentration of 0.85 ppbv (Daum et al., 1989).

Klockόw et al. (1989) determined atmospheric HNO_3 using an automatically operating thermodenuder system. Average HNO_3 levels, measured at a coastal site in the Netherlands, Petten, ranged from 0.17 to 2.7 $\mu g.m^{-3}$.

A recently performed field comparison of nitric acid measurement methods (Hering et al., 1988) showed that statistically significant,

systematic differences in nitric acid determinations do exist. Reported concentrations varied among simultaneously collected samples by more than a factor of 2 and as much as factor of 4. For the period with the highest nitric acid levels reported, concentrations ranged from 191 to 800 neq.m^{-3}.

The above listed references include only some of the most recently published data on nitric acid measurements. It is beyond the scope of this work to give a complete overview of all methods and results regarding nitric acid determinations in ambient air. It is however clear from the above listed values that nitric acid levels in urban or near-urban areas may vary from less than 1 μg.m^{-3} to 10 μg.m^{-3}, with peak values up to 50 μg.m^{-3}.

1.3.3 Laboratory generation of test aerosols and atmospheres

1.3.3.1 Laboratory generation of NaCl particles

A very simple and efficient method for the generation of a polydisperse aerosol is the pneumatic nebulization of a NaCl solution. Figure 1.5 shows the laboratory setup used. The principle of all pneumatic nebulizers is identical, although important differences occur in geometry of the setup. Pressurised air is forced through a small tube. The low pressure created by the Bernoulli effect at the end of the tube results in the rising of the NaCl solution through the second tube. The solution leaves the tube as a thin liquid filament which is accelerated in the air stream and decomposes into droplets. The largest droplets impact on the wall of the recipient. The smaller droplets are carried into the silicagel-filled diffusion dryer. At the end of the diffusion dryer dry NaCl particles can be collected.

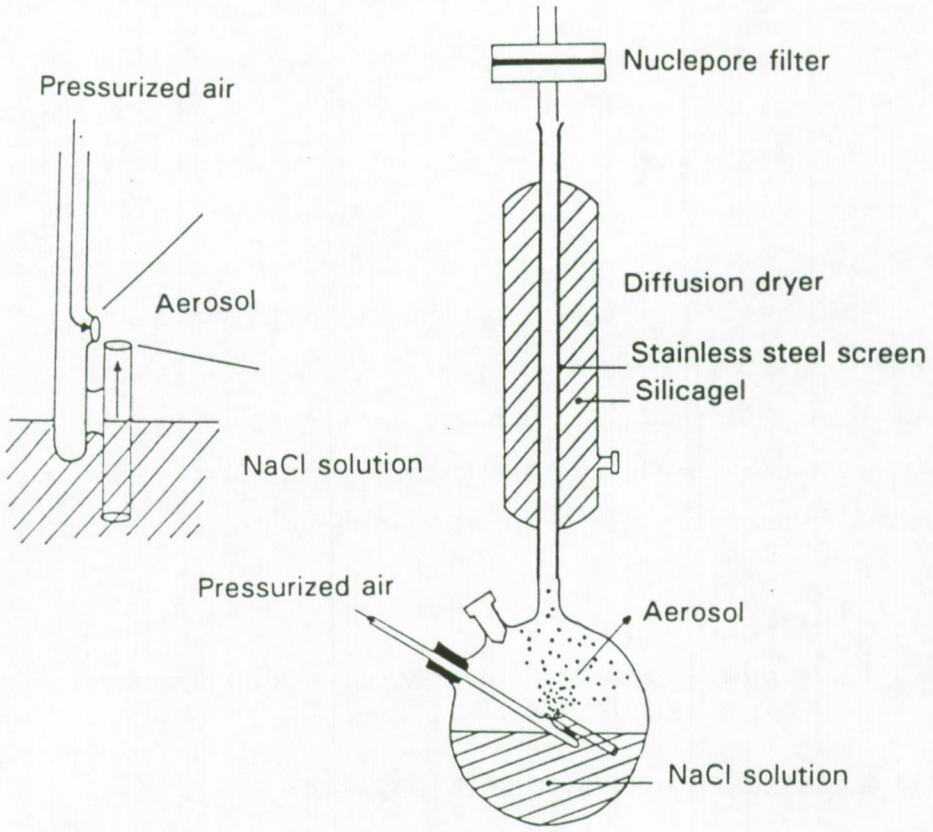

Figure 1.5: Generation of a polydisperse NaCl aerosol

In order to assure high reproducibility, the recipient was filled with exactly the same amount of solution while the level of the air tubes was carefully checked before sampling. The flow rate of the nebulizing agent was kept constant at 3 $l.m^{-1}$.

It is possible to calculate the size spectrum of the droplets generated by a pneumatic nebulizer, starting from the density, the surface tension and the viscosity of the solution, the flow rate of the gas and the flow rate of the liquid.

The average diameter of the generated NaCl particles was measured by collecting the NaCl particles on a 47 mm diameter Nuclepore

polycarbonate membrane filter with pore size 0.45 μm. The diameter of 1000 individual NaCl particles was measured with an electron microscope. A total of 8 experiments were performed using two different setups, one with a horizontally placed diffusion dryer and one with a vertically placed diffusion dryer. The average diameter of the collected NaCl particles as function of the molarity of the NaCl solution is given in Figure 1.6. It is clear that larger particles can be deposited by gravitation in the setup with the horizontally placed diffusion dryer.

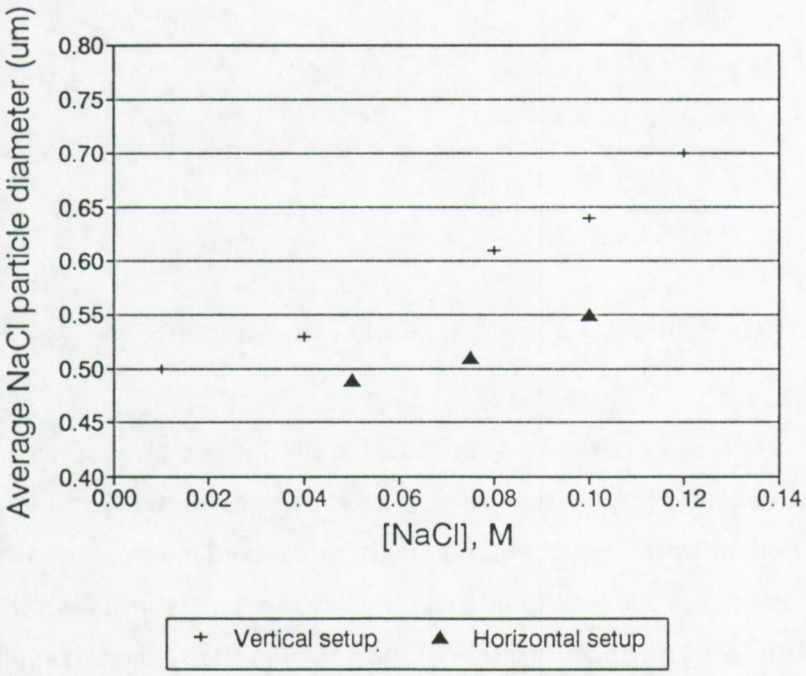

Figure 1.6: Average diameter of the polydisperse NaCl aerosol as a function of the molarity of the nebulized solution

1.3.3.2 Generation of a HNO_3 test atmosphere

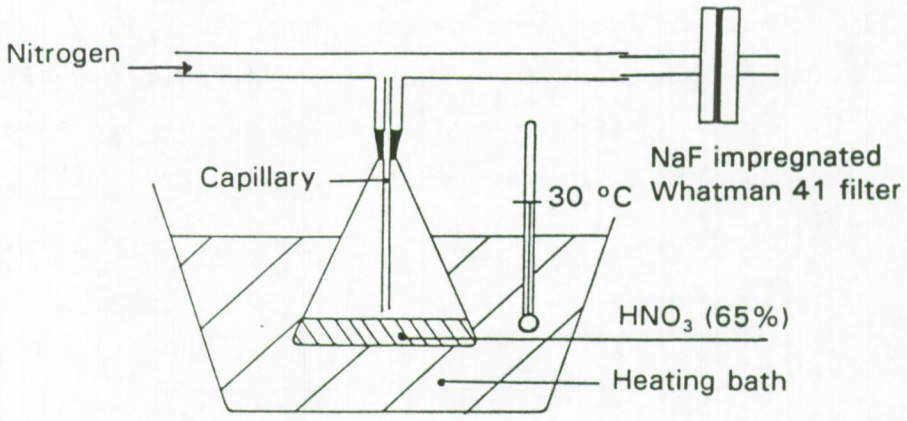

Figure 1.7: Generation of a nitric acid test atmosphere

In order to generate a reproducible HNO_3 test atmosphere, the procedure described by Slanina et al.(1981) was followed (Fig 1.7).

A concentrated HNO_3 solution is thermostated in a water bath and the HNO_3 vapour is allowed to diffuse through a capillary into a stream of diluting nitrogen. The concentration of the gaseous HNO_3 can be regulated by changing the different experimental setup parameters like the temperature of the water bath, the length and diameter of the capillary and the flow rate of the diluting nitrogen. It was measured by collecting the HNO_3 on a NaF impregnated Whatman 41 cellulose filter and by analyzing the extract with ion chromatography. When the temperature is kept constant within 1 °C, and a diluting stream of 1 $l.min^{-1}$ is used, a nitric acid concentration of 1.6 ± 0.2 $\mu g.l^{-1}$ (n = 5) is obtained.

1.3.4 Laboratory experiments on NaCl - nitric acid interaction

Stage 2 (particles between 2 and 4 μm) of a single-orifice cascade impactor was loaded with approximately 75000 NaCl particles (the equivalent of 1.0 μg NaCl) by sampling a NaCl test atmosphere during 20 s. The output flow rate of the test atmosphere generator is 3 $l.min^{-1}$ while the operational flow rate for the impactor is 1 $l.min^{-1}$. Therefore only one third of the generated aerosol is collected by the impactor.

In the next step, the impactor, with only stage 2 loaded with NaCl particles, was placed behind the nitric acid atmosphere generating system, During 40 s, nitric acid contaminated air was passed through the impactor. During this sampling time, a total amount of 1.0 μg HNO_3 passes the impactor (Figure 1.8).

The use of equal amounts of NaCl on the impactor stage and nitric acid in the test-atmosphere may seem an arbitrary choice. The sea salt concentration varies with the wind speed over a very wide range: 0.5 to 500 $\mu g.m^{-3}$ (Woodcock, 1953). Above the North Sea an average concentration of 4.7 $\mu g.m^{-3}$ was measured between 1984 and 1988 (see also Chapter 2). On the other hand, the Southern Bight of the North Sea is surrounded by highly industrialized countries emitting large quantities of NO_x that are converted to nitric acid. For meteorological situations above the North Sea where the wind is coming from polluted areas and the wind speed is not too high, comparable concentrations of NaCl and HNO_3 can be expected.

After the experiment, the Formvar coated electron microscope grid, that acted as an impaction surface, was transferred directly to the sample chamber of the LAMMA-500.

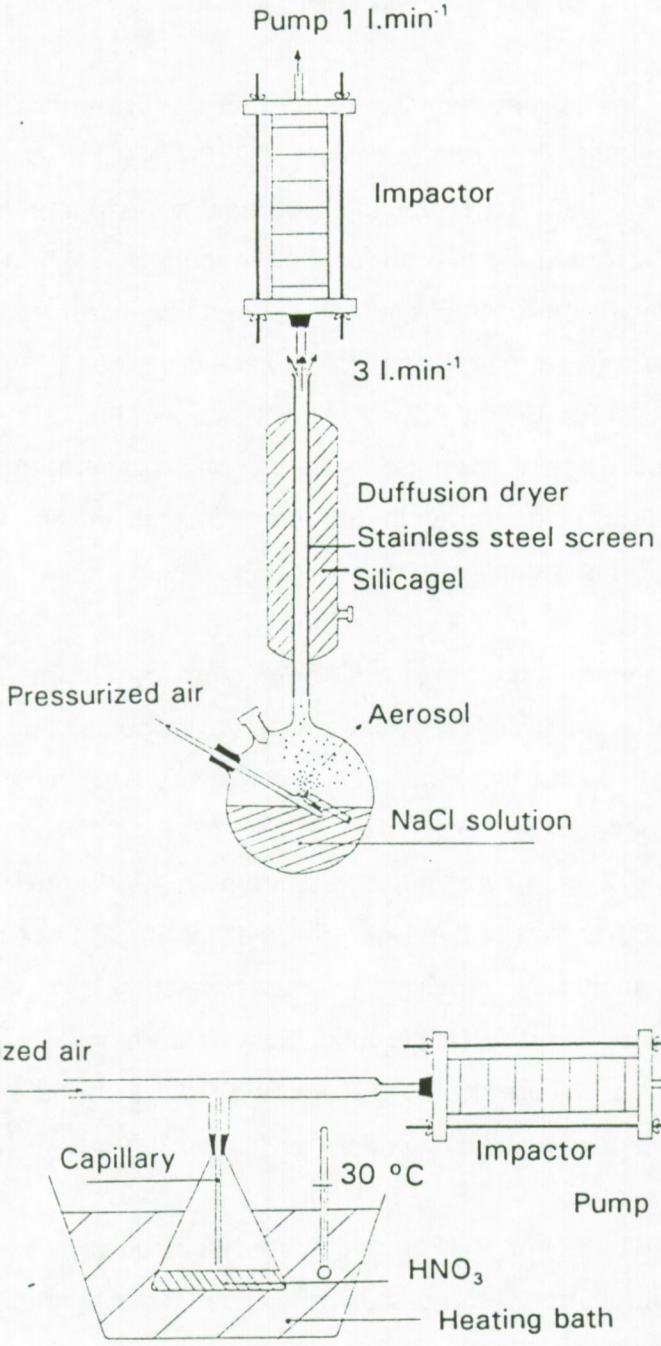

Figure 1.8: Laboratory simulation of NaCl aerosol sampling with an impactor in an nitric acid contaminated atmosphere

1.3.5 Results of single particle analysis

1.3.5.1 Qualitative LMMS

LMMS was performed on NaCl aerosol particles both before and after a HNO_3 atmosphere was passed through the impactor. All mass spectra were recorded in the negative mode, since for anions in general and for chloride and nitrate specifically, more peaks for identification are available in the negative mode spectra. Fig 1.9 shows the mass spectra at full laser energy, and thus evaporating the particle completely in one single laser shot, of particles before and after reaction with HNO_3. It is clear that in the latter case, nitrate peaks can be identified in the mass spectrum, confirming the reaction between impacted NaCl particles and nitric acid contaminated atmosphere which was passed through the impactor. When using an attenuated laser energy, the spectrum of pure $NaNO_3$ is obtained (Figure 1.9).

Figure 1.10 shows a secondary electron image of a NaCl particle after reaction with nitric acid. The central NaCl cube is surrounded by $NaNO_3$.

In a second experiment, the cascade impactor was loaded with NaCl droplets by sampling a test atmosphere without using a diffusion dryer. After passing nitric acid vapour through the impactor, the particles were analyzed with LMMS. The same observations were made as with dry particles: NaCl droplets do react with HNO_3 vapour that passes through the impactor.

In a third experiment a mixed $NaCl/NaNO_3$ (1/1 w/w) solution was used for aerosol generation. LMMS analysis of the resulting particles yields the same results as for the two previuos experiments indicating that fractional crystallization of $NaCl/NaNO_3$ mixed droplets leads also to particles that consist of a central NaCl cube, surrounded by $NaNO_3$.

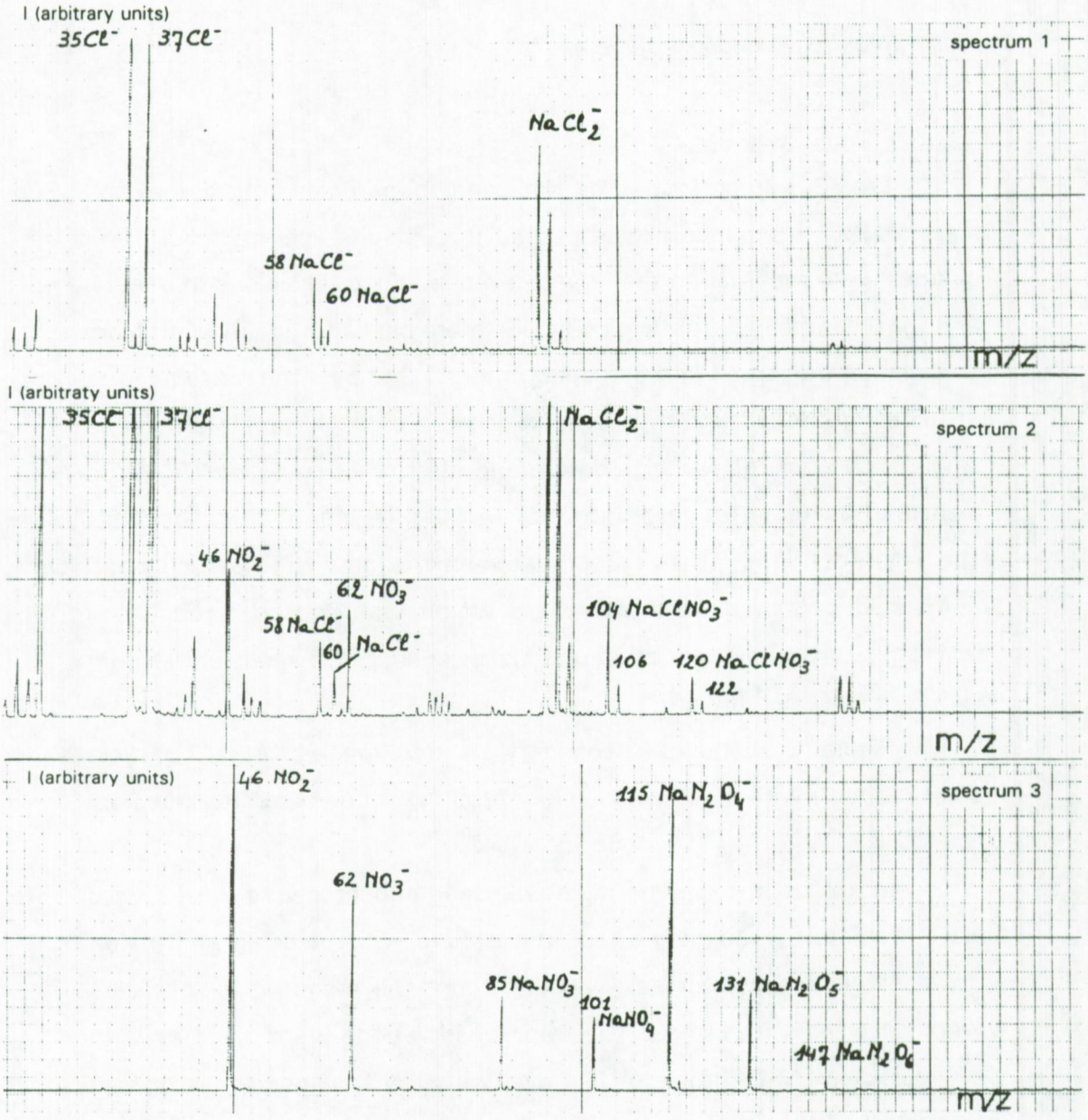

Figure 1.9: LMM spectra of NaCl aerosols before (full laser energy, spectrum 1) and after (full laser energy, spectrum 2 and attenuated laser energy, spectrum 3) a nitric acid spiked atmosphere was passed through the impactor.

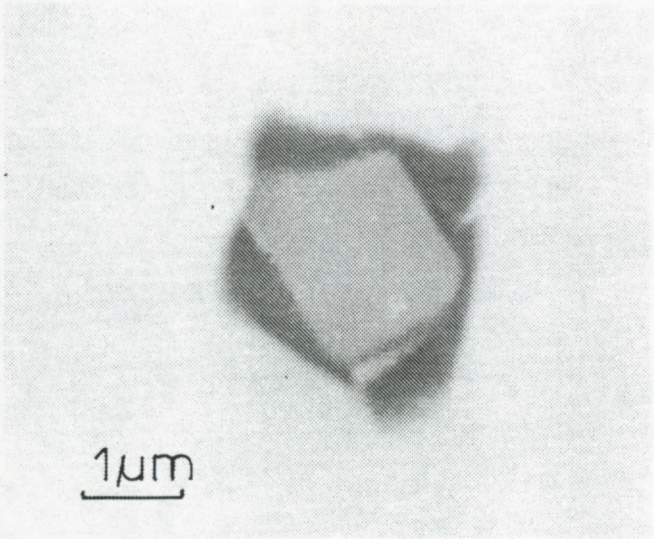

Figure 1.10: Secondary electron image of a NaCl particle after reaction with HNO_3

1.3.5.2 Quantitative LMMS

The ratio of Cl^-/NO_3^- ions in marine particles is an indication of the pollution degree of the marine atmosphere. A certain bulk chloride to nitrate ratio is not necessarily correlated with the same chloride to nitrate ratio for all aerosol particles. If the chloride to nitrate ratio in single particles varies over a wide range, this could be measured with LMMS.

Six mixed sodium chloride nitrate double salts were prepared by nebulizing solutions with 5, 20, 35, 50, 65, 80 and 95 equivalent % chloride respectively. The resulting aerosol particles were analyzed with LMMS on three separate occasions. The chloride/nitrate was calculated from the ratio of the mass peaks Cl^{-1} (m/z = 37), $NaCl^{-1}$ (m/z = 58,60), $NaCl_2^{-1}$ (m/z = 93,95,97), $Na_2Cl_3^{-1}$ (m/z = 151,153,155) to NO_3^{-1} (m/z = 62), $NaNO_3^{-1}$ (m/z = 85), $NaNO_4^{-1}$ (m/z = 101), $NaN_2O_4^{-1}$ (m/z = 115), $NaN_2O_5^{-1}$ (m/z = 131), $NaN_2O_6^{-1}$ (m/z = 147). The $^{35}Cl^{-1}$ and the $^{62}NO_3^{-1}$ peaks were not taken into account because of frequent signal overflow. The results of these measurements are listed in Table 1.1. A shot-to-shot

reproducibility of about 80% makes it quite difficult to estimate the chloride to nitrate ratio in single aerosol particles.

Using an average sensitivity factor of 3 (as calculated from Table 1.1), an average weight ratio of chloride/nitrate of 7.9 was derived for 20 NaCl particles exposed to nitric acid, as described above.

Table 1.1
Chloride/nitrate ratios in single particles
LMMS results of measurements on standard aerosols

equiv. % Cl	Cl/NO_3 aerosol (1)	Cl/NO_3 LMMS (2)	Sensitivity Factor (3)
5	0.053	0.1	2.5
20	0.250	0.4	1.4
35	0.540	1.1	2.0
50	1.000	2.2	2.2
65	1.900	4.7	2.5
80	4.000	24.0	6.0
95	19.000	89.0	4.7

(1): Element to element equivalent ratio in the aerosol particles
(2): Measured LMMS intensity ratio of the chloride to nitrate peaks (average of 30 measurements)
(3): Defined as the ratio of the measured intensity (2) to the ratio (1)

1.3.6 Denuders

In order to avoid reaction between NaCl particles or droplets and nitric acid vapour during sampling of ambient particulate matter with filters and impactors, the reactive gaseous component has to be removed from the atmosphere quantitatively, while the distribution and composition of the aerosol particles has to remain unchanged. In order to achieve this, a device called diffusion-denuder or simply denuder can be used.

1.3.6.1 Theoretical description of diffusion denuders

A diffusion denuder is a tube of which the inner wall is coated with a chemical component which reacts rapidly with the gaseous component that has to be removed. For nitric acid different coatings have been used

so far: NaF, NaCl and Na_2CO_3 (Perrino et al., 1990).

When a HNO_3 containing atmosphere is passed through a NaF coated tube, the HNO_3 molecules close to the inner wall will react with the NaF coating. In this way, a concentration gradient will be formed between the centre and the inner wall of the tube. Diffusion of nitric acid molecules will result in a net drift towards the tube wall. Since the diffusion coefficient of particles is much smaller than that of gas molecules, no particulate matter will be lost when the aerosol passes through the tube.

Gormley and Kennedy (1949) calculated the theoretical efficiency of a denuder. If a is the radius of the tube, V the velocity of the gas at any point at a distance r from the axis and Q the volume passing per second, then:

$$V = \frac{2\,Q}{\pi\,a^4}\,(a^2 - r^2) \qquad (1.3)$$

Consider reference axes x, y, z with origin in the centre of the face of the tube, and the flow being parallel to the z-axis. If u, v and w are the velocity components of the nuclei relative to the fixed axes, then the equations of motion are:

$$\begin{aligned} D\,\frac{\partial \Psi}{\partial x} &= -\,\Psi\,u \\ D\,\frac{\partial \Psi}{\partial y} &= -\,\Psi\,v \\ D\,\frac{\partial \Psi}{\partial z} &= -\,\Psi\,(w - V) \end{aligned} \qquad (1.4)$$

where D is the diffusion coefficient of the nuclei and Ψ is the partial pressure of the nuclei. Substituting u, v, and w in the equation of continuity:

$$\frac{\partial}{\partial x}(\Psi u) + \frac{\partial}{\partial y}(\Psi v) + \frac{\partial}{\partial z}(\Psi w) = 0 \qquad (1.5)$$

gives:

$$\nabla \Psi - \frac{1}{D}\frac{\partial}{\partial z}(\Psi V) = 0 \qquad (1.6)$$

Using cylindrical coordinates r, θ and z, the equation becomes:

$$\frac{1}{r}\frac{\partial}{\partial r}\left(r\frac{\partial \Psi}{\partial r}\right) + \frac{1}{r^2}\frac{\partial^2 \Psi}{\partial \theta^2} + \frac{\partial^2 \Psi}{\partial z^2} - \frac{1}{D}\frac{\partial}{\partial z}(\Psi V) = 0 \qquad (1.7)$$

In the first approximation, $\frac{\partial^2 \Psi}{\partial z^2}$ is neglected, and for reasons of symmetry, $\frac{\partial \Psi}{\partial \theta} = 0$, so that:

$$\frac{\partial^2 \Psi}{\partial r^2} + \frac{1}{r}\frac{\partial \Psi}{\partial r} - \kappa (a^2 - r^2)\frac{\partial \Psi}{\partial z} = 0 \qquad (1.8)$$

where $\kappa = 2Q/(\pi a^4 D)$.

Since nuclei are destroyed at the walls, $\Psi = 0$ when $r = a$. The number of nuclei at a distance z is proportional to:

$$\int_0^a \Psi r (a^2 - r^2)\, dr \qquad (1.9)$$

If $\Psi = \Psi_0$ when $z = 0$, then the ratio of the number of nuclei at a distance z to the number n_0 at the entrance $z = 0$ is:

$$\frac{n}{n_0} = \frac{4}{a^4 \Psi_0} \int_0^a \Psi \, r \, (a^2 - r^2) \, dr \qquad (1.10)$$

The final solution is then given by:

$$f = 0.819 \exp(-3.567 \, \alpha) + 0.097 \exp(-22.3 \, \alpha) + 0.033 \exp(-57 \, \alpha)$$

where f = *fractional penetration*

$$\text{and } \alpha = \frac{\pi \, d \, L}{F} \qquad (1.11)$$

using D = *diffusion coefficient*
L = *lenght of tube*
F = *flow rate*

The efficiency of the denuder is independent of the diameter of the tube, since an increase in tube diameter would automatically lead to a decrease in flow rate and an analogue increase in residence time in the tube, which allows the pollutant to reach the wall of the tube over the same length.

Possible loss of aerosol particles in the denuder can be the result of different processes: electrostatic interaction, turbulence, diffusion and gravitation. Loss of particles by electrostatic interaction is strongly dependant on the material of which the tube is made. Steen and Andreasson (1973) (Ferm, 1979) stated that deposition of particles between 0.3 and 13 μm is the smallest for glass tubes.

Loss of particles by turbulence can be avoided by assuring that the flow regime inside the tube is laminar. In the beginning of the tube, the flow regime will be turbulent. In practice therefore, the first part of the

tube is left uncoated. The length of the uncoated part, L, is given by:

$$L > 0.05 * d * Re \quad and \quad Re < 2000 \qquad (1.12)$$

where d is the inner diameter of the tube and Re is the Reynolds number.

Particle loss by diffusion becomes important for particles with a diameter below 0.1 μm. Gravitational deposition of particles can be avoided by placing the denuder always in a vertical position.

Possanzini et al. (1983) presented a new design of a high-performance denuder. Instead of using a single cylindrical tube, a double annular geometry is used. Theoretical considerations show that annular denuders are superior to cylindrical ones in terms of collection efficiency and absorption capacity. A short annular denuder can be used at much higher flow rates than a cylindrical one, because the laminar flow conditions, dependent on the Reynolds number and on the inner diameter of the annular denuder, are still met at flow rates which are 10 times higher than the maximum flow rate allowed in a cylindrical denuder.

1.3.6.2 Preparation of a NaF denuder for nitric acid removal

The efficiency for a HNO_3 denuder is calculated for a flow rate of 1 $l.min^{-1}$ (flow rate of the impactor used) and a diffusion coefficient of 0.16 $cm^2.s^{-1}$. Under these conditions a 20 cm tube would collect 92% of the HNO_3 passing the tube, a 40 cm tube 99% and a 60 cm tube 99.9%.

Tubes of 6 mm inner diameter were prerinsed with a concentrated chromic acid solution to remove all organic contaminants and the rinsed with Milli-Q bidistilled water. A 5 min etching procedure with concentrated (40%) HF was then followed. After rinsing again with bidistilled water, the tube was filled with 0.1 M NaF solution and empties again 5 min later. Then, the tube was dried at a temperature of 120 °C in an oven. Tubes were kept sealed off with Parafilm until use.

1.3.6.3 Experimental measurement of the denuder efficiency

The experimental setup shown in Figure 1.11 was used for evaluation of the efficiency of the denuder. A 65% HNO_3 was kept at a constant temperature of 30 °C. The HNO_3 was allowed to diffuse through a capillary and diluted with a 1 $l.min^{-1}$ N_2 stream. The resulting 1.6 $\mu g.l^{-1}$ HNO_3 containing air stream was led through a 75 cm long denuder tube with 60 cm NaF coating. At the end of the tube a 0.1 M NaF impregnated Whatman 41 cellulose filter was placed to trap any nitric acid which was not collected on the denuder surface.

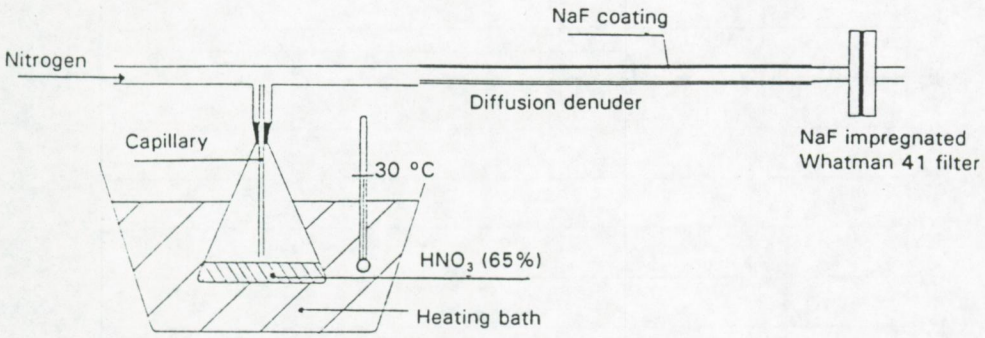

Figure 1.11: Evaluation of the HNO_3 collection efficiency of a NaF denuder

Tubes and filters were ultrasonically extracted with 10 ml bidistilled water. The final solution was measured with ion chromatography using an eluent of 0.015 M $NaHCO_3$ and 0.010 M Na_2CO_3 with a flow rate of 1.5 $ml.min^{-1}$.

Fig 1.12 shows the results of seven experiments where different amounts of nitric acid were passed trhough the denuder. The maximum capacity of the denuders is 30 to 35 μg while 100% efficiency is reached up to 25 to 30 μg.

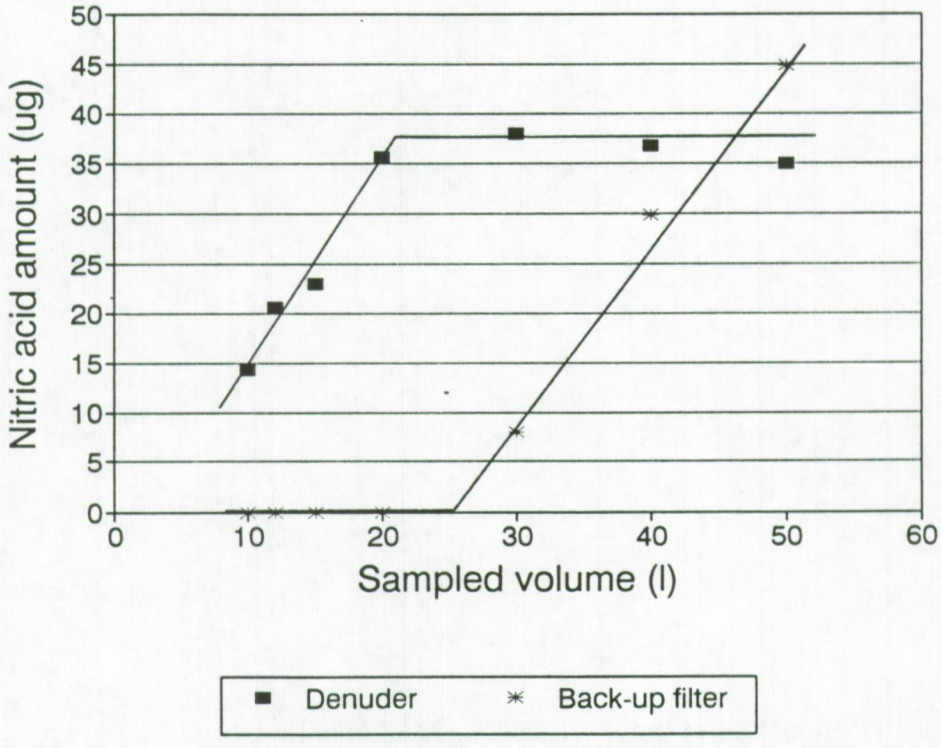

Figure 1.12: Experimental determination of the collection efficiency and maximum capacity of NaF denuders for HNO_3 sampling

An additional set of seven experiments using unetched glass tubes showed that the maximum capacity decreased to about 10 μg for a 60 cm coated tube, which indicates that the NaF is deposited more efficiently to an etched glass surface.

In a recent study, Eatough et al. (1985) presented a critical evaluation of the collection efficiency of denuders for HNO_3 sampling in ambient air. Field and laboratory experiments with both tungstic acid and nylon denuders indicate that the species sampled as gas-phase nitric acid is $HNO_3.xH_2O$. The diffusion coefficient for the collected nitric acid species was calculated by measuring the deposited amount in subsequent sections of the denuder and by using the Gormley and Kennedy (1949) equation. The measured diffusion coefficient is dependent on the atmospheric water content. An average value of 0.076 $\pm$ 0.020 $cm^2.s^{-1}$ was calculated. In practice however, this would only implicate that the efficiency of our 60 cm NaF coated denuder for nitric acid sampling decreases from 99.9% to 99.6%.

1.3.7 An alternative system for HNO_3 removal during impactor sampling

The use of NaF coated glass tubes was shown to be quite efficient in removing HNO_3 from the air stream entering an impactor during aerosol sampling. In practice however, this system offers some disadvantages. The denuders have to be placed in a protective housing and the length of the total system might make it more difficult to handle on a ship in bad weather conditions. Since our main interest lies in marine aerosols and collection of those marine particles on the North Sea itself, we would be interested in a more compact and less fragile system, but with the same characteristics of efficiency.

If we consider again the starting point of the whole problem, we see that the essential phenomenon that we are studying is the reaction of

NaCl particles on an impaction surface with HNO_3 in the vapour phase passing through the impactor. If we would place one or more extra stages in front of the impactor, load them with an excess of reactive NaF or NaCl aerosols, we might be able to remove the HNO_3 quantitatively from the air stream before the particles are collected on the following stages. Since the aerosol distribution may not be changed during the sampling procedure, the extra stages would need to have a higher cut-off diameter than the first stage.

In our case the impactor consists of 5 stages of 4, 2, 1, 0,5 and 0.25 μm cut-off diameter. This impactor was equipped with two extra stages of cut-off diameter 16 and 8 μm. In a series of six experiments, stages 0 and 00 (with cut-of diameter 8 and 16 μm, respectively) were loaded with 80, 100, 200, 250, 300 and 400 μg of NaCl aerosols generated by the nebulizer. In the next step a nitric acid contaminated air stream was passed through the impactor, allowing 8 μg HNO_3 to pass through. Only in the first experiment, nitrate was detected by ion chromatography on both stage 00 and stage 0. In all other cases, the nitric acid was quantitatively captured on the first extra-stage, stage 00. Back-up filters that were also loaded with approximately 80 μg of NaCl aerosols did not show any presence of nitrate after the nitric acid was passed through the impactor.

It can be concluded from these few experiments that a single extra-stage, loaded with at least a ten-fold amount (relative to the amount of HNO_3 that is expected to pass through the impactor during sampling) of 1 to 2 μm NaCl particles can remove any free nitric acid quantitatively during sampling of aerosol particles. When using an extra-stage with a cut-off diameter of 16 μm, no smaller ambient aerosol particles will be lost during sampling.

1.4 H_2SO_4 - NH_3 interaction

1.4.1. Sulphuric acid in the atmosphere

Sulphuric acid is not produced directly by any natural or anthropogenic source. It is the reaction product of reduced sulphur compounds with oxidizing agents. It is generally accepted that sulphate in the atmosphere can be formed from SO_2 (Meszaros, 1981) by different reactions:

1. Sulphuric acid is an end product of homogeneous gas phase reactions including photochemical and thermal steps. Sulphuric acid droplets are then formed by vapour condensation.
2. SO_2 is oxidized in fog and cloud droplets after absorption.
3. SO_2 is oxidized on the surface of existing aerosol particles.

1.4.2 Ammonia in the atmosphere

Ammonia plays an important role in the nitrogen cycle. Natural emission occurs from biological decomposition of nitrogenous matter, both in terrestrial and aquatic environments. Anthropogenic emission of ammonia is generated by activities as coal combustion in urban and industrial areas and by extensive use of nitrogen rich fertilizers in agricultural areas.

Ammonia is removed from the atmosphere naturally by microbiological nitrogen fixation, by physical processes such as wet and dry deposition and by chemical reactions like oxidation to nitrogen oxides and neutralization with acidic gases and particles. These reactions are related to the acid rain phenomenon, because ammonia is the major alkaline gas that can neutralize acidic species like nitric and sulphuric acid. In airborne particulate matter, ammonium is closely associated with

sulphate in the sub micrometer particle size range.

Reported concentrations of ammonia and ammonium are higher in summer than in winter periods and higher at ground levels than in upper levels of the troposphere. In marine environments, values are normally lower than in continental areas.

1.4.3 Laboratory simulation of ammonia-sulphuric acid interaction during sampling of particulate matter with a cascade impactor.

1.4.3.1 Generation of a sulphuric acid test aerosol

A sulphuric test aerosol was generated with the setup described in section 1.3.1.1, with the filling solution being 0.1 M H_2SO_4. A Na_2SO_4 solution was used for measurement of the size distribution, since sulphuric acid will evaporate in the high vacuum of the electron microscope.

1.4.3.2 Ammonia permeation tube

A stable NH_3 atmosphere can be obtained by the use of a permeation tube (Figure 1.13) (Altshuller and Cohen, 1960; O'Keeffe and Ortman, 1966). This tube consists of a pyrex-glass tube which acts as a reservoir and a Teflon seal which acts as a permeation device (Teckentrup and Klockow, 1978).

Gaseous NH_3 is liquified by adiabatic expansion and kept in a cooling mixture of carbon dioxide ice and aceton. The reservoir is filled with liquid ammonia and sealed off rapidly. Then, the permeation tube is allowed to heat up to room temperature. Because of the high pressure difference between the inside of the tube and the surrounding atmosphere, the ammonia will diffuse through the Teflon seal. The amount of ammonia that permeates is a function of temperature and the characteristic dimensions of the tube itself. In order to ensure a stable,

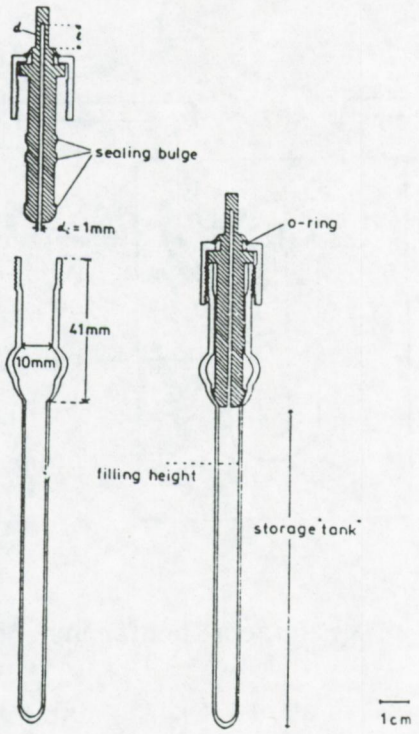

Figure 1.13: Ammonia permeation tube

reproducible output rate, the tube is kept at a constant temperature in a thermostated water bath. The concentration in the final ammonia atmosphere is regulated by the flow rate of the ammonia free nitrogen gas passing over the permeation tube (Figure 1.14).

1.4.3.3 Quantification of the ammonia output rate

The output rate of the permeation tube is measured experimentally by passing the ammonia atmosphere through a 0.1 N oxalic acid impregnated Whatman 41 cellulose filter. This filter is then ultrasonically extracted and the ammonia is measured with the Nessler method. A second determination method used is the gravimetric measurement of the

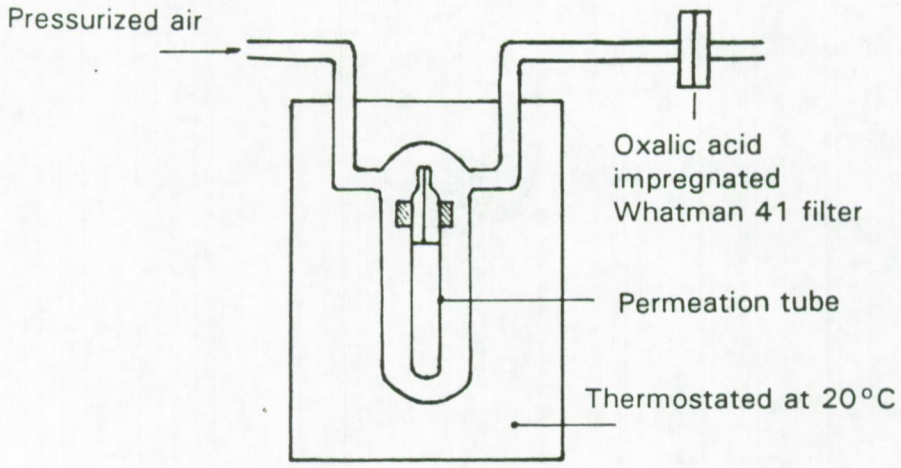

Figure 1.14: Production of an ammonia contaminated atmosphere

permeation tube (Scaringelli et al., 1970). The output rate of ammonia is then given by the loss in weight of the tube as a function of time.

At 20°C, a permeation rate of 1.6 μg.min^{-1} (n = 5, σ = 10%) was measured.

1.4.3.4 Laboratory tests

Stage 4 (aerodynamic cut-off diameter of 0.5 μm) was loaded with approximately 1.0 μg of sulphuric acid aerosol generated with the setup discussed in section 1.3.1.1. Formvar coated electron microscopy grids cannot be used for aerosol collection in this case, because the organic film is damaged or even completely destroyed by the sulphuric acid. Instead, Mylar foil was used as an impaction surface. In an other set of experiments the vacuum seal of the LAMMA-500 sample chamber was used as the impaction surface of the cascade impactor. Subsequently, an air stream containing ammonia (0.06 m^3, 16 μg.m^{-3}) was passed trough the impactor.

Visual inspection (Figure 1.15) of the sample clearly indicated the presence of crystalline ammonium sulphate. LMM spectrometric analysis confirmed the presence of ammonium sulphate on the impaction surface. As we could expect from the laboratory simulations on $NaCl\text{-}HNO_3$ interaction, sulphuric acid droplets collected with an impactor can be neutralized by ammonia which is still present in the atmosphere during sampling.

This artifact reaction can be avoided in an analogous way as with the $NaCl\text{-}HNO_3$ interaction. Gaseous ammonia can be removed by using a 40 cm oxalic acid coated denuder.

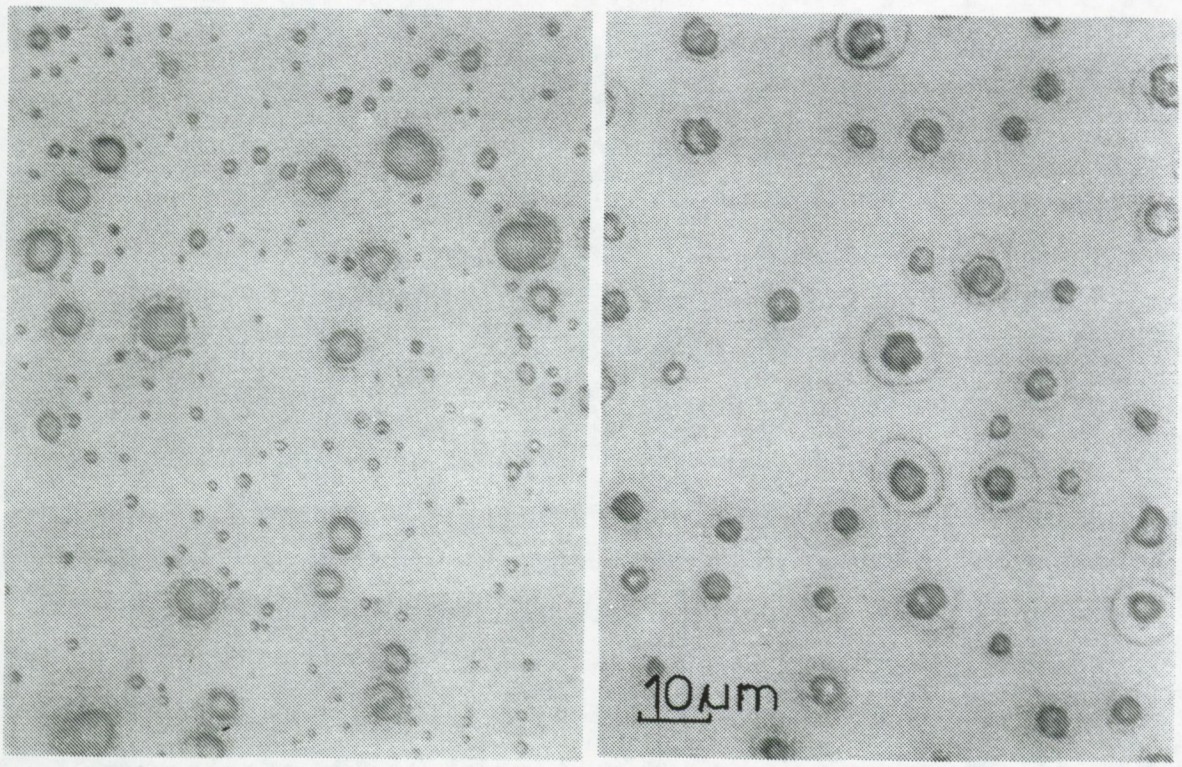

Sulphuric acid particles

Ammonium sulphate particles

Figure 1.15: Visual microscope picture of sulphuric acid aerosols and ammonium sulphate aerosols on a Mylar foil.

1.5 Single particle analysis of ammonium compounds

1.5.1 Electron microscopy

The detection of thermally unstable compounds such as ammonium salts with single particle techniques is not a straightforward procedure. In electron microscopy the high energy electron beam will heat up the particle that is being analyzed, resulting in partial or even complete evaporation of the thermally unstable compounds inside the particle. However, with the aid of so-called film tests, these compounds can be identified with electron microscopy.

For analysis of unstable nitrates, nitron can be used. Reaction of nitron with for instance ammonium nitrate will result in the formation of a large number of sharp needle-like structures that can be identified unambiguously in an electron microscope (Bigg et al., 1974). Possible interference of sodium sulphate and sodium sulphite can be avoided by using a fixation procedure with $BaCl_2$ (Ayers, 1978).

Mamane and Pueschel (1980) used nitron-precoated Formvar membranes to collect airborne particles. In this way, volatile nitrate salts, such as NH_4NO_3 react with the coating during sampling and can thus be detected afterwards by electron microscopy. If one uses uncoated sampling membranes, the volatile species will disappear during the coating process, which takes place under vacuum conditions.

Sulphuric acid, ammonium sulphate and partially neutralized sulphuric acid can be identified by using a combination of a shadowing procedure with SiO_2 or with Au-Pd and complete neutralization with ammonia. The different compounds will still have their specific morphological structure from before neutralization, making identification with electron microscopy possible (Ferek et al., 1983).

1.5.2 LMMS of inorganic ammonium compounds

1.5.2.1 LMMS of standard inorganic ammonium salts

The LMMS technique offers some possibilities for the analysis of unstable compounds. Heinen et al. (1984) proposed a modified sampling chamber to analyze compounds unstable in high vacuum conditions. The unstable particles are placed on the side of the incident laser beam and not on the side of the mass spectrometer. No quartz seal is used but instead a Formvar foil which acts both as a sample support and a vacuum seal. A single laser pulse will perforate the Formvar foil and generate ions which can be extracted into the mass spectrometer. Up to 10 single laser shots can be fired before the high vacuum conditions are lost inside the sample chamber.

For compounds which are stable in vacuum but thermally unstable (inorganic ammonium salts, for instance), the LMMS technique can be used in its normal configuration. Analysis of ammonium salts in individual particles can be performed directly without any special sample preparation. This is an important advantage of the LMMS technique compared with other microprobe techniques such as electron probe micro-analysis.

Standard 0.1 M solutions of different inorganic ammonium salts (ammonium chloride, ammonium nitrate and ammonium sulphate) were nebulized and collected through a diffusion dryer on a Formvar coated EM grid placed in a cascade impactor.

Spectra of the standard ammonium compounds are shown in Figures 1.16 through 1.18. The three ammonium salts are stable in the vacuum conditions of the LAMMA-500 instrument. Cluster-ion formation is quite similar in the case of ammonium chloride and nitrate. The following clusters can be detected (X = Cl or NO_3): NH_4^+, $(NH_3)NH_4^+$, $(NH_3)_2NH_4^+$, $(NH_4X)NH_4^+$ and $(NH_4X)(NH_3)NH_4^+$ in the positive-ion mode

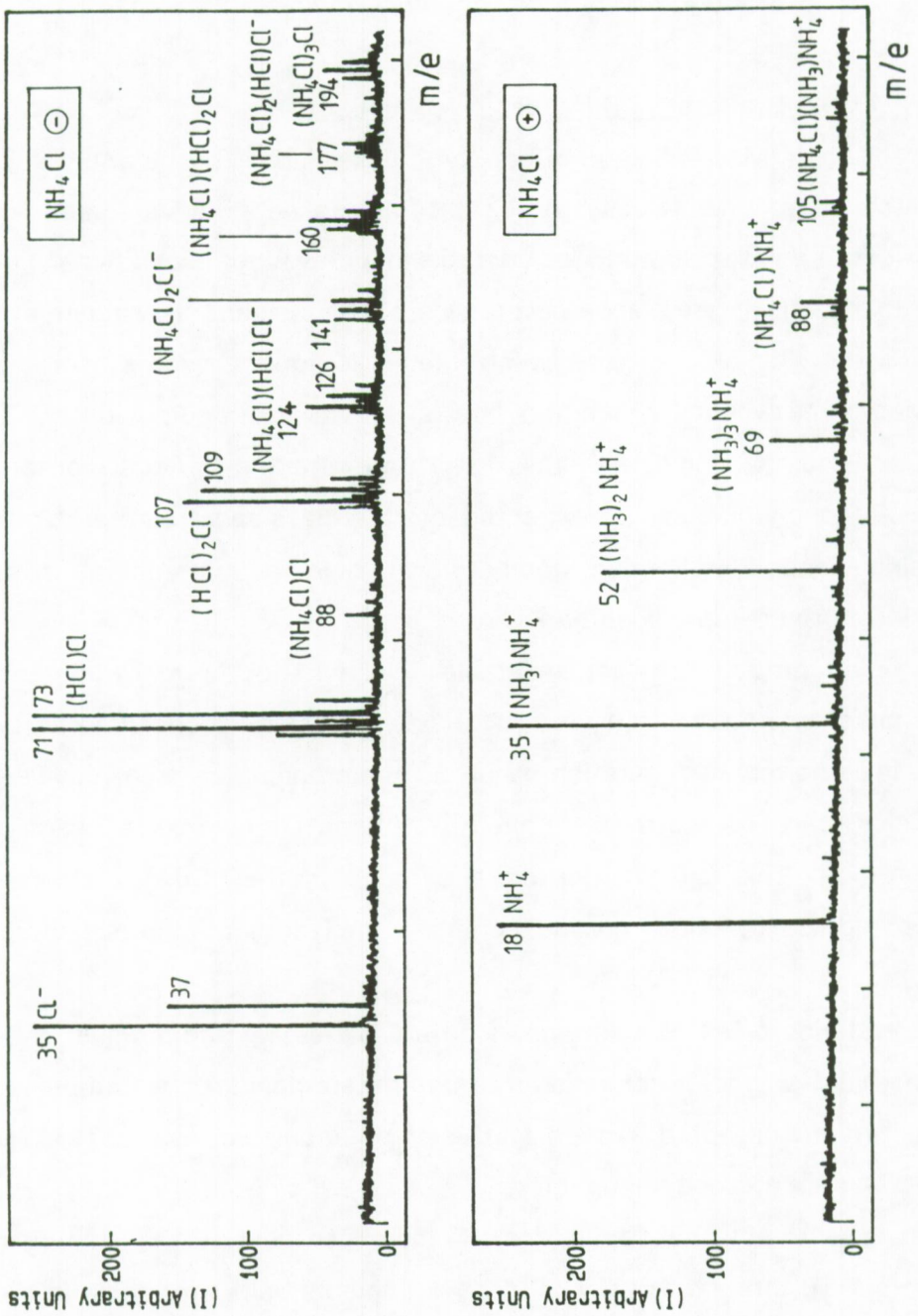

Figure 1.16: LMM spectra of ammonium chloride

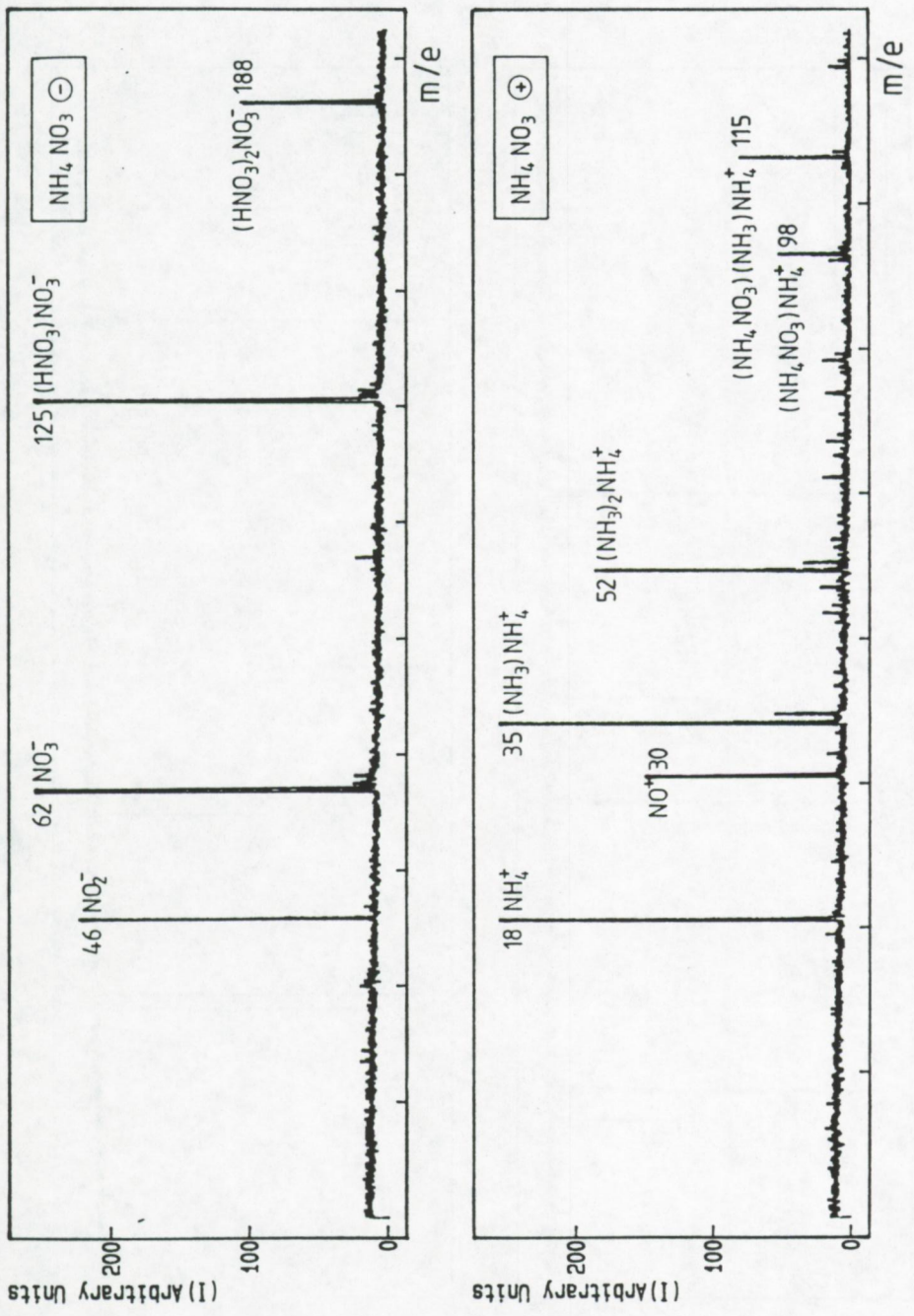

Figure 1.17: LMM spectra of ammonium nitrate

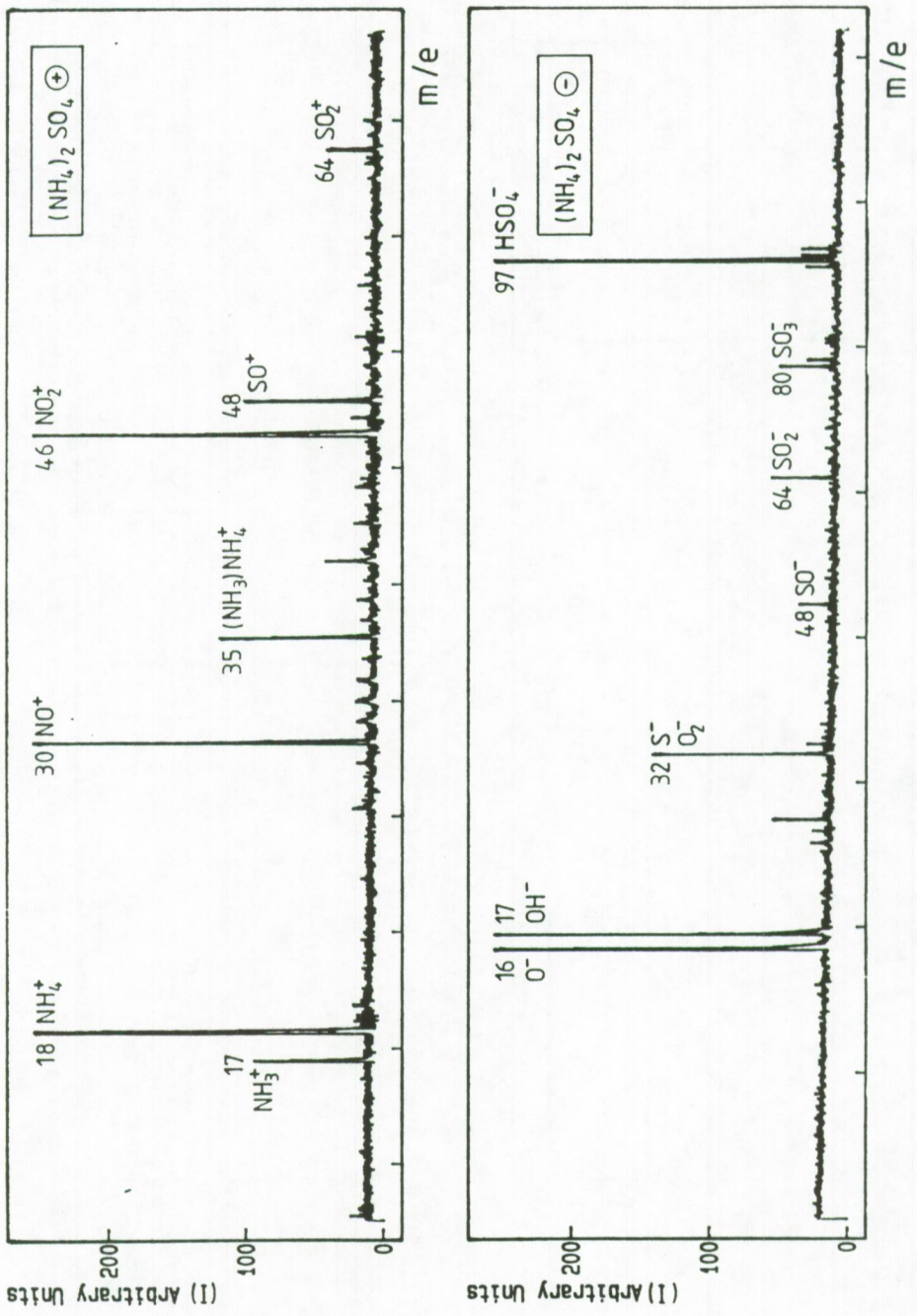

Figure 1.18: LMM spectra of ammonium sulphate

and X^-, $(HX)X^-$ and $(HX)_2X^-$ in the negative-ion mode. The m/z = 46 (NO_2^-) to m/z = 62 (NO_3^-) ratio is <1 in the case of ammonium nitrate in contrast with other nitrate salts (Bruynseels and Van Grieken, 1985). Spectra for ammonium sulphate in both modes provide no evidence for clusters with NH_4^+.

1.5.2.2 Sensitivity of LMMS for different cations

In order to obtain any quantitative results with the LAMMA-500 instrument, it is necessary to know the relative sensitivities for different ions in a marine aerosol matrix. Therefore mixed aerosol particles were made containing different $Na^+/K^+/NH_4^+$ ratios in a chloride matrix.

The results of the measurements of mixed $NH_4^+/Na^+/K^+/Cl^-$ particles are given in Table 1.2. The Na^+/NH_4^+ peak intensity ratio, measured with the LAMMA-500 instrument, $(Na/NH_4)_L$, divided by the stoichiometric Na^+/NH_4^+ ratio in the aerosol particles, $(Na/NH_4)_P$, is defined as the relative sensitivity coefficient for Na^+ to NH_4^+, $(Na/NH_4)_{L/P}$ (and analogously for K^+).

TABLE 1.2

Relative sensitivity of the LAMMA-500 instrument for NH_4^+, Na^+ and K^+ in mixed standard $NH_4^+/Na^+/K^+/Cl^-$ aerosols

$(Na/NH_4)_P$	$(Na/NH_4)_L$	L/P	$(K/NH_4)_P$	$(K/NH_4)_L$	L/P
0.001	0.10	100	0.0004	0.15	370
0.002	0.26	130	0.0008	0.48	600
0.004	0.50	130	0.0016	1.0	650
0.01	1.3	130	0.004	2.4	590
0.02	4.0	200	0.008	5.4	680
0.04	63	1800	0.016	47	3000
0.1	130	1300	0.04	150	3800
0.2	—	—	0.08	—	—

It is clear from Table 1.2 that this LMMS technique is much more sensitive for sodium and potassium than for ammonium in mixed chloride aerosol particles. The sensitivity factors for sodium and potassium relative to ammonium are not constant, but this is merely an artifact of the limited dynamic range of the Biomation transient recorder which was used for signal storage of the secondary electron multiplier output in the LAMMA-500 apparatus. At a 100 MHz sampling rate, this dynamic range is limited to about 2.3 bits or a factor of 5. If only the values obtained by using the LMMS intensity ratios that lie between 0.2 and 5 are considered, then the values found are 150 for $(Na/NH_4)_{L/P}$ and 630 for (K/NH_4). This means that the ammonium/sodium ratios in particles that lie between 30 and 750 (97 to 99.9% of ammonium) can be measured accurately.

In marine aerosol particles, other cations and anions are generally present. To extrapolate the results to a more general marine aerosol matrix, a mixture of NH_4^+, Na^+, Mg^{2+}, Al^{3+}, K^+, Ca^{2+} and Fe^{3+} together with Cl^-, NO_3^- and SO_4^{2-} was prepared. The results of these measurements are given in Table 1.3.

TABLE 1.3

Relative sensitivity of the LAMMA-500 instrument for the seven cations in the mixed standard aerosol matrix

Element (X^+)	$(X/NH_4)_P$	$(X/NH_4)_L$	L/P[a]	Element (X^+)	$(X/NH_4)_P$	$(X/NH_4)_L$	L/P[a]
NH_4^+	1.000	1.000	1.000	K^+	0.00164	1.08	660 (29)
Na^+	0.00514	0.95	185 (6)	Ca^+	0.0384	0.49	12.8 (1.1)
Mg^+	0.0571	0.59	10.3 (0.7)	Fe^+	0.0415	0.50	12.1 (0.6)
Al^+	0.0245	0.41	16.8 (1.4)				

[a] Standard deviation of the mean of 100 spectra is given in parentheses.

Because LMMS is much more sensitive for other cations than for ammonium, it is very suitable for detecting low concentrations of metal ions in a single particle made up of ammonium salts. The detection limit for Pb, an element frequently detected in ambient ammonium sulfate aerosol particles with LMMS, is 30 ppm in a 1 μm particle (Bruynseels et al., 1985).

1.5.2.3 Ammonium content of single particles collected on the North Sea

Marine aerosol particles, collected during two cruises on the North Sea, were investigated for their ammonium compounds. A first set of samples was taken in August 1985 in the Southern Bight of the North Sea during mainly westerly winds. Ammonium was not detected directly, since the peak at m/z = 18 was mostly absent in the positive ion mode, except in some particles of size between 0.25 and 0.5 μm. A large m/z = 97 peak (HSO_4^-) is usually detected in the negative mode, confirming the presence of an important amount of ammonium sulfate. The ratio of the m/z = 143 $(Na_2SO_4)H^+$ peak to the m/z = 165 $(Na_2SO_4)Na^+$ peak also indicates the presence of a hydrogen source. These findings are in agreement with numerous other measurements (Lewin et al., 1986); ammonium and sulfate are highly associated and mostly abundant in the submicrometer particle size range.

A second set of samples was taken during a cruise in March 1986. During this cruise, the meteorological situation was quite different from the first cruise. A weak, variable wind, mainly from eastern direction, resulted in the transport of large amounts of ammonia emitted in Belgium and the Netherlands into the North Sea atmosphere. In addition, a low temperature inversion height inhibited the natural dispersion of pollutants.

In almost all particles (more than 90%) on all five stages of the cascade impactor, ammonium was detected in the positive mode (m/z = 18, NH_4^+). With the relative sensitivity factors obtained from the

standard aerosols, the relative cationic content of the particles can be calculated from the measured intensity ratios, assuming that the particles anionic content does not differ greatly from the standard aerosols. The intensities of the m/z = 18 (ammonium), m/z = 23 (sodium), m/z = 24 (magnesium), m/z = 27 (aluminium), m/z = 39 (potassium), m/z = 40 (calcium) and m/z = 56 (iron) are multiplied by the relative sensitivity factors L/P and normalized to the sum. The peak at m/z = 40 (Ca^+) is corrected for the contribution of MgO^+ and the peak at m/z = 56 (Fe^+) is corrected for the contribution of CaO^+. These contributions were measured by analysis on standard magnesium and calcium salts. Table 1.4 lists the measured Na^+/NH_4^+ intensities and calculated mol % of ammonium in the total cations, taking into account the presence of Na, Mg, Al, K, Ca, and Fe.

TABLE 1.4

Measured Na^+/NH_4^+ ratios in four marine aerosols collected during the second cruise (10—14/3/1986) in the North Sea

Stage[a]	Measured Na/NH_4 intensity				NH_4 (mol·% cations)			
	1	2	3	4	1	2	3	4
1	—	—	5.3	4.1	0	0	77	79
2	48	16	5.4	2.3	47	53	74	89
3	9.6	57	3.4	13	30	79	88	57
4	19	47	4.7	5.3	45	49	75	79
5	11	63	3.5	8.6	39	75	92	85

[a] Diameters of stages 1—5 are 4, 2, 1, 0.5 and 0.25-μm aerodynamic diameter, respectively.

It is obvious that particles from all five stages contain very large amounts of ammonium ion, up to 90% of the total cationic content. In the large particles, ammonium is associated with nitrate and sulfate, in the smaller particles only with sulfate. Sample 4, taken at the end of the cruise with the wind direction changing slowly from east to southeast, shows the highest ammonium concentrations on all stages of the cascade impactor.

1.5.3 Identification of mixed ammonium compounds in single particles with LMMS in samples collected at the University of Antwerp (UIA) campus.

In section 1.5.2 we showed that it is possible to identify simple inorganic ammonium salts in single aerosol particles in a direct way. Some indirect electron microscope measurements (see section 1.5.1) had already proven the existence of pure simple ammonium salts in single particles.

Sturges and Harrison (1989) reported on the identification of mixed ammonium salts in ambient particulate matter. High volume cascade impactors were sampled in the outskirts of Toronto, Ontario. Analysis of the samples with X-ray diffraction resulted in the identification of NH_4Cl, $(NH_4)_2SO_4$, $(NH_4)_2SO_4.2NH_4NO_3$, $(NH_4)_2SO_4.3NH_4NO_3$, $CaSO_4.(NH_4)_2SO_4.H_2O$ and $PbSO_4.(NH_4)_2SO_4$.

The ammonium nitrate sulphate double salts were prepared by Sturges and Harrison (1989) using the granulation method of Coates and Woodward (1963) by hydrating mixtures of finely ground ammonium nitrate and ammonium sulphate. A small amount of the two double salts was transferred to a Formvar coated electron microscope grid for LMMS analysis. Figure 1.19. shows the negative mode spectrum for $(NH_4)_2SO_4.3NH_4NO_3$. Negative mode spectra are identical for the two

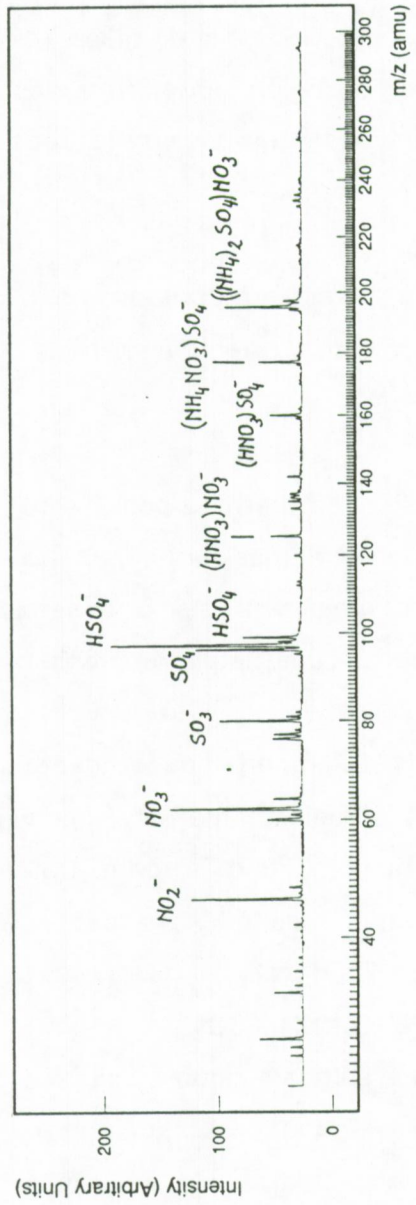

Figure 1.19: Negative ion mode LMM spectrum of $(NH_4)_2SO_4.3NH_4NO_3$

compounds. Due to the low shot-to-shot reproducibility of the used LMMS technique, it is not possible to identify both salts unambiguosly from a single mass spectrum. However, the prescence of different combined peaks would allow us to investigate the presence of ammonium nitrate sulphate double salts in ambient particulate matter samples.

A few samples were collected with a five stage cascade impactor on a roof of one of the university buildings during the winter of 1987-1988. The university is located at 10 km south of the Antwerp city centre in a suburban area. Figure 1.20 and 1.21 shows some of the negative mode spectra. In the larger particles (stage 1 and 2, cut-off diameter 4 and 2 μm, respectively) chloride, nitrate and sulphate peaks are simultaneously detected. Not one spectrum yielded pure chloride or pure nitrate peaks. In the lower particle-size fraction (stage 4 and 5, cut-off diameter 0.5 and 0.25 μm, respectively) no chlorides were detected, but in most cases (> 50%) nitrate and sulphate salts were present together. Although pure ammonium chloride and ammonium nitrate particles have been identified by other authors in the past, we were unable to find them in these samples. The presence of combined ammonium chloride nitrate sulphate triple salts cannot be attributed to reaction on the impactor since particle loadings were too low to allow particle-particle interactions, and an ammonia removing denuder was used in front of the impactor so that gas-particle interactions on the impaction surface can also be ruled out. It is possible that the combined ammonium salts are really internally mixed aerosol particles as a results of redistribution inside cloud or fog droplets.

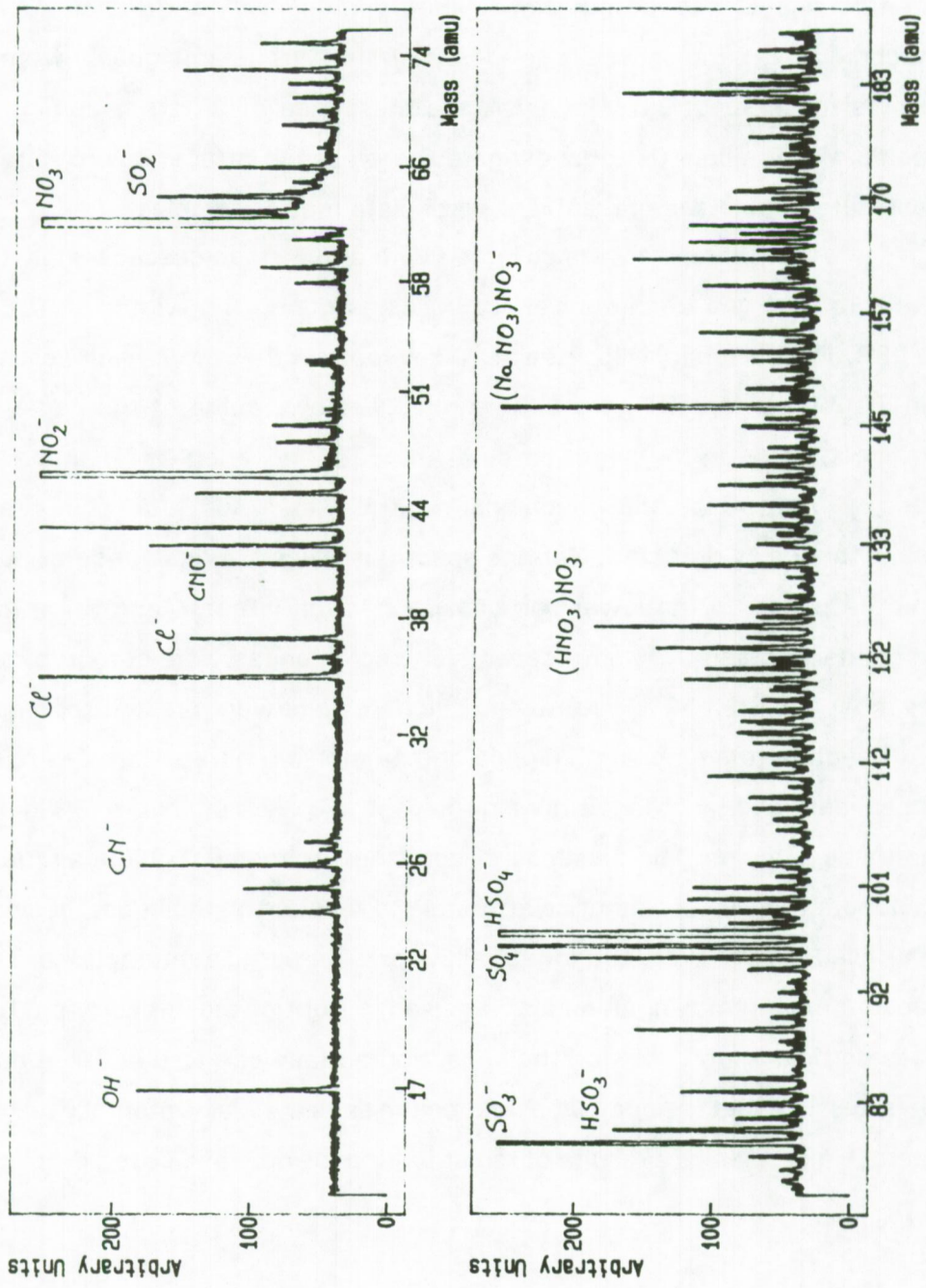

Figure 1.20: Negative ion mode LMM spectrum of a mixed ammonium salt particle collected in ambient air (impactor stage 2)

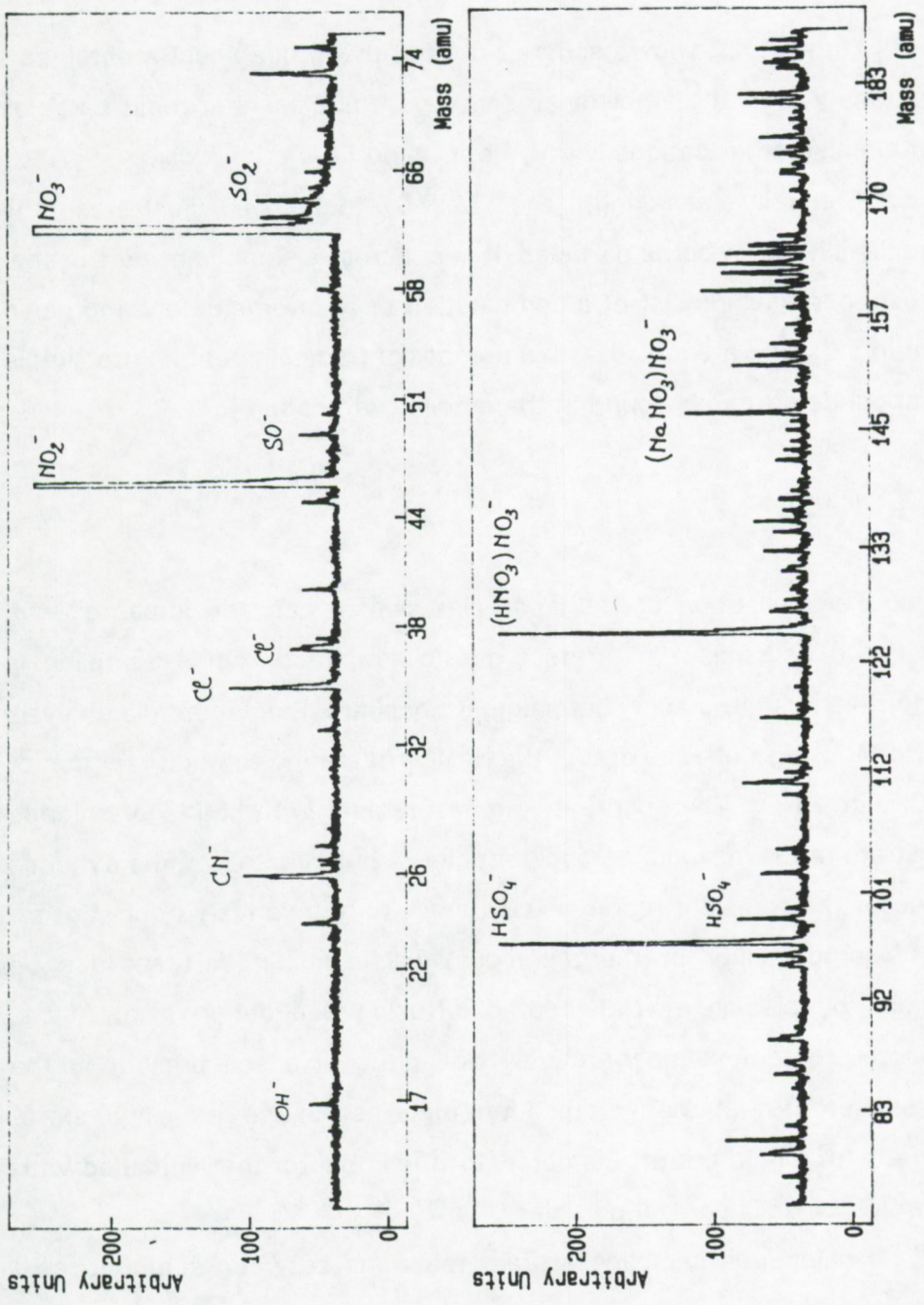

Figure 1.21: Negative ion mode LMM spectrum of a mixed ammonium salt particle collected in ambient air (impactor stage 3).

Figure 1.22 shows some of the positive mode spectra obtained from analysis of the ambient air samples. It is clear that most particles contain also other cations like V, Pb, Ca and Fe.

Generally speaking, the LMMS technique illustrates the complexicity or airborne particles. It seems that a significant part of the aerosol particles consist of a combination of both organic and inorganic compounds that are mixed with a number of trace elements. Pure simple compounds are rarely found in the ambient atmosphere.

1.6 Conclusion

The collection of NaCl particles with a cascade impactor was proven to be subject to artifact nitrate formation, when sampling is performed in a nitric acid containing atmosphere. Single particle analysis with LMMS was used to detect the $NaNO_3$ formation through reaction of NaCl with HNO_3. The quantitative measurement with LMMS of chloride to nitrate ratios in single aerosol particles is both limited by the dynamic range of the transient recorder used and by the relatively poor shot-to-shot reproducibility of the technique. This sampling artifact can be avoided by placing a NaF coated diffusion denuder in front of the impactor to remove quantitatively any nitric acid still present in the atmosphere. An alternative procedure involves the use of a single extra-stage, with a high cut-off diameter, for the impactor that is loaded with a surplus of NaCl aerosol particles.

Analoguous sampling artifact reactions between sulphuric acid aerosols and gaseous ammonia were simulated in laboratory tests. The LMMS technique has proven to be useful for direct detection of thermally unstable inorganic ammonium compounds in single aerosol particles. Ammonium chloride, ammonium nitrate and ammonium sulphate can be identified unambiguously on the basis of their positive and negative mass

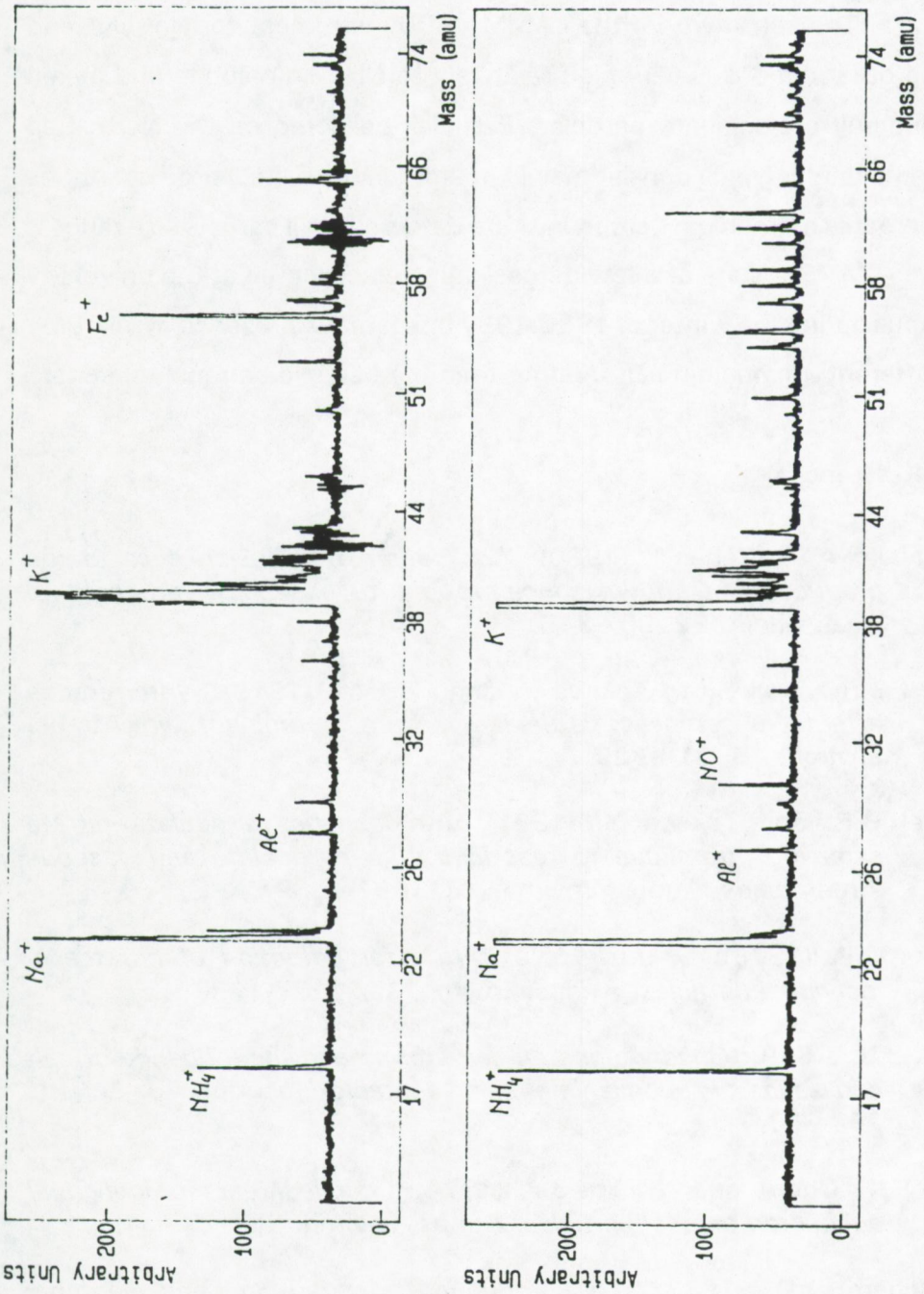

Figure 1.22: Positive ion mode LMM spectra of mixed ammonium salt particle collected in ambient air.

spectra. The sensitivity of the LAMMA-500 instrument for Na^+, K^+ and some other cations is very high relatively to NH_4^+ in chloride and mixed chloride/nitrate/sulphate particles. Particles collected on the North Sea during easterly winds consist mainly of ammonium salts. Large quantities of inorganic ammonium compounds are detected in all particle size ranges.

LMMS results of a few aerosol samples collected at the university campus during the winter of 1986-1987 indicate the presence of mixtures of different ammonium salts, rather than pure simple ammonium salts.

1.7 References

Altshuller A.P., Cohen I. (1960): *Application of diffusion cells to the production of known concentrations of gaseous hydrocarbons.* Anal. Chem. 32, 802-810.

Appel B.R., Wall S.M., Tokiwa Y. and Haik M. (1979): *Interference effects in sampling particulate nitrate in ambient air.* Atmos. Environ. 13, 319-325.

Appel B.R. and Tokiwa Y. (1981): *Atmospheric particulate nitrate sampling errors due to reactions with particulate and gaseous strong acids.* Atmos. Environ. 15, 1087-1089.

Ayers G.P. (1978): *On the use of nitron for detection of nitrates in individual particles.* Atmos. Environ. 12, 1227-1230.

Beck J.B. (1819): *Observations on salt storms and the influence of salt and saline air upon animal and vegetable life.* Amer. J. Sci., 1, 388-397.

Bigg E.K., Ono A. and Williams J.A. (1974): *Chemical tests for individual submicron aerosol particles.* Atmos. Environ. 8, 1-13.

Blanchard D.C. (1983): *The production, distribution, and bacterial enrichment of the sea-salt aerosol.* In Air-sea Exchange of Gases and Particles. Eds. Liss P.S and Slinn W.G.N., NATO-ASI Series C-108, 407-454.

Bruynseels F.J. and Van Grieken R.E. (1985): *Direct detection of sulfate and nitrate layers on sampled marine aerosols by Laser microprobe mass analysis.* Atmos. Environ. 19, 1969-1970.

Cadle R.D. (1973). *Chemistry of the lower atmosphere.* Plenum Press, New York.

Cadle S.H. (1985): *Seasonal variations in nitric acid, nitrate, sulfuric acid, and ammonia in an urban area.* Atmos. Environ. 19, 181-188.

Coates R.V. and Woodward G.D. (1963): *X-ray powder* diffraction data for solid solutions and double salts occuring in granular compound fertilizers. J. Sci. Fd. Agric. 14, 398-404.

Dasch J.M. and Cadle S.H. (1986): *Dry deposition to snow in an urban area.* Wat. Air Soil Pollut. 29, 297-308.

Dasch J.M., Cadle S.H., Kennedy K.G. and Mulawa P.A. (1989): *Comparison of annular denuders and filter packs for atmospheric sampling.* Atmos. Environ. 23, 2275-2782.

Daum P.H., Kelly T.J., Tanner R.L., Tang X., Anlauf K., Bottenheim J., Brice K.A. and Wiebe H.A. (1989): *Winter measurements of trace gas and aerosol composition at a rural site in southern Ontario.* Atmos. Environ. 23, 161-173.

Eagan M.L. and Dubois L. (1974). *The determination of ammonium ion in airborne particlulates with selective electrodes.* Anal. Chim. Acta, 70, 157-167.

Eatough D.J., White V.F., Hansen L.D., Eatough N.L. and Ellis E.C. (1985): *Hydration of nitric acid and its collection in the atmosphere by diffusion denuder.* Anal. Chem. 57, 743-748.

Ferm M. (1979): *Method for the determination of atmospheric ammonia.* Atmos. Environ., 13, 1385-1393.

Ferek R.J., Allen L.L. and Winchester J.W. (1983): *Electron microscopy of acidic aerosols collected over the norheastern United States.* Atmos. Environ. 17, 1545-1561.

Forrest J., Tanner R.L., Spandau D.J., D'Ottavio T. and Newman L. (1980): *Determination of total inorganic nitrate utilizing collection of nitric acid on NaCl-impregnated filters.* Atmos. Environ. 14, 137-144.

Gormley P. and Kennedy M. (1949): *Diffusion from a stream flowing through a cylindrical tube.* Proc. R. Irish Acad. 52A, 163-169.

Harrison R.M. and Pio C.A. (1983): *Size-differentiated composition of inorganic atmospheric aerosols of both marine and polluted continental origin.* Atmos. Environ. 17, 1733-1738.

Harrison R.M. and Allen A.G. (1990): *Measurements of atmospheric HNO_3, HCl and associated species on a small network in eastern England.* Atmos. Environ. 24A, 369-376.

Heinen H.J. and Holm R. (1984): *Recent development with the Laser microprobe mass analyzer (LAMMA).* S.E.M., 1129-1138.

Hering S.V., Lawson D.R., Allegrini I., Febo A., Perrino C., Possanzini M., Sickles J.E., Anlauf K.G., Wiebe A., Appel B.R., John W., Ondo J., Wall S., Braman R.S., Sutton R., Cass G.R., Solomon P.A., Eatough D.J., Eatough N.L., Ellis E.C., Grosjean D., Hicks B.B., Womack J.D., Horrocks J., Knapp K.T., Ellestad T.G., Paur R.J., Mitchell W.J., Pleasant M., Peake E., MacLean A., Pierson W.R., Brachazek W., Schiff H.I., Mackay G.I., Spicer C.W., Stedman D.H., Winer A.M., Biermann H.W. and Tuazon E.C. (1988): *The nitric acid shootout: Field comparison of measurment methods.* Atmos. Environ. 22, 1519-1539.

Junge C.E. (1956): *Recent investigation in air chemistry.* Tellus, 8, 127-139

Kiang C.S., Stauffer D., Mohnen V.A., Bricard J. and Vigla D. (1973): *Heteromolecular nucleation theory apllied to gas-to-particle conversion.* Atmos. Environ. 7, 1279-1283.

Klockow D., Niessner R., Malejczyk M., Kiendl H., vom Berg B., Keuken M.P., Wayers-Ypelaan A. and Slanina J. (1989): *Determination of nitric acid and ammonium by means of a computer-controlled thermodenuder system.* Atmos. Environ. 23, 1131-1138.

Mamane Y. and Pueschel R.F. (1980): *A method for the detection of individual nitrate particles.* Atmos. Environ. 14, 629-639.

Meszaros E. (1981): *Atmospheric Chemistry. Fundamental Aspects.* Elsevier Scientific Publishing Company, Amsterdam.

Niessner R. and Klockow D. (1983): *A new approach to the determination of atmospheric strong acids.* J. Aerosol Sci. 13, 175-179.

Perrino C., De Santis F. and Febo A. (1990): *Criteria for the choice of a denuder sampling technique devoted to the measurement of atmospheric nitrous and nitric acids.* Atmos. Environ. 24A, 617-626.

O'Keeffe A.E. and Ortman G.C. (1966): Primary standards for trace gas analysis. Anal. Chem. 38, 760-763.

Okita T., Morimoto S. and Izawa M. and Konno S. (1976): *Measurements of gaseous and particulate nitrate in the atmosphere.* Atmos. Environ. 10, 1085-1089.

Possanzini M., Febo A. and Liberti A. (1983): *New design of a high performance denuder for the sampling of atmospheric pollutants.* Atmos. Environ. 17, 2605-2610.

Platt U., Perner D., Winer A.M., Harris G.W. and Pitts J.N.Jr. (1980): *Detection of NO_3 in the polluted troposphere by differential optical absorption.* geophys. Res. Lett. 7, 89.

Ruprecht H. and Sigg L. (1990): *Interactions of aerosols (ammonium sulfate, ammonium nitrate and ammonium chloride) and of gases (HCl and HNO_3) with fogwater.* Atmos. Environ. 24A, 573-584.

Savoie D.L. and Prospero J.M. (1982): *Particle size distribution of nitrate and sulfate in the marine atmosphere.* Geophys. Res. Lett., 9, 1207-1210.

Scaringelli F.P., O'Keeffe A.E., Rosenberg E. and Bell J.P. (1970): *Preparation of known concentrations of gases and vapors with permeation devices calibrated gravimetrically.* Anal. Chem. 42, 871-876.

Sickells J.E., Hodson L.L., McLenny W.A., Paur R.J., Ellestad T.G., Mulik J.D., Anlauf K.G., Wiebe H.A., MacKay G.I., Schiff H.I. and Bubacz D.K. (1990): *Field comparison of methods for the measurement of gaseous and particulate contributors to acidic dry deposition.* Atmos. Environ. 14A, 155-165.

Slanina J., v. Lamoen-Doornebal L., Lingerak W.A., Meilof W., Klockow D. and Niessner R. (1981): *Application of a thermo-denuder analyzer to the determination of H_2SO_4, HNO_3 and NH_3 in air.* Int. J. Envir. Analyt. Chem. 9, 59-70.

Small H., Stevens T.S. and Bauman W.C. (1975): *Novel ion exchange chromatographic method using conductometric detection.* Anal. Chem, 47, 1801-1809.

Steen B. and Andreasson K. (1973): *Deposition of ambient air particles in tubes of 4.5-6.5 mm diameter at flow rates of 1.4 and 3 $l.min^{-1}$.* IVL-Publication B129, Swedish Water and Air Pollution Research Laboratory.

Sturges W.T. and Harrison R.M. (1989): *Semi-quantitative X-ray diffraction analysis of size-fractionated atmospheric particles.* Atmos. Environ. 23, 1083-1098.

Tanner R.L., Kelly T.J., Dezaro D.A. and Forrest J. (1989): *A comparison of filter, denuder and real-time chemiluminescence techniques for nitric acid determination in ambient air.* Atmos. Environ. 23, 2213-2222.

Teckentrup A. and Klockow D. (1978): *Preparation of refillable permeation tubes.* Anal. Chem., 50, 1728.

Woodcock A.H. (1953): *Salt nuclei in marine air as a function of altitude and wind force.* J. Met., 10, 362-371.

Chapter 2

Elemental concentrations in atmospheric particulate matter sampled from the R/V Belgica on the North Sea

2.1 Introduction

The North Sea is characterized by an area of 575000 km^2 and an average depth of 94 m. It is surrounded by relatively highly industrialized and densely populated countries: Norway, Denmark, West-Germany, The Netherlands, Belgium and the United Kingdom. Human activities on and around the North Sea have important biological, chemical and geological effects.

The North Sea atmosphere contains an immense variety of natural and man-made components, both in gaseous and in particulate form. The sea itself produces sea salt droplets that are involved in various chemical reactions (see also Chapter 1). Anthropogenic pollutants emitted on land can reach the North Sea atmosphere through physical dispersion and transport processes. Human activities on the sea itself such as oil and gas field exploitation and the use of diesel engine powered ships for transportation result in a direct injection of pollutants into the marine atmosphere.

In order to understand more about the North Sea aerosol constituents and their sources and their fate, an extensive sampling program was set up with the R/V Belgica, a recently built Belgian oceanographic research vessel. Between December 1984 and June 1988, 71 aerosol samples were collected under different meteorological situations and from different regions, covering the complete North Sea and the Channel.

Particulate matter, collected on membrane-type filters was analyzed with energy-dispersive X-ray fluorescence (EDXRF) yielding atmospheric concentrations for Al, Si, P, S, Cl, K, Ca, Ti, V, Cr, Mn, Fe, Ni, Cu, Zn and Pb. In section 2.2 a brief theoretical description of EDXRF and of the apparatus used, a Spectrace 5000 unit (Tracor, USA), is given. Calibration procedures involving thin film mono-element standards are discussed next. Sampling equipment is described in section 2.3 with

special emphasis on contamination-free sampling procedures.

The results of EDXRF measurements on 71 filter samples collected during 10 different sampling campaigns are discussed in section 2.4. A multi-variate technique, factor analysis, is used for determination of the underlying structure of the total data set.

Our experimental results are compared with literature data on measurements of trace elements in air performed at coastal stations around the North Sea (section 2.5) and from another ship (section 2.6). An overview is given of all data that are available on North Sea atmosphere measurements over the last 20 years.

Finally a comparison is made between our experimental values for atmospheric Pb concentrations above the North Sea and model-predicted concentrations.

2.2 Analytical procedure

2.2.1 Energy dispersive X-ray fluorescence

Energy-dispersive X-ray fluorescence is a powerful multi-element technique which allows analysis of solid samples without pretreatment and is essentially non-destructive. It is based on the interaction between electromagnetic radiation and matter. When an X-ray photon (0.1 keV to 100 keV) hits an element, the photon can be absorbed completely by an electron which results in the ejection of the electron with an energy equal to the difference between the energy of the incident X-ray photon and the binding energy of the electron in its shell. This photo-electric effect results in the creation of an electron vacancy in the atom which leads to transitions of electrons from outer to inner shells. The energy lost in each transition is emitted as an X-ray photon that can escape the atom as an element-characteristic X-ray or can expel an outer electron of the atom, a so-called Auger-electron. Auger absorption occurs predominantly in low

Z elements, while the emission of characteristic X-rays is more probable for high Z elements (Figure 2.1).

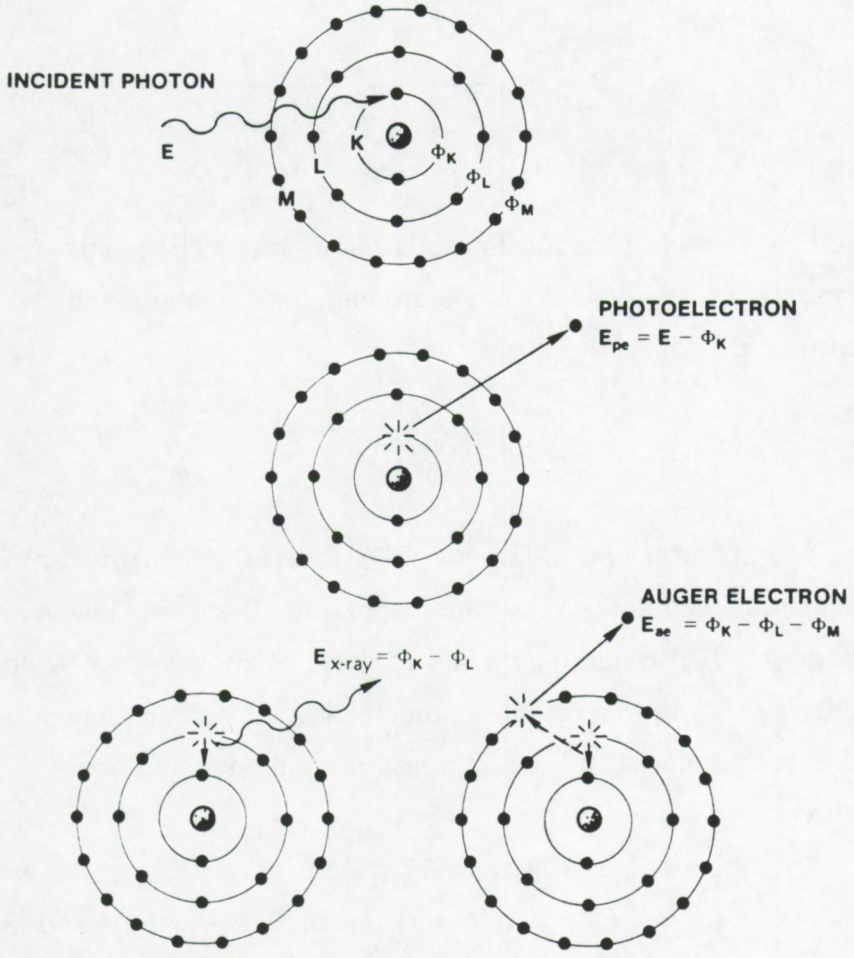

Figure 2.1: Photo-electric interactions between an incident X-ray photon and an atom (Jenkins et al., 1981).

Besides photo-electric interaction, incident X-rays can also be scattered. Elastic or coherent scattering does not lead to energy loss of the incident photons. Inelastic or Compton scattering results in a loss of energy and a change in direction of the original photon:

$$E = \frac{E_0}{1 + (\frac{E_0}{m_0 c^2})(1 - \cos\theta)} \qquad (2.1)$$

where E = energy of the inelastic scattered photon, E_0 = energy of the incident photon, c = velocity of electromagnetic radiation, and θ = angle of scattering.

2.2.2 Instrumentation: Spectrace-5000

The Spectrace 5000 (Tracor, USA) is an EDXRF instrument which is completely controlled by and operated from an IBM-AT type microcomputer. This instrument has a sample chamber with a 10-position sample tray that can be rotated automatically. The sample chamber can be used both under atmospheric pressure conditions and under vacuum conditions.

The Spectrace 5000 uses a 17.5 Watt power X-ray tube with Rh anode target. It operates within a range of 6 to 50 keV and with a maximum current intensity of 0.35 mA. The X-ray beam passes a 127 μm thick Be window, is collimated and finally passes through a filter system. The filter system allows the use of either no filter at all or a selection from five different filter types: a cellulose filter, a 127 μm Al filter, a 50 μm Rh filter, a 127 μm Rh filter or a 630 μm Cu filter.

At 90 degrees relative to the incident X-ray beam, the characteristic X-rays from the sample and the scattered X-rays are detected by an energy-dispersive Si(Li) detector. This detector has an active area of 0.3 cm^2 x 0.3 cm and a resolution of approximately 160 eV

at the Mn K_α line. The gain of the system is 20 eV/channel; spectra can be recorded into a 10, 20 or 40 keV region. Data acquisition and display is done by the personal computer. Figure 2.2 shows a typical energy-dispersice X-ray spectrometer.

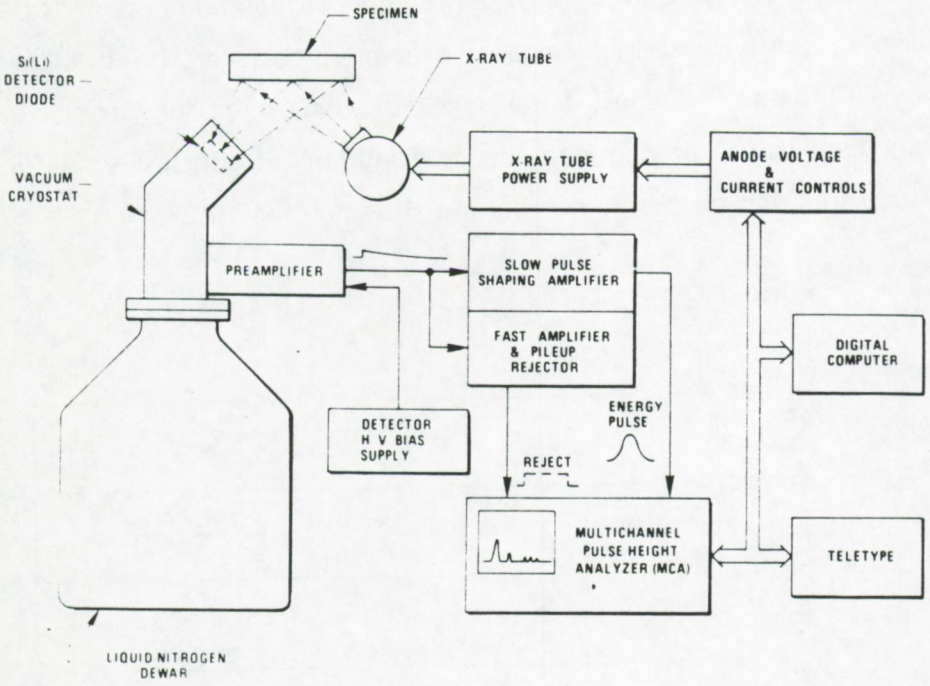

Figure 2.2: EDXRF - Block diagram (Jenkins et al., 1981).

2.2.3 Calibration

In the calibration procedure followed, a series of thin film reference standards, composed of pure elements or simple inorganic compounds evaporated on a 4 μm thick Mylar foil (Micromatter, Seattle, WA, USA), were used. Assuming that the standards are infinitely thin and all matrix effects are negligible, the intensity of a characteristic X-ray can be written as:

$$I_i = K_i \; i \; t \; C_i \qquad (2.2)$$

where I_i = intensity of characteristic line i, K_i = sensitivity coefficient for line i of element i, i = tube current, t = irradiation time and C_i = concentration in $\mu g.cm^{-2}$ of element i.

Low Z element standards are analyzed with an accelerating voltage of 15 kV, using a current of 0.35 mA and an irradiation time of 1000 sec. No collimator was used. Because of overlap between the Rh-L lines and the Cl-K and S-K lines, a cellulose filter was used for filtration of the incident polychromatic X-ray beam. The resulting sensitivity coefficients as a function of atomic number are shown in Figure 2.3.

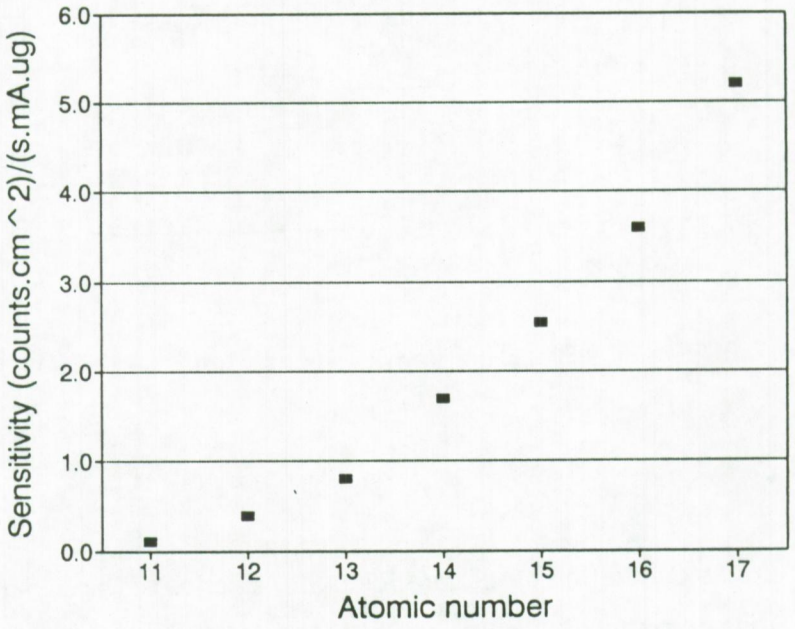

Figure 2.3: Low Z-element XRF calibration curve.

For high Z element standards, irradiation was done during 1000 sec with a 35 kV beam using a 0.35 mA current and a thin Rh-filter. The resulting sensitivity coefficients are shown in Figure 2.4.

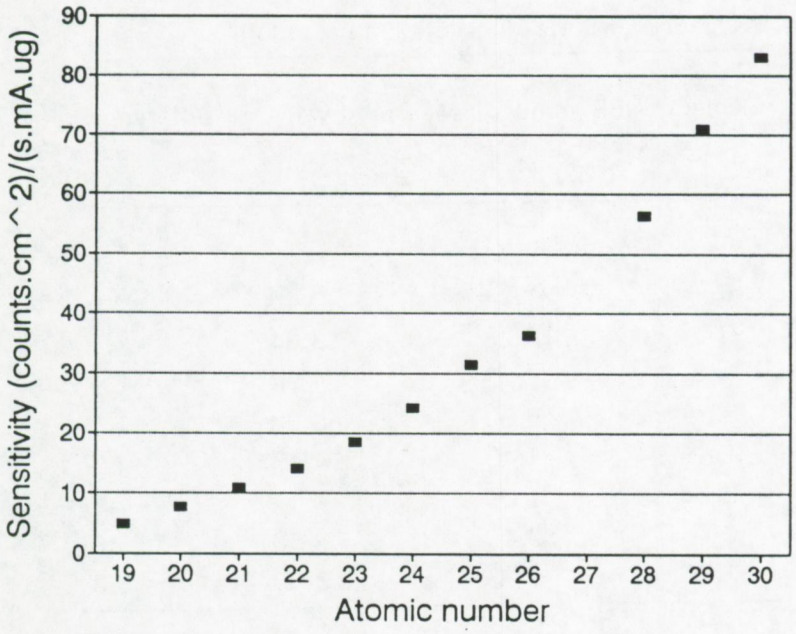

Figure 2.4: High Z-element XRF calibration curve.

For Pb, the L lines are used for calibration.

X-ray spectra are analyzed with the AXIL software (Van Espen et al. 1986). The AXIL software package is an integrated system for EDXRF spectrometric analysis. It runs on an IBM-PC or compatible computer and performs such tasks as: communication with external multi-channel analyzers, conversion of spectral data, analysis of spectra using non linear least-squares fitting, calculation of quantitative analysis results and plotting and printing of data.

The calibration procedure was evaluated by analyzing two NBS reference standards consisting of a Nuclepore membrane with a deposited glass layer. Table 2.1 compares the certified values with the ones obtained through calibration with Micromatter standards.

Table 2.1:
Evaluation of the XRF calibration procedure

Element	NBS standard Certified value ($\mu g.cm^{-2}$)	Measured value ($\mu g.cm^{-2}$)	% Difference
K	17.90	18.17	+1.5
Ca	21.94	22.49	+2.5
Ti	13.23	13.64	+3.1
V	5.09	4.97	- 2.4
Mn	5.09	5.03	- 1.1
Fe	14.48	14.15	- 2.3
Co	1.09	1.11	+1.5
Cu	2.46	2.39	- 3.0
Zn	3.73	3.80	+1.9

Table 2.2 lists the detection limits for airborne particulate matter samples, assuming 10 m^3 of air was drawn through a 47 mm diameter Nuclepore filter. Detection limits are calculated as three times the standard deviation on the peak surfaces, obtained by analysis of a blank filter. High Cl detection limit is due to the interference of incompletely filtered Rh-L lines that coincide with the Cl-K lines.

Table 2.2
Detection limits in $ng.m^{-3}$, assuming a sample volume of 10 m^3 and a filter diameter of 47 mm.

Al	200	Cl	600	V	2.0	Ni	0.5
Si	140	K	9	Cr	1.5	Cu	0.4
P	70	Ca	6	Mn	0.9	Zn	0.4
S	80	Ti	2.5	Fe	0.4	Pb	8

2.3 Sampling strategy

2.3.1 R/V Belgica

The R/V Belgica is a modern oceanographic vessel that came into operation in July 1984. A crew of 15 and a scientific team of 15 are involved in a large number of research tasks. The ship offers sampling facilities for sediments, seawater and airborne constituents. Fishing activities are also included. Four fully equipped laboratories assure sample storage and analysis possibilities. A central computer is used for continuous data collection with regard to both meteorological parameters and physical seawater parameters. Figure 2.5 shows a picture of the R/V Belgica on the North Sea during a sampling campaign in October 1989.

2.3.2 Air sampling equipment

Total airborne particulate matter is collected by using a 47 mm diameter, 0.4 μm pore size polycarbonate membrane-type filter (Nuclepore, aerosol-grade). In some cases, a dual filter unit was used, consisting of a 8.0 μm pore size filter, followed by a 0.4 μm pore size one. This double filter sampler allows to separate the coarse particle fraction (>2 μm) from the fine particle fraction during sampling. The filters are placed in a plexiglass filter holder which has a hat-type cover (Figure 2.6) to protect the filter from any contamination by seawater droplets that are ejected in the air through wave breaking by the ship itself.

Table 2.3 shows the results of electron microscope measurements on five dual samples, with and without hat, taken on the North Sea. From the particle size distributions, the number of particles with a diameter larger than 2 μm was calculated. There is no systematic difference between the sampler with hat and the sampler without hat. The

Figure 2.5: The R/V Belgica.

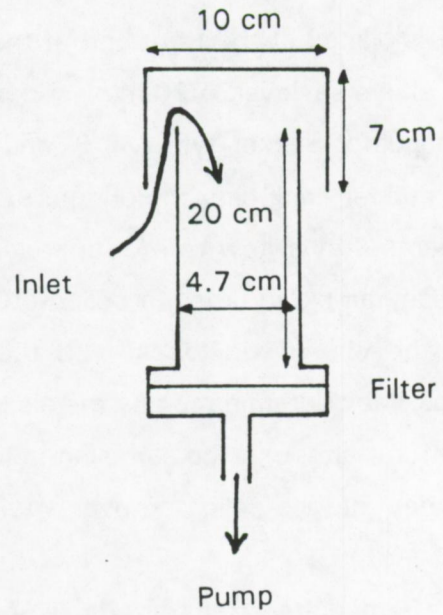

Figure 2.6: Filter holder for air sampling.

percentage of mass (calculated from the number size distribution by assuming the same density and shape for all particles), represented by particles with a diameter larger than 2 μm is nearly the same with the two setups used.

Table 2.3
Sampling efficiency of hat-type filter system

% of particles > 2 μm		% of mass represented by particles > 2 μm	
with hat	without hat	with hat	without hat
2.4	7.9	66	72
3.0	2.3	63	75
1.5	2.7	66	68
5.8	2.3	88	80
9.1	8.6	89	90

The filter holder is placed at the front end of the ship at a height of approximately 10 m above sealevel. A 20 m plastic hose connects the filter unit to a vacuum pump (Becker type VT 6) and a dry gas meter which are placed at the upper deck near the bridge.

The pump is operated at a flow rate of approximately 35 $l.min^{-1}$ during 4 to 12 h for each sample in order to collect 10 m^3. Sampling is discontinued whenever the relative wind direction to the ship is $<-45°$ or $>45°$ for reasons of possible contamination by the diesel engine exhaust of the ship itself. Therefore, although the sampling volume is nearly the same for all samples, they may be collected over a wide range of total sampling times.

Filter samples are immediately transferred to a flow hood inside the chemical laboratory on the ship and are placed in a plastic box until further analysis by EDXRF in the laboratory of the university.

2.4 Results

In this section, an overview is given of all results concerning atmospheric concentrations of trace elements in the North Sea atmosphere. Although some of the earlier samples (sampling campaign 1 and 2 with 4 and 15 aerosol samples, respectively) have been collected and analyzed by others (Bruynseels, 1987), they are included to give a complete survey of the total data set.

2.4.1 Campaign 1: December 12 - December 16, 1984

2.4.1.1 General sampling data and meteorological information

During campaign 1, from December 12 to December 16, 1984, four aerosol samples were collected from the R/V Belgica on the Southern Bight of the North Sea, more specifically on the Belgian Continental Shelf.

Two-dimensional, 96 h backward air mass trajectories were

calculated by the Belgian weather service KMI for the 1000 mbar level, i.e. sea level. Corresponding back trajectories for all four filters are shown in Figure 2.7.

These air mass trajectories indicate the origin and the history of the collected airborne particulate material. They often include more useful information than wind speed and wind direction data at the sampling site, since two samples collected at the same location under similar local meteorological conditions may have a completely different air mass history due to differences in the large-scale meteorological situation, i.e. the distribution of high and low pressure areas and the presence of cold and warm fronts.

2.4.1.2 XRF results

Table 2.4 lists the atmospheric concentrations as obtained by EDXRF. In sample 1, the highest S, K, V, Ni, Cu, Zn and Pb concentrations are found. From the air mass history (Figure 2.7), we can see that the collected airborne material originated from the London area and the southern part of the United Kingdom.

Sample 2 was collected under continental (France) influences (Figure 2.7). Most concentrations are lower than in sample 1, except for Ca (+80%) and Fe (+55%). The Zn concentration is the same in sample 1 and 2.

The third sample was collected at higher wind speeds, up to 15 $m.s^{-1}$. In addition, the sampled air mass had a relatively more marine origin (Figure 2.7). This is reflected in a higher Cl concentration, while the concentrations of all other elements are much lower than in sample 1 and 2.

The fourth sample was collected again under more continental influence and at lower wind speeds, resulting in higher concentrations for anthropogenic elements and a lower Cl concentration compared to the previous sample. Although there is only an interval of 12 hours between

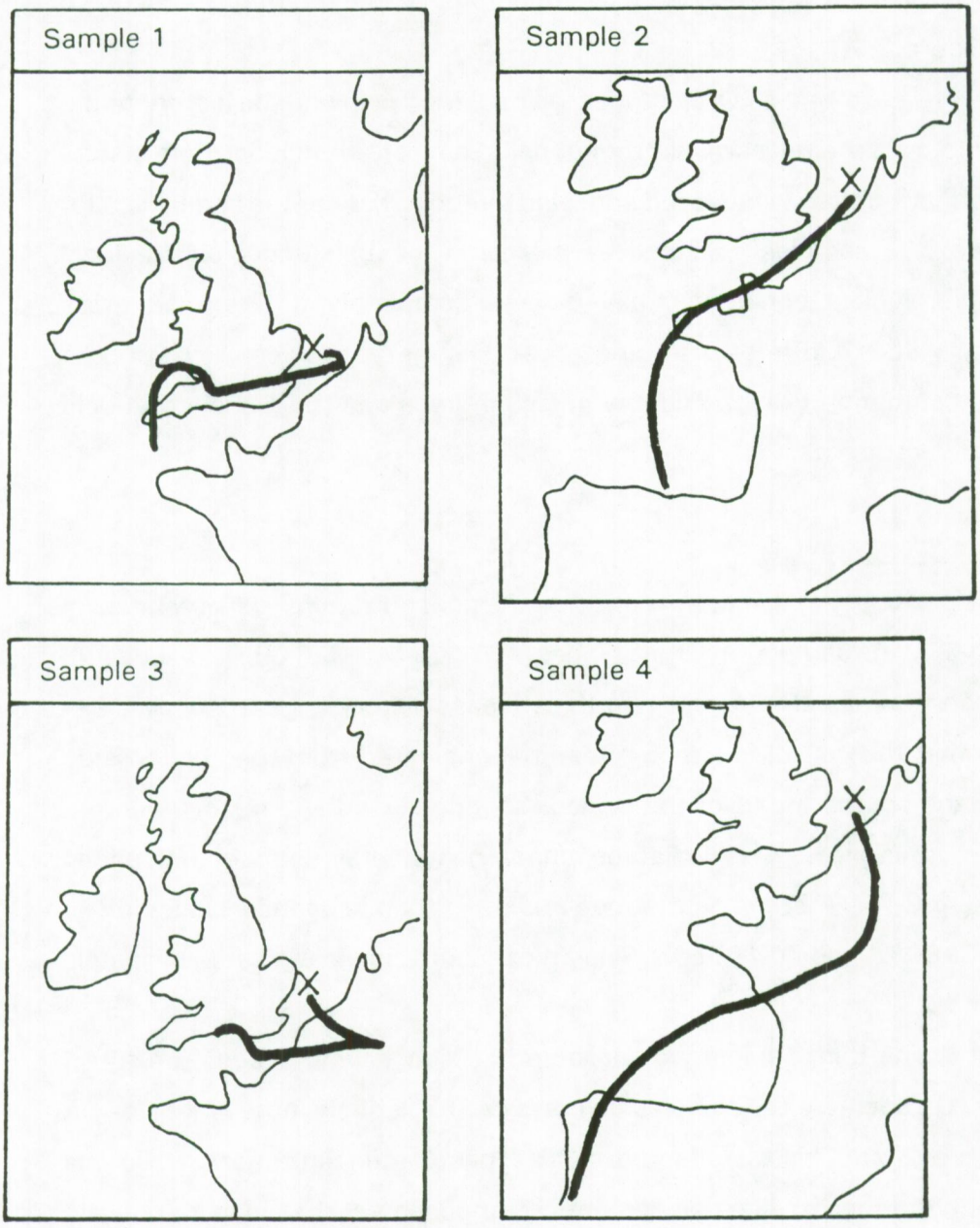

Figure 2.7: 96 h backward air mass trajectories for samples of campaign 1, December 1984 (sample location indicated by an x).

Table 2.4:
XRF results in ng.m^{-3} - Campaign 1, December 1984

Sample / Element	1	2	3	4
S	4600	1650	600	1510
Cl	800	620	1350	<600
K	310	310	190	270
Ca	250	450	120	140
V	70	32	18	30
Fe	470	720	300	740
Ni	15	7.0	<0.5	<0.5
Cu	33	8.0	<0.4	<0.4
Zn	180	180	32	80
Pb	210	150	40	140

the third and the fourth sample, concentrations differ significantly; the Pb concentration goes up by a factor of 3.5 from 40 to 140 ng.m^{-3}. Rapid changes in the meteorological situation are reflected without delay in the atmospheric concentrations of trace elements.

2.4.2 Campaign 2: April 20 - May 10, 1985

2.4.2.1 General sampling data and meteorological information

Between April 20 and May 10, 1985, a three week sampling campaign was organized with the R/V Belgica. During the first part of the campaign, between Zeebrugge (Belgium) and Bergen (Norway), 8 aerosol samples were collected on a 0.4 μm pore size Nuclepore filter. During the second part of the campaign, between Bergen and Zeebrugge, another 7 samples were collected, this time by using a stacked filter unit consisting of a 8.0 μm pore size Nuclepore filter, followed by a 0.4 μm one.

Table 2.5 summarizes the available meteorological information for campaign. Figure 2.8 shows the track followed by the R/V Belgica.

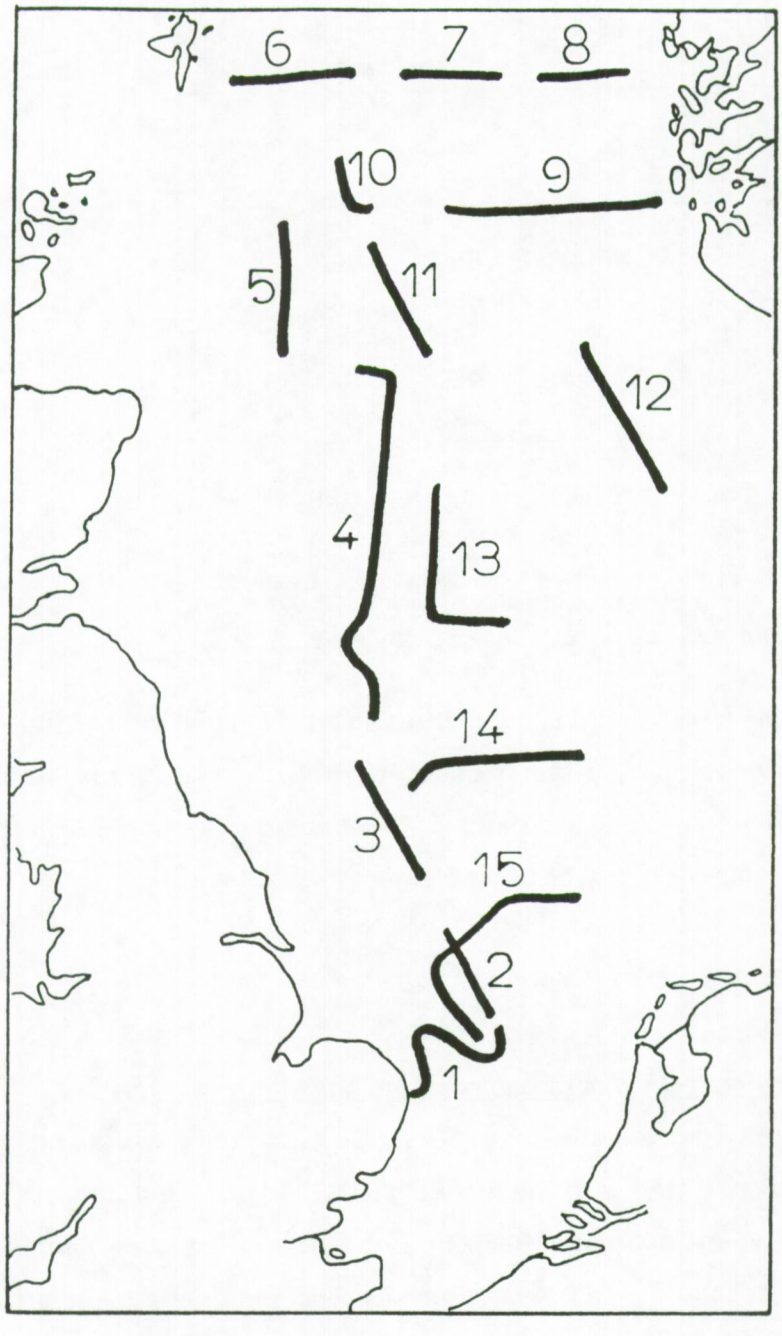

Figure 2.8: Track of campaign 2 - April, 1985 (the numbers refer to the sample numbers).

Table 2.5:
Meteorological information - Campaign 2, April 1985

Sample	Wind direction (sector)	Wind speed ($m.s^{-1}$, range)	Air mass history
1	NW - NE	1-9	UK, northern Atlantic
2	NE - N	2-9	northern Atlantic, North Sea
3	NE - NW	8-10	Norway, northern Atlantic
4	NW	4-11	Norway, northern Atlantic
5	NW	11-18	northern Atlantic
6	W	2-9	northwestern Atlantic
7	NE	15-22	northwestern Atlantic
8	NE	4-15	Norway, northern Atlantic
9	NE - N	6-11	Norway
10	N - W	2-11	Norway
11	VARIABLE	4-6	Norway, North Sea
12	SE - E	10-13	North Sea
13	S - NE	4-6	North Sea, FRG, Denmark
14	N - NE	5-8	FRG, Poland, Baltic Sea
15	NW	5-8	UK, North Sea

2.4.2.2 XRF results

Table 2.6 lists the XRF results for samples 1 to 8 of campaign 2. Sample 1 shows an extremely high Cu concentration (420 $ng.m^{-3}$), probably due to contamination, although it is not clear what could be the source for this contamination. Sample 5 has high concentrations for all elements, although the meteorological information suggests that this sample should be comparable to sample 4 and sample 6. The most likely explanation is that sample 5 was contaminated by sea spray droplets from breaking waves at the bow of the ship. This is illustrated by the extremely high Cl concentration (99600 $ng.m^{-3}$).

Table 2.6:
XRF results in ng.m^{-3} - Campaign 2, April 1985
First part of campaign 2: single filter used for particle collection

Sample / Element	1	2	3	4	5	6	7	8
P	<70	89	<70	120	<70	89	<70	<70
S	2400	900	650	500	14100	620	630	100
Cl	20700	2490	5050	3140	99600	2600	3040	910
K	560	110	140	80	4100	100	110	24
Ca	440	120	130	99	3100	82	94	31
Mn	<0.9	2.0	1	1	<0.9	<0.9	<0.9	<0.9
Fe	30	19	12	23	17	<0.4	10	2.0
Ni	3.0	<0.5	1.0	1.0	<0.5	<0.5	1	<0.5
Cu	420	1	2	1	14	1	1	0.5
Zn	12	3	5.0	3.0	35	5.0	<0.4	2.0
Pb	14	<8	<8	<8	<8	<8	<8	<8

Generally speaking, concentrations go down rapidly after the first sample and then remain low. S and Ca concentrations are plotted as a function of time in Figure 2.9 .

The air mass history indicates that the first sample was collected under partial influence of emissions from the UK, while sample 2 to 8 were collected under predominantly northern wind with very little continental influence.

Table 2.7 lists the XRF results for the second part of campaign 2, for the coarse particle fraction. The highest wind speed, measured during collection of sample 12, is demonstrated in a Cl concentration of 17200 ng.m^{-3}. For samples 9 to 11, the wind direction was mainly north and sampled air masses had very little continental influence, resulting in low concentrations for all elements except Cl. As the wind direction turned more to the east and the sampled air mass passed over Germany,

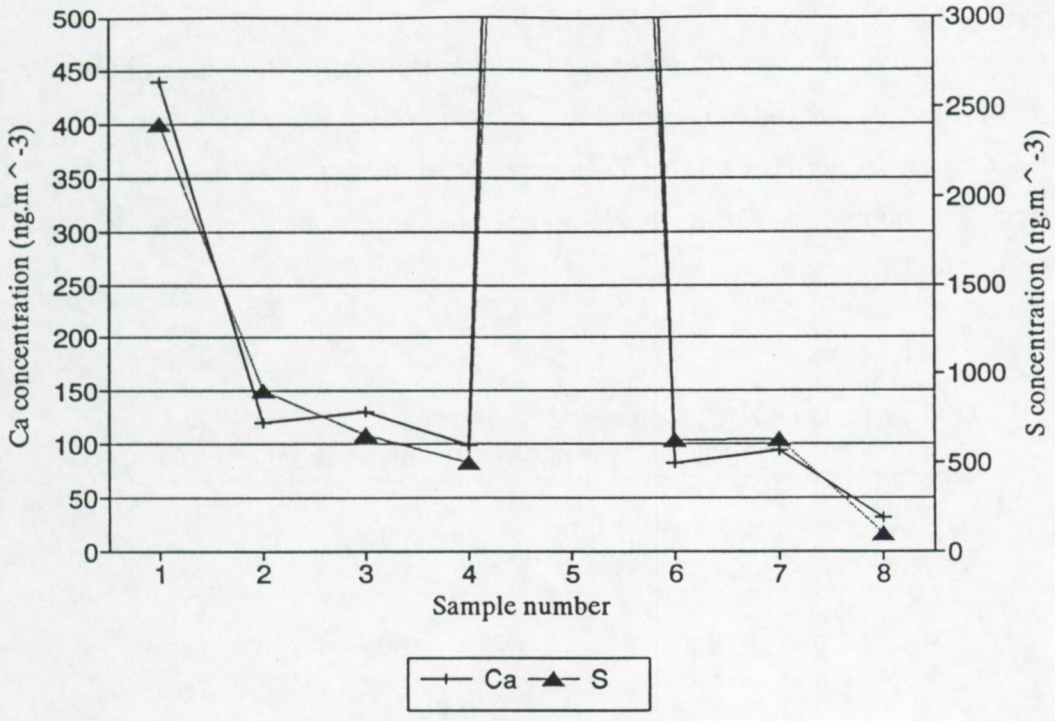

Figure 2.9: Ca and S concentrations during the first part of campaign 2.

Table 2.7:
XRF results in ng.m^{-3} - Campaign 2, April 1985
Second part of campaign 2: Coarse particle fraction (> 2 μm)

Sample / Element	9	10	11	12	13	14	15
S	740	180	120	1300	365	640	860
Cl	6200	1370	665	17200	3020	2500	4000
K	170	40	26	300	110	200	250
Ca	230	31	26	380	93	370	450
Ti	<2.5	<2.5	7	<2.5	<2.5	25	<2.5
Fe	24	5	15	19	35	145	110
Cu	2	1	<0.4	<0.4	<0.4	<0.4	<0.4
Zn	6	<0.4	<0.4	3	3	10	13
Pb	13	<8	<8	10	10	9	16

concentrations start to increase. In the fine fraction results (Table 2.8) this is even more clearly the case. Pb concentrations in the fine fraction go up from below the detection limit (< 8 $ng.m^{-3}$) in samples 9 to 11 to 9-27 $ng.m^{-3}$ in samples 12 to 15. Zn concentrations increase respectively from 1-4 $ng.m^{-3}$ to 10-19 $ng.m^{-3}$ and S concentrations from 460-940 $ng.m^{-3}$ to 1580-2550 $ng.m^{-3}$.

Table 2.8:
XRF results in $ng.m^{-3}$ - Campaign 2, April 1985
Second part of campaign 2: Fine particle fraction (< 2 μm)

Sample / Element	9	10	11	12	13	14	15
S	940	660	460	1580	2550	640	1660
Cl	<600	<600	<600	<600	<600	2500	<600
K	34	21	8	38	85	200	81
Ca	28	12	10	23	23	370	29
Ti	<2.5	<2.5	<2.5	<2.5	<2.5	25	<2.5
V	<2.0	<2.0	<2.0	10	5	<2.0	11
Mn	<0.9	3	<0.9	2	3	<0.9	7
Fe	11	4	4	26	30	145	28
Ni	1	1	1	2	2	<0.5	6
Cu	4	1	<0.4	2	2	<0.4	4
Zn	4	2	1	14	19	10	19
Pb	<8	<8	<8	19	18	9	27

2.4.3 Campaign 3: August 21 - August 31, 1985

2.4.3.1 General sampling data and meteorological information

The track followed during campaign 3 is shown in Fig 2.10. Three filter samples were collected on the way north from Zeebrugge (Belgium) to Hull (UK), while three others were collected on the way back to Zeebrugge. Wind speed and wind direction data are listed in Table 2.9.

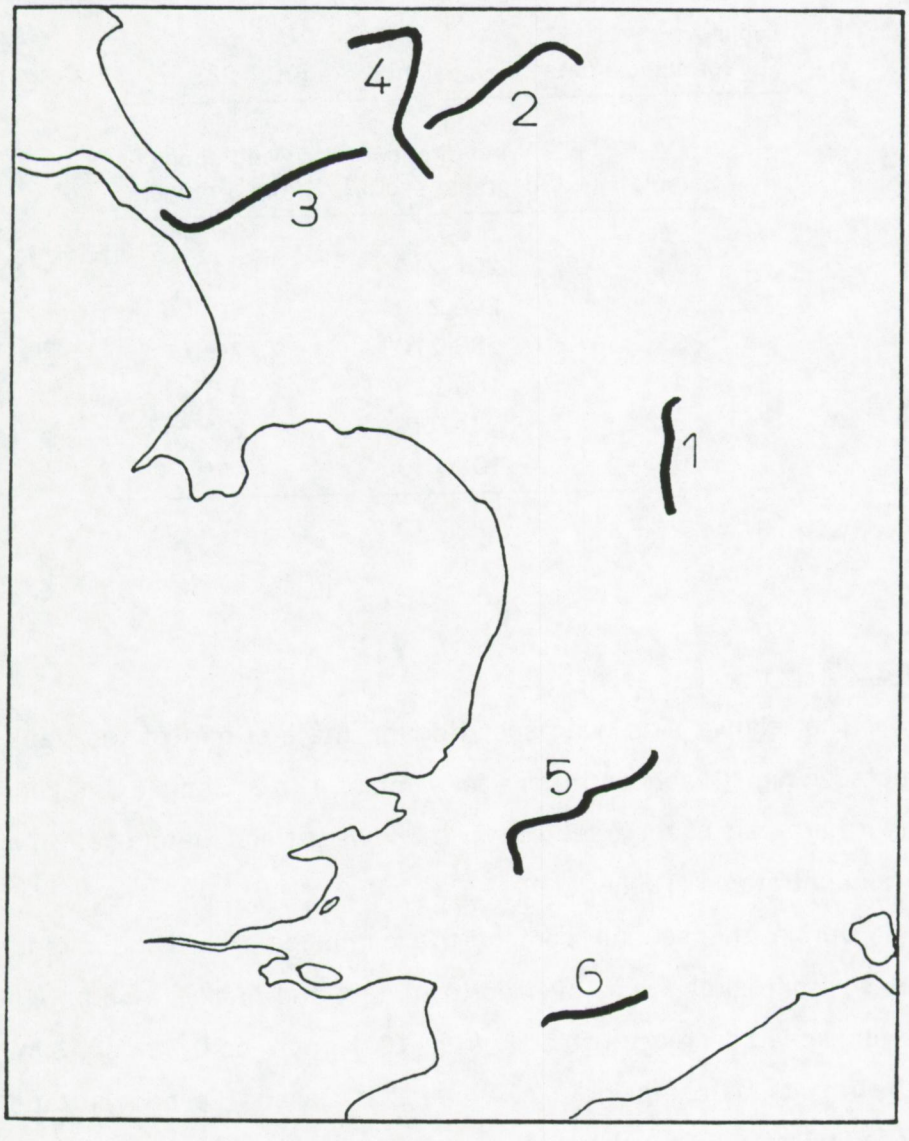

Figure 2.10: Track of campaign 3, August 1985 (the numbers refer to the sample numbers).

Table 2.9:
Meteorological data - Campaign 3, August 1985

Sample	Wind direction (degrees, sector)	Wind speed ($m.s^{-1}$, range)
1	200-210	7-10
2	200-210	4-6
3	200-210	7-9
4	180-220	3-6
5	35-100	2-4
6	100-150	5-10

2.4.3.2 XRF results

The relative high wind speed during the first part of the track is reflected in high Cl concentrations for samples 1 to 3. Sample 3, taken at the northern part of the track shows the lowest trace metal (Cu, Zn and Pb) concentrations (Table 2.10).

During the second part of the campaign, the wind direction changed from south-west, over north to east and finally to south while the wind speed decreased steadily from 10-15 $m.s^{-1}$ to 0-5 $m.s^{-1}$. Similar to the results of campaign 1, we see that Ca and Fe concentrations increase relatively more than other trace metal concentrations, when the wind turns to the south.

Table 2.10:
XRF results in ng.m^{-3} - Campaign 3, Agust 1985

Sample / Element	1	2	3	4	5	6
Si	<140	260	<140	680	190	870
P	120	<70	<70	<70	<70	<70
S	1630	870	640	2740	4510	4960
Cl	6060	3960	5070	910	730	730
K	420	230	340	840	420	700
Ca	360	360	210	170	170	700
Ti	<2.5	26	<2.5	23	<2.5	<2.5
V	<2.0	<2.0	<2.0	29	74	20
Cr	31	6.0	55	11	97	46
Mn	<0.9	<0.9	<0.9	22	15	68
Fe	130	180	110	320	610	840
Ni	4.0	5.0	8.0	14	30	11
Cu	6.1	3.9	<0.4	6.8	5.0	8.5
Zn	53	34	23	86	4.2	86
Pb	34	31	<8	53	18	69

2.4.4 Campaign 4: March 11 - March 14, 1986

2.4.4.1 General sampling data and meteorological information

Fig 2.11 shows the track followed by the R/V Belgica during campaign 4 between March 11 and March 14, 1986. The first 6 samples were collected with east wind. During sample 7 and 8, the wind direction slightly changed to south-east. The wind speed never exceeded 7 m.s^{-1} and was most of the time lower than 5 m.s^{-1}.

2.4.4.2 XRF results

Table 2.11 shows the XRF results for the eight samples collected during campaign 4. Cl was not detected in a single sample. At very low wind speeds, the sea produces little sea spray droplets. In addition, high acid pollution concentrations will react with the few NaCl aerosols in the marine atmosphere, resulting in a release of HCl.

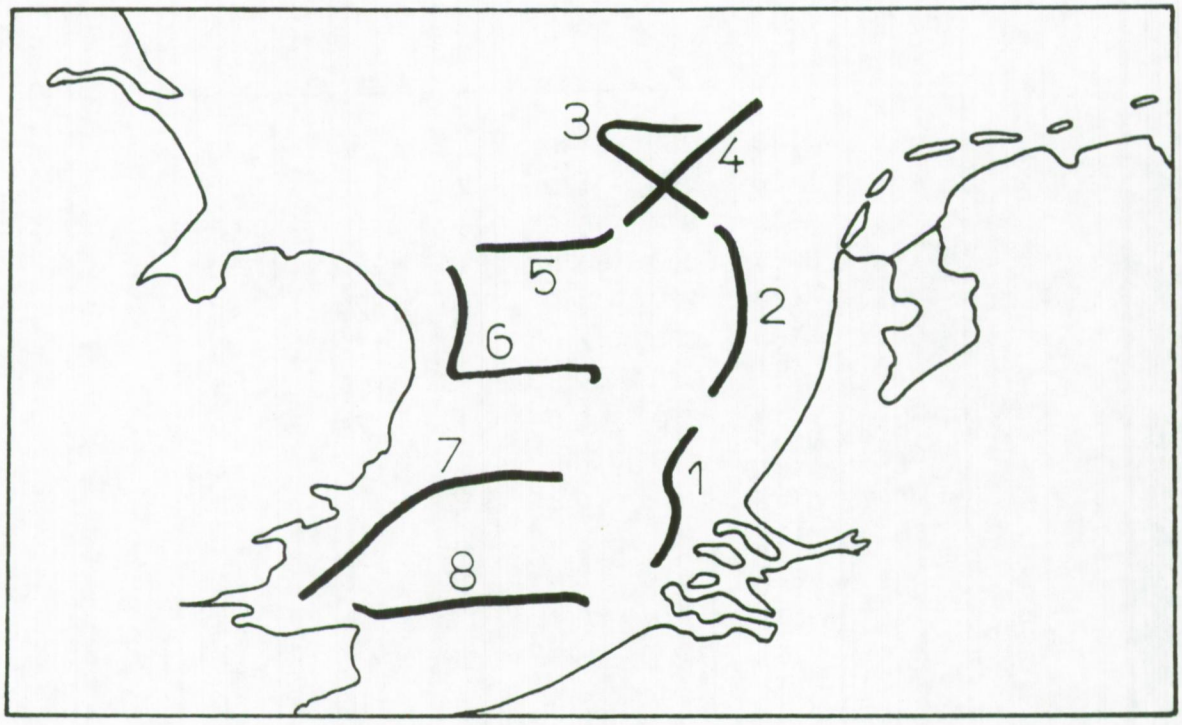

Figure 11: Track of campaign 4, March 1986 (the numbers refer to the sample number).

All anthropogenic elemental concentrations measured during this campaign are very high. Pb concentrations vary from 46 to 280 $ng.m^{-3}$, Zn concentrations from 110 to 790 $ng.m^{-3}$ and S concentrations from 6400 to 15200 $ng.m^{-3}$. It is well known that, during the meteorological conditions present during this campaign, pollutant concentrations tend to rise rapidly. A combination of a low temperature inversion and low wind speeds limit natural dispersion of pollutants. Furthermore, the absence of any form of precipitation restricts the possibilities of concentration decrease through wet deposition processes. At the end of campaign 4, the wind direction gradually shifted from east to south-east, resulting in the highest concentrations for all elements. (Table 2.11 and Figure 2.12)

Table 2.11:
XRF results in ng.m^{-3} - Campaign 4, March 1986

Sample Element	1	2	3	4	5	6	7	8
Si	840	1130	1120	940	1200	1860	2490	4820
P	290	420	370	380	380	600	690	690
S	6360	9600	8250	8790	8740	12900	14500	15200
K	300	340	330	420	400	560	740	1560
Ca	180	150	250	160	240	520	980	1970
Ti	11	20	31	15	26	69	100	180
V	14	18	13	11	17	33	42	46
Cr	2.3	4.2	7.5	21	7.4	8.3	14	27
Mn	17	17	19	23	21	33	46	180
Fe	370	360	410	400	530	980	1170	2760
Ni	7.6	7.8	5.6	7.3	7.3	15	21	24
Cu	11	10	15	16	14	22	21	39
Zn	140	150	110	200	150	200	220	790
Pb	120	76	46	84	73	140	170	280

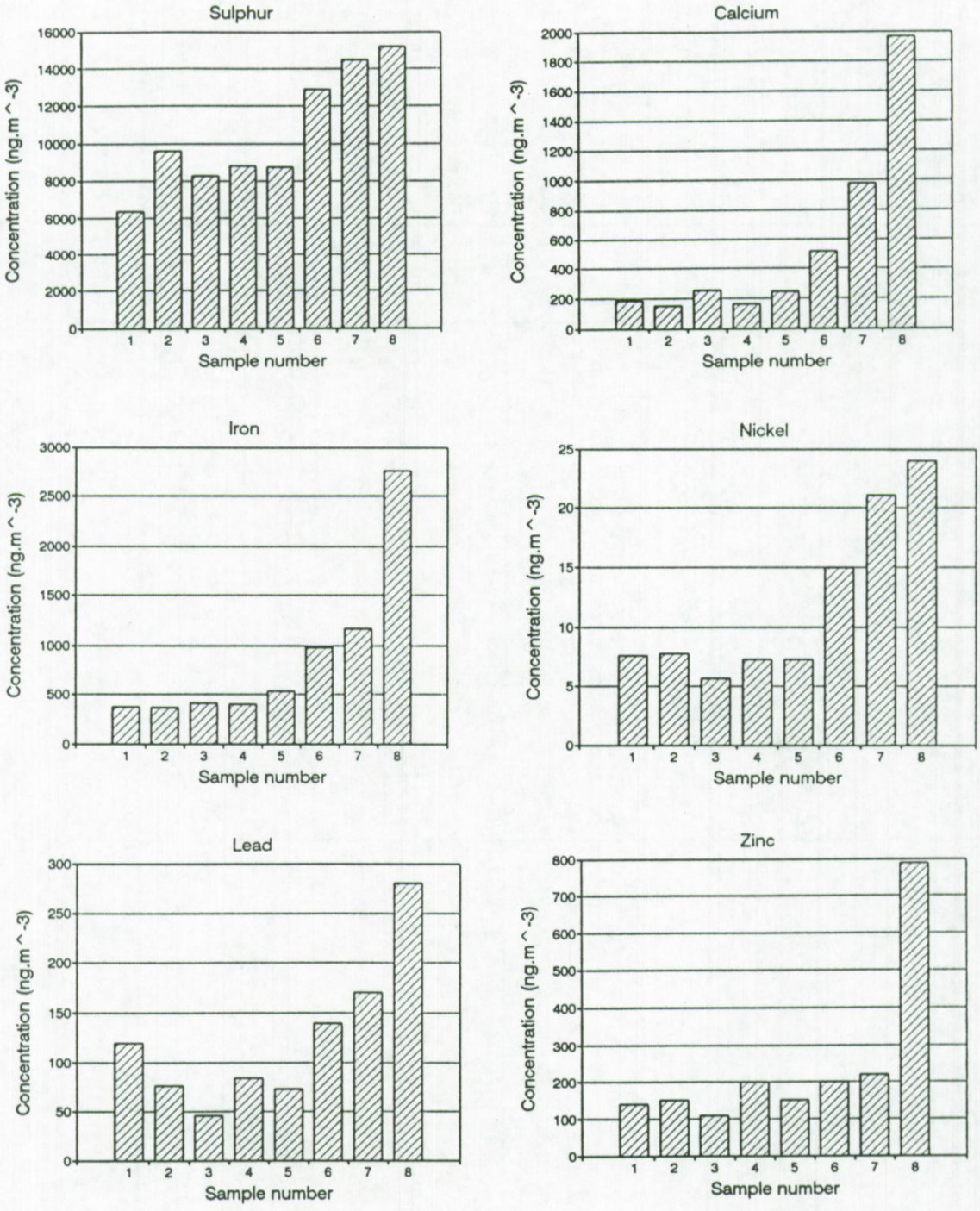

Figure 12: Atmospheric concentrations during campaign 4, March 1986.

2.4.5 Campaign 5: May 12 - May 17, 1986

2.4.5.1 General sampling data and meteorological information

Campaign 5 was performed in the English Channel, between Zeebrugge (Belgium) and the border of the English Channel and the Atlantic Ocean at 5 °W. The track followed during this sampling campaign is shown in Fig 2.13

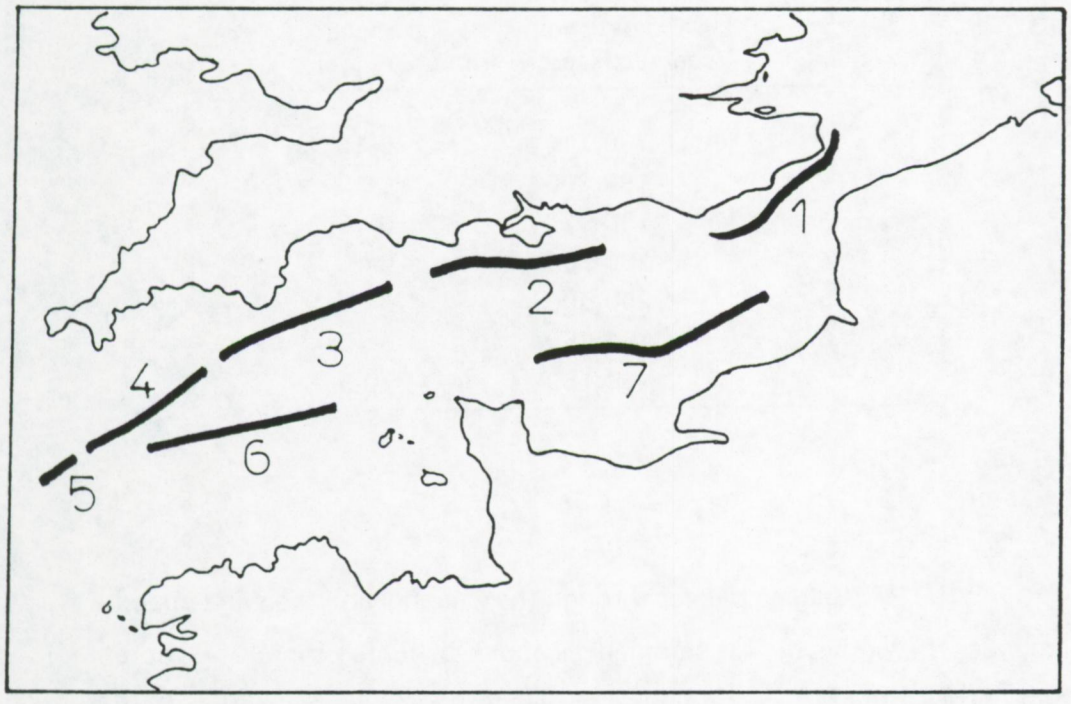

Figure 2.13: Track of campaign 5, May 1986.

During the first half of the sampling campaign, a moderate wind speed of 10 $m.s^{-1}$ increased gradually to 15 $m.s^{-1}$, while the wind direction was south-west to west. During the second half of campaign 5, the wind speed rapidly decreased to below 5 $m.s^{-1}$ and the wind direction changed to east to south-east (Table 2.12).

Table 2.12:
Meteorological data - Campaign 5, May 1986

Sample	Wind direction (degrees, sector)	Wind speed ($m.s^{-1}$, range)
1	200-210	5-10
2	190-200	10-15
3	190-220	10-15
4	280-300	10-15
5	250-300	5-10
6	150-250	5-10
7	60-150	0-5

2.4.5.2 XRF results

As the R/V Belgica passes through the Channel and the wind speed increases, the origin of the sampled air mass becomes more and more marine. This reflected in a steady decrease in the S concentration from sample 1 to 5. While the wind direction changes from south-west to south east and the wind speed decreases at the end of the campaign, concentrations for most elements go up again (Table 2.13). The continental influence and the very low wind speed during sample 7 is illustrated by the low Cl concentration : < 600 $ng.m^{-3}$ versus 3190 $ng.m^{-3}$ in the previous sample.

Table 2.13:
XRF results in $ng.m^{-3}$ - Campaign 5, May 1986

Sample / Element	1	2	3	4	5	6	7
Al	<200	230	<200	230	<200	<200	<200
Si	180	270	150	220	<140	<140	<140
P	140	300	200	260	78	82	<70
S	1360	1530	870	860	410	590	1200
Cl	3270	10400	7190	9990	3560	3190	<600
K	150	280	150	180	69	95	89
Ca	180	230	150	170	80	93	160
Ti	<2.5	<2.5	<2.5	<2.5	<2.5	<2.5	17
V	12	9.2	<2.0	<2.0	2.3	5.9	18
Cr	6.8	7.2	<1.5	<1.5	<1.5	<1.5	<1.5
Mn	1.7	<0.9	<0.9	<0.9	<0.9	<0.9	3.4
Fe	48	4.6	4.1	3.7	7.3	16	105
Ni	4.5	4.5	<0.4	<0.4	<0.4	<0.4	4.8
Cu	<0.4	<0.4	<0.4	<0.4	<0.4	<0.4	2.5
Zn	5.6	1.6	<0.4	<0.4	<0.4	2.3	27
Pb	10	<8	<8	<8	<8	<8	<8

2.4.6 Campaign 6: June 22 - June 26, 1987

2.4.6.1 General sampling data and meteorological information

Between June 22 and June 26, 1987, a second sampling campaign through the English Channel was organized. Seven filter samples were collected between Zeebrugge (Belgium) and the most westerly point of the followed track. The 96 h backward air mass trajectories are shown in Figure 2.14.

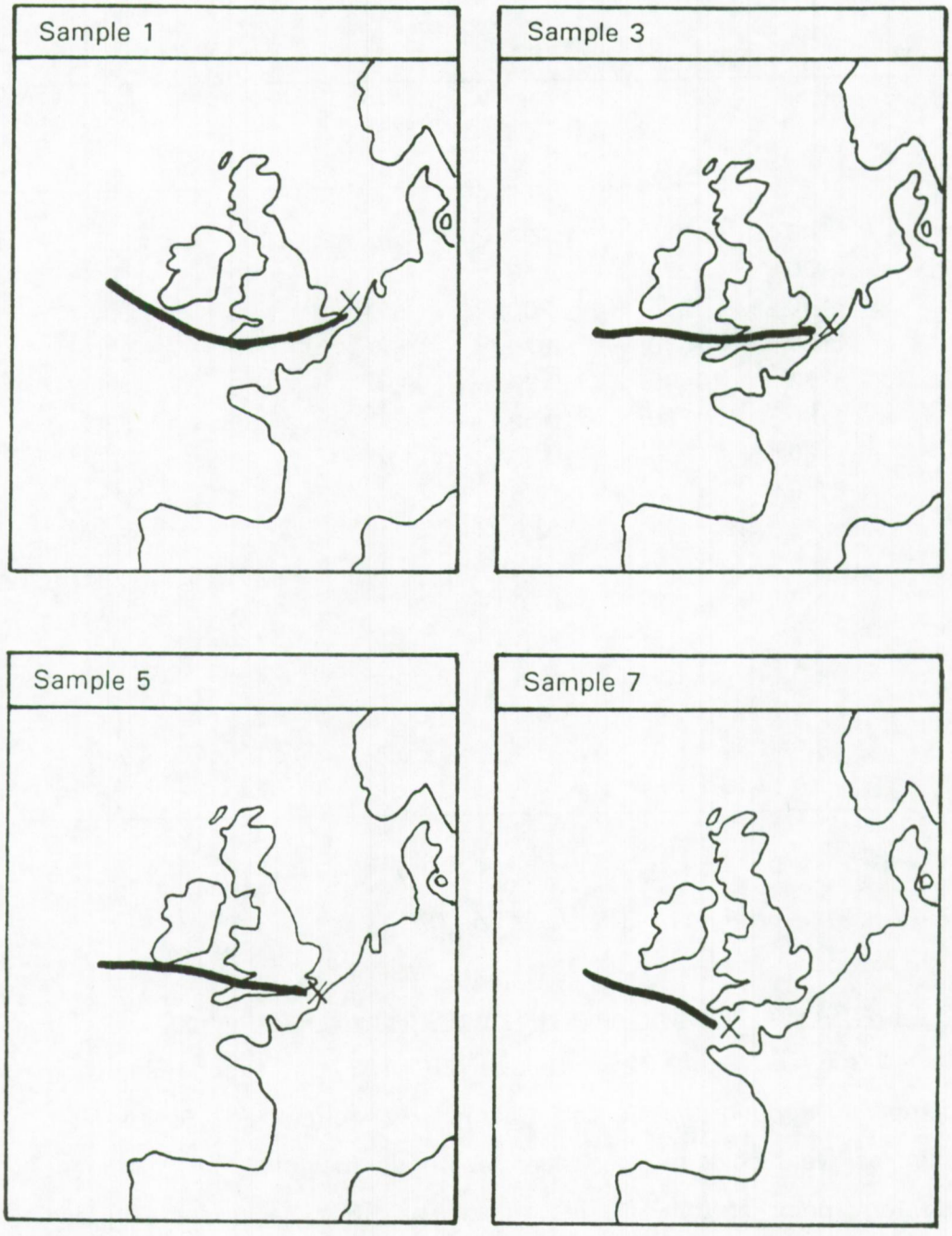

Figure 2.14: 96 h back trajectories for campaign 6, June 1987 (sampling location indicated by an x.

2.4.6.2 XRF Results

Table 2.14 lists the XRF results for sampling campaign 6. Analogue to campaign 5, the concentration of most elements go down steadily, as the Belgica passes through the channel and the origin of the collected air mass is mostly marine.

Table 2.14:
XRF results in $ng.m^{-3}$ - Campaign 6, June 1987

Sample / Element	1	2	3	4	5	6	7
Al	250	<200	<200	<200	<200	<200	<200
Si	510	190	210	170	140	140	300
P	220	79	110	<70	<70	<70	85
S	1890	1310	1080	1010	410	570	1040
Cl	5440	<600	2470	<600	<600	<600	1910
K	480	72	84	49	10	<9	<9
Ca	320	62	86	48	10	6.6	<6
V	7.8	3.4	<2.0	3.3	2.0	<2.0	<2.0
Mn	1.0	<0.9	0.9	<0.9	<0.9	<0.9	<0.9
Fe	28	12	5.9	15	3.1	1.0	1.3
Ni	3.0	0.6	<0.5	1.1	<0.5	<0.5	0.7
Cu	1.0	<0.4	<0.4	0.7	<0.4	0.4	0.5
Zn	6.7	0.4	0.6	<0.4	<0.4	0.5	<0.4
Pb	<8	10	<8	<8	<8	<8	<8

2.4.7 Campaign 7: October 27 - October 29, 1987

2.4.7.1 General sampling data and meteorological information

Figure 2.15 shows the track followed during campaign 7. The 96 h backward air trajectories for the four samples collected are shown in Figure 2.16. A stacked filter unit was used for collection of the airborne particulate material.

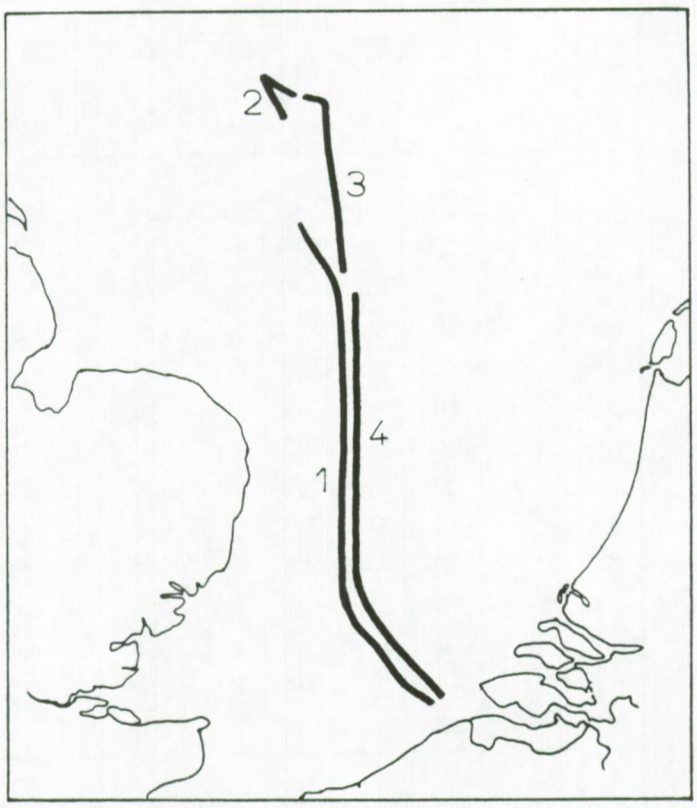

Figure 2.15: Track of campaign 7, October 1987 (the numbers refer to the sample numbers).

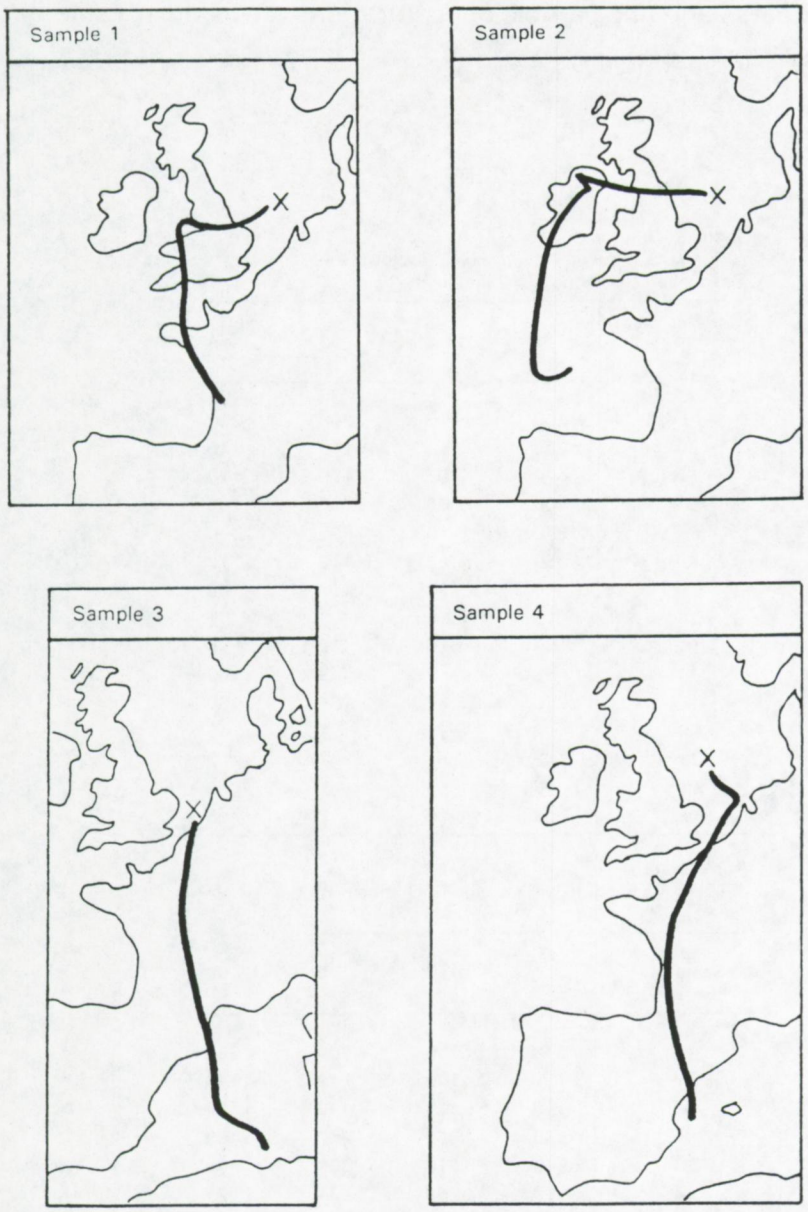

Figure 3.16: 96 h backward trajectories for campaign 7, October 1987 (sampling location indicated with an x).

2.4.7.2 XRF results

The coarse and fine particle concentrations are listed in Table 2.15 and Table 2.16 respectively.

Table 2.15:
XRF results in ng.m^{-3} - Campaign 7, October 1987
Coarse particle fraction (>2 μm)

Sample / Element	1	2	3	4
Al	300	<200	<200	<200
Si	750	150	<140	<140
P	<70	81	120	<70
S	400	400	590	460
Cl	1930	4140	4890	2300
K	150	93	110	77
Ca	46	91	110	68
Ti	20	<2.5	<2.5	<2.5
V	<2.0	<2.0	<2.0	5
Mn	5	<0.9	<0.9	<0.9
Fe	260	57	34	180
Ni	4	1	1	6
Cu	2	1	1	3
Zn	15	3	1	6
Pb	<8	<8	9	<8

Table 2.16:
XRF results in ng.m^{-3} - Campaign 7, October 1987
Fine particle fraction (<2 μm)

Sample / Element	1	2	3	4
Al	240	<200	<200	<200
Si	150	<140	<140	<140
P	190	<70	130	<70
S	1150	660	740	1480
Cl	6540	1610	5300	<600
K	150	59	24	77
Ca	35	18	14	12
V	3	<2.0	<2.0	<2.0
Cr	<1.5	5	<1.5	<1.5
Mn	3	1	<0.9	<0.9
Fe	40	5	7	42
Ni	2	<0.5	1	4
Cu	<0.4	<0.4	1	1
Zn	11	3	3	11
Pb	13	<8	9	9

The air mass collected during samples 1 and 4 has an important influence from emissions in France, while samples 2 and 3 are rather influenced by emissions in the UK. In the coarse particle fraction this is illustrated by higher Fe concentrations in samples 1 and 4 compared with samples 2 and 3. On the other hand, Ca concentrations are higher in samples 2 and 3 compared with samples 1 and 4. This is in contradiction with the findings during campaign 1 and campaign 3, where both Ca and Fe concentrations are higher when the origin of the collected air mass is to the south rather than to the west.

In the fine particle fraction (Table 2.16), K, S, Ni and Zn concentrations are higher in samples 1 and 4 than in samples 2 and 3.

2.4.8 Campaign 8 : November 6 - November 17, 1987

2.4.8.1 General sampling data and meteorological information

The track followed during campaign 8 is shown in Figure 2.17. The corresponding 96 h backward trajectories are shown in Figure 2.18 for samples 1 to 5. For samples 6 to 8, no back trajectories are available. Samples 7 and 8 were collected when the wind direction changed to the south west and the wind speed rapidly increased up to 10-11 Bft. For safety reasons, sampling was discontinued afterwards.

2.4.8.2 XRF results

Table 2.17 shows the coarse particle fraction results for sample 1 to 8. Cl concentrations go down until sample 6, then a sudden increase due to a violent change in wind direction and wind speed results in a Cl concentration of 5000-6000 $ng.m^{-3}$. Fe, Zn and Pb concentrations decrease abruptly at sample 7.

Table 2.18 lists the fine particle fraction results for campaign 8. S, K, Fe, V, Zn and Pb all show the same profile: an abrupt decrease as the meteorological situation changes rapidly.

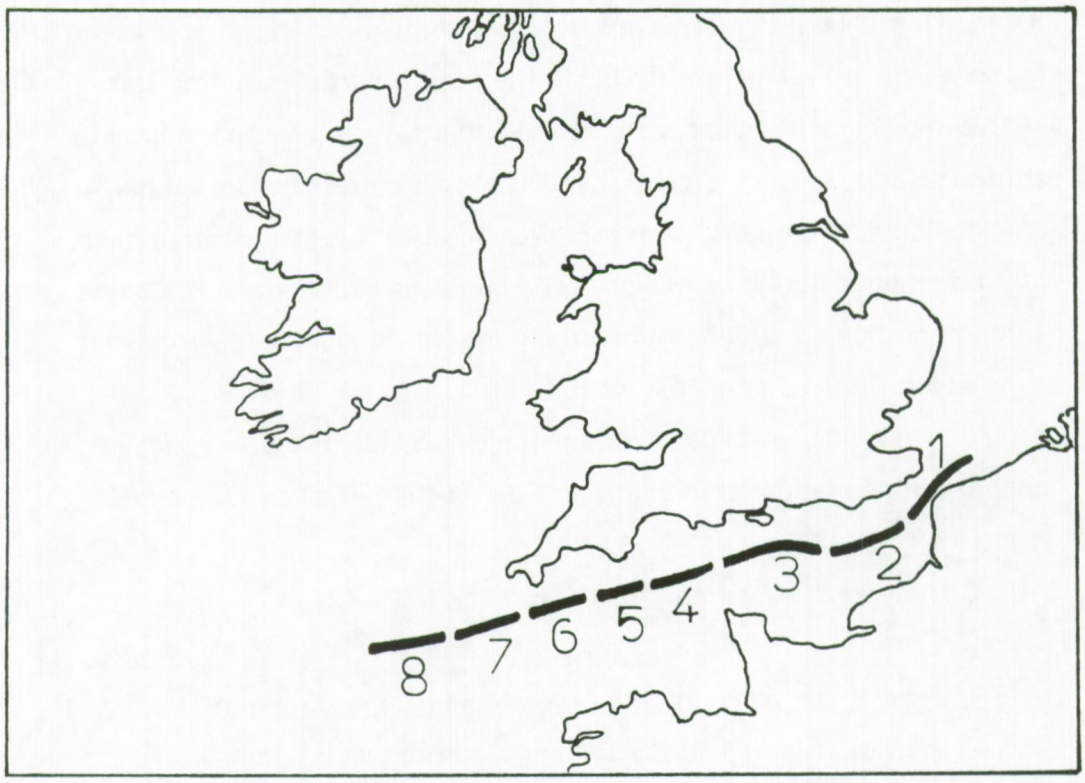

Figure 2.17: Track of campaign 8, November 1987 (the numbers refer to the sample number).

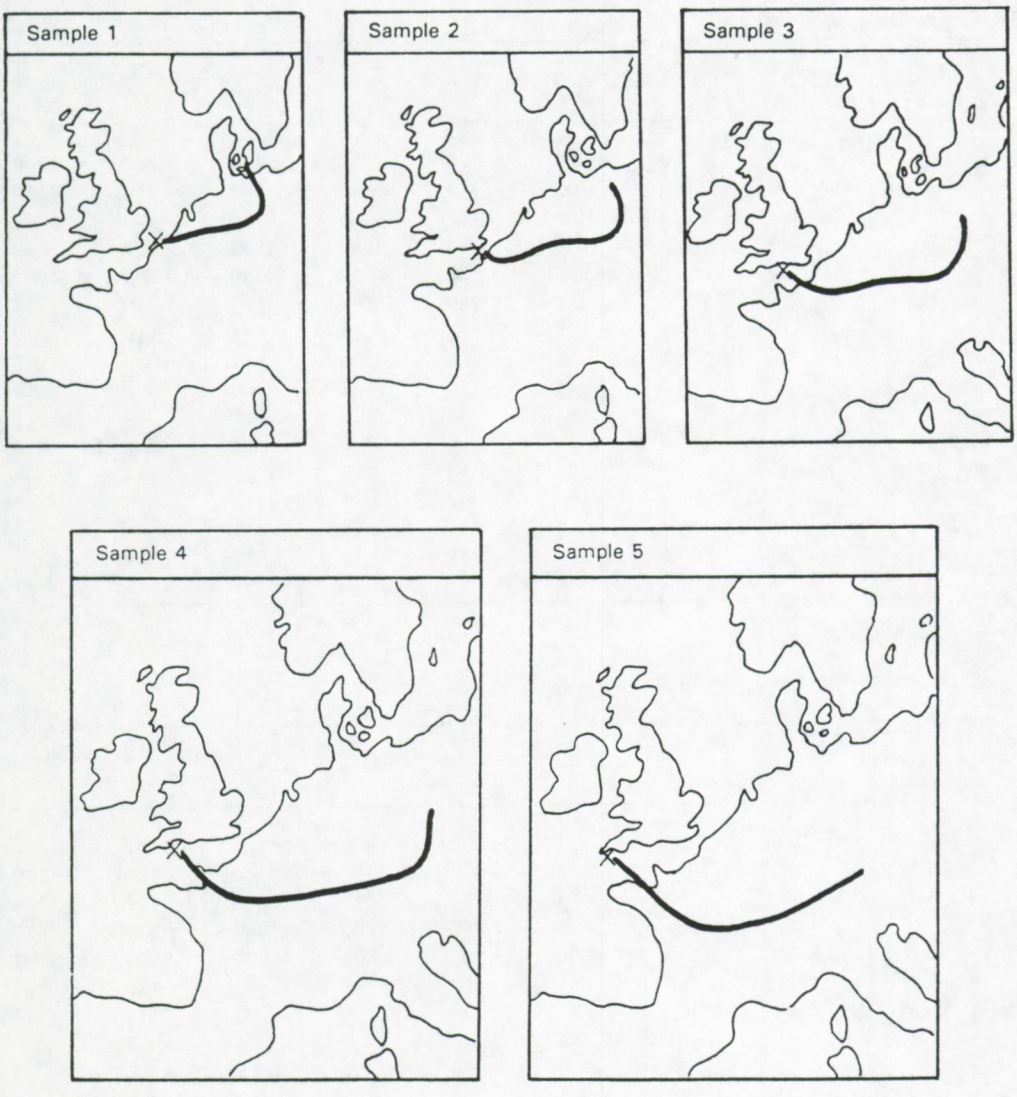

Figure 2.18: 96 h backward air mass trajectories for campaign 8, November 1987 (sampling location indicated with an x).

Table 2.18:
XRF results in $ng.m^{-3}$ - Campaign 8, November 1987
Fine particle fraction (< 2 μm)

Sample / Element	1	2	3	4	5	6	7	8
Al	210	<200	<200	<200	200	<200	<200	<200
Si	160	180	160	<140	<140	<140	<140	<140
P	220	200	130	190	180	170	<70	<70
S	3930	3470	2660	3780	3680	3200	92	<80
Cl	610	<600	<600	<600	<600	<600	<600	<600
K	200	320	190	240	140	110	10	<9
Ca	15	33	<6	7	<6	7	<6	<6
Ti	7	3	<2.5	3	<2.5	4	<2.5	5
V	20	16	10	10	8	6	2	6
Cr	6	3	2	2	<1.5	<1.5	4	6
Mn	13	18	10	6	5	4	<0.9	<0.9
Fe	197	159	25	18	9	5	<0.4	<0.4
Ni	3	5	2	2	1	1	<0.5	<0.5
Cu	3	8	3	1	<0.4	<0.4	<0.4	<0.4
Zn	68	107	43	32	23	20	<0.4	<0.4
Pb	66	135	58	52	31	31	<8	<8

Table 2.17:
XRF results in $ng.m^{-3}$ - Campaign 8, November 1987
Coarse particle fraction (> 2 μm)

Sample / Element	1	2	3	4	5	6	7	8
Al	310	230	<200	<200	<200	<200	<200	<200
Si	520	510	150	220	190	140	<140	<140
P	130	100	<70	<70	<70	<70	120	130
S	1720	1300	550	880	760	1060	510	670
Cl	1450	710	<600	<600	<600	<600	5080	5900
K	110	160	51	100	79	62	110	300
Ca	280	400	90	120	110	71	110	260
Ti	48	21	4	6	<2.5	4	<2.5	<2.5
V	2	3	<2.0	<2.0	<2.0	<2.0	<2.0	<2.0
Mn	11	71	2	2	3	2	<0.9	<0.9
Fe	490	290	67	96	73	57	4	3
Ni	3	2	2	<0.5	1	1	1	2
Cu	3	4	1	1	1	1	<0.4	1
Zn	51	48	17	20	16	18	2	3
Pb	24	32	9	17	<8	15	13	<8

2.4.9 Campaign 9, March 1988

2.4.9.1 General sampling data and meteorological information

6 samples were collected when crossing the Southern Bight of the North Sea, between Zeebrugge and London. The wind direction was stable during the sampling period and remained between 280° and 320°. Samples 5 and 6 were collected during entrance of the Thems estuary in the direction of London.

2.4.9.2 XRF results

Table 2.19:
XRF results in $ng.m^{-3}$ - Campaign 9, March 1988

Sample / Element	1	2	3	4	5	6
Si	<140	<140	<140	<140	250	550
S	900	1970	1480	1070	4830	7940
Cl	4520	6200	9840	6440	<600	970
K	280	270	640	230	330	530
Ca	330	290	1090	290	210	820
Ti	20	<2.5	20	13	17	48
V	20	11	12	<2.0	10	17
Cr	15	40	26	17	19	48
Mn	170	<0.9	7.9	<0.9	14	20
Fe	87	68	110	41	280	550
Ni	10	4.7	6.0	1.5	4.9	8.2
Cu	8.2	8.1	15	3.2	7.1	15
Zn	74	13	64	10	72	140
Pb	19	13	18	<8	65	120

Table 2.19 shows the XRF results for campaign 9. The very high Mn concentration in sample 1 is probably due to an unknown source of contamination. Samples 1 to 4 have comparable concentrations for most elements. The 10-fold increase in Fe and Zn concentrations is clearly associated with emissions from the London area and the industry in northern England. Cu and Ni concentrations go up by a factor of 5.

2.4.10 Campaign 10, June 1988

2.4.10.1 General sampling data and meteorological information

Figure 2.19 shows the track followed during campaign 10 in June 1988. All samples were collected under similar meteorological conditions. The wind direction stayed within the northern sector, between 320 and 30 degrees.

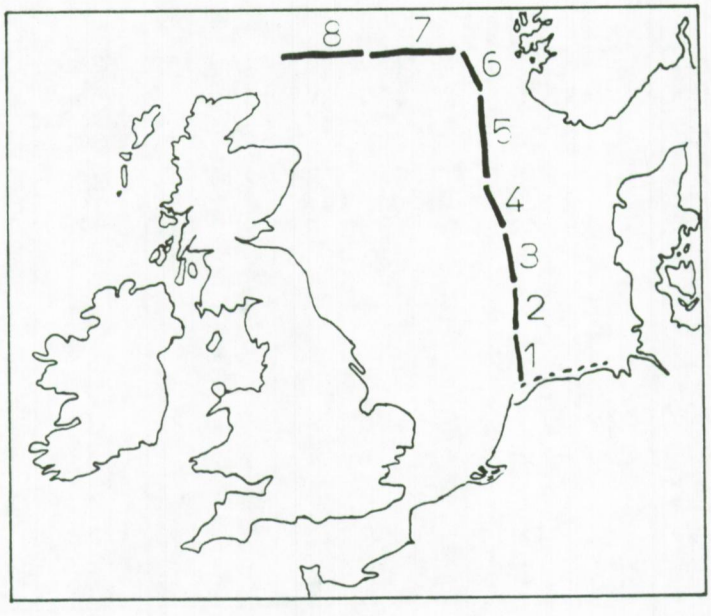

Figure 2.19: Track of campaign 10, June 1988 (the numbers refer to the sample numbers).

2.4.10.2 XRF results

Table 2.20 lists the XRF results of campaign 10. All concentrations in all eight samples are quite low. Not much variation is found as a function of time, which is in agreement with the constant wind direction and thus the fairly constant air mass history.

Table 2.20:
XRF results in ng.m^{-3} - Campaign 10, June 1988

Sample / Element	1	2	3	4	5	6	7	8
S	290	220	230	220	130	340	140	300
Cl	1030	670	950	<600	<600	2400	<600	<600
K	49	35	88	17	16	100	34	17
Ca	60	52	28	25	49	110	20	<6
Ti	23	<2.5	7.0	15	20	13	9.2	11
V	12	6.1	5.0	<2.0	6.1	<2.0	<2.0	7.7
Cr	30	18	12	19	21	16	12	22
Fe	43	38	16	51	35	23	22	28
Ni	3.2	2.0	1.5	<0.5	3.5	<0.5	3.1	2.7
Cu	6.8	3.8	3.1	3.8	4.7	3.6	4.4	4.9
Zn	7.5	3.5	2.9	3.7	1.9	2.3	3.3	4.2

2.4.11 Averages

Statistical data on the complete data set of aerosol samples are listed in Table 2.21: average, median, first quartile and fourth quartile concentration. The averages listed in Table 2.21 were calculated by leaving out two (probably) contaminated samples of campaign 2 (April

1985). Furthermore, values that were below the detection limit are replaced by half the detection limit in order to calculate the average. For samples that were collected with a stacked filter unit, the total concentrations is calculated as the sum of the concentration of the two filters. The numbers listed in Table 2.21 can be considered as average concentrations for the total North Sea, including the English Channel.

Table 2.22 lists the average concentration for the total North Sea, the Southern Bight of the North Sea (defined as the area of the North Sea below the 54°N latitude), and the northern part of the North Sea. 35 samples were collected between 51° N and 54° N. These are considered to be representative for the atmosphere above the Southern Bight of the North Sea.

It is obvious from Table 2.22 that concentrations in the northern part of the North Sea are much lower than in the Southern Bight. Mn, Zn, Pb and Fe all show concentrations that are more than 10 times higher in the southern part of the North Sea compared to the northern part. Si, S, Ti and Cu concentrations are 4 to 6 times higher in the south. K, Ca, V and Ni have very similar 'southern part to northern part' concentration ratios: 3.6 to 3.9. Al, P and Cr show the least difference between northern part concentrations and southern part ones. This is merely a result of the large number of observations that were below the detection limit of the analytical technique used. Average Cl concentrations are within 5% identical.

Table 2.21:
Average, median, first and fourth quartile concentrations in $ng.m^{-3}$

Element	Average	Median	First quartile - Fourth quartile
Al	139	<200	<200-<200
Si	399	<140	<140-270
P	174	<70	<70-200
S	2750	1400	630-3900
Cl	2890	1400	<600-4500
K	254	200	88-340
Ca	239	150	78-320
Ti	14.0	0.7	<2.5-17
V	12.4	5.9	<2.0-17
Cr	12.1	2.6	<1.5-15
Mn	13.6	<0.9	<0.9-10
Fe	229	48	16-320
Ni	4.7	2.7	0.7-7.0
Cu	5.5	3.1	0.6-8.0
Zn	54.9	12	2.7-74
Pb	40.6	13	<8-53

Table 2.22
Average atmospheric concentrations in $ng.m^{-3}$

Element	Average	Southern Bight	Northern North Sea
Al	139	193	112
Si	399	725	119
P	174	249	96.8
S	2750	4780	778
Cl	2890	2960	2830
K	254	401	110
Ca	239	382	100
Ti	14.0	24.9	4.6
V	12.4	18.8	4.9
Cr	12.1	14.2	10.1
Mn	13.6	28.5	0.8
Fe	229	432	31.3
Ni	4.7	7.5	2.0
Cu	5.5	9.2	1.9
Zn	54.9	107	4.7
Pb	40.6	77	5.0

2.4.12 Factor analysis

2.4.12.1 Principle

Factor analysis is a multi-variate technique that is used to find the underlying structure in a large data set. The main goal of applying factor analysis is to try to reduce a large number of variables (in our case 16 elemental concentrations) measured in a system (in our case the North Sea atmosphere) to a limited number of independent factors that explain the variation of the observed system.

A number of p correlated variables is transformed to a number of p factors that are linear combinations of the original variables. The total variance is explained completely by p factors. Factors are classified so that the first factor explains the largest percentage of variance. A limited number of factors is selected in order to explain a large fraction of the observed variance. The choice of the number of factors to be retained is somewhat arbitrary and can be based on the eigenvalues of the subsequent factors or on the cumulative percentage of variance that is explained.

The relation between the factors and the original variables is given by the factor loadings matrix. Variables that are highly loaded on one factor can serve to identify that factor. If the variables are atmospheric elemental concentrations, the factors can be associated with specific aerosol sources.

Factor analysis was performed using STATGRAPHICS version 2.6 software that runs on AT-type personal computer.

In a first set of calculations, factor analysis was performed on all samples that were collected with stacked filter units. The calculations were done on the results for the coarse and the fine fraction separatively. In a second experiment, factor analysis was applied to all samples collected in the Southern Bight of the North Sea, because these samples have little missing values for most elements.

2.4.12.2 Factor analysis on coarse fraction and fine fraction samples

19 aerosol samples were collected with a stacked filter unit consisting of a 8.0 μm pore size Nuclepore polycarbonate-membrane filter followed by a 0.4 μm pore size one: samples 9 to 15 from campaign 2, samples 1 to 4 from campaign 7 and samples 1 to 8 from campaign 8. Factor analysis was performed on this limited sample set in order to evaluate any difference in inter-element correlations between the coarse and the fine particle fraction.

Table 2.23 shows the results of factor analysis performed on 19 coarse-fraction aerosol samples. Since in a significant number of samples several elements are not detected, only seven variables were selected: S, Cl, K, Ca, Fe, Zn and Pb.

90.0 % of the total variance can be explained by the first three independent factors. The first factor is heavily loaded with Pb (0.94), S (0.79) and Zn (0.72) and represents sulphate particles that are rich in trace metals. The second factor with K (0.96), Cl (0.83) and Ca (0.77) is associated with sea salt particles. The third factor is heavily loaded with Fe (0.90) and can be associated with soil dust particles or metallurgic sources.

Factor analysis on the fine particle fraction (Table 2.24) yields four factors that explain 91.9% of the observed variance. Factor 1 with S (0.91), K (0.85), Pb (0.76) and Zn (0.75) is again identified with trace metal rich sulphate particles. Factor 2 is loaded with Cu (0.88), Ni (0.86) and Zn (0.62). Factor three with Ca (0.95) and Fe (0.67) is associated with $CaSO_4$ and fly-ash emissions. The fourth factor, with Cl (0.98), is typical for the marine aerosol.

Table 2.23:
Factor analysis results
Coarse particle fraction

Factor	Eigenvalue	% Variance	Cumulative variance
1	3.6	51.7	51.7
2	2.3	32.9	84.5
3	0.4	6.3	90.9
4	0.4	5.6	96.4
5	0.1	1.9	98.4
6	0.1	1.2	99.6
7	0.0	0.4	100.0

Variable	Estimated communality
S	0.871
Cl	0.826
K	0.931
Ca	0.861
Fe	0.952
Zn	0.975
Pb	0.943

Varimax rotated factor loading matrix

Variable / Factor	1	2	3
S	0.79	0.37	0.33
Cl	0.05	0.83	0.38
K	0.05	0.96	0.04
Ca	0.48	0.77	0.21
Fe	0.37	0.03	0.90
Zn	0.72	0.13	0.66
Pb	0.94	0.05	0.22

Table 2.24:
Factor analysis results
Fine particle fraction

Factor	Eigenvalue	% Variance	Cumulative variance
1	4.97	55.2	55.2
2	1.68	18.6	73.8
3	0.85	9.4	83.3
4	0.78	8.7	91.9
5	0.38	4.2	96.1
6	0.23	2.6	98.7
7	0.87	1.0	99.7
8	0.28	0.3	100.0
9	0.02	0.0	100.0

Variable	Estimated communality
S	0.925
Cl	0.997
K	0.933
Ca	0.949
Fe	0.863
Ni	0.790
Cu	0.899
Zn	0.972
Pb	0.946

Varimax rotated factor loading matrix

Variable / Factor	1	2	3	4
S	0.91	0.14	0.17	0.21
Cl	0.10	0.12	0.10	0.98
K	0.85	0.29	0.35	0.10
Ca	0.07	0.17	0.95	0.10
Fe	0.46	0.45	0.67	0.05
Ni	0.20	0.86	0.11	0.06
Cu	0.32	0.88	0.07	0.13
Zn	0.75	0.62	0.11	0.09
Pb	0.76	0.59	0.04	0.09

2.4.12.3 Factor analysis on samples collected on the Southern Bight of the North Sea

35 samples were collected when the R/V Belgica was on the Southern Bight of the North Sea, between 51 and 54 N. Factor analysis was performed on this data set using the following variables: S, Cl, K, Ca, V, Fe, Ni, Cu, Zn and Pb.

Table 2.25 shows that 91.5% of the observed variance can be explained by three factors. Sea salt particles are identified by the third factor with a high loading for Cl (0.92). Factor 2 is heavily loaded with V (0.92) and Ni (0.91), two elements that are typical for oil burning residue. The first factor contains all other elements: Zn (0.91), Ca (0.89), Cu (0.87), K (0.85), Fe (0.84), Pb (0.83) and S (0.69).

It seems that factor analysis applied to our data is only able to reveal a limited number of aerosol particle sources: sea salt particles, oil burning residue and trace metal rich particles. Although there may be a larger number of particle sources and thus different particle types, the emission occurs mainly on land. After dispersion and transport, the continental aerosol will reach the marine atmosphere as a well mixed aerosol. In this way, factor analysis on bulk results cannot reveal the original sources. The fact that emissions from oil burning are often recognized as an independent source above the sea, suggests that this source has a somewhat different behaviour than other pollution sources. This might be explained by the emission of Ni and V through diesel engine exhaust of ships, present on the North Sea.

If one would try to differentiate the various continental aerosol sources, other analysis techniques should be used. Specially single particle techniques such as electron microprobe can offer more information here.

Figure 2.20 shows the Ni-V and the Zn-Pb concentrations as a function of chronological sample collection. It is obvious that both for Ni and V and for Pb and Zn trends can be observed.

Table 2.25:
Factor analysis results
Southern Bight samples

Factor	Eigenvalue	% Variance	Cumulative variance
1	6.86	68.7	68.7
2	1.30	13.0	81.7
3	0.98	9.8	91.5
4	0.29	2.9	94.4
5	0.17	1.7	96.2
6	0.12	1.2	97.3
7	0.11	1.1	98.4
8	0.09	0.9	99.3
9	0.05	0.5	99.8
10	0.02	0.2	100.0

Variable	Estimated communality
S	0.854
Cl	0.899
K	0.889
Ca	0.915
V	0.960
Fe	0.937
Ni	0.973
Cu	0.903
Zn	0.932
Pb	0.890

Varimax rotated factor loading matrix

Variable / Factor	1	2	3
S	0.69	0.26	0.56
Cl	0.08	0.21	0.92
K	0.85	0.41	0.03
Ca	0.89	0.24	0.25
V	0.25	0.92	0.24
Fe	0.84	0.43	0.21
Ni	0.36	0.91	0.15
Cu	0.87	0.26	0.27
Zn	0.91	0.20	0.25
Pb	0.83	0.16	0.41

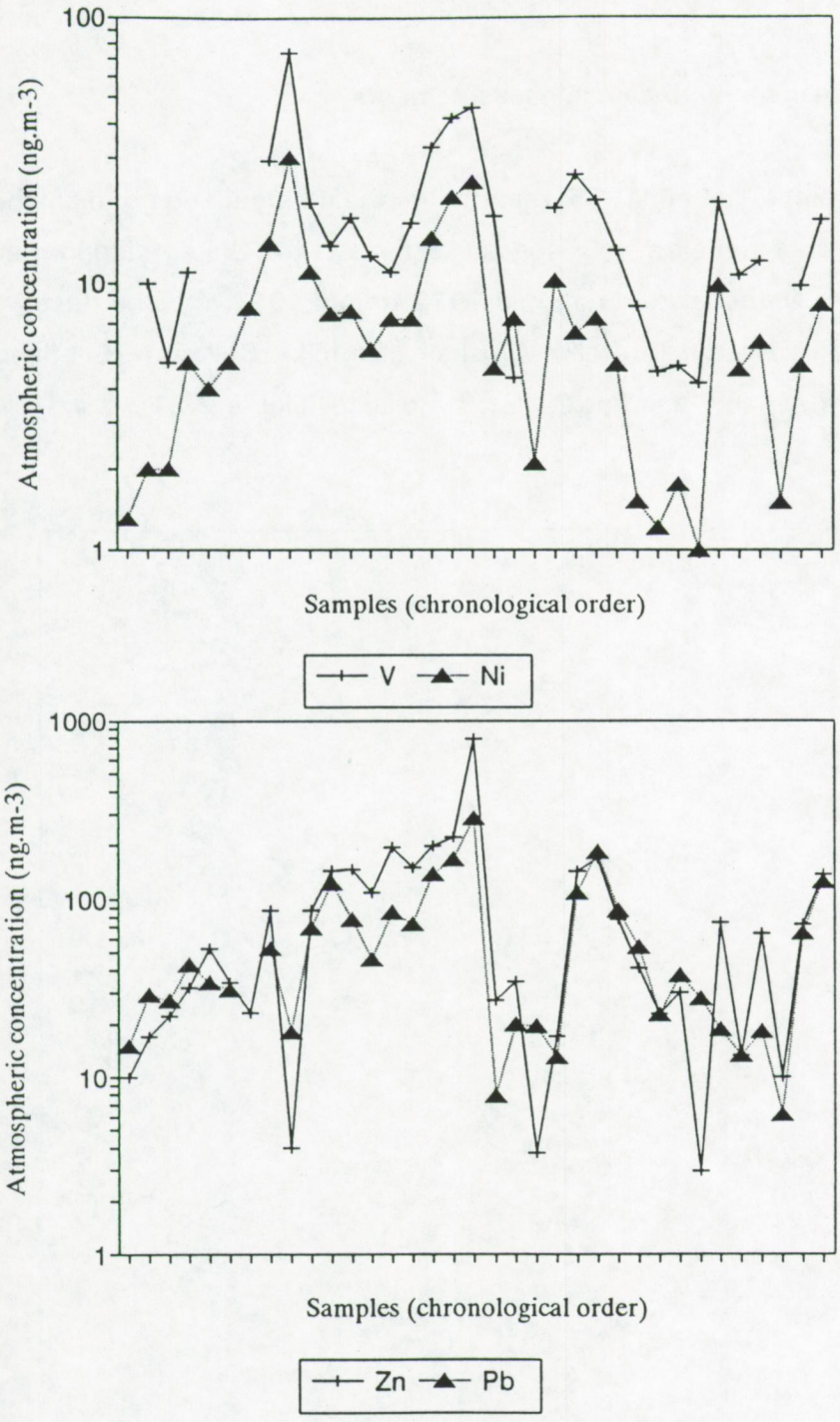

Figure 2.20: Ni and V (upper) and Zn and Pb (lower) concentrations as a function of chronological sample collection.

2.5 Comparison with coastal measurements

Cambray et al. (1975) reported on the determination of elemental concentrations in air at four coastal stations in the United Kingdom and one in the Netherlands. From mid-1972 to mid-1973 airborne dust was collected at Leiston (Suffolk), Gresham (Norfolk), Collafirth (Shetland), Lerwick (Shetland) and Petten (North-Holland) (Figure 2.21).

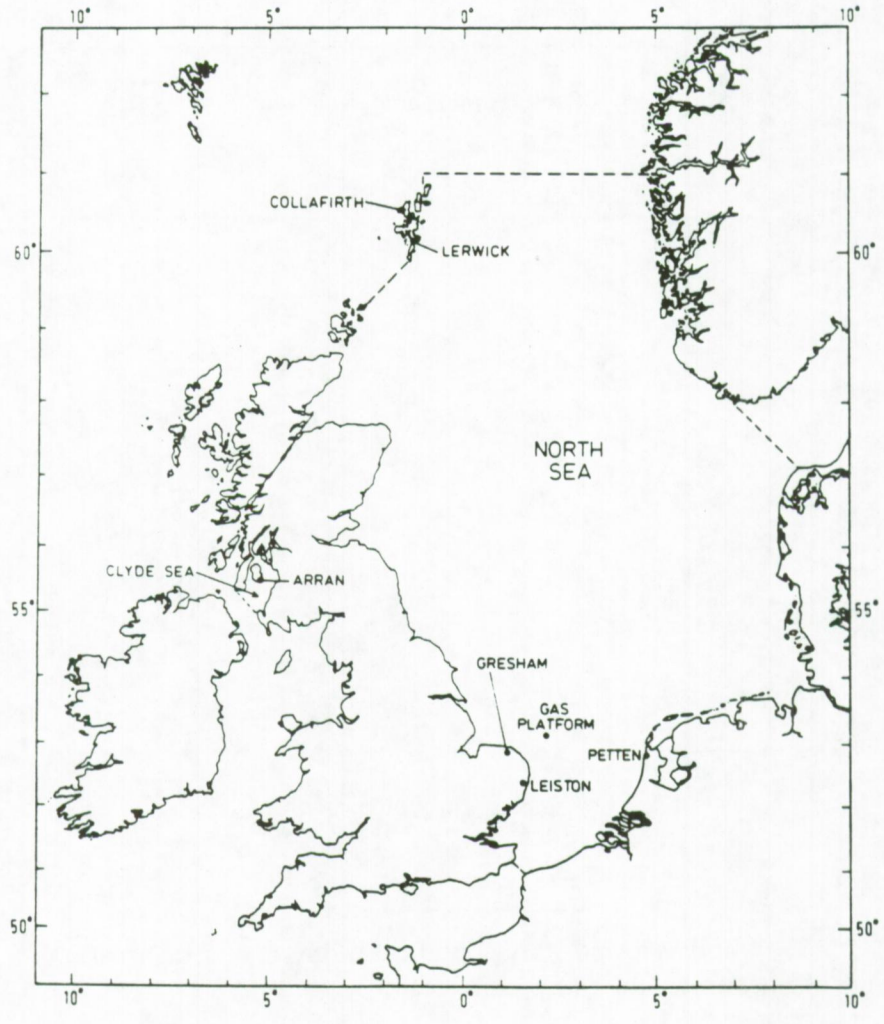

Figure 2.21: Sampling stations around and on the North Sea (Cambray et al., 1975).

Atmospheric particulate material was collected by means of a Whatman 40 (6 cm diameter) filter. With a flow rate of 6 $l.min^{-1}$, particles up to 150 μm could be collected. Samples were collected on a monthly basis. Chemical analysis was performed on the samples by using a variety of techniques such as neutron activation analysis, X-ray fluorescence, atomic absorption and classical methods. For the measurement of airborne dust samples a relative standard deviation of 25% was calculated.

Table 2.26 compares our atmospheric concentration values for the total North Sea and the Southern Bight of the North Sea with the experimental values obtained by Cambray et al. (1975) in five coastal stations around the North Sea. The averages listed in Table 2.26 were calculated by Cambray et al. (1975) by leaving out the values obtained at Lerwick (Shetland) since they were thought to be contaminated by sea spray, possibly enriched in trace metals. This assumption was based on the fact although airborne elemental concentrations are nearly the same, rainwater concentrations were much higher in Lerwick (Shetland) than in Collafirth (Shetland) and the fact that the main difference between the two sampling sites was the distance to the sea, Lerwick being closer to the sea than Collafirth.

Van Aalst et al. (1983) compiled all experimental measurements of heavy metals in the atmosphere, regarding the North Sea atmosphere, up to 1981. In Table 2.27 average concentrations based on a three-year measurement period in Leiston (Suffolk) and Collafirth (Shetland) reported by Cawse (1975, 1976, 1977) are listed. The range of yearly average concentrations, measured by DCMR (1978, 1979, 1980) at the Noordzeeweg in the Rijnmond area near Rotterdam are also included. In addition some incidental measurements reported by Diederen and Guicherit (1981) and Slanina (1981) are included. The extremely high values obtained at Haamstede must be relativated since they are the average of only four measurements, two with west wind and two with east wind.

Table 2.26:
Atmospheric concentrations in $ng.m^{-3}$.
Comparison of our results with the experimental measurements performed at five coastal stations around the North Sea by Cambray et al. (1975)

	Cambray et al. (1975)						This work	
Location / Element	Leiston	Gresham	Petten	Collafirth	Lerwick	Average	North Sea	Southern Bight
Al	270	305	200	56	56	210	140	190
Cl	2540	3180	3300	3400	3300	3200	2890	2960
V	14	13	11	2.2	2.3	10	12	19
Cr	6.9	4.3	3.9	1.3	0.9	4.1	12	14
Mn	25	27	18	4.1	3.2	18	14	29
Fe	390	410	370	89	62	320	230	430
Ni	6.1	6.9	9.3	3.7	3.4	6.5	4.7	7.5
Cu	<14	<11	<8	<5	<10	9.5	5.5	9.2
Zn	150	135	95	32	30	105	55	110
Pb	165	165	120	39	29	125	41	77

Table 2.27:
Atmospheric concentrations in $ng.m^{-3}$.
Comparison of our results with those of different authors, as reported by Van Aalst et al. (1983)

	Cawse (1975, 1976, 1977)		DCMR (1978-1981)	Diederen and Guicherit (1981)		Slanina (1981)	This work	
Location / Element	Leiston	Collafirth	Rijnmond	Haamstede	Schier-monnikoog	Petten	North Sea	Southern Bight
Cr	2.5	0.8		7.5	0.8	7	12	14
Ni	5.6	3.7	8-20	22	5		4.7	7.5
Cu	13	15	10-11	350	11.5	3	5.5	9.2
Zn	106	15		130	20	10	55	110
Pb	116	24	160-205	180	30	50	41	77

During the period between May 1972 and April 1977, daily average levels of heavy metals were determined routinely in Ostend at the Belgian coast (Kretzschmar and Cosemans, 1979). Atmospheric dust was collected on a Whatman 41 cellulose filter by means of a hi-vol sampling device. The monitoring station was located at the end of the East Pier in Ostend (Belgium). Determination of heavy metal levels was done by emission spectrography. In Table 2.28 concentrations for four different wind sectors, as calculated from the original data set of Kretzschmar and Cosemans, 1979, are listed together with our experimental data.

Table 2.28:
Atmospheric concentrattions in $ng.m^{-3}$.
Comparison of our results with a five year study of atmospheric heavy metal concentrations at the Belgian coast as reported by Krezschmar and Cosemans (1979).

	Kretzschmar and Cosemans (1979)					This work	
Sector / Element	Average	north sector	east sector	south sector	west sector	North Sea	Southern Bight
V	28	29	50	51	27	12	19
Cr	13	6.5	15	15	6.4	12	14
Mn	81	22	77	89	13	14	29
Fe	1430	400	1320	1660	300	230	430
Ni	13	6.7	13	14	6.9	4.7	7.5
Cu	19	10	25	22	5.7	5.5	9.2
Zn	300	110	310	360	61	55	110
Pb	278	100	290	350	63	41	77

Atmospheric heavy metal levels during east and south wind are very similar, as are concentrations during north and west wind. A fairly good agreement is found between our values for the Southern Bight area and the values reported by Kretzschmar and Cosemans (1979) for north and west wind situations. Concentrations during continental wind are a

factor of 2 to 5 higher than those measured during situations were the wind was coming from the sea.

Although not explicitly North Sea coastal measurements, the data collected by Flament et al. (1987) at the French coast in the Channel and those collected by Schneider (1987) in the Kiel Bight offer a good basis for intercomparison of results. Flament (1987) collected airborne dust samples at five different locations on the French coast of the east Channel (Bray-Dunes, Gravelines, Tardighen, Wimereux and Fort-Mahon Plage). Table 2.29 lists the average concentrations obtained by Flament et al. (1987) together with our values.

Table 2.29:
Atmospheric concentrations in $ng.m^{-3}$.
Comparsion of our data with results from experimental measurements made by Flament et al. (1987) on the coast of the East Channel.

Element	Flament et al. (1987) East Channel	This work North Sea	This work Southern Bight
Al	547	140	190
Mn	131	14	29
Fe	496	230	430
Cu	19.8	5.5	9.2
Zn	100	55	110
Pb	56	41	77

Al, Mn and in a lesser extent Cu concentrations at the French coast are much higher than our values for the Southern Bight of the North Sea. Pb, Zn and Fe levels are quite comparable. Any possible influence of local metallurgic industry in the area can not be excluded, although it is not quite clear why this wouldn't have any effect on the Zn concentration.

Schneider (1987) reported on 59 air filter samples collected on a weekly basis from a lighthouse in the Kiel Bight. The lighthouse was located on an artificial island about 20 km from the city of Kiel. During weekly sampling about 100-200 m^3 of air was drawn through a double filter consisting of cellulose (Whatman 41) and PTFE (Sartorius SM11807). Samples were analyzed by neutron activation for Na, Al, V and Mn, and after digestion with HNO_3, by total reflection fluorescence for K, Ca, Ti, Cr, V, Mn, Fe, Ni, Cu, Zn, As, Se, Rb, Sr, Ba and Pb. Table 2.30 compares our values for the total North Sea and for the Southern Bight of the North Sea with those from Schneider (1987) for the Kiel Bight.

Table 2.30:
Atmospheric concentrations in $ng.m^{-3}$.
Comparison of our results with experimental measurements performed by Schneider (1987) in the Kiel Bight.

	Schneider (1987)		This work	
Element	Average	1 σ range	North Sea	Southern Bight
Al	394	68-720	140	190
K	300	124-476	250	400
Ca	435	86-787	240	380
Ti	27	5-49	14	25
V	9.7	4.9-15	12	19
Cr	2.9	0.2-5.6	12	14
Mn	15	4-26	14	29
Fe	369	90-648	230	430
Ni	4.0	1.7-6.3	4.7	7.5
Cu	7.7	1.3-14	5.5	9.2
Zn	57	8-106	55	110
Pb	53	14-92	41	77

For a number of elements, very good agreement is found: the average Pb concentration over the kiel Bight is 53 $ng.m^{-3}$ while the average concentration over the total North Sea is 40 $ng.m^{-3}$ and over the Southern Bight is 70 $ng.m^{-3}$. Zn (55 $ng.m^{-3}$ for the Kiel Bight and 55 $ng.m^{-3}$, total North Sea), Cu (7.7 $ng.m^{-3}$ for the Kiel Bight and 5.4 $ng.m^{-3}$ for the total North Sea), Ni (4.0 $ng.m^{-3}$ for the Kiel Bight and 4.7 $ng.m^{-3}$ for the total North Sea) and Mn (15 $ng.m^{-3}$ for the Kiel Bight and 13 $ng.m^{-3}$ for the total North Sea) are quite comparable.

2.6 Comparison with platform and ship based measurements

In contrast with measurements performed at coastal stations around the North Sea, much less data are available on experimental determination of airborne elemental concentrations in samples taken on the North Sea itself. It is nevertheless obvious that atmospheric concentrations above the North Sea are not necessarily the same as those measured at the coast. In the centre of the North Sea, no anthropogenic sources of pollutants (except, ships and oil and gas rigs) are present. The sea itself might be a source of atmospheric pollution through ejection of sea salt aerosols that can be enriched in trace metals. However, at the coast, with its more frequent wave breaking and subsequent aerosol spray production, the contribution of the sea as a source for atmospheric pollution would be greater than in the open sea. Therefore it is quite plausible to expect that atmospheric concentrations of anthropogenic elements will be lower above the open sea than at the coast.

Cambray et al. (1975) used an unmanned gas platform, located at position 52° 46′ N, 4° 40′ E, to collect airborne dust on a monthly basis with a Whatman 40 paper filter. The inlet of the filter was pointed downward and placed at an altitude of 25 m. The concentrations measured at the gas platform are quite comparable with those obtained from samples collected at the coast in Leiston (Suffolk), Gresham

(Norfolk) and Petten (North-Holland) (see also section 2.5). In Table 2.31 concentrations measured at the gas platform by Cambray et al. (1975) are listed together with our results.

Table 2.31:
Atmospheric concentrations in $ng.m^{-3}$.
Comparison of our results with platform based measurements as reported by Cambray et al. (1975).

	Cambray et al. (1975)	This work	
Element	Gas platform	North Sea	Southern Bight
Al	155	140	190
Cl	5700	2890	2960
V	9.7	12	19
Cr	3.7	12	14
Mn	17.5	14	29
Fe	270	230	430
Ni	8.2	4.7	7.5
Cu	<17	5.5	9.2
Zn	125	55	110
Pb	120	41	77

For most elements, reasonable agreement is found. Pb values for the gas platform are relatively high (120 $ng.m^{-3}$) compared with our observations for the Southern Bight (70 $ng.m^{-3}$). Also Cl concentrations are a factor of 2 higher at the platform (5700 $ng.m^{-3}$) than the average value we measured (2600 $ng.m^{-3}$). Our Cr concentrations are relatively high, but this is probably due to contamination since we find approximately the same concentration for the Southern Bight area as for the total North Sea.

Dedeurwaerder (1988) collected 96 aerosol samples between January 1980 and August 1985 from different ships, the Westhinder, the

Mechelen, The Alkaid and the Belgica, on the North Sea. The largest number was collected from the light vessel Westhinder, located at position 51.23.5 N, 02.21.5 E. Total particulate matter was collected by drawing air trough a 11 cm diameter Whatman 41 cellulose filter. After acid digestion of the filters, the resulting solution was analyzed with atomic absorption spectroscopy. Table 2.32 compares our results with those of Dedeurwaerder (1988). The average concentration given by Dedeurwaerder (1988) is calculated by removing all samples that were not taken in the Southern Bight of the North Sea, below 53° N. Besides the average concentration, the median concentration is listed. In addition, atmospheric concentrations, measured when the wind direction was within 050° and 230° degrees (the so-called continental wind sector), are listed.

Table 2.32:
Atmospheric concentrations in $ng.m^{-3}$.
Comparison of our results with ship based measurements as reported by Dedeurwaerder (1988).

	Dedeurwaerder (1988)			This work	
Element	Average	Median	Continental sector*	North Sea	Southern Bight
Al	390	165	700	140	190
Mn	58	13	49	14	29
Fe	560	248	910	230	430
Cu	17	14.9	22	5.5	9.2
Zn	150	98	250	55	110
Pb	150	111	200	41	77

* wind direction between 50° and 230°

The atmospheric concentrations measured at the Westhinder by Dedeurwaerder (1988) are significantly higher than the concentrations we observed for the Southern Bight of the North Sea. Al, Cu and Pb values are a factor of two higher, Fe and Zn are 50% higher, while the average Mn concentration is merely 8% higher.

One possible explanation for this is the fact that the sampling point that was used by Dedeurwaerder (1988) was located in the southern part of the Southern Bight of the North Sea, an area that is relatively close to the different pollutant sources on the continent and in the UK. Indeed, the Westhinder lightvessel is only separated from the coastline by a relative small distance and it is located at a very dense traffic channel on the North Sea.

2.7 Comparison with model calculations

A number of groups have calculated the atmospheric concentrations of heavy metals above the North Sea by using a theoretical model. The TREND-model developed by Van Jaarsveld (1986) is the most elaborated one available. Another model, developed by Krell and Roeckner (1988) is more directed towards calculation of atmospheric deposition of anthropogenic pollutants in the North Sea, rather than towards calculation of airborne concentrations.

The TREND-model starts from the anthropogenic element emission-inventory for Europe (Pacyna, 1985), adjusted for recent industrial evolution in the Netherlands. A Langragian model is used for the description of the dispersion and transport of pollutants. Transport of particles is calculated for five separate particle size classes.

A statistical approach is used for the determination of long term average concentrations by grouping meteorological situations in a limited number of size classes and by calculating representative values for the different classes and by multiplying them with the frequencies of occurrence of the classes. The classification is based on data about the wind direction, atmospheric stability, mixing height layer and transport distance.

Fig 2.22 shows the calculated average atmospheric lead concentration for 1983 for the total North Sea area. Model calculated Pb

Figure 2.22: Model calculation of the average Pb concentration in the North Sea atmosphere (Van Jaarsveld et al., 1986).

concentrations vary from 10 to 15 ng.m^{-3} in the atmosphere above the northern North Sea, while for the Southern Bight area values of 50 to 100 ng.m^{-3} are calculated.

The average atmospheric Pb concentration that we observed for the whole North Sea area between 1984 and 1988 (40 ng.m^{-3}) compares very well with the average calculated concentration (33 ng.m^{-3}) for the year 1983. Our value for the Southern Bight of the North Sea (70 ng.m^{-3}) is also in very good agreement with TREND-model calculated value (70 ng.m^{-3}).

Emissions of trace elements may vary from year to year, depending

on industrial expansion (economic variations) and environmental legislation (emission restrictions). Consequently also concentrations will vary from year to year. It would be interesting therefore to compare our experimental results for the period 1984-1988 with model calculations for the same period. In addition, other elements should be looked at too.

2.8 Conclusion

Atmospheric concentrations of different elements in the lower troposphere above the North Sea are highly variable as a function of both time and location. Rapid changes in the meteorological situation are reflected without delay in the atmospheric concentrations of trace elements.

Average Cl concentrations above the northern part of the North Sea are approximately the same as above the Southern Bight of the North Sea. Mn, Zn, Pb and Fe concentrations are 10 times lower in the northern North Sea atmosphere than in the southern part. Si, S, Ti, Cr, K, Ca, V and Ni concentrations are on the average 3 to 6 times lower above the northern North Sea, compared to the Southern Bight atmopshere.

Factor analysis performed on all samples collected with a stacked filter unit resulted in the identification of three fctors for the coarse particle fraction (sulphate particles with trace metals, sea salt particles and soil dust or metallurgic particles containing Fe) and four factors for the fine particle fraction (sea salt, sulphate with Pb and Zn, trace metal particles with Cu, Ni and Zn and fly-ash particles).

Factor analysis performed on all samples collected above the Southern Bight of the North Sea (total aerosol filtration samples) yielded three factors: sea salt particles, particles enriched in Ni and V, originating from natural oil combustion and particles containg a variety of elements such as S, K, Ca, Fe, Pb, Cu and Zn.

Compared with coastal measurements of trace elements in the

atmosphere, a relative good agreement can be found. In some cases however large discrepancies between results from our ship-based measurements and coastal station results can be attributed to the probable influence of local emission sources such as industrial areas.

Compared to the ship based measurements performed by the Dedeurwaerder (1988) our results for the Southern Bight of the North Sea are up to 50% lower. This difference can be most likely be attributed to the fact that Dedeurwaerder (1988) collected aerosol samples in the very southern part of the North Sea, whereas we collected samples, covering the whole area of the Southern Bight of the North Sea below 54°N.

Model calculations by Van Jaarsveld et al. (1986) for Pb show a good agreement with our observed Pb concentrations between 1984 and 1988.

2.9 References

Bruynseels F. (1987): *Applications of laser microprobe mass analysis in aerosol research.* Ph. D. Thesis, University of Antwerp, UIA, Antwerp.

Cambray R.S., Jeffereies D.F. and Topping G. (1975): *An estimate of the input of atmospheric trace elements into the North Sea and the Clyde Sea (1972-3).* AERE-Report 7733.

Cawse P.A. (1975, 1976, 1977): *A survey of atmospheric trace elements in the UK.* AERE-Report R 8038, R 8398, R 8869.

D.C.M.R. (1978, 1979, 1980): *Quarterly and yearly reports.* DCMR, Schiedam.

Diederen H.S.M.A. and Guicherit R. (1981): *Bronherkenning van aerosolen door middel van cocentratiemetinegen van elementen in de buitenlucht.* IMG-TNO Report G 799.

Dedeurwaerder H.L. (1988): *Study of the dynamic transport and of the fall-out of some ecotoxicological heavy metals in the troposphere of the Southern Bight of the North Sea.* Ph.D Thesis, University of Brussels, VIB, Brussels.

Flament P., Noel S., Auger Y., Leman G., Puskaric E. and Wartel M. (1984): *Les retombées atmosphériques sur le littoral Nord-Pas-de-Calais.* Poll. Atmos., 262-270.

Jenkins R., Gould R.W. and Gedcke D. (1981): *Quantitative X-Ray Spectrometry.* Marcel Dekker, Inc., New York.

Krell U. and Roeckner E. (1988): *Model simulation of the atmospheric input of lead and cadmium into the North Sea.* Atmos. Environ. 22, 375-381.

Kretzschmar J.G. and Cosemans G. (1979): *A five year survey of some heavy metal levels in air at the Belgian North Sea coast.* Atmos. Environ. 13, 267-277.

Schneider B. (1987): *Source characterization for atmospheric trace metals over Kiel Bight.* Atmos. Environ. 21, 1275-1283.

Van Aalst R.M., Van Ardenne R.A.M., De Kreuk J.F. and Lems Th. (1983): *Pollution of the North Sea from the atmosphere.* TNO-Report CL 82/152.

Van Espen P., Janssens K. and Nobels J. (1986): *AXIL-PC, Software for the analysis of complex X-ray spectra.* Chemometrics and Intelligent Laboratory System, 1, 109-114.

Van Jaarsveld J.A., Van Aalst R.M. and Onderlinden D. (1986): *Deposition of metals from the atmosphere into the North Sea.* RIVM-Report 842015002.

Chapter 3

Aircraft-based measurements of atmospheric Cd, Cu, Pb and Zn above the Southern Bight of the North Sea

3.1 Introduction

Emission of pollutants on land occurs at different altitudes, which are essentially the different stack heights. Pollutant plumes may or may not rise in the air as a function of the plume temperature, the environmental lapse rate (i.e. the variation of temperature with altitude) and the atmospheric stability. In addition, large scale air motions are the result of interaction between cold and warm fronts and the existence of changing high and low pressure areas. Particulate matter can be entrained in air parcels over very long distances. Asian mineral dust has been found back as far as the central North Pacific Ocean (Schneider et al., 1990). It is obvious that characterization of aerosol particles in the North Sea atmosphere, or in any other atmosphere for that matter, requires three-dimensional sampling. The use of an aircraft for aerosol sampling has the additional advantage of the possibility to cover a large area as to avoid any contamination by local sources of pollutants.

Ship-based sampling as well as sampling from coastal stations can possibly be biased by contamination of the samples e.g. by sea spray. The generation of marine aerosol particles by the sea includes the formation of film and jet drops form the upper microlayer of the sea surface. These particles may be enriched relatively to the seawater composition in organics and in trace metals. Collection of airborne particulate matter close to the sea surface can therefore result in measurements of high trace metal concentrations. An aircraft has the technical possibility of both sampling at very low altitudes, in our case down to 10-15 m above sea level, and at much higher altitudes. Therefore an evaluation can be made of the contribution of the sea itself as a source for trace metals in the air.

In this chapter, attention is focused on atmospheric concentrations of Cd, Cu, Pb and Zn, heavy metals that have toxic effects on different forms of natural life. Pacyna (1984) calculated the emission of 15 anthropogenic elements in Europe for the year 1979. The data were

obtained on the basis of trace element emission factors and statistical information on the consumption of ores, rocks and fuels and the production of various types of industrial goods.

Cd is largely emitted by primary Zn-Cd production (57%) and primary Cu-Ni production (22%). Industrial and residential combustion of fuels is responsible for 5.7% of the total Cd emission in Europe. Conventional thermal power plants emit 3.7% of the total Cd amount.

51% of the total European Cu emission originates from primary Cu-Ni production. The second largest source is industrial and residential combustion of fuels (13%). Some 11% is emitted by iron and steel manufacturing, 9.7% by wood combustion and 8.9 % by conventional thermal power plants.

In 1979, 60% of the total Pb emission in Europe originated from gasoline combustion. This source has decreased steadily over the last few years. 11.9% of the Pb emission comes from iron and steel manufacturing. Primary Pb, Cu-Ni and Zn-Cd production is responsible for 8.5%, 7.5% and 6.4%, respectively, of the total Pb emission.

Zn is mainly emitted by primary Zn-Cd production (61%). The second largest source for Zn is iron and steel manufacturing (13%). Refuse incineration and wood combustion are responsible for 7.4% and 5.7%, respectively, of the total Zn emission in Europe.

It is quite obvious that anthropogenic emissions will vary from year to year as a function of changing economic activity, industrial expansion and environmental legislation, i.e. emission criteria. Generally speaking, Cd, Cu, Pb and Zn are emitted by the ferro and non-ferro industry and by combustion of all sorts of fuels.

In section 3.2, the aircraft is described and the sampling equipment is characterized. Special attention is paid to isokinetic sampling and the sampling of large particles. Then, in section 3.3, the analytical procedure followed for analysis of Cd, Cu, Pb and Zn in atmospheric particulate matter is discussed. Section 3.4 and 3.5 include the results of measurements of total atmospheric particulate Cd, Cu, Pb and Zn

concentrations and of size-differentiated concentrations, respectively. The variation of concentrations as a function of altitude, wind direction, air mass history and season is investigated. Finally, the aircraft-based results are compared with the results of ship-based measurements of Cu, Pb and Zn, as discussed in Chapter 2.

3.2 Sampling strategy

3.2.1 PH-ECO: Technical description (Figure 3.1)

The aircraft used is a twin-engine Piper Chieftain (PA-31-350, call-sign PH-ECO) of the Geosens B.V. company (Rotterdam, The Netherlands). It has been modified in order to perform a large variety of atmospheric research tasks. Besides a pilot and a co-pilot, two operators are involved in each flight. One additional passenger can be included. When fully equipped and using a crew of four persons, the flight time is limited to four and half hours. Considering the transfer time between the Rotterdam airport and the North Sea, a useful sampling time of three and a half hours is available during each flight. Sampling flights are limited by a maximum flight level of approximately 24000 ft. Normal cruise speed of the aircraft is 150 kn (270 $km.h^{-1}$ or 70 $m.s^{-1}$).

Table 3.1 lists the main technical specifications of the PH-ECO aircraft.

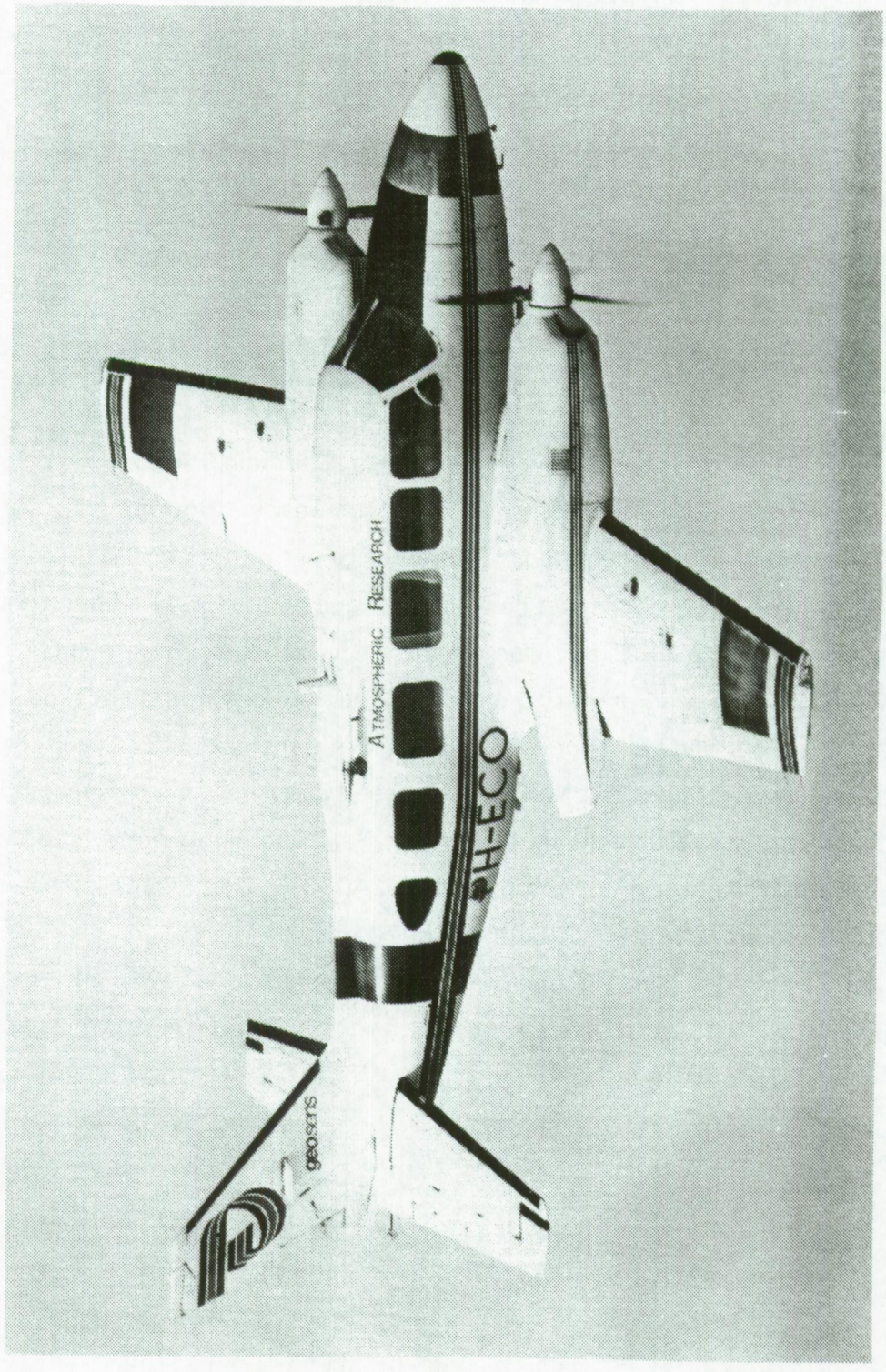

Figure 3.1: The PH-ECO sampling aircraft.

Table 3.1:
PH-ECO (Geosens B.V.) aircraft specifications

1	A/C Type	Piper Chieftain PA-31-350
2	Owner	Geosens B.V.
3	Operator	Geosens B.V.
4	Engines	2
5	Weights:	
	Maximum take off	7000 lbs
	Empty	4319 lbs
	Payload	2681 lbs
	Fuel capacity	890 lbs
6	Number of crew	5
7	Fuel sort	AVGAS 100LL
8	Fuel consumption	165 lbs/h
9	Endurance	4.5 h
10	Range at 5000 ft	650 NM*
11	Cruise	150 kn**
12	Max. cruise speed at SL	185 kn
13	Max. cruise at FL 100	210 kn
14	Stalling speed	75 kn
15	Ceiling	24000 ft
16	Take off dist., 50 ft obst.	>500 m
17	Acc. stop distance	>800 m
18	Rate of climb at SL	1000 ft/min
19	Rate of climb at FL 50	800 ft/min
20	Approved for	IMC + Icing

*: NM = nautical mile (1850 m)
**: kn = NM/h

3.2.2 Isokinetic inlet

3.2.2.1 The Pennsylvania State University (PSU) isokinetic sampler

Sampling of airborne particulate matter under isokinetic conditions is essential in order to avoid distortion of the particle size distribution. Anisokinetic sampling (Figure 3.2) may be the result of the difference between the average intake speed of the instrument, u, and the aircraft speed, u_0. Misalignment of the intake can also result in anisokinetic sampling, although this is of minor importance to aircraft sampling.

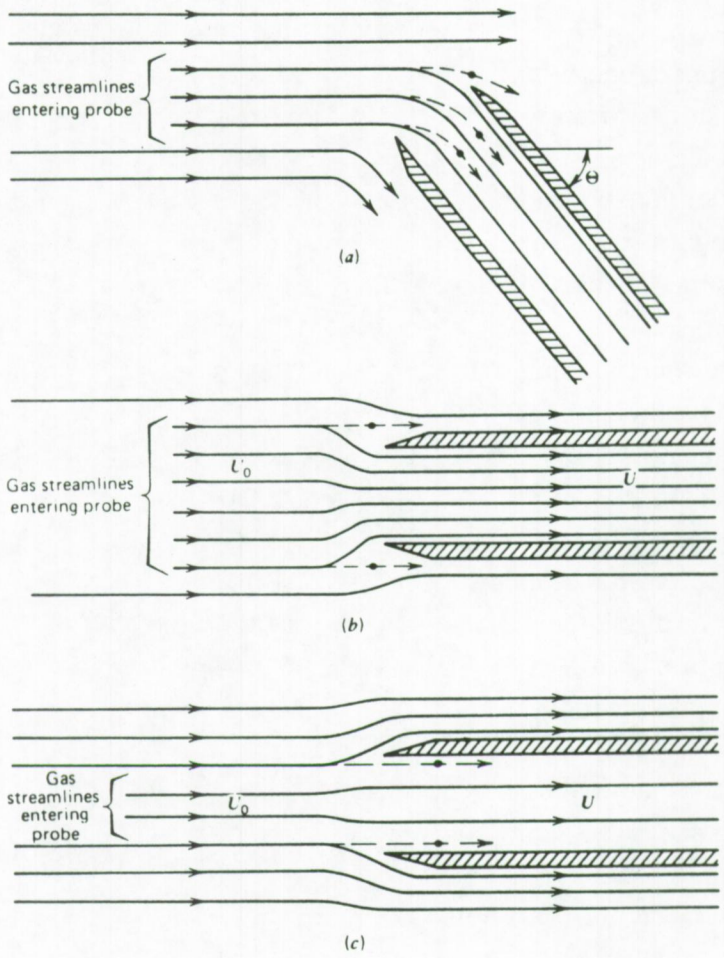

Figure 3.2: Anisokinetic sampling conditions (Hinds, 1982).

The distortion in the particle concentration resulting from anisokinetic sampling can be described by:

$$\frac{C_s}{C_0} = 1 + \left(\frac{u_0}{u} - 1\right) \beta\ (K) \qquad (3.1)$$

where C_s and C_0 are the concentration in the sample and in the free air, respectively, and K is the particles Reynolds number:

$$K = \frac{\rho_p\ u_0}{18\ \eta\ D} d_p^2 \qquad (3.2)$$

where ρ_p and d_p are the particle density and diameter, respectively, η the air viscosity and D the internal diameter of the intake. The value of β(K) is given by:

$$\beta(K) = \frac{BK}{1 + BK} \qquad (3.3)$$

and B is given by:

$$B = 2.0 + 0.62\ \frac{u}{u_0} \qquad (3.4)$$

Because of the problem of operating simultaneously several instruments with different intake speeds and covering a wide range of particle sizes, Pena et al. (1977) designed a single isokinetic decelerator with a common sampling chamber, in which the air velocity would be equivalent to light to moderate wind speeds. The Pennsylvania State University (PSU) isokinetic sampler (Figure 3.3) includes additional fine tuning by tailoring each individual intake for the various instruments to meet the isokinetic requirements between the chamber environment and the sampling line.

Air enters the sampler through a carefully designed circular intake of 2.03 cm diameter and is reduced in speed through a 7° conical expansion that terminates in a cylindrical sampling chamber. The expansion angle of 7° minimizes both dissipative losses and flow

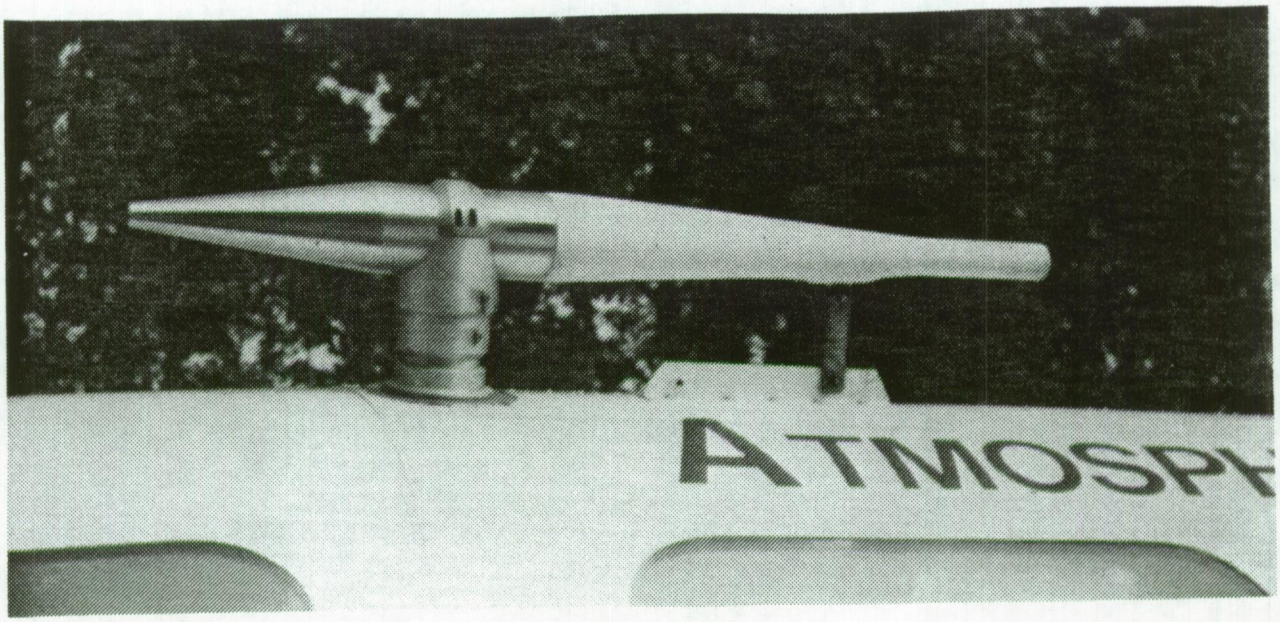

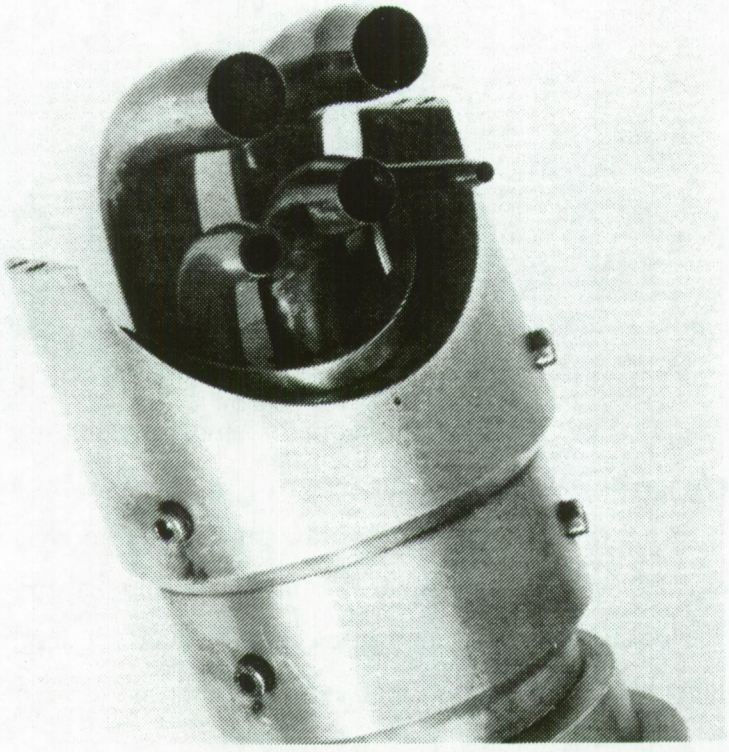

Figure 3.3: PSU isokinetic sampler: overall view and detail of the individual intakes inside the central sampling chamber.

separation. The air speed is reduced by a factor of 16.6 from the aircraft speed.

The sample chamber has an inner diameter of 8.28 cm and a total length of 22.86 cm. The tubes leading to the individual instruments are located in the area limited by the distances 7.5 cm and 12.5 cm from the entrance to the chamber. In this chamber a small fraction (< 10%) of the total air flow is removed by the aerosol instruments. The tubes leading to the individual instruments all have a gradual 90° bend and are adopted for isokinetic sampling by using an appropriate nozzle size to match the local air speed in the sample chamber to the instrument flow rate.

Behind the sampling chamber, the air is accelerated along a second conical section to the exhaust port. The pumping action of the air stream in passing the exhaust can be used to compensate for losses inside the sample chamber so as to maintain a total flow that represents isokinetic sampling at the intake.

The PSU sampler is mounted on the roof of the aircraft in such way that the intake is located outside the boundary layer of the aircraft and that no particulate or gaseous matter coming from the exhaust of the two engines can be sampled.

3.2.2.2 Sampler performance

The performance of the PSU isokinetic sampler was tested by Pena et al. (1977) by measuring the velocity profile inside the sample chamber and by calculating the isokinetic efficiency from:

$$\frac{u_0}{u} = \frac{u_0 R_0^2}{v_m (R_s - \delta^*)^2} \qquad (3.5)$$

where R_0 is the radius of the intake, R_s is the radius of the sampling chamber, v_m is the average velocity in the sampling chamber, obtained from velocity profile measurements and δ^* is given by:

$$\delta^* = 1.74 \left(\frac{\nu \chi}{v_\infty}\right)^{\frac{1}{2}} \qquad (3.6)$$

where ν is the kinetic air viscosity (0.17 $cm^2.s^{-1}$), χ is the distance from the entrance of the chamber (10 cm) and v_∞ is the air velocity at the centre line of the sample chamber in $cm.s^{-1}$.

Wind tunnel tests (Pena et al., 1977) showed that the turbulence intensity is low (5%) and that no flow separation occurred in the expansion section. In addition it was proven that there is negligible sensitivity to angle of attack up to 8°.

The isokinetic efficiency C_s/C_0, calculated for three different particle densities and selected particle sizes showed that particles up to 5.0 μm are collected with an efficiency up to 80%.

3.2.2.3 Experimental determination of the 50% cut-off diameter of the complete filter sampling system used.

When calculating a cut-off diameter for a specific sampling system, the complete sampling line should be taken into account, not only the sampler intake. Indeed, particles may be lost between the initial intake and the final collection on a filter, in bends and valves that do not have 100% isokinetic characteristics.

In order to evaluate the cut-off diameter of the filter sampling system used in the PH-ECO, a comparison has to be made between the particle size distribution as measured on the filter and the particle size distribution as it is present in the ambient air before the aerosol particles encounter or pass any intake device. To achieve this, a direct impaction rod was designed.

A 1 cm diameter rod, covered with particle-free sticky tape (Scotch, 3M), is placed on a vertical bar (Figure 3.4). The surface of the

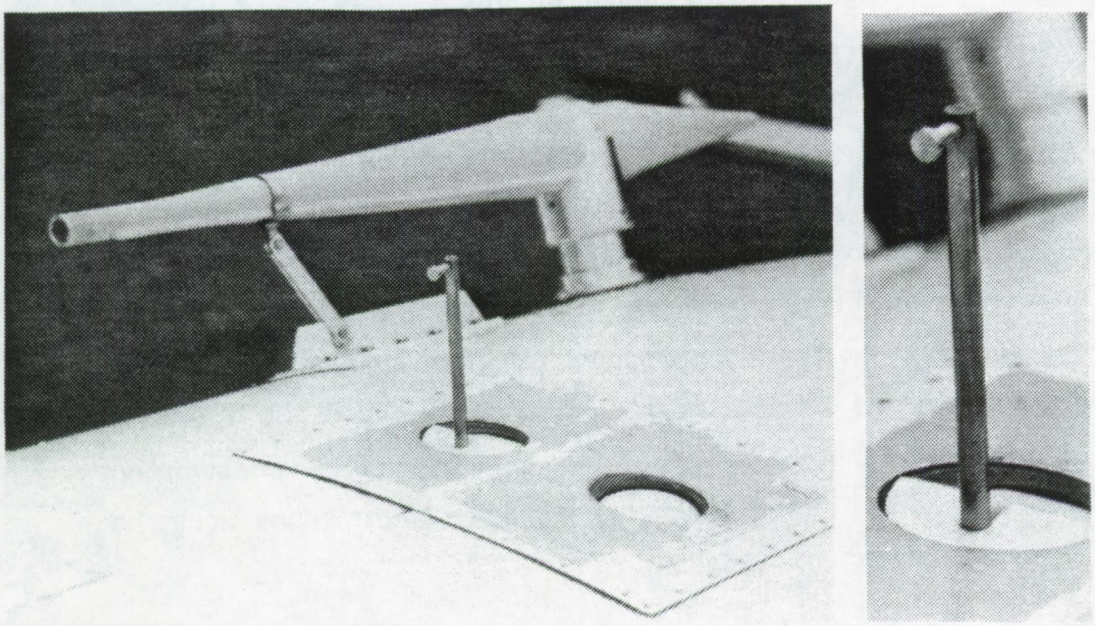

Figure 3.4: Direct impaction rod mounted on the PH-ECO next to the PSU-inlet.

rod is perpendicular to the flight direction and the streamlines of the air around the aircraft. Particles are impacted on the rod with an efficiency given by:

$$E_I \sim \frac{\rho_p \, d_p^2 \, U \, C_c}{9 \, \eta \, d_c} \qquad (3.7)$$

where E_I is the impaction efficiency, C_c is the Cunningham slip correction factor and d_c is the collector size i.e. a characteristic impactor size. The smaller the impaction rod, the more efficient particles will be collected. Large particles will be collected with 100 % efficiency, assuming there is no bounce-off effect.

On January 11, 1989, a PSU calibration flight was performed at 400 m altitude in the Rotterdam harbour area. In this highly industrialized area, a large number of particle emission sources are present, resulting in

the presence of an important amount of large particles.

At 270 km/h true air speed, the impaction rod collects particulate material with an equivalent flow rate of 350 $l.min^{-1}$, while the Nuclepore filter is operated at a flow rate of approximately 50 $l.min^{-1}$. In order to assure sufficient loading of the Nuclepore filter and to avoid overloading of the impaction rod, sampling times are different for the filter (30 min) and for the impaction rod (5 min). The particle size distribution was measured with an electron microscope using a magnification of 1000x. Results from two separate samples are shown in Figure 3.5. It is clear from Figure 3.5 that the 50% cut-off diameter of the total filter sampling system, including the PSU inlet, the sample lines, the connections and valves, is situated around 2.5 μm.

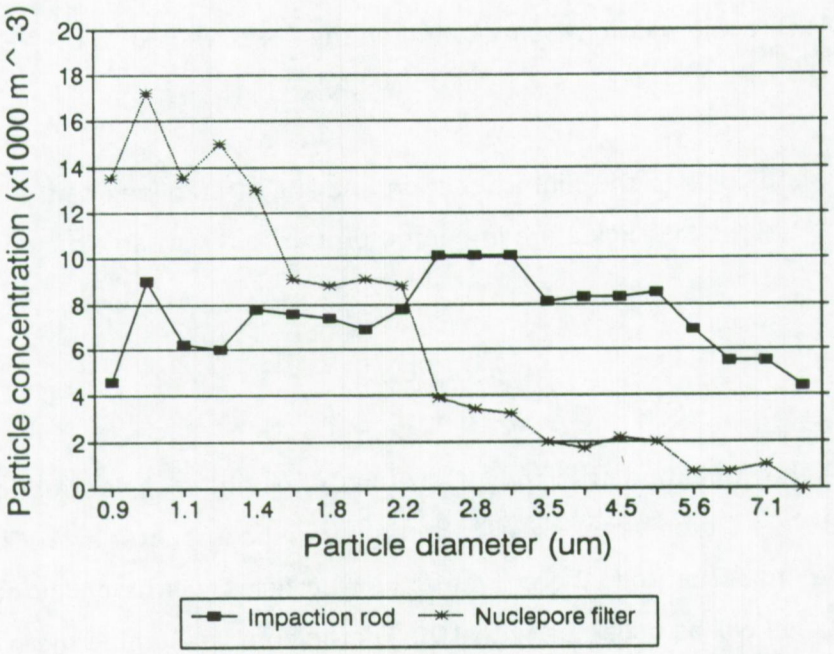

Figure 3.5: Particle size distribution on the Nuclepore filter and the direct impaction rod.

3.2.3 Sampling of atmospheric gases: SO_2 and O_3

In situ SO_2 measurements are performed with a pulsed fluorescence monitor (Thermo Electron, model 43A). The flow rate of the apparatus has been modified in order to increase the response time up to 12 seconds. The detection limit is 1 ppb and the accuracy about 1.5%.

Ozone is measured with a Bendix model 8002 (Combustion Engineering) chemiluminescence monitor. A detection limit of 0.2 ppb, an accuracy of 1 % and a response time of 4 seconds can be achieved with this apparatus.

Results of SO_2 and O_3 measurements during 23 sampling flights above the Southern Bight of the North Sea are presented in Chapter 5.

The PH-ECO includes also the possibility of measuring burden SO_2 (integrated SO_2 concentration between the flight level and the ground level) with a Barringer Research model Cospec 4 apparatus and burden NO_x with a Moniteq model Marrs 101 apparatus.

3.2.4 Sampling of particulate matter with filters

Filtration has become the most widely used technique for aerosol sampling because of the low cost and simplicity. By appropriate choice of a so-called 'air moving' system, filter medium and filter size, almost any sample quantity desired can be collected in a given sampling interval.

Filters remove particles from a gas stream by a number of different mechanisms. These include interception, impaction, diffusional deposition, electrical interaction and gravitational deposition. The one or more of these mechanisms that dominate for a given filtration system will depend on the flow rate, the filter medium and the aerosol characteristics. For our purposes two filter types were used: a 0.4 μm pore size Nuclepore filter of 47 mm diameter and a 1.0 μm pore size Teflon filter (Millipore, type FA) of 47 mm diameter.

3.2.4.1 Filter type I: Nuclepore filter

Nuclepore filters are membrane filters that are made by placing a 10 μm thick polycarbonate sheets in contact with uranium sheets. U-235 fission fragments produce holes in the plastic. Subsequent treatment in an etch solution enlarges the holes to a specific size. Nuclepore filters have a smooth filtering surface, with cylindrical pores, almost uniform in diameter and perpendicular to the filter surface (Lippmann, 1978). Liu and Lee (1976) measured the collection efficiency for Nuclepore filters for submicrometer aerosol particles between 0.03 an 1.0 μm. The filtration efficiency of a 0.6 μm Nuclepore filter for different pressure drops is illustrated in Figure 3.6. The most penetrating particle size decreases as the filter pressure drop increases. The filter efficiency approaches 100% as the particle size approaches the filter pore size.

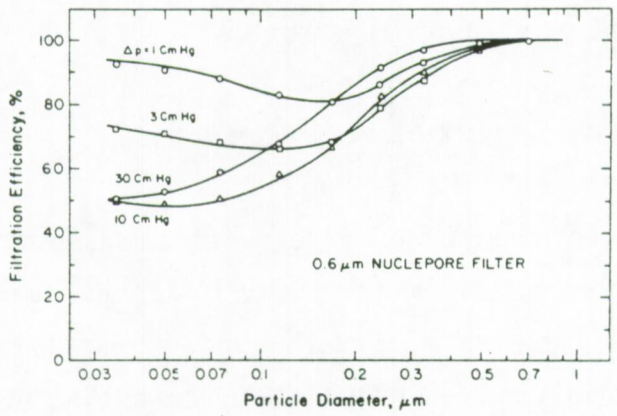

Figure 3.6: Collection efficiency of a 0.6 μm pore size Nuclepore filters for different filter pressure drops (Liu and Lee, 1976).

In our experimental setup, a 47 mm diameter 'aerosol-grade' Nuclepore filter with 0.4 μm pore size is used. It has a thickness of 10 μm and a mass/area of 0.8 mg.cm^{-2}. The operational flow rate of approximately 50 l.min^{-1} results in a face velocity of 60-70 cm.s^{-1} and a filter pressure drop of about 20 cm Hg. The collection efficiency is estimated to be >90% for particles with a diameter >0.2 μm.

3.2.4.2 Filter type II: Teflon filter

Besides the Nuclepore filter, a 47 mm diameter Teflon filter (Millipore, type FA) with 1 μm pore size is used. This filter has a thickness of 180 μm and a mass/area of 2.2 mg.cm^{-2}. The results of Liu and Lee (1976) show that, for this type of filter, collection efficiencies >99.99% are found for particles between 0.03 and 1 μm under all considered circumstances.

3.2.4.3 Air moving system

Electric power supply is limited in the PH-ECO aircraft as it is in any aircraft. In addition extra weight means less fuel can be carried along and thus the flight time and the effective sampling time is reduced. The use of heavy-weight high-volume pumps that require too much electric power must be avoided as much as possible.

In the PH-ECO a quadruple Venturi-effect based pump-system is installed that requires no electric power at all and is capable of drawing approximately 50 l.min^{-1} of air through two parallel filters of 47 mm diameter and 0.4 to 1.0 μm pore size.

The so-called 'Venturi-pump' consists of an inner and outer tube (Figure 3.7). The inner tubes narrows from 26 mm diameter to 16 mm diameter after 1 cm. In this way, the air speed in the narrow section will be higher than the true air speed of the aircraft and thus the pressure at that section will be lower than the ambient pressure. At the narrow section the slit-type exhaust of the aerosol sampling lines are placed. Because of the Venturi-effect, air is drawn from the exhaust and the Venturi operates as a pump. The use of four Venturis placed on the wings results in a slight increase in aerodynamic resistance of the aircraft and thus a slightly higher fuel consumption if the same speed is to be held (which is necessary if isokinetic sampling conditions are to be met).

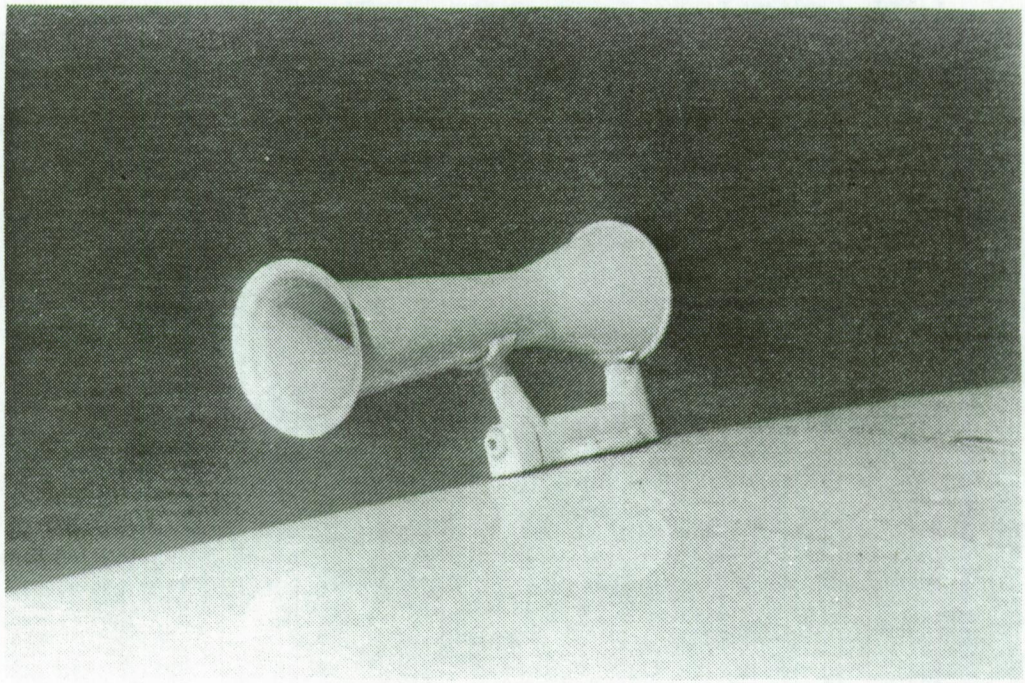

Figure 3.7: Venturi-effect based aspiration system for aerosol sampling.

3.2.4.4 Flow rate measurements

Since the aircraft is used for sampling at different heights, and thus under different atmospheric pressures, standard flow rate devices cannot be used because their performances are highly dependent on the ambient pressure. For the flow rate measurements of the Nuclepore and the Teflon filter a Brooks model 5811N thermal mass flow-meter was used in combination with a model 5851 pressure controller. In the range between 0 an 100 $l.min^{-1}$, an accuracy of 5% can be achieved with this apparatus.

3.2.5 Sampling of particulate matter with impactors

3.2.5.1 Berner impactor

For size-differentiated aerosol sampling, a nine stage low pressure cascade impactor (with cut-off diameters of 0.06, 0.125, 0.25, 0.5, 1.0, 2.0, 4.0, 8.0 and 16 μm) was used: the Berner LPI/0.06/30 (Berner and

Lurzer, 1980).

The use of low pressure results in a reduction of the frictional forces of the gas on the particles; the slip correction factor increases significantly for particles with size around 1 μm when the pressure is reduced. In addition, a reduction in pressure results in an increase in volume flow through the smaller jets and a correlated increase in inertial forces. Hence at lower pressures smaller particles are deposited in an impactor (Berner et al., 1979).

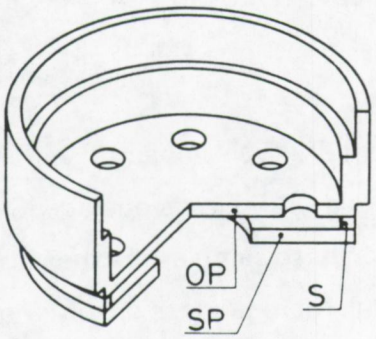

Figure 3.8: Single stage of the Berner impactor.
(OP = orifice plate, SP = stagnation plate and S = spacer)

A cross section of one impactor stage is represented in Figure 3.8. Besides the entrance stage, which has a single orifice in order to precipitate particles larger than 16 μm, each stage has several equally sized orifices arranged symmetrically around the centre of the stage. This arrangement ensures symmetric flow patterns and symmetric particle deposition. The aerosol jets coming from the orifices are deflected by the stagnation plate (SP), which has a large centered hole for the flow to pass to the next stage. This design inhibits that bounced-off particles are transferred into deposits of the subsequent stages. The distance between

the orifice and stagnation plates is made by a removable circular spacer (S). A critical orifice, which is placed behind the final impactor stage controls a constant flow rate of 30 $l.min^{-1}$.

The deposits are collected on 10 μm thick aluminum foils which are held in place by the spacer. If the foils are used uncoated, as was the case for all the sampling flights, particles may be lost from the first three stages. These particles will however not be found back on subsequent stages (Berner and Lurzer, 1980).

A flow rate of 30 $l.min^{-1}$ was maintained through the use of a high volume pump which was powered by the 24 V generator of the aircraft.

3.2.5.2 Battelle impactor

A single orifice Battelle type impactor with five stages (cut-off diameters of 4, 2, 1, 0.5 and 0.25 μm) is equipped with Formvar coated electron microscope grids. These samples are then analyzed with a single particle technique (Laser microprobe mass spectrometry, LMMS) in order to obtain information about sulphur and nitrogen speciation and about trace element concentrations in individual particles.

3.2.5.3 Quartz-Crystal Microbalance impactor

A Quartz-Crystal Microbalance (QCM) impactor is used for experimental determination of the total amount of suspended particulate material in the atmosphere and of the particle mass size-distribution. Particles are separated into 10 size classes. The cut-off diameters of the individual stages are: 25, 12.5, 6.4, 3.2, 1.6, 0.8, 0.4, 0.2, 0.1 and 0.05 μm.

Figure 3.9 shows a typical QCM impactor stage. Transmitted particles impact on a surface of a piezo electrical quartz crystal. Particle mass deposition results in a monotonic decrease in crystal frequency. The output signal from this sensor is compared with a second crystal that is shielded from particle deposition and acts as a reference crystal. The resulting beat frequency is monitored as a function of time. Differentiation

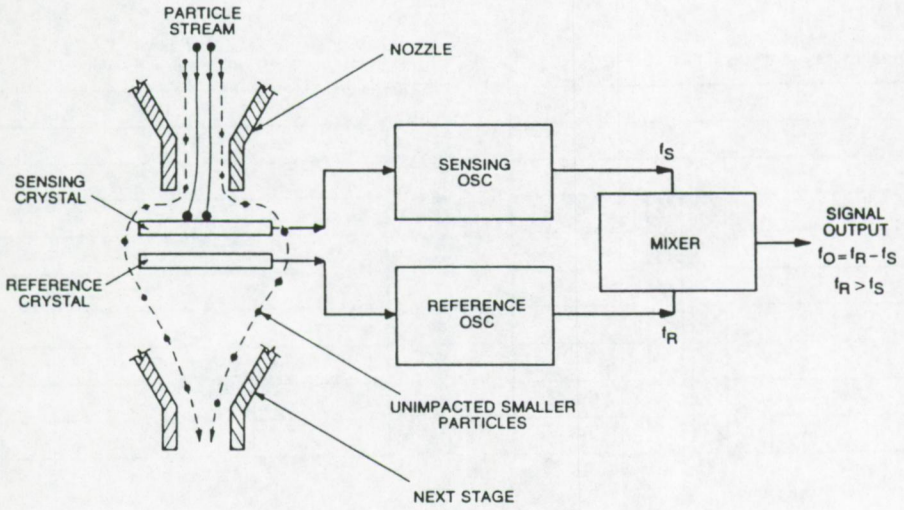

Figure 3.9: Single stage of a QCM impactor.

of the beat frequency gives particle mass concentration for the size class of interest. The stages have to be cleaned regularly as to avoid overloading and inaccurate measurements. According to the manufacturer's specifications, the QCM impactor can be used for particle mass distribution measurements when the total amount of suspended particulate matter lies between 10 $\mu g.m^{-3}$ and 60 $mg.m^{-3}$.

A number of test-measurements were carried out during Flight 11, on January 13, 1989. Sampling time was limited to 5 minutes in order to have relatively high time resolution. Although the total amount of suspended particulate matter was between 1.5 and 9.1 $\mu g.m^{-3}$, and thus beyond the manufacturer's limits, a number of interesting observations can be made on the eight samples collected during that flight. Figure 3.10 and Figure 3.11 show the measured particle mass size distributions of two sets of four samples.

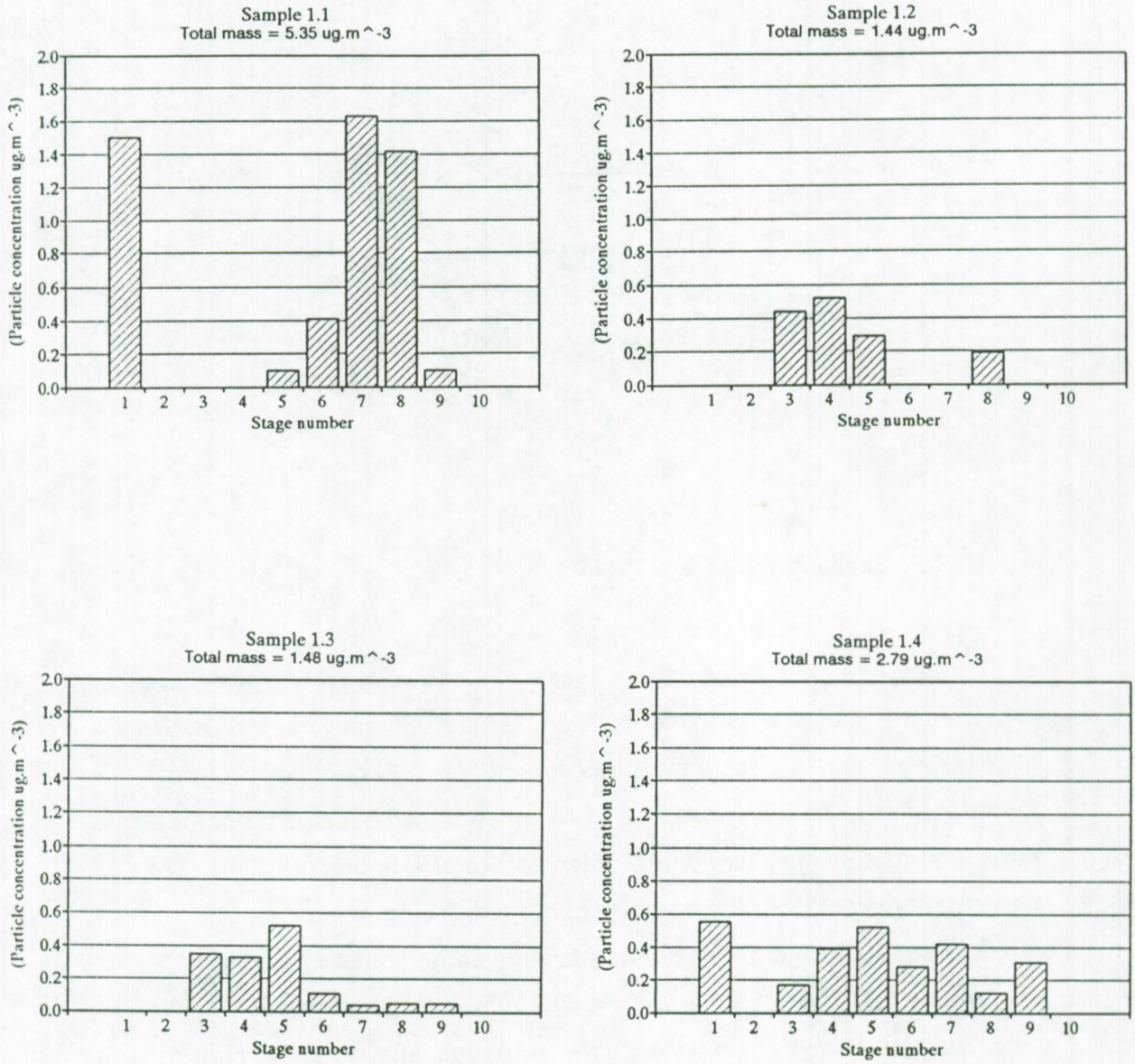

Figure 3.10: Mass size distributions of North Sea aerosol - sample set 1.

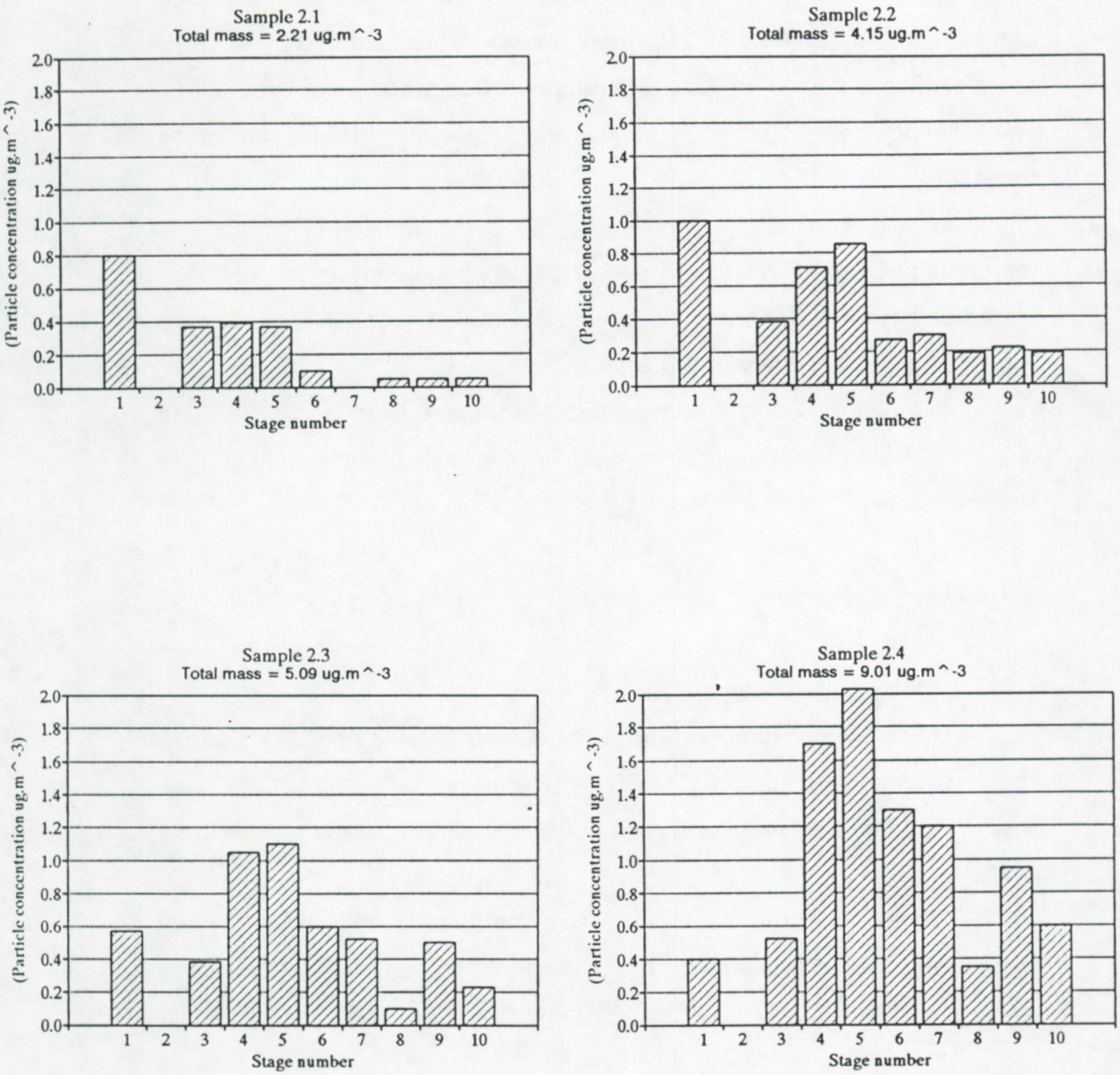

Figure 3.11: Mass size distributions of North Sea aerosols - sample set 2.

Stage 1 shows relatively high loadings in several samples, although particles with a diameter > 25 μm are unlikely to be sampled by the PSU sampler. Stage 2 gave erroneous results and was probably overloaded or badly cleaned before use. Blank measurements resulted also in high values for stage 2.

Of the eight samples collected, 5 have a maximum at stage 5 (particles between 1.6 and 3.2 μm), 2 have a maximum at stage 4 (particles between 3.2 and 6.4 μm) and 1 sample has maximum at stage 7 (particles between 0.4 and 0.8 μm).

Samples 6, 7 and 8 show a second maximum on stage 9 (0.1 to 0.2 μm) indicating the presence of a bimodal particle mass size-distribution.

3.2.6 Other equipment

3.2.6.1 Meteorological parameters

The ambient temperature is measured with a PT-100 thermo couple (Rosemount, model 102 E). Temperatures between -20 °C and +40 °C can be measured with an accuracy of 0.25 °C and a maximum resolution of 0.01 °C.

The dew point is measured with a Meteolabor A.G. model PT3-S device that has a measuring range from -30 °C to +40 °C with a resolution of 0.1 °C.

3.2.6.2 Navigational parameters

Velocity (true air speed) and height are measured with two pressure meters, a PDCR 10/2L and a PDCR 10/T for measurements between 0 and 1050 hPa and between 0 and 200 hPa, respectively.

The height above the ground can be measured with a King Radar Altimeter, model KRA 10/10a. A 5% accuracy is obtained for measurements between 20 and 2500 ft.

The use of a Doppler 91 sensor unit with a RNS 252 Navigation

compass (Racall) allows determination of the position with an accuracy of 0.1 nautical mile and measurement of the wind speed with an accuracy of 1 $m.s^{-1}$.

3.2.6.3 Data collection and transmittance

Three recorders (BBC model SEA430) with each three channels allow real time recording on paper of 9 parameters. A modified Olivetti PC model M21 with 5 1/4" diskette is used for the collection of all parameters with a frequency of 12 data-set collections per minute. If necessary, data-transmission to a ground station is possible with a HF radio-connection.

3.2.7 Flight conditions and flight scheme

All sampling flights were performed in the same way. Before take-off at Rotterdam and during transit to the Goeree platform (position 51°55'N, 03°40'E) all equipment is tested. One spiral track is performed at Goeree. During this spiral track, sulphur dioxide and ozone concentrations, as well as temperature and dew point are monitored in order to localize the temperature inversion height which is taken as the boundary of the mixing layer.

Then 6 horizontal tracks (25 minutes, 60 miles) at different heights are flown under the temperature inversion layer. The last track is performed at minimum altitude (10-15 m above sea level). All tracks are flown parallel to the wind direction in order to sample an air mass of which the history can be traced back as a well defined back trajectory (Figure 3.12).

SO_2 and O_3 are measured continuously. A Nuclepore and Teflon filter and a Battelle, rod and QCM impactor are sampled during each track. The Berner impactor is sampled continuously during the first five tracks.

A general sampling and analysis scheme is shown in Figure 3.13.

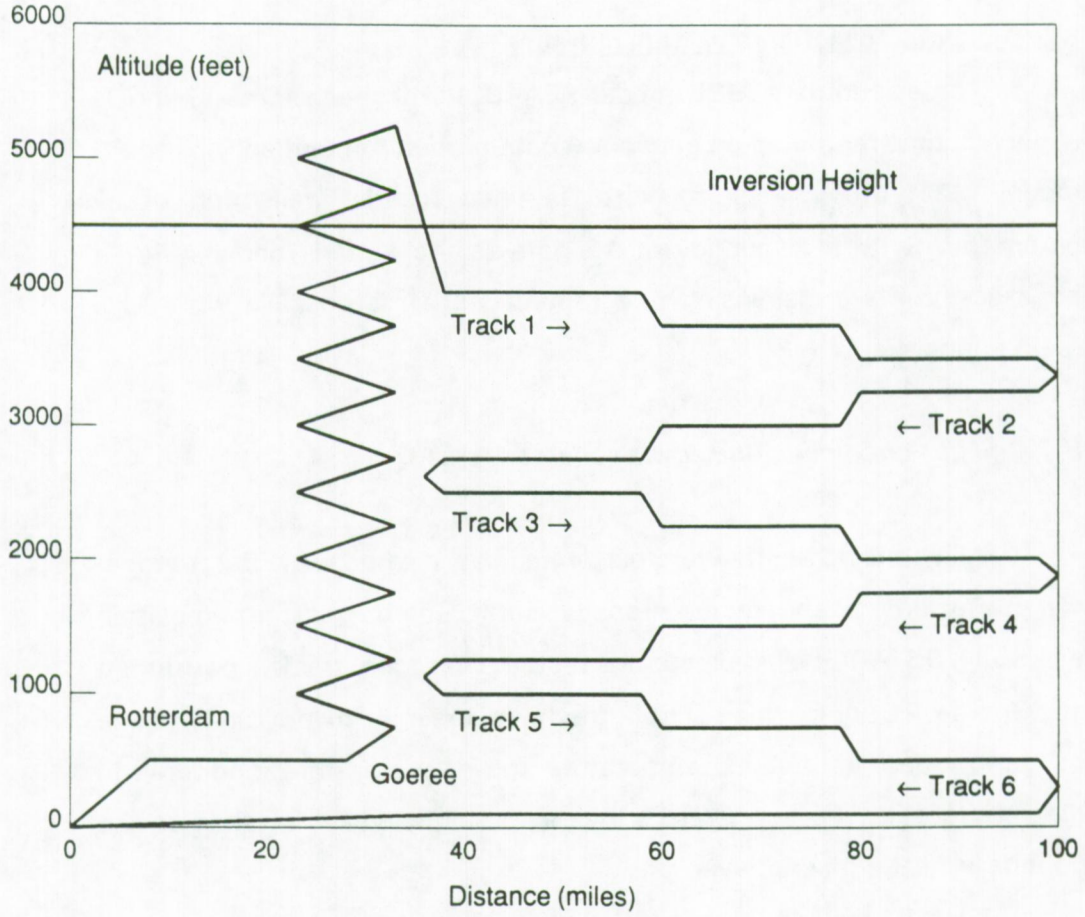

Figure 3.12: Flight scheme for an assumed temperature inversion height of 6000 feet (approximately 2000 m).

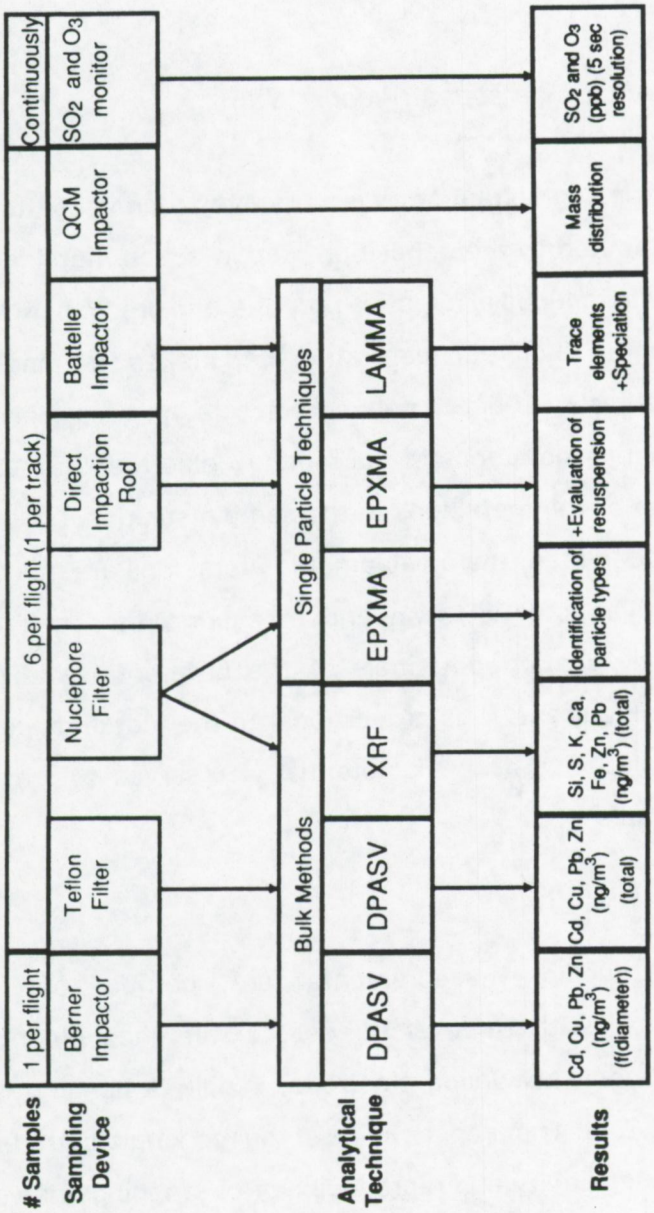

Figure 3.13: General sampling and analysis scheme.

3.3 Analytical technique: Differential pulse anodic stripping voltammetry (DPASV).

3.3.1 Theoretical considerations (Wang, 1985)

Anodic stripping voltammetry is a two-step technique. Its extreme sensitivity is attributed to the deposition step in which metal ions in the sample solution are reduced at negative potential and preconcentrated into a mercury electrode. The preconcentration step makes stripping analysis much more sensitive than direct polarographic techniques, because the concentration of the metal ions in the mercury electrode are 100-1000 higher than those of the metal ions in the sample solution.

In the second step, the amalgamated metal ions are measured by applying a positive potential scan and measuring the peak currents produced as the oxidation potentials of the different metal ions are reached. The peak current, i_p, is proportional to the metal concentration in the sample solution. The peak potential, E_p, serves to identify the metals in the sample.

3.3.1.1 Electrodes

Anodic stripping measurements are carried out in an electrochemical cell with three electrodes, a reference electrode, an auxiliary electrode and a working electrode, usually a hanging mercury drop electrode (HMDE). The proper choice of the working electrode is very important for the sensitivity and reproducibility of stripping analysis. The ideal working electrode should have a favourable electrochemical behaviour of the analytes of interest, a reproducible surface area and a low background current.

3.3.1.2 Oxygen removal

Dissolved oxygen interferes in stripping analysis through reduction to H_2O_2 and H_2O in acidic media and reduction to H_2O_2 and OH^- in neutral

or basic media. These reduction steps result in an increase in background current. In addition, oxygen may oxidize the metals in the electrode amalgam and hydroxyl ions can precipitate metal ions in the vicinity of the working electrode.

The method most frequently used for removing oxygen from a solution consists of bubbling an electro-inactive gas through the sample solution. Residual oxygen can be removed from nitrogen by bubbling through a vanadous chloride solution.

Following the purge time, nitrogen is still passed over the sample to maintain an oxygen-free atmosphere over the sample during further analysis.

3.3.1.3 The deposition step

In anodic stripping voltammetry, the metal ions of interest are reduced at a negative potential. At the mercury working electrode, the reaction is:

$$M^{n+} + ne^- \rightarrow M(Hg) \qquad (3.8)$$

The deposition potential imposed on the working electrode is chosen according to the species to be determined and is maintained for a deposition period depending on the analyte concentrations. This potential is usually several tenths of a volt more negative than the reversible potential calculated from the Nernst equation for the least easily reduced species to be determined. The formation of an amalgam depends mainly on the solubility of the metal in mercury.

Because of the hydrogen evolution background reaction that occurs at negative potentials, care must be taken not to apply very negative deposition potentials. As the acidity of the solution increases, a gradual loss in sensitivity for ions with negative peak potentials is observed.

For measurements in the ppb range, using the differential pulse mode, deposition times of 5 to 15 min are sufficient. The use of long deposition times may result in interferences because of formation of

intermetallic compounds or saturation of the mercury.

The deposition is usually facilitated by convective transport of the metal ions to the surface of the working electrode through solution stirring. For the deposition current at the hanging mercury drop electrode in a stirred solution, a semi-empirical equation has been derived (Wang, 1985):

$$i_L = knr_0^2 D^{2/3} C_b U^{1/2} + 4\pi r_0 nFDC_b \qquad (3.9)$$

where k is a constant, n is the number of electrons involved in the redox reaction, r_0 is the mercury drop radius, D is the diffusion coefficient of the ion, C_b is the concentration of the analyte, U is the stirring speed and F is the Faraday constant.

As the forced convection is stopped at the end of the deposition period, a uniform concentration distribution is established in about 30 s when using a HMDE.

The rest period also ensures that the subsequent stripping step is performed in a solution where convection is absent. During the rest period, deposition through diffusional transport is continued at the working electrode.

3.3.1.4 The stripping step

The stripping step consists of scanning the potential anodically toward positive potentials, linearly, or in another potential-time waveform. When the potential reaches the standard potential of a metal-metal-ion couple, that particular metal is reoxidized into solution and a current is flowing:

$$M(Hg) \rightarrow M^{n+} + ne^- \qquad (3.10)$$

The resulting voltammogram (measured current as a function of applied potential) recorded during the stripping step provides the analytical information of interest. The stripping current is proportional to the concentration of the metal in or on the working electrode, and therefore, to its concentration in the sample solution. Peak potentials serve to identify the different metal ions in the sample.

3.3.1.5 Background current

In linear-scan anodic stripping voltammetry, the total current is given by the sum of the stripping peak current and the background current. The detection limit and the accuracy are determined by the uncertainty in measuring the peak current and thus the background current. The background current has one component associated with redox reactions of impurities, decomposition of the electrolyte or solvent and reaction of the electrode itself. Another component, that is the most important, is called the charging current. At the electrode-solution interface a separation of charges takes place resulting in an electrical double-layer. When the potential of the working electrode is changed, a current must flow to charge or discharge the electrical double-layer that acts as a capacitor.

3.3.1.6 Differential pulse mode

The most widely used stripping mode is differential pulse voltammetry, designed to compensate the for the charging background current. In the differential pulse stripping mode, pulses of equal amplitude are superimposed on an anodic potential scan (Figure 3.14).

The currents are sampled twice: prior to the pulse application and just before the pulse termination. The first current is subtracted automatically from the second one and the difference is plotted as a function of the potential.

When the potential is suddenly applied, the total current in the system increases because of the resultant increase in faradaic and

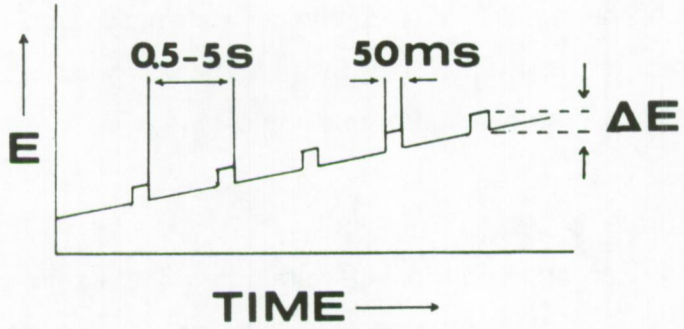

Figure 3.14: Anodic potential scan with superimposed pulses (Wang, 1985).

charging currents. The induced charging current decays more rapidly than does the faradaic current. Therefore, the sampled current, at the end of the pulse life, is mostly faradaic. Because the charging current is essentially the same at the two sampling points, the difference between the readings is attributed mainly to the faradaic reaction.

An additional gain in overall sensitivity occurs because some of the metal ions stripped from the electrode during the pulse are re-reduced into the electrode during the waiting period between the pulses. Therefore, the same material is stripped and re-reduced many times and repetitive contributions are made to the measured current. The gain in sensitivity over linear-scan voltammetry amounts up to a factor of 1000 when using a HMD electrode.

Lund and Onshus (1976) derived a simplified equation for the differential pulse stripping peak current at a hanging mercury drop electrode:

$$\Delta i_p = knr\Delta EU^{1/2}t_dC_b \qquad (3.11)$$

where ΔE is the pulse amplitude.

3.3.2 Sample preparation

3.3.2.1 Extraction method

Colovos et al. (1973) reported on the determination of trace amounts of Zn, Cd, Pb and Cu in airborne particulate matter. The destruction of the organic collection filter and of the sample is achieved by a low-temperature ashing procedure. Millipore filters are impregnated with 0.1 M potassium sulphate solution, before ashing at a temperature of 50-100 °C. Conventional muffle furnace dry ashing proved to be unreliable because of the losses due to the volatility of certain elements such as Pb, Cd and Zn.

MacLead and Lee (1973) also used a low temperature asher for sample destruction. The residue was dissolved in 1:1 perchloric-nitric acid solution. Recovery studies indicated that with the followed procedure 73 to 93% of the Cd was recovered, >81% of the Pb and >87% of the Cu.

Janssens and Dams (1973; 1974) described a procedure for particulate matter removal from a Whatman 41 cellulose filter by means of an ultrasonic treatment with an eluting acid. This procedure has the additional advantage that impurity levels of the filter itself are less critical. Filter sections were extracted ultrasonically with different concentrations of nitric acid. A nitric acid solution of 0.1 M resulted in the highest net readings during atomic absorption analysis. A single extraction of 5 min resulted in an average recovery of 88%, while a double extraction yielded 99% recovery. It was concluded that ultrasonic removal of Cd from filters in 0.1 M HNO_3 is a quantitative elution method (Janssens and Dams, 1974), as it was proven to be for Pb also (Janssens and Dams, 1973).

For our Teflon filter samples, the extraction consisted of a single 60 minute ultrasonic extraction by placing the Teflon filter in 10 ml ultrapure water, prepared by a Millipore Milli-Q purification unit, and acidifying with 70 μl of Merck Suprapure concentrated nitric acid.

3.3.3.2 Evaluation of the extraction method

Ten airborne particulate matter samples were analyzed with proton induced X-ray emission (PIXE) and with DPASV after extraction with 0.1 M nitric acid. The recovery rate ranged from 80 to 107% for Cu with an average of 82%, from 18 to 64% for Pb and from 12 to 90% for Zn. The recovery rate for Pb and Zn is very variable, which is in contradiction with the data from Janssens and Dams (1973) and the observations made by Losno et al. (1988).

NBS standards of fly-ash particles were analyzed for Cd with DPASV after extraction with 0.1 M nitric acid. 85 to 93% of the Cd was recovered in this way, with an average of 89%.

Individual DPASV results for Cd an Cu are corrected with a factor 1/0.89 and 1/0.82, respectively, while Pb and Zn results are not used for further calculation of the total Pb and Zn concentration in the atmosphere. Instead, the Pb and Zn concentrations as obtained by PIXE analysis are used. In PIXE analysis, the samples are irradiated with a 2.4 MeV proton beam, supplied by the compact isochronous cyclotron at the University of Ghent. No matrix corrections were carried out in view of the light sample load. Full details about PIXE can be found elsewhere (Maenhaut, 1989).

3.3.3 Analytical procedure

Cd, Cu, Pb and Zn determinations were carried out with a Model 264 polarographic analyzer/ stripping voltammeter (EG&G Princeton Applied Research, Princeton, NJ, USA) using a Model 303 static mercury drop electrode (EG&G Princeton Applied Research, Princeton, NJ, USA).

The 10 ml extract is placed in a 25 ml teflon electrochemical cell. Oxygen is removed by bubbling nitrogen through the sample solution during 4 minutes. Next, trace metals are deposited at -1.0 V into the mercury electrode using a deposition time of 250 s. After 30 s of equilibration time, a positive potential scan up to +0.05 V (5 $mV.s^{-1}$) is applied. Quantification was done by standard addition using 2 spikes for

each element. Calculation of the concentration was based on measurement of the peak heights.

For the determination of Zn, the sample was neutralized to pH 4.0 by adding 1500 μl of 0.1 M NaAc. Then, deposition of Zn (and other trace metals) was performed at -1.1 V.

The average relative standard deviation per measurement appeared to be between 10 and 15% for the overall analytical procedure.

Blank levels, measured by extracting blank Teflon filters and measuring them in an identical way as the samples were measured, were 0.01 ± 0.01 ppb for Cd, 0.34 ± 0.08 ppb for Pb, 0.39 ± 0.09 ppb for Cu and 0.46 ± 0.15 ppb for Zn. For the aluminum impactor samples, blank levels were 0.03 ± 0.02 ppb for Cd, 0.37 ± 0.12 ppb for Pb, 1.47 ± 0.70 ppb for Cu and 2.07 ± 0.85 ppb for Zn.

3.4 Results of individual flights: total atmospheric concentrations of Cd, Cu, Pb and Zn.

3.4.1 Meteorological information

The use of wind direction and wind speed data alone is not sufficient for characterization of the individual samples. Backward air mass trajectories are necessary for identification of the different sources that contribute to trace metal concentrations of the samples.

For each flight four 36 hour back trajectories were calculated for four different levels (1000, 900, 850 and 700 mbar), for two sampling points (the Goeree platform and a second point depending on the flight direction) and for two sampling times (at the beginning and at the end of each sampling flight). The KNMI (De Bilt, The Netherlands) calculated back trajectories were interpolated to yield trajectories for the six sampling flight levels (Rojas, 1990). Figures 3.15 and 3.16 show the back trajectories for the different sampling flights at 1000 mbar (sea level).

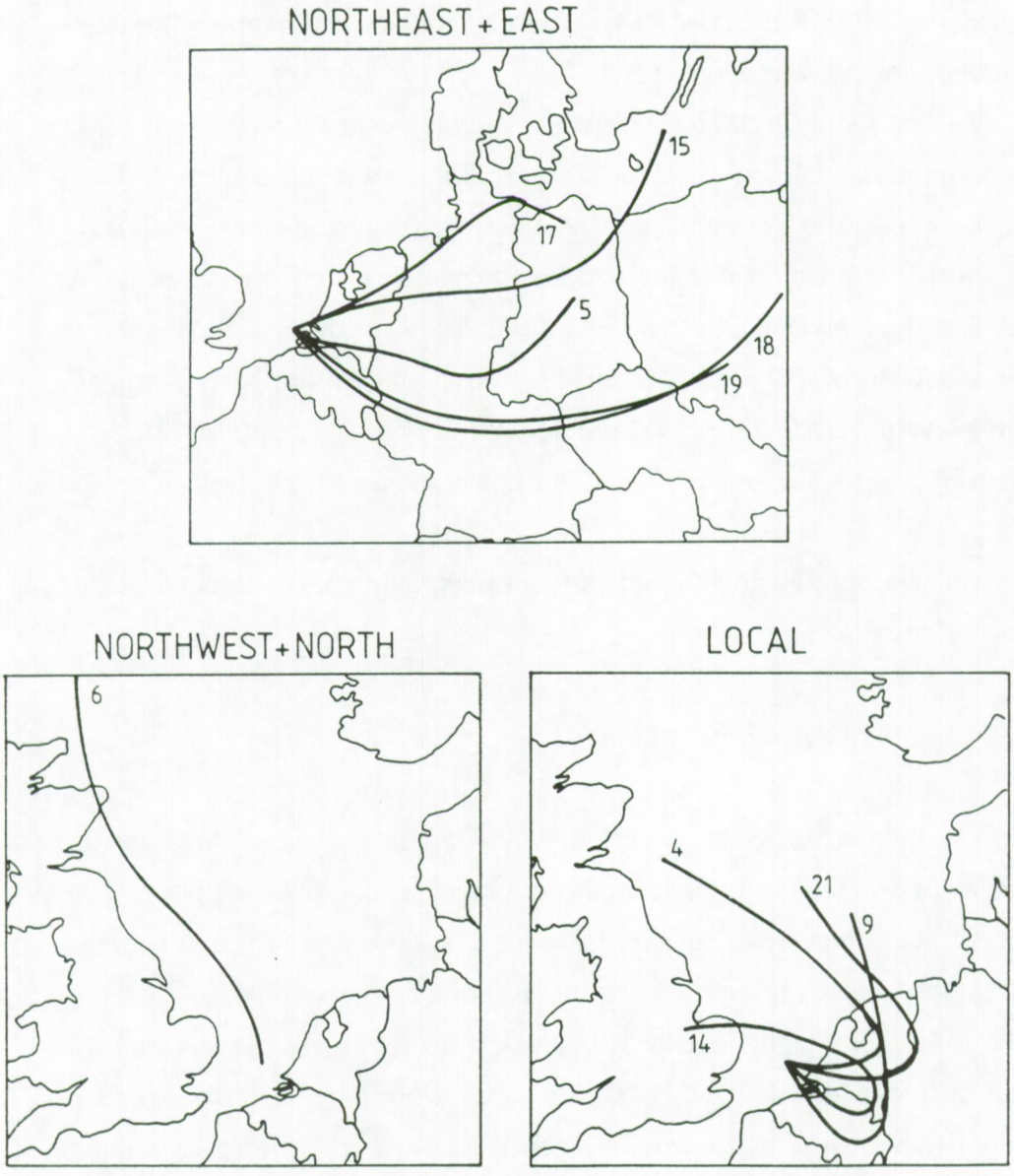

Figure 3.15: 1000 mbar back-trajectories for flights of the northeast + east, the northwest + north and the local or variable sector. The numbers refer to the flight numbers.

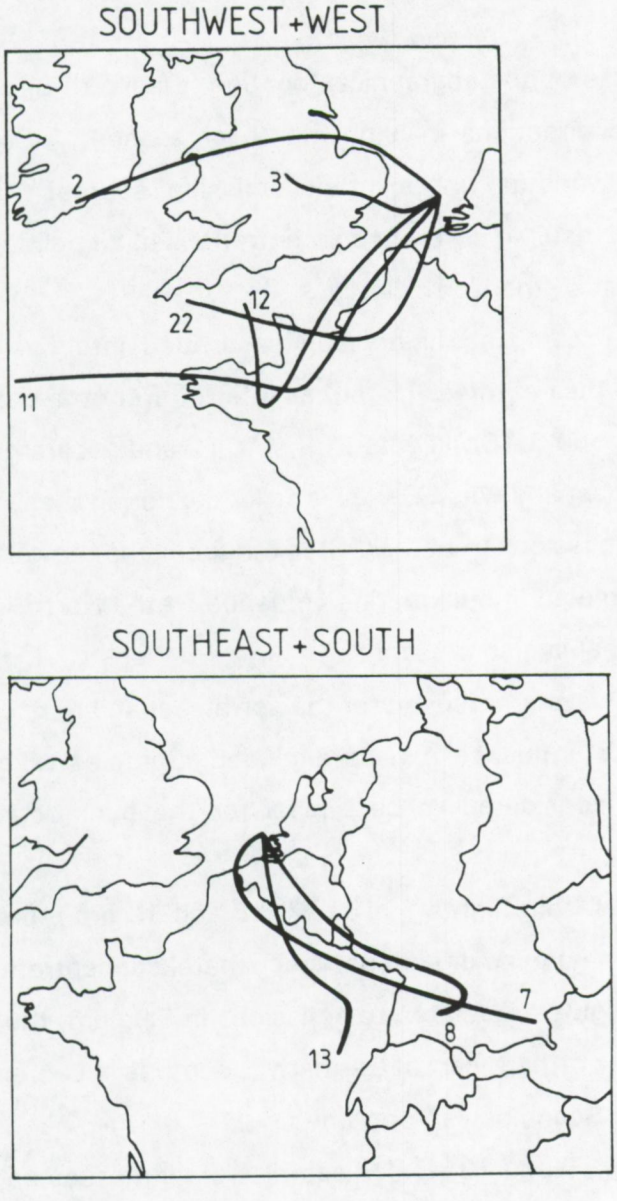

Figure 3.16: 1000 mbar back-trajectories for flights of the southwest + west and the southeast + south sector. The numbers refer to the flight numbers.

3.4.2 Concentrations as a function of wind direction

Because of its geographical location, the North Sea is affected by variable wind directions in each month or season. As a result of the geographical variation in pollutant emission sources, different wind directions will result in different concentrations of air pollutants above the Southern Bight of the North Sea.

The 18 sampling flights can be divided into five wind sectors depending on their air-mass history as inferred from the back-trajectories (Figures 3.15 and 3.16). Flights 2, 3, 11, 12 and 22 are gathered in the sector southwest and west. Samples collected during these flights include influence by emissions from the United Kingdom and the northeastern part of France. Some additional marine influence by the North Atlantic Ocean and the Channel is also present.

Flight 6 is characteristic for the northwest and north sector, where any continental influence can be excluded. Samples taken during this flight can be considered to be typical for the background North Sea atmosphere.

Samples from flights 5, 15, 17, 18 and 19 are representative for northeast and east wind directions. Trace metal concentrations measured during these flights are related to emissions in Belgium, the Netherlands, the central and northern part of Germany, countries in Eastern Europe, the Baltic Sea and Scandinavian countries.

Flights 7, 8 and 13 yielded samples of air masses originating from the south-east and the south sector. Emissions in Belgium, the northern part of France and the southern part of Germany are responsible for the concentrations of heavy metals measured during these flights.

Finally, samples collected during flights 4, 9, 14 and 21 were obtained under low wind speed and variable wind direction conditions.

Table 3.2 lists the average Cd, Cu, Pb and Zn concentrations below the temperature inversion layer for the different wind sectors. A wind-direction weighted average concentration can be calculated by using

the wind direction distribution data as reported by Hohn (1973) for the southern part of the North Sea.

The highest concentrations are found for the sector south to south-east for Cd, Pb and Zn. The average atmospheric trace metal concentrations for this sector are a factor of 2 higher than the average concentrations for all sectors, except for Cu. Cu concentrations are higher for the west to southwest sector, but this is merely the result of one outlier (more than 50 $ng.m^{-3}$ for flight 22).

The lowest concentrations are found in sector northwest to north. Actual trace metal levels for this wind sector may be even lower as stated in Table 3.2 because the measured concentrations were close to or even less than the analytical detection limit.

Average Pb and Zn concentrations are quite similar for east, west and variable wind sectors. Within each wind-sector, the heavy metal concentrations may vary quite significantly. It is obvious that although two flights can be classified in the same wind sector, there may still exist important differences in the air mass history. Small changes in the backward air-mass trajectories may have a large influence on the atmospheric concentration, since some of the more important emission sources such as industrial areas can be concentrated geographically.

Furthermore, it should be stressed that not only the wind direction has an important influence on the final atmospheric concentration of trace metals above the Southern Bight of the North Sea. Other meteorological parameters such as the atmospheric stability and the height of the mixing layer may largely influence trace metal levels in air.

Table 3.2:
Average concentrations ($ng.m^{-3}$) as a function of wind direction

Sector SOUTHWEST-WEST	Cd	Cu	Pb	Zn
Flight 2	2.8	19.8	40	34
Flight 3	3.2	20.9	72	74
Flight 11	0.6	1.1	42	48
Flight 12	0.5	3.0	69	54
Flight 22	4.1	55.6	38	56
Sector NORTHWEST-NORTH				
Flight 6	0.2	1.1	7	2
Sector NORTHEAST-EAST				
Flight 5	5.5		55	97
Flight 15	0.2	1.7	24	48
Flight 17	0.7	8.2	69	87
Flight 18	0.4	7.4	49	61
Flight 19	0.3	1.7	50	75
Sector SOUTHEAST-SOUTH				
Flight 7	2.3	16.5	114	158
Flight 8	0.3	9.4	107	151
Flight 13	8.8	23.9	149	144
Sector VARIABLE				
Flight 4	0.2	9.1	16	16
Flight 9	1.1	23.1	85	109
Flight 14	2.3	8.1	68	56
Flight 21	0.6	16.2	49	60
Averages				
SOUTHWEST-SOUTH	2.2	20.1	52	53
NORTHWEST-NORTH	0.2	1.1	7	2
NORTHEAST-EAST	1.4	4.7	49	74
SOUTHEAST-SOUTH	3.8	16.6	123	151
VARIABLE	1.1	14.1	55	60
ALL SECTORS	2.1	14.3	61	73

3.4.3 Concentrations as a function of altitude

3.4.3.1 Concentrations above and under the temperature inversion layer

Several tracks were flown just above the temperature inversion layer. These include track 1 and 2 of flight 3, track 1 of flight 5, track 1 of flight 8, track 1, 2, 3 and 4 of flight 9, track 1, 2, 3 and 4 of flight 11, track 1, 2 and 3 of flight 12 and track 1, 2, 3 and 4 of flight 19. Table 3.3 compares the average concentrations above and under the temperature inversion layer.

Table 3.3:

Average concentrations in $ng.m^{-3}$ above and under the temperature inversion layer (T.I.L.).

	Cd	Cu	Pb	Zn
Above T.I.L.	0.4	8.8	16	16
Under T.I.L.	2.1	14.3	61	73

The concentration above the temperature inversion layer is clearly lower than the concentration under the temperature inversion layer: a factor of 5 for Cd and Zn, a factor of 4 for Pb and a factor of 2 for Cu. In some individual cases, the observed differences are not so important. This can be explained by the fact that the height of the temperature inversion layer and the height of the mixing layer are not necessarily located at the same altitude. The mixing height may be somewhat higher than the temperature inversion layer as a function of the temperature difference between the stack-emitted air parcels and the ambient air.

3.4.3.2 General concentration profiles

If all samples from all flights are divided into 10 classes of altitude (0-100m, 100-200m, 200-400m, 400-600m, 600-800m, 800-1000m, 1000-1200m, 1200-1400 m, 1400-1800m and 1800-2700 m), and an average concentration is calculated for each altitude-class, then a general concentration profile can be calculated (Figure 3.17 and Figure 3.18)

The high value for the Cu concentration between 1200 and 1400 m is due to one outlier concentration of 189 $ng.m^{-3}$. Discarding this one value, the highest concentrations are found between 100 and 200 m for all four elements.

3.4.3.3 Concentration profiles from individual flights

In individual flights, concentration profiles are not consistently the same. Variations can partly be explained by variation of the air mass back-trajectories with altitude. Samples collected at different heights may have different origins and will yield different concentrations. The environmental lapse rate and the atmospheric stability can also have an effect on the vertical distribution of pollutants in the mixing layer.

The Cd profile of flight 13 shows high concentrations at 120, 200, 240 and 270 m, while the levels at 15 and 80 m are much lower. During flight 14 a sharp maximum Cd concentration is found at 60 m. The Cd profile of flight 18 is quite uniform except for the altitude of 1120 m, where the concentration is a factor of two higher than at all other altitudes (Figure 3.19).

Cu concentration profiles also show high variability from flight to flight. A reasonably uniform profile with a maximum at 480 m is found during flight 7. A much sharper maximum is found during flight 13 at 200 m altitude. Cu concentartions during flight 17 are low at the lowest tracks (15 and 400 m). Then a maximum is found at track 3 (900 m) while at

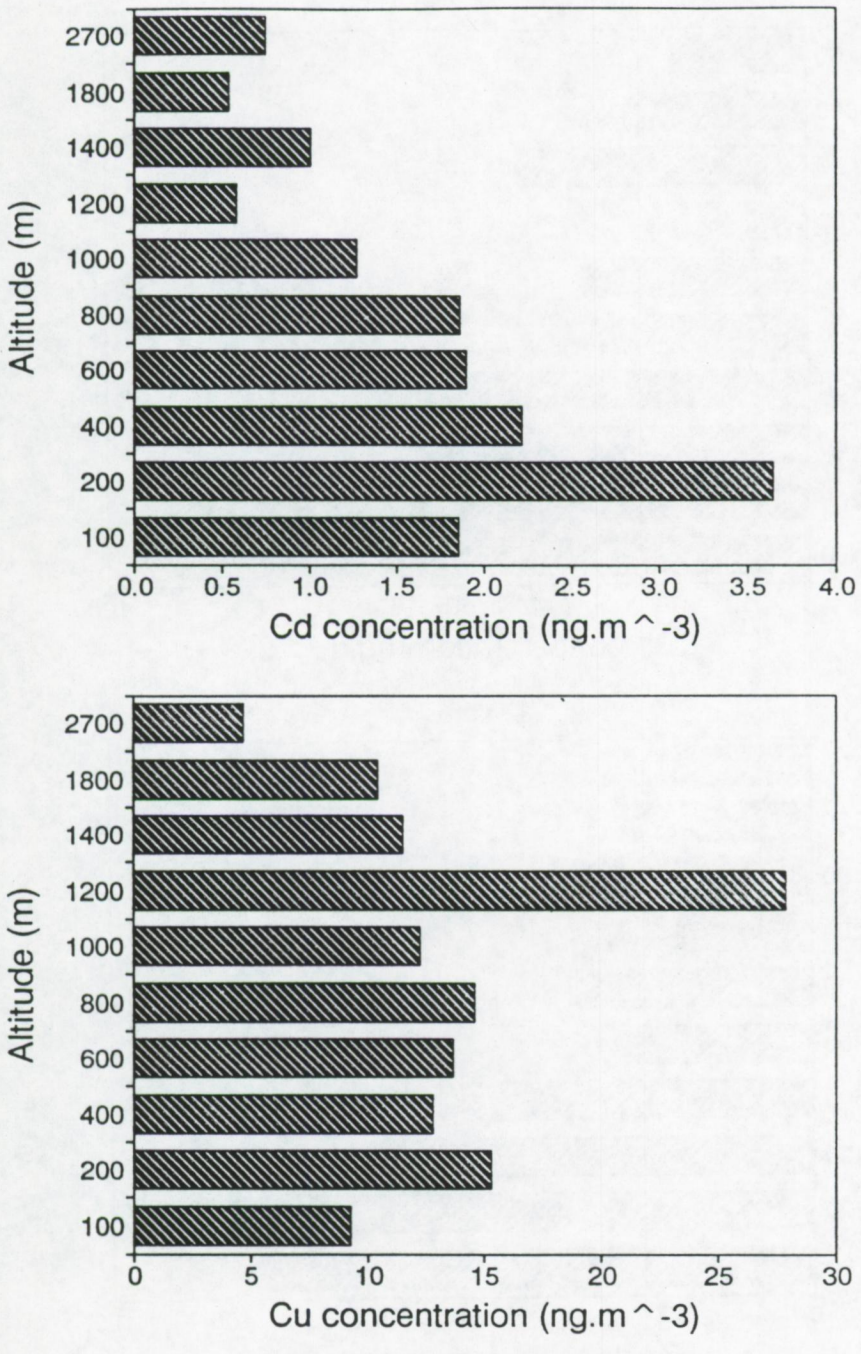

Figure 3.17: Cd and Cu concentration as a function of altitude (all samples).

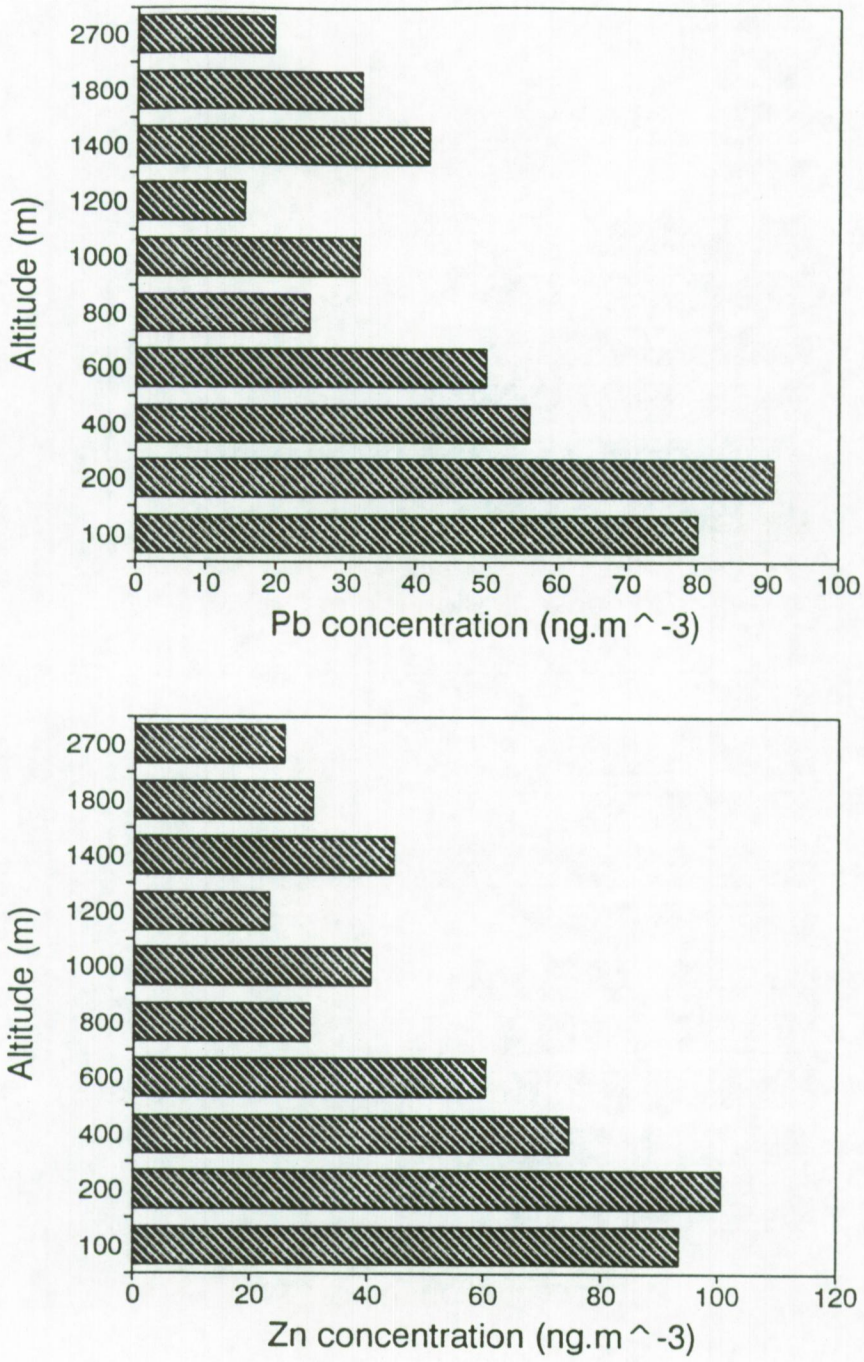

Figure 3.18: Pb and Zn concentration as a function of altitude (all samples).

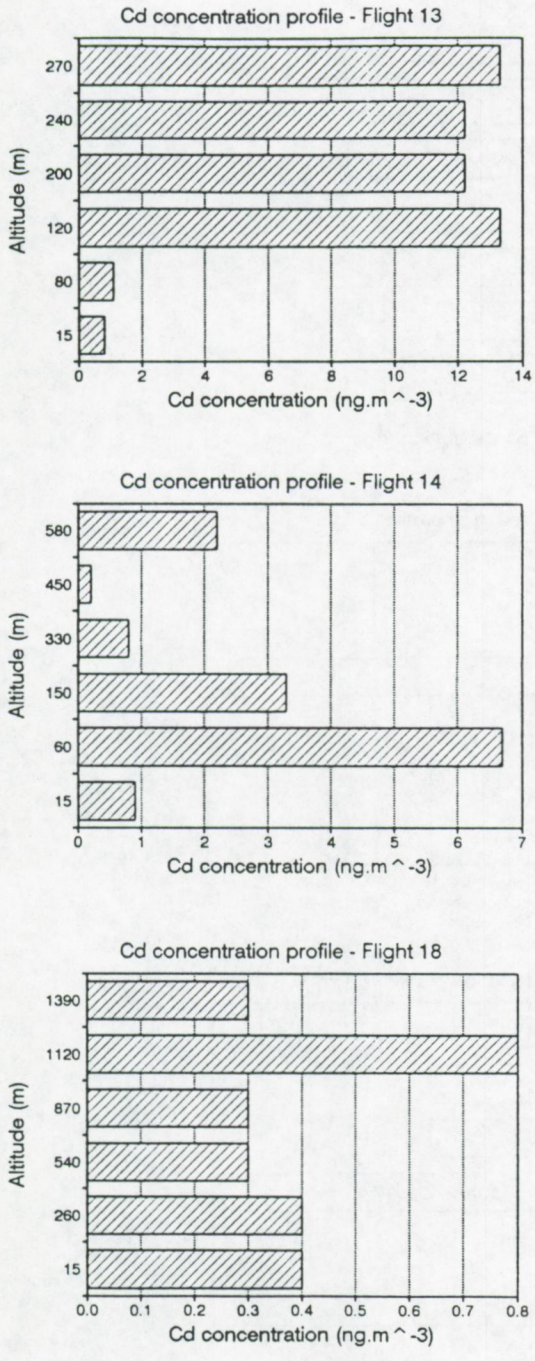

Figure 3.19: Cd concentration profiles of flights 13, 14 and 18.

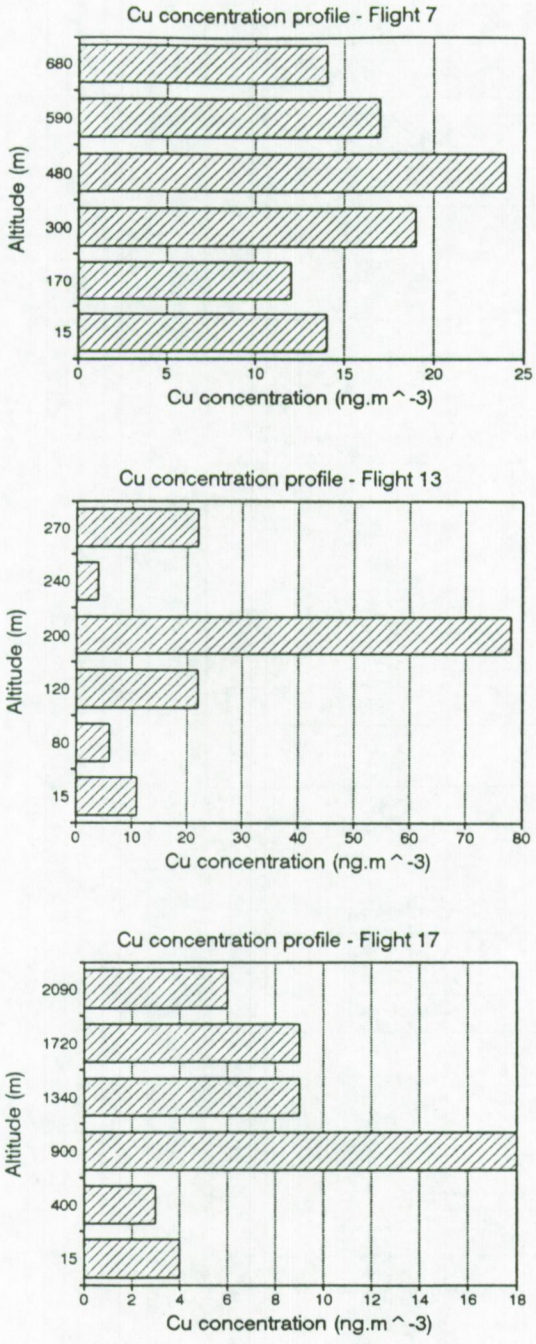

Figure 3.20: Cu concentration prodiles of flights 7, 13 and 17.

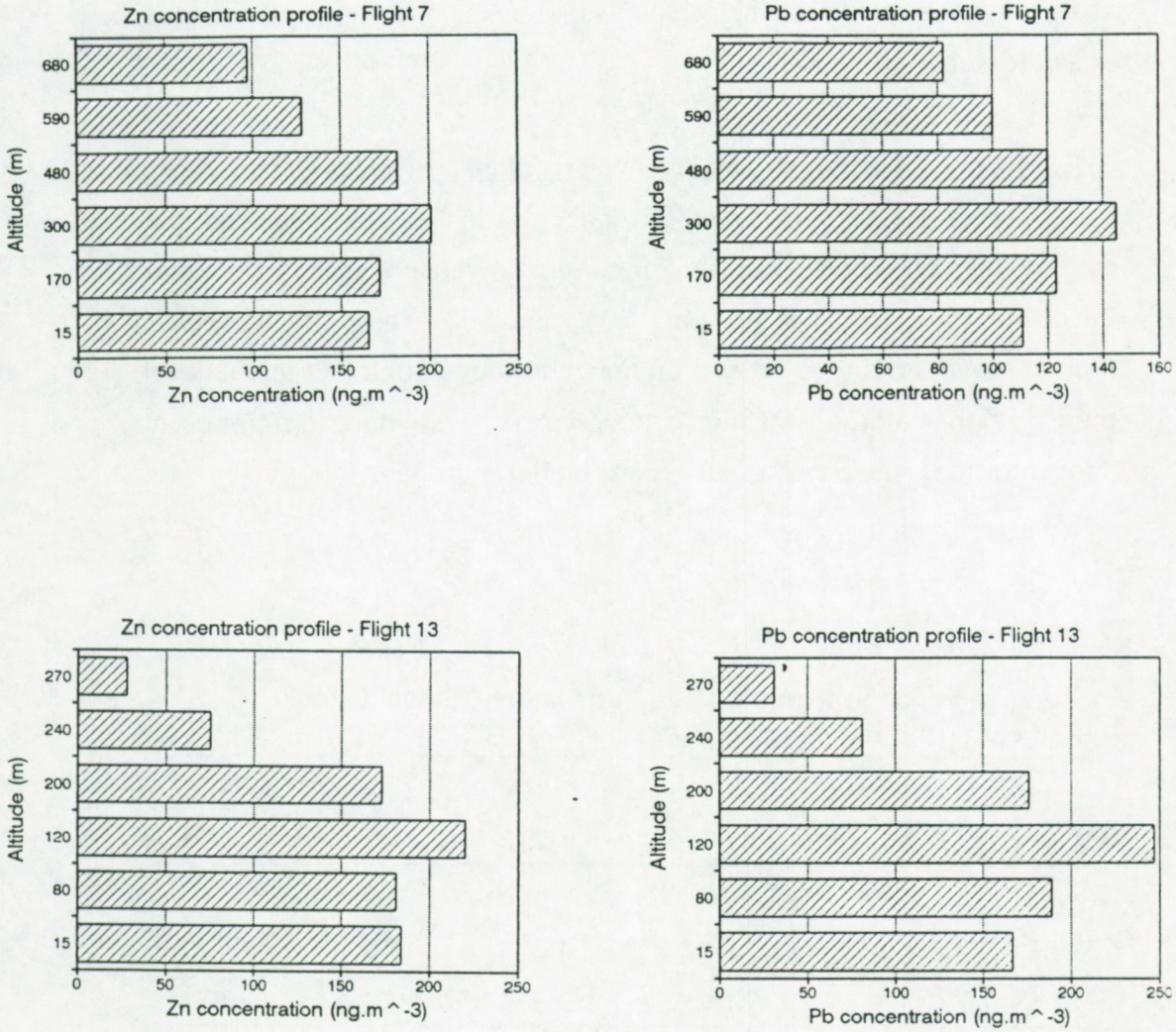

Figure 3.21: Zn and Pb concentration profiles of flights 7 and 13.

higher altitudes, the concentrations decrease again (Figure 3.20). Zn and Pb profiles (Figure 3.21) are very similar for flights 7 and 13 (both southeast sector). In both flights, the concentration increases from sealevel to the middle of the temperature inversion layer and decreases again at higher altitudes.

3.4.3.4 Concentrations at sea level versus higher altitudes

Table 3.4 lists the average concentration at sea level and the average concentration under the temperature inversion layer. The Pb and Zn concentrations at sea level are 20% and 15%, respectively, higher than at higher altitudes. Cd and Cu concentrations are lower at sea level than at higher altitudes. There is however no systematic difference in concentrations close to the sea and at higher altitudes.

Table 3.4:

Average concentrations in $ng.m^{-3}$ at sea level (lowest track) and under the temperature inversion layer (T.I.L.).

	Cd	Cu	Pb	Zn
Under T.I.L.	2.1	14.3	61	73
Sea level	1.3	9.8	73	83

The possible contribution of the sea to trace metal levels at the lower altitudes is probably insignificant for the Southern Bight of the North Sea. Flight 6 was performed under northwest wind. The aerosol particles collected during this flight could not come from any pollution source. Therefore, trace metal concentrations measured under these conditions could be attributed to only one source, namely the sea itself.

Samples taken during flight 6 yield concentrations below the detection limit for all elements for all flight levels. Also at the sea level, no trace metals were detected although the samples were collected at a relatively high wind speed and thus sea spray formation was surely present. It is therefore clear that in an area such as the Southern Bight of the North Sea, the contribution of the sea as a source of trace metals in the atmosphere is small compared to other, continental, sources.

3.4.4 Comparison with ship-based measurements

Table 3.5 compares the aircraft-based measurements versus ship-based measurements. Although the samples were collected in different periods (1984-1988 for the ship and 1988-1989 for the aircraft), they were collected in the same area and with comparable equipment. Reasonable agreement can be found between both data sets.

Table 3.5:

Aircraft-based versus ship-based measurements.
Concentrations in $ng.m^{-3}$.

	Cu	Pb	Zn
R/V Belgica:			
North Sea	5.5	41	55
Southern Bight	9.2	77	110
PH-ECO:			
Mixing layer (under T.I.L.)	14.3	61	73
Sea level (lowest track)	9.8	73	83

3.5 Atmospheric Cd, Cu, Pb and Zn concentrations as a function of particle size.

Impactor samples (each one collected between the start of track 1 and the end of track 5 with a total sampling volume of 4.5 m^3) from 11 flights were analyzed with DPASV for Cd, Cu, Pb and Zn. Table 3.6 and Table 3.7 list the individual results for all impactors. For Cd, Cu and Zn a large fraction of the measurements yielded concentrations below the analytical detection limit of the used technique: 67% for Cd, 59% for Cu and 60% for Zn.

Figures 3.22 and 3.23 show the average size distribution of Cd, Cu, Pb and Zn for two separate calculation methods: values below the detection limit are replaced by zero on one hand and by the detection limit itself on the other hand. Because of the significant amount of missing values, there is a large uncertainty for the Cd, Cu and Zn distributions. The Zn size distribution shows a maximum for stage 3 (4 to 8 μm). The average Cd size distribution has a first maximum at the lowest size range (0.06 to 0.125 μm) and a second for particles between 8 and 16 μm. The average Cu distribution has also two maxima, at stage 8 (0.125 to 0.25 μm) and at stage 1 (>16 μm).

The average Pb size distribution has lower uncertainties (except for stage 1) than the other elements. It has a clear bimodal structure with a first maximum at stage 7 (particles between 0.25 and 0.5 μm) and a second maximum at stage 2 (particles between 8 and 16 μm).

Pb size distributions vary from flight to flight, but some general features are apparent (Figure 3.24). The size distributions of flight 8 and flight 12 show a clear bimodal structure, while the Pb distribution from flight 11 is unimodal. Flight 15 yielded an intermediate form between a unimodal and a bimodal one.

Recent size distribution measurements performed by Steiger et al. (1989) on a platform in the North Sea indicated the occurrence of different Pb distributions, both unimodal and bimodal ones.

Table 3.6a:
Size-differentiated concentrations of Cd in $ng.m^{-3}$

Stage (μm)	0.060	0.125	0.25	0.50	1	2	4	8	16
Flight number									
5	0.1	0.3	0.2	<0.1	0.1	<0.1	0.3	-	<0.1
6	0.1	<0.1	<0.1	<0.1	<0.1	<0.1	0.2	<0.1	<0.1
8	0.7	<0.1	0.7	<0.1	<0.1	0.4	0.5	1.0	0.2
9	-	0.3	<0.1	<0.1	<0.1	<0.1	0.1	0.2	<0.1
11	-	<0.1	<0.1	<0.1	<0.1	<0.1	<0.1	2.0	0.7
12	-	<0.1	0.1	0.1	1.3	<0.1	0.2	0.1	<0.1
14	<0.1	<0.1	<0.1	<0.1	<0.1	<0.1	<0.1	<0.1	0.1
15	<0.1	<0.1	<0.1	0.1	<0.1	<0.1	<0.1	<0.1	<0.1
17	0.1	<0.1	<0.1	0.1	<0.1	<0.1	<0.1	0.1	<0.1
18	1.7	<0.1	<0.1	<0.1	0.2	<0.1	<0.1	0.1	<0.1
19	<0.1	<0.1	<0.1	<0.1	0.1	<0.1	<0.1	<0.1	<0.1

Table 3.6b:
Size-differentiated concentrations of Cu in $ng.m^{-3}$

Stage (μm)	0.060	0.125	0.25	0.50	1	2	4	8	16
Flight number									
5	<2	9	<2	<2	4	<2	<2	-	<2
6	7	3	5	<2	<2	18	18	8	2
8	46	70	2	<2	2	3	4	12	7
9	-	6	<2	3	<2	<2	<2	<2	70
11	-	<2	<2	<2	<2	<2	<2	<2	10
12	-	11	<2	<2	15	6	5	<2	<2
14	3	7	4	<2	<2	<2	<2	<2	4
15	<2	<2	4	7	6	<2	4	3	<2
17	<2	<2	<2	<2	<2	4	<2	<2	<2
18	<2	<2	<2	<2	6	11	<2	<2	<2
19	<2	<2	<2	<2	4	9	3	<2	<2

Table 3.7a:
Size-differentiated concentrations of Pb in $ng.m^{-3}$

Stage (μm)	0.060	0.125	0.25	0.50	1	2	4	8	16
Flight number									
5	2	<2	4	4	<2	7	8	-	9
6	2	<2	2	<2	2	4	2	3	<2
8	2	2	24	13	<2	3	7	10	<2
9	-	34	10	9	3	<2	<2	8	<2
11	-	3	9	14	7	3	<2	<2	<2
12	-	9	11	31	7	<2	15	16	6
14	9	10	5	5	2	2	2	4	<2
15	6	20	6	4	3	4	5	7	2
17	4	2	<2	<2	<2	<2	<2	<2	<2
18	3	3	<2	<2	2	2	2	<2	4
19	<2	14	32	3	<2	<2	4	<2	<2

Table 3.7b:
Size-differentiated concentrations of Zn in $ng.m^{-3}$

Stage (μm)	0.060	0.125	0.25	0.50	1	2	4	8	16
Flight number									
5	<6	9	<6	14	<6	14	<6	-	17
6	22	<6	18	<6	<6	20	25	<6	<6
8	<6	<6	<6	<6	12	16	20	21	12
9	-	<6	<6	<6	<6	<6	22	8	<6
11	-	<6	<6	<6	<6	<6	40	16	14
12	-	13	<6	<6	<6	<6	10	<6	<6
14	<6	<6	<6	6	<6	<6	<6	14	13
15	7	<6	13	6	<6	<6	19	18	<6
17	<6	9	<6	<6	<6	13	14	9	<6
18	<6	<6	<6	<6	8	12	7	<6	<6
19	<6	<6	7	9	8	7	<6	<6	<6

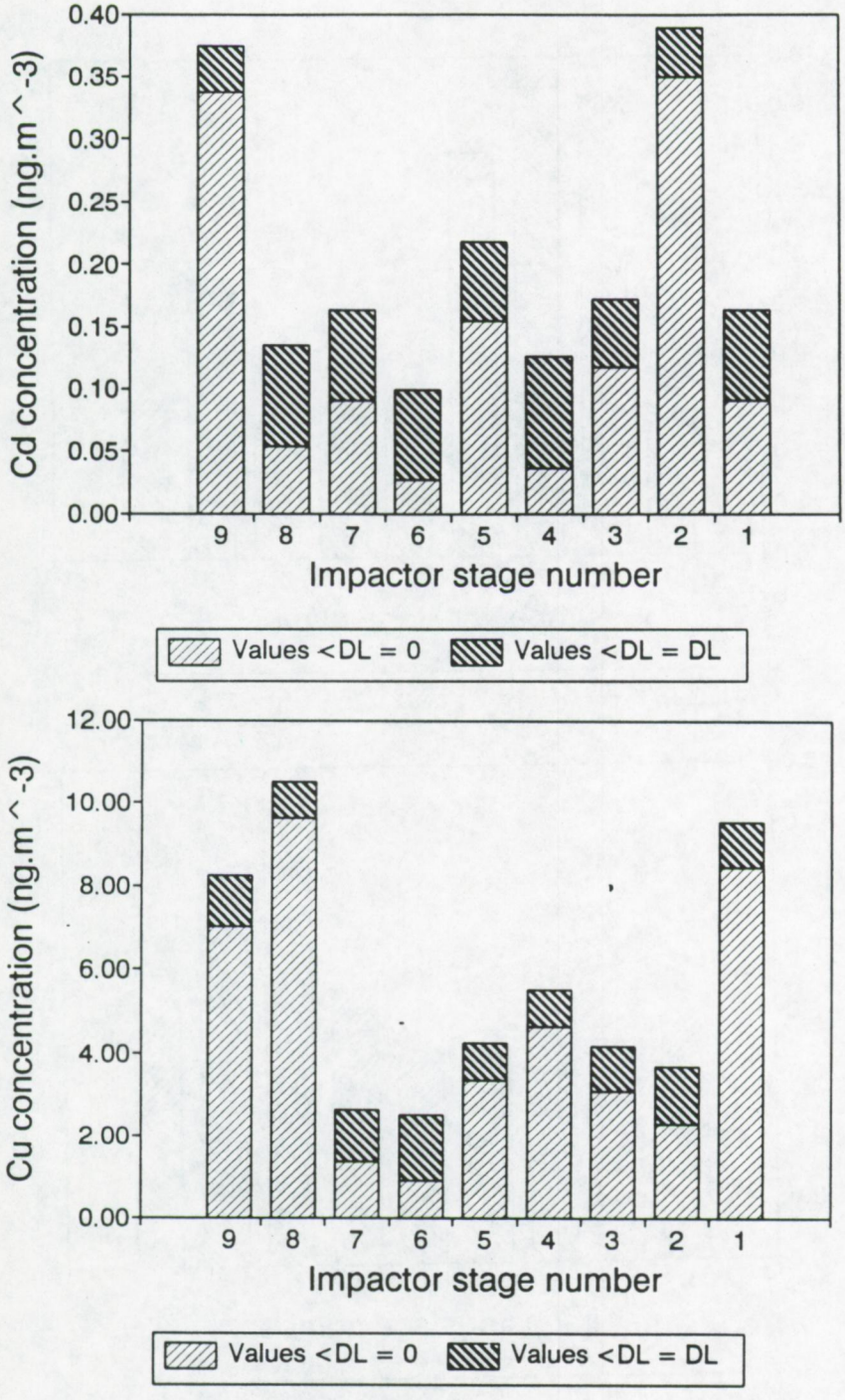

Figure 3.22: Average Cd and Cu concentration as a function of particle size.

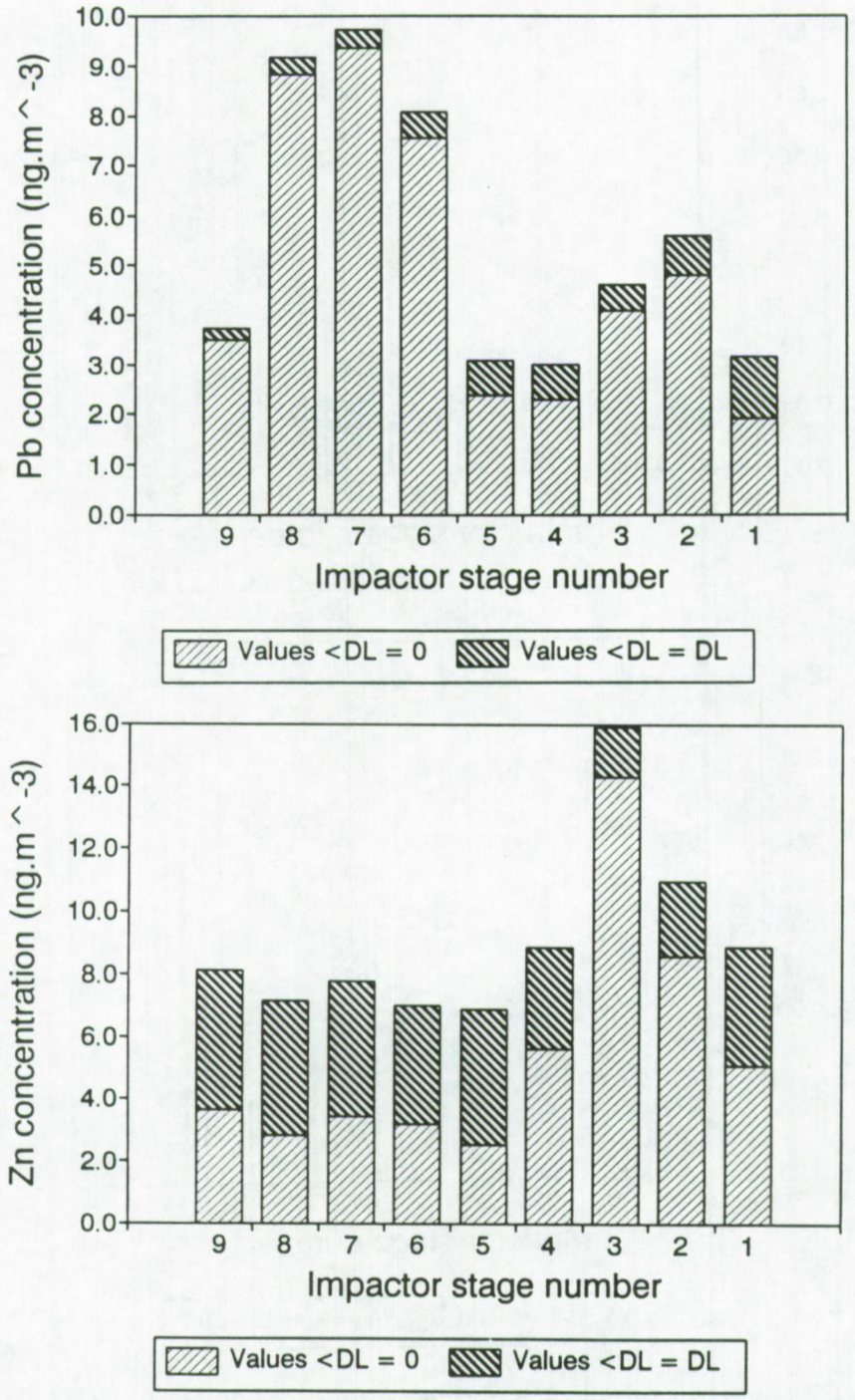

Figure 3.23: Average Pb and Zn concentration as a function of particle size.

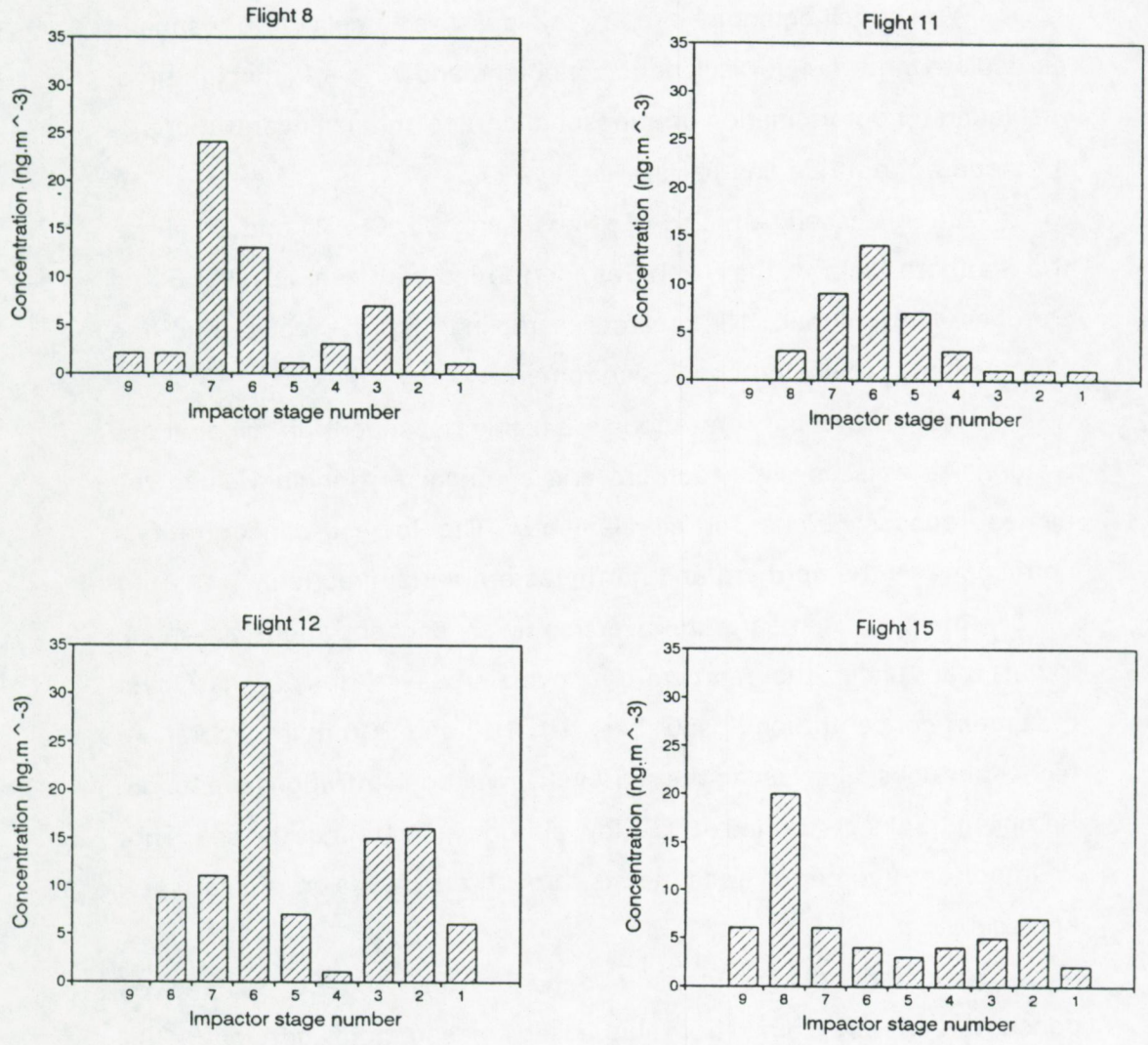

Figure 3.24: Individual Pb size distributions for flights 8, 11, 12 and 15.

3.6 Conclusion

With a well-equipped aircraft, it is possible to collect atmospheric particulate matter under isokinetic conditions and with a fairly high time-resolution for determination of atmospheric trace metal concentrations as a function of altitude and particle size.

Aircraft based sampling of atmospheric Cd, Cu, Pb and Zn above the Southern Bight of the North Sea, performed between July 1988 and October 1989 during 18 separate sampling flights, resulted in the formulation of following conclusive remarks.

Heavy metal concentrations are highly dependent on the air mass history. Air masses with southern and southeastern origin yielded the highest concentrations for all elements. The lowest concentrations correspond to the northern and northwestern wind direction.

Above the temperature inversion layer, concentrations are much lower than under the temperature inversion layer. Inside that layer maximum concentrations occur between 100 and 200 m in general. At higher altitudes and close to the sea level, lower concentrations are found. Sampling tracks performed at very low altitude indicate that the sea is not an important source for trace metals through resuspension of sea water aerosols.

A very good agreement is found between the Cu, Pb and Zn concentrations as obtained from ship-based measurements between 1984 and 1988 and concentrations as obtained by aircraft sampling.

Size-differentiated measurements of Pb concentrations show highly variable size distributions. Both unimodal and bimodal distributions are observed. The average Pb distribution shows a maximum for particles between 0.25 and 0.5 μm and a second maximum for larger particles between 8 and 16 μm. This has some important implications for the calculation of deposition fluxes of trace metals to the sea surface, as will be discussed in more detail in the next Chapter.

3.7 References

Berner A., Lurzer Ch., Pohl F., Preining O. and Wagner P. (1979): *The size distribution of the urban aerosol in Vienna.* Sci. Tot. Environ. 13, 245-261.

Berner A. and Lurzer C. (1980): *Mass size distributions of traffic aerosols at Vienna.* J. Phys. Chem. 84, 2079-2083.

Colovos G., Wilson S. and Moyers J. (1973): *The determination of trace amounts of zinc, cadmium, lead and copper in airborne particulate matter by anodic stripping voltammetry.* Anal. Chim. Acta, 64, 457-464.

Hinds W.C (1982): *Aerosol Technology.* John Wiley and Sons, New York.

Hohn R. (1973): *On the Climatology of the North Sea.* In: North Sea Science, Goldberg E.D. (Ed.), NATO North Sea Science Confererence, Aviemore, Scotland, 15-20 November 1971.

Janssens M. and Dams R. (1973): *Determination of lead in atmospheric particulates by flameless atomic absorption spectrometry with a graphite tube.* Anal. Chim. Acta. 65, 41-47.

Janssens M. and Dams R. (1974): *Determination of cadmium in air particulates by flameless atomic absorption spectrometry with a graphite tube.* Anal. Chim. Acta. 70, 25-33.

Lippmann M. (19): *Filter media and filter holders for air sampling.* In: Air Sampling Instruments, American Conference of Governmental Industrial Hygienists, Cincinnati, Ohio.

Liu B.Y.H. and Lee K.W. (1976): *Efficiency of membrane and Nuclepore filters for submicrometer aerosols.* Environ. Sci. Technol. 10, 345-350.

Losno R., Bergametti G. and Buat-Menard P. (1988): *The partitioning of zinc in Meditteranean rainwater.* Geophys. Res. Lett. 15, 1389-1392.

Lund W. and Onshus D. (1976): *The determination of copper, lead and cadminum in sea water by differential pulse anodic stripping voltammetry.* Anal. Chim. Acta. 86, 109-122.

Maenhaut W. (1989): *Analytical techniques for atmospheric trace elements.* In Control and Fate of Atmospheric Trace Metals, Pacyna J. and Ottar B. (Eds.), Kluwer Academic Publisher, Dordrecht, The Netherlands.

McLead K.E. and Lee R.E., Jr. (1973): *Selected trace metal determination of spot tape samples by anodic stripping voltammetry.* Anal. Chem. 45, 2380-2383.

Pacyna J.M. (1984): *Estimation of the atmospheric emissions of trace elements from anthropogenic sources in Europe.* Atmos. Environ. 18, 41-50.

Pena J.A., Norman J.M. and Thomson D.W. (1977): *Isokinetic sampler for continuous airborne aerosol measurements.* J. Air Poll. Contr. Ass. 27, 337-340.

Rojas C. (1991): Ph.D. Thesis, University of Antwerp, Belgium (in preparation).

Schneider B., Tindale N.W. and Duce R.A. (1990): *Dry deposition of Asian mineral dust over the central North Pacific.* J. Geophys. Res. 95, 9873-9878.

Steiger M., Schulz M., Schwikowski M., Naumann K. and Danecker W. (1989): *Variability of aerosol size distributions above the North Sea and its implication to dry deposition estimates.* J. Aerosol Sci. 20, 1229-1232.

Wang J. (1985): *Stripping Analysis: Priciples, Instrumentation and Applications.* VCH Publishers Inc., Deerfield Beach, Florida.

Chapter 4

Dry and wet deposition of atmospheric Cd, Cu, Pb and Zn into the Southern Bight of the North Sea

4.1 Introduction

From an environmental point of view, it is imperative to determine not only the concentrations of trace metals in the atmosphere but also the mass of trace metals deposited from the atmosphere to the sea surface. It is well known that trace elements can be enriched in the biological food chain or rather food web. An increase in the seawater concentration would therefore result ultimately in an increase in trace metal levels of marine biota. A precise relationship between the actual trace metal concentrations e.g. in fish and the metal burden of the relevant habitat is complicated, since several factors have to be taken into account (Harms and Kerkhoff, 1988).

As will be discussed further on, there is no straightforward procedure to measure or calculate the trace metal flux to the sea. Atmospheric particles can reach the sea surface trough a number of physical processes which are divided into two categories: dry and wet deposition.

This chapter starts with a description of the different dry deposition processes. Several methods for calculating the dry deposition velocity are described and evaluated: the horizontal concentration gradient method, the vertical concentration gradient method, direct deposition measurement, the model of Sehmel and Hodgson (1978), the model of Slinn and Slinn (1980), the model of Williams (1982) and the dual tracer method (Friedlander et al., 1986 and Main and Friedlander, 1990).

Wet deposition processes, in-cloud and below-cloud scavenging are described next. Different methods for evaluating the wet fall-out are discussed: direct measurement of rainwater, the use of scavenging ratios or washout factors, and the use of scavenging rates or scavenging coefficients.

In section 4.3 the dry flux (calculated from size-differentiated airborne concentrations and dry deposition velocities obtained with the

model of Slinn and Slinn (1980), taking into account particle properties and meteorological variables) and the wet flux (calculated from airborne concentrations as a function of altitude, estimated rainfall intensities, mixing height information and theoretically calculated scavenging rates) of trace metals to the Southern Bight of the North Sea is compared with experimental deposition measurements around and over the North Sea.

Next, in section 4.4 results from theoretical modelling of atmospheric deposition by Van Jaarsveld et al. (1986) and by Krell and Roeckner (1988) are compared with our deposition rates.

In section 4.5 the deposition fluxes of trace elements to the North Sea are compared with fluxes reported for other marine areas, both polluted and unpolluted.

Finally, in section 4.6, a critical evaluation is made of the relative contribution of the atmosphere as an individual input source to the total load of heavy metals to the North Sea. The atmospheric input is compared to the riverine input, input by direct discharges and input by dumping.

4.2 Theoretical considerations

4.2.1 Dry deposition processes

Dry deposition of particles to the sea surface is the sum of all physical removal processes that take place when there is not any form of precipitation (rain, snow or hail). Particles can reach the sea surface by gravitational settling, turbulent diffusion, Brownian diffusion or impaction.

Gravitational settling is more important for larger particles and can be described by Stokes' law:

$$v_g = \frac{g\ \rho_p\ d_p^2}{18\ \mu} \qquad (4.1)$$

where v_g = gravitational settling velocity, g = gravitational acceleration

constant, ρ_p = particle density, d_p = particle diameter and μ = dynamic viscosity of air.

Turbulent diffusion itself is not a direct deposition process, but rather a transport process, since particles have to cross a laminar boundary layer at the air/sea interface by gravitational settling or Brownian diffusion before they are actually deposited to the sea surface.

Brownian diffusion of particles is the result of a particle concentration gradient that exists because the particle concentration near the air/sea interface is zero, since particles are deposited to the sea surface. Deposition by diffusion is relatively more important for small particles.

Impaction occurs at irregularities in the sea surface, i.e. waves and can be described by an impaction parameter ϕ (Ranz and Wong, 1952):

$$\phi = \frac{A\ \rho_p\ u_h\ d_p^2}{18\ \mu\ d_c} \qquad (4.2)$$

where A = Cunningham-Stokes slip correction factor, u_h = horizontal wind speed and d_c is a typical length for the impactor which can be associated with the height of waves. Impaction of particles is more efficient for larger particles and at higher wind speeds.

An important number of factors influence the different dry deposition processes. Meteorological data such as the friction velocity, the aerodynamic surface roughness and the atmospheric stability are related to the deposition of particles. The first two parameters are used to describe the wind velocity profile above the deposition surface. Humidity gradients and rainfall characteristics such as rain intensity and rain drop size distributions all affect the deposition of particles.

Pollutant properties (particles can by either hydrophobic or hygroscopic, for instance) which may vary with temperature, humidity and electrostatic gradients at the sea surface will result in a variation of

the deposition characteristics of particles.

Logically, surface properties such as perfect or non-perfect sink conditions and resuspension characteristics must have an effect on the dry and wet fluxes of particles to the sea.

4.2.2 Dry deposition velocity

It is reasonable to expect that the dry deposition flux F_d of particles is proportional to the concentration of particles in air C_a near the air/sea interface:

$$F_d \sim C_a \tag{4.3}$$

If the units of F_d are $kg.m^{-2}.s^{-1}$ and C_a has $kg.m^{-3}$ as units, then the proportionality constant must have $m.s^{-1}$ as units and is defined as the dry deposition velocity v_d:

$$v_d = \frac{F_d}{C_a} \tag{4.4}$$

Several authors have developed models for evaluating v_d. As will be shown below, most models still lack a final formulation for the dry deposition velocity which takes into account all dry deposition processes and all parameters influencing that dry deposition. The following models will be discussed: the horizontal concentration gradient method, the vertical concentration gradient method, direct measurement of deposition and atmospheric particle concentrations, the model of Sehmel and Hodgson (1978), the model of Slinn and Slinn (1980), the model of Williams (1982) and the dual tracer method (Friedlander et al., 1986 and Main and Friedlander, 1990).

4.2.2.1 Horizontal concentration gradient method

Lodge (1978) used a simple box model (Figure 4.1) to obtain:

$$C_a(x) - C_a(x_0) \exp\left[-\frac{x\, v_d}{u\, H}\right] \qquad (4.5)$$

where x = distance travelled by the air mass, u = wind speed and H = height of the mixing layer or boundary layer.

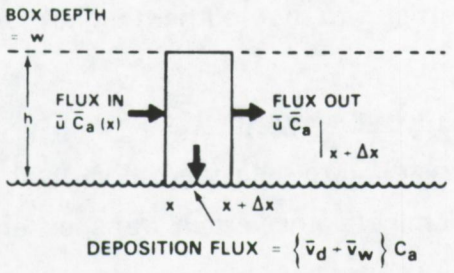

Figure 4.1: Box model for evaluation of v_d (Lodge, 1978)

Experimental measurements of the particle concentration decrease as a function of the distance travelled over sea by the air mass yields v_d. In practice however, this approach can only be used with very low wind speeds and rather high deposition velocities. Assuming v_d = 0.2 cm.s^{-1}, u = 5 m.s^{-1} and H = 1 km, then a 10% decrease of the concentration is measured at a distance of 250 km. Experimental measurements of the horizontal gradients due to dry deposition are therefore quite difficult to perform.

Furthermore equation 4.5 was obtained by assuming a constant mixing height. In reality, the mixing height changes in the course of the day and as the air mass travels across the sea (see also Chapter 5, page 5.36). A reviewed box model (Slinn, 1983) yields:

$$\frac{dC_a}{dx} = -\left[\frac{v_d}{u} + \frac{dH}{dx}\right]\frac{C_a}{H} \qquad (4.6)$$

For v_d = 0.2 cm.s^{-1}, u = 5 m.s^{-1}, dH/dx becomes the dominant term in eq. 4.6 from 5 m per km. Such small variations in the mixing height cannot be measured experimentally with reasonable accuracy.

We must conclude that the horizontal concentration gradient method is not applicable in determining values for the dry deposition velocity of atmospheric particles to the Southern Bight of the North Sea.

4.2.2.2 Vertical concentration gradient method

An alternative approach is to measure the vertical concentration profile where turbulence dominates the vertical transport and assume the vertical flux to be given by (Slinn, 1983):

$$F_d = K_z \frac{\partial C_a}{\partial z} = v_d C_a \qquad (4.7)$$

where K_z is the turbulent diffusion coefficient.

K_z has to be calculated from the vertical wind profile and the momentum flux, assuming the particle flux is constant. To obtain these constant flux assumptions however, the experimentalist would need to perform his experiments in a very thin layer at a large distance downward from any source (Slinn, 1983). In addition a very rapidly responding equipment to measure particle concentrations as a function of height is needed.

Sievering (1981) used profile measurements to compare particle mass transfer with momentum transfer over the Lake Michigan. He used the expression of Gilette (1972) to calculate dry deposition velocity v_d:

$$v_d(z) = -\rho_a \frac{C_D u_z^2 (C_H - C_L)}{(u_H - u_L) C_z} \qquad (4.8)$$

where C_D = drag coefficient and L, z and H are measuring heights with $L < z < H$. Three minute measurements of aerosol particles were performed at 3.7, 5.0 and 6.4 m.

Sievering (1981) concluded that the successful use of the profile method may in part depend on the absence of local contaminant aerosol sources. It appeared that particle mass transfer may be enhanced when large wind speed and/or strong temperature stability changes occur in the surface layer. The overall uncertainty of the v_d estimates was 40 - 90%.

4.2.2.3 Measurement of actual deposition

Via experimental measurements of the actual dry flux, F_d, the dry deposition velocity, v_d, can be evaluated with equation 4.4 if also the particle concentration in air is measured. The performance characteristics of air sampling equipment is quite well known, but the properties of dry deposition collectors like the structure of the laminar boundary layer above the collector and the collection efficiency still remain uncertain. It is not at all clear how far the deposition to the surrogate surface can be compared with deposition to the natural sea surface.

Another practical limitation is, that if the deposited mass is measured, the results may be affected importantly by the deposition of a few large particles. Since v_g is proportional to a^2 (for larger particles, gravitational settling is the dominant process and the dry deposition can be decribed adequatly by taking into account Stokes' law) and the particle mass is proportional to a^3, the deposited mass is a function of a^5. A single 10 μm particle will therefore contribute as much to the total deposited mass as 100000 particles of 1 μm. This will make it extremely difficult to measure dry deposition of trace metals directly if even only a small fraction of these metals is present in the large particle-size fraction.

4.2.2.4 The model of Sehmel and Hodgson (1978)

Sehmel and Sutter (1974) measured the dry deposition rate of monodisperse particles onto a water surface in a wind tunnel. They performed experiments for different wind speeds and particle sizes. Figure 4.2 shows the measured deposition velocities for particles with a density of 1.5 g.cm^{-3}.

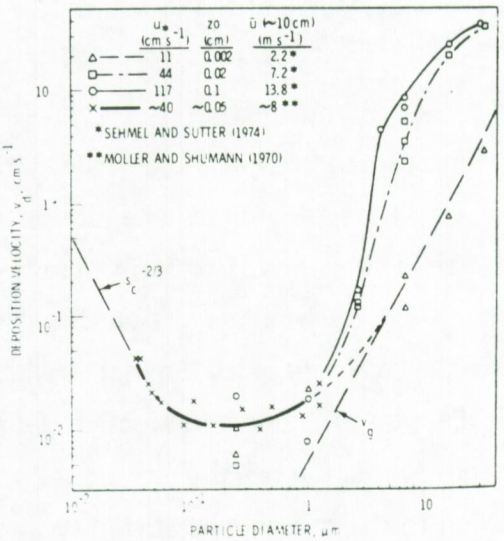

Figure 4.2: Deposition velocities to a water surface: experimental measurements in a wind tunnel (Sehmel and Sutter, 1974 and Möller and Schumann, 1970)

Sehmel and Hodgson (1978) predicted deposition velocities as a function of particle diameter (0.01 to 100 μm), friction velocities (10 to 200 cm.s^{-1}), aerodynamic roughness height (0.001 to 10 cm), particle density (1 to 11.5 g.cm^{-3}) and stable and unstable atmospheres. Predictions indicate that the dry deposition velocity increases as the roughness height increases, usually as the friction velocity increases, and that it is nearly independent of the atmospheric stability. Figure 4.3 shows

predicted deposition velocities at 1m for u_* (friction velocity) = 30 $cm.s^{-1}$ and particle densities of 1, 4 and 11.5 $g.cm^{-3}$.

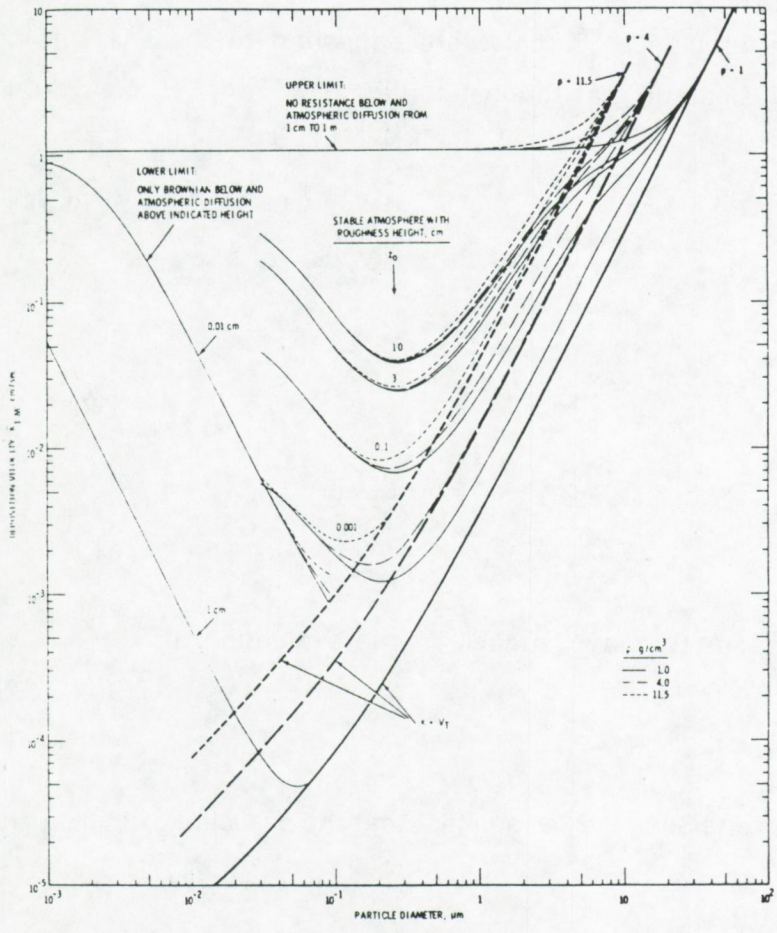

Figure 4.3: Predicted dry deposition values (Sehmel, 1980)

4.2.2.5 The model of Slinn and Slinn (1980)

In this model, the atmosphere beneath a convenient reference height (z = h, usually 10 m) is divided into two layers. In the upper layer, vertical transport of particles is dominated by turbulent diffusion. For larger particles (> 10 μm), gravitational settling is a competing process. The lower layer (z = δ, approximately 100 μm) is characterized by the absence of turbulence. Particles are deposited to the sea surface by thermal diffusion and gravitational settling (Figure 4.4).

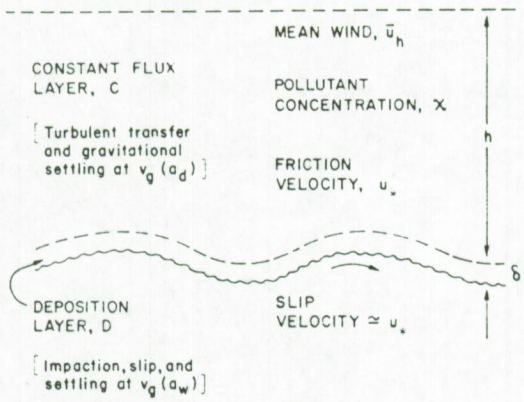

Figure 4.4: A two layer model for the evaluation of v_d (Slinn and Slinn, 1980)

Slinn and Slinn (1980) suggest that the particle flux can be written as:

$$F_d = [K_z + K_p + D] \frac{\partial C_a}{\partial z} + (v_g - w_s) C_a \qquad (4.9)$$

where K_p = particle diffusivity, D = Brownian diffusivity and w_s = particle slip velocity. A slip velocity has to be introduced, since particles may "slip" relatively to the fluid motion if they cannot exactly follow rapid fluid motions or because of different phoretic effects, such as Stefan flow and electrophoresis.

Because particles will grow near the air/sea interface due to the high humidity, a wet particle radius a_w is introduced for particles travelling through the deposition layer. The flux at the reference height h and at the boundary layer δ is given by:

$$F_d\,(z{=}h) = \acute{k}_c\,(C_h - C_\delta) + (v_g\,(a_d) - w_s)\,C_h \qquad (4.10)$$

$$F_d\,(z{=}\delta) = \acute{k}_d\,(C_\delta - C_0) + (v_g\,(a_w) - w_s)\,C_\delta \qquad (4.11)$$

where k'_c = constant flux layer transfer velocity, k'_d = deposition layer transfer velocity, a_d = particle dry radius, a_w = particle wet radius and C_0 = particle concentration at the air/sea interface.

Assuming that there is no particle resuspension ($C_0 = 0$), that the flux is constant (steady-state: $F_d(z=h) = F_d(z=\delta)$) and defining $v_d = F_d(z=h)/(C_h-C_0)$, the following equation can be obtained:

$$\frac{1}{v_d} = \frac{1}{k_c} + \frac{1}{k_d} + \frac{v_g\,(a_d)}{k_c\,k_d} \qquad (4.12)$$

where $k_c = k'_c + v_g(a_d)$ and $k_d = k'_d + v_g(a_w)$.

For calculations, following approximations are made:

$$\acute{k}_c = \beta\,C_D\,u_h \qquad (4.13)$$

$$\acute{k}_d = \frac{\beta}{\beta-1}\,C_D\,u_h\,(Sc^{-\frac{1}{2}} + 10^{-\frac{3}{St}}) \qquad (4.14)$$

where ß = 5/3 (Slinn, 1976), C_D = drag coefficient, Sc = Schmidt number and St = Stokes number.

Results of theoretical calculations by Slinn and Slinn (1980) are shown in Figure 4.5.

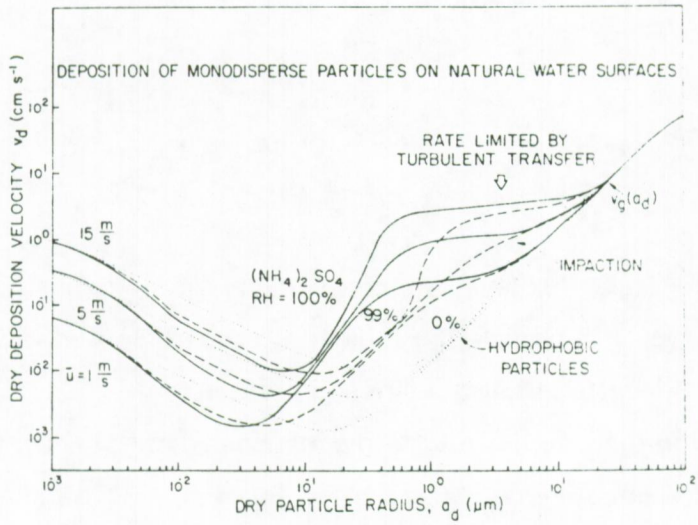

Figure 4.5: Dry deposition velocities as a function of particle size, wind speed and relative humidity (Slinn and Slinn, 1980)

4.2.2.6 The model of Williams (1982)

The model of Williams claims to be an improvement of earlier models. It includes the dependence of the dry deposition velocity on particle diameter, wind speed, spray formation at high wind speeds, particle growth in the high humidities near the air/sea interface, variation of turbulent transfer with wind speed, air/water temperature difference and surface roughness.

Analogue to the model of Slinn and Slinn (1980), the atmosphere is divided into two separate layers (Figure 4.6).

In the very thin lower layer, particles can be transported to the sea surface in two parallel ways. Part of the surface is thought to be smooth,

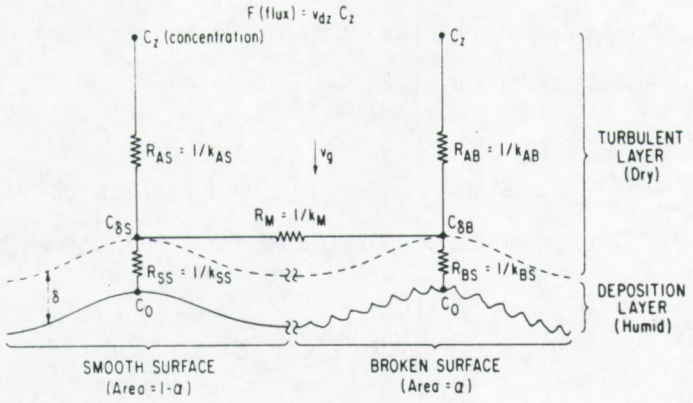

Figure 4.6: Model of Williams (1982) for evaluating v_d

while another fraction is broken up by waves and spray formation. Horizontal transport between the smooth and the broken surface is also a possible interaction.

Within the constant flux layer, the dry flux of particles is given by:

$$F_d(z-h) = (1-\alpha)\, k_{as}\, (C_h - C_{\delta s}) + \alpha\, k_{ab}\, (C_h - C_{\delta b}) + v_g(a_d)\, C_h \qquad (4.15)$$

where α = the fractional surface that is broken by spray, k_{as} = turbulent transfer coefficient in the constant flux layer over the smooth surface deposition layer, k_{ab} = turbulent transfer coefficient in the constant flux layer over the broken surface deposition layer, $C_{\delta s}$ and $C_{\delta b}$ are the concentrations at the top of the deposition layer over the smooth and broken surfaces.

At the dry deposition layer, the flux is given by:

$$F_d(z - \delta) = (1 - \alpha)\, k_{ss}\, (C_{\delta s} - C_0) + \alpha\, k_{bs}\, (C_{\delta b} - C_0) + (1 - \alpha)\, v_g(a_w)\, C_{\delta s} + \alpha\, v_g(a_w)\, C_{\delta b} \qquad (4.16)$$

where k_{ss} and k_{bs} are transfer coefficients in the deposition layer to the broken and the smooth surfaces.

Horizontal transfer between the two regions allows interaction between the smooth and the broken surfaces and is given by:

$$F_{sb} = k_m (C_{\delta s} - C_{\delta b}) \tag{4.17}$$

where k_m = lateral transfer coefficient.

Defining $v_d = F_d(z=h)/(C_z - C_0)$ and assuming perfect sink for particles $C_0 = 0$ and steady state conditions $F_d(z=h) = F_d(z=\delta)$, then the following expression can be evaluated for v_d:

$$v_d = \left(\frac{A}{B}\right) \times \left[(1-\alpha)(k_{ss} + v_g(a_w)) + \frac{k_m \alpha (k_{bs} + v_g(a_w))}{k_m + \alpha (k_{ab} + k_{bs} + v_g(a_w))} \right] + \frac{\alpha (k_{bs} + v_g(a_w)) \alpha (k_{ab} + v_g(a_d))}{k_m + \alpha (k_{ab} + k_{bs} + v_g(a_w))} \tag{4.18}$$

$$\text{where } A = k_m [(1-\alpha) k_{as} + \alpha k_{ab} + v_g(a_d)] + (1-\alpha)(k_{as} + v_g(a_d)) \alpha (k_{ab} + k_{bs} + v_g(a_w)) \tag{4.19}$$

$$\text{and } B = k_m [(1-\alpha)(k_{as} + k_{ss}) + \alpha (k_{ab} + k_{bs} + v_g(a_w)) + (1-\alpha)(k_{as} + k_{ss} + v_g(a_w)) \alpha (k_{ab} + k_{bs} + v_g(a_w)) \tag{4.20}$$

For calculations, the following approximations are made:

$$k_{ax} = \frac{\kappa u_*}{\left[\ln\frac{z}{z_0} - \Phi_H\left(\frac{z}{L}\right)\right]} \qquad (4.21)$$

where x = s or b, κ = von Karman's constant = 0.4, z = reference height, z_0 = roughness height and Φ_H = stability dependent correction function for particles (z/L = Monin-Oboukhov stability parameter).
The particle wet radius is given by (Fitzgerald, 1975):

$$a_w = 4.5\ a_d^{1.04} \quad (r.h. = 99\%) \qquad (4.22)$$

where a_w = particle wet radius and a_d = particle dry radius.
The fractional surface broken by spray is given by (Wu, 1979):

$$\alpha = 1.7 \times 10^{-6}\ u_z^{3.75} \qquad (4.23)$$

where u_z = wind speed at the reference height.
The transfer coefficient to the smooth surface is given by the expression of Slinn and Slinn (1980):

$$k_{ss} = \left(\frac{u_*^2}{\kappa u}\right)\left(10^{-\frac{3}{St}} + Sc^{-\frac{1}{2}}\right) \qquad (4.24)$$

The transfer coefficient to the broken surface, k_{bs}, is governed by processes such as scavenging by impaction and coagulation with spray droplets. These processes are thought to be quite efficient in capturing particles, so that a rather high value for k_{bs} is proposed: 10 $cm.s^{-1}$. Figure 4.7 shows the results of Williams for k_{bs} = 10 $cm.s^{-1}$.

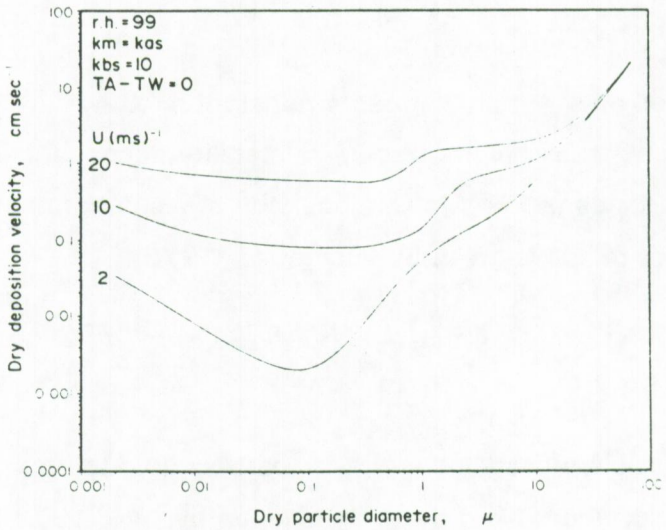

Figure 4.7: Dry deposition velocities as a function of wind speed and particle size (Williams, 1982)

4.2.2.7 The dual tracer method

Friedlander et al. (1986) proposed a new method for the evaluation of a dry deposition velocity. When two species originate from the same source and one of them is a conserved species and the other is depositing, then a dry deposition velocity can be evaluated from measurements of the ratio of the depositing species to the non-depositing species.

Main and Friedlander (1990) used this method to calculate dry deposition velocities of Pb containing aerosols. The ratio of the ambient [Pb]/[CO] ratio to the source [Pb]/[CO] ratio is defined as the fraction of aerosol remaining airborne. The dry deposition velocity is then calculated from the [Pb]/[CO] ratios using a continuously-stirred atmospheric box model. For particles < 1 μm, a dry deposition velocity of 0.13 $cm.s^{-1}$ is found. A mass average dry deposition of 0.28 $cm.s^{-1}$ is found when all

size ranges are taken into account. Figure 4.8 shows the resulting dry deposition velocities as a function of the mean Stokes diameter.

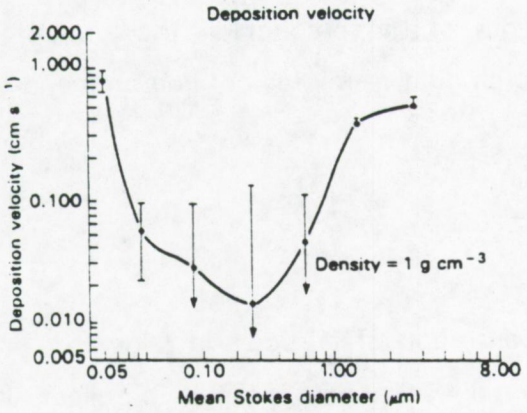

Figure 4.8: Calculated dry depsoition velocities as a function of Stokes diameter (Main and Friedlander, 1990)

4.2.3 Wet deposition

Wet deposition is the combination of rainout (in-cloud scavenging of particles) and washout (below-cloud scavenging of particles). Capture of particles by cloud droplets does not automatically lead to removal of the particles from the atmosphere, since cloud droplets may evaporate on their way to the earth's surface. This merely results in a redistribution of the aerosol.

In contrast with removal of particles by dry deposition, scavenging of particles is a discontinuous process. The main problem in understanding wet fluxes of particles is the description of the scavenging process, while the actual transport to the earth's surface can be described quite simply.

4.2.3.1 Calculation of the wet deposition from rainwater concentrations and rainfall statistics

The wet flux of particles, F_w, can be written as the sum over all individual rain events of the product of the amount of particles in rainwater times the amount of rainfall per unit area and unit time:

$$F_w = \sum_i C_{p,i}\, p_i \qquad (4.25)$$

where $C_{p,i}$ = concentration of particles in rainwater and p_i = rainfall intensity. Experimentally, it is quite difficult to collect all individual rain events over a longer period. This is certainly the case for rainwater collection over sea. Therefore eq. 4.25 is usually approximated.

In a first very simple approximation, the wet flux is given by the average rainwater concentration times the yearly precipitation rate:

$$F_W = C_p\, P \qquad (4.26)$$

where P = yearly precipitation rate ($mm.year^{-1}$).

Precipitation is a discontinuous process. Whenever a precipitation rate p (small caps) is used, this represents the instanteneous precipitation rate during a single rain event. p is usually in the order of 1 $mm.hr^{-1}$ for an average rain event.

In order to calculate average wet fluxes, an average yearly precipitation rate P (large caps) is used. In other words, P is the precipitation rate if it would rain continuously throughout the whole year. P is usually in the order of 500-1000 $mm.year^{-1}$ or 0.05-0.1 $mm.hr^{-1}$ on the North Sea and its surrounding countries.

Dedeurwaerder (1988) developed a more elaborated procedure for approximation of the wet flux. Concentrations of trace metals in rain water were plotted against the precipitation volume (or precipitation

intensity). Usually a hyperbolic relationship can be found:

$$C_{p,i} = A + \frac{B}{p_i} \qquad (4.27)$$

A can be associated with the background concentration of a certain element in cloud water, while B is related to the scavenging efficiency of rain drops for that specific element. Therefore:

$$F_w = \sum_i (A + \frac{B}{p_i})\, p_i = A\, P + B\, N \qquad (4.28)$$

where N = number of rain events per year.

4.2.3.2 Wet flux from scavenging ratios and particle concentrations in air

If the wet flux is normalized to the concentration of particles in air, a wet deposition velocity can be defined:

$$v_w = \frac{F_w}{C_a} = \frac{C_p}{C_a} P = s\, P \qquad (4.29)$$

where s = scavenging ratio or washout factor, i.e. the ratio of the concentration of particles in rainwater to the concentration of particles in air.

Washout factors are generally found to be in the range of 100,000 to 2,000,000 if concentrations are measured in volume units. Some authors use mass-mixing ratios and take into account the density of air so that the resulting scavenging ratios are a factor of 1000 smaller. Scavenging ratios or washout factors tend to be less variable than concentrations in rain themselves. The use of scavenging ratios assumes there is linear relationship between the concentration in air and in rainwater. Rain concentrations represent a removal of particulate matter over the total air column through which rain is falling and they are not necessary related to the atmospheric particle concentration close to the

sea surface.

In urban or near continental areas (like the Southern Bight of the North Sea) scavenging ratios are related to the mass mean diameter of the particles in air. In general scavenging ratios increase with increasing particle size (Figure 4.9). In remote marine air, such a relationship is not found (Arimoto et al,. 1985 and Buat-Menard et al., 1983).

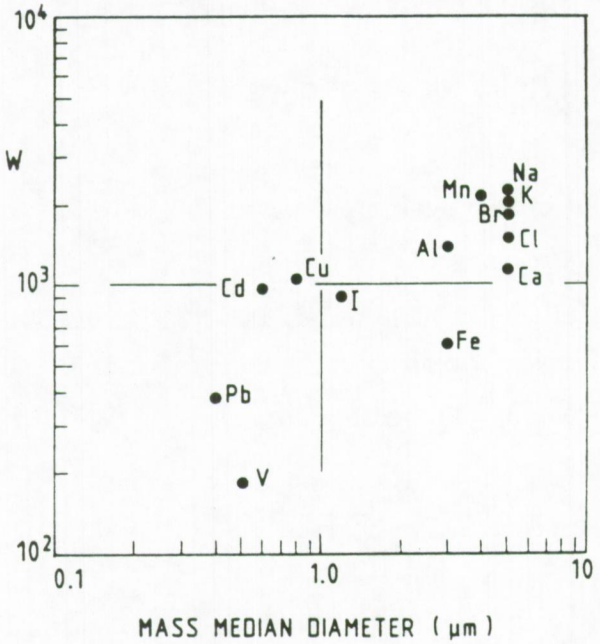

Figure 4.9: Scavenging ratios as a function of mass median diameter (Buat-Menard, 1986).

4.2.3.3 Wet flux as a function of scavenging rates

The scavenging rate Ψ(a) for a given size class of particles a to a+da is defined as the instantaneous fraction of particles removed per unit time by precipitation:

$$\Psi(a) = \lim_{\Delta t \to 0} -\frac{\Delta C_a / C_a}{\Delta t} = -\frac{1}{C_a}\frac{dC_a}{dt} \qquad (4.30)$$

The minus sign will be omitted further on, since we are only interested in the magnitude of the scavenging rate.

The wet flux is the fraction of the particle concentration that is removed from the air by the precipitation on its way to the earth's surface:

$$F_w = \int_0^\infty \Psi \, C_a \, (z) \, dz \qquad (4.31)$$

The scavenging of particles can be described as an impaction phenomenon. Consider a raindrop with radius R falling at its terminal velocity v_t. Suppose the particles have radius a and their gravitational settling speed is $v_g(a)$. If there is no bounce-off or deflection of the flow pattern, then, during a time interval dt, all particles within the volume $(v_t - v_g(a))\pi dt(R+a)^2$ would be captured by the drop. However a collection efficiency has to be introduced, since particles will bounce off and the flow pattern will be disturbed by the falling droplet. The collection efficiency E' can be written as the product of the collision efficiency E and a retention efficiency η.

If there are n(a) particles per unit volume and N(R)dR drops per unit volume and of radii R to R + dR, the number of particles collected per unit volume by all drops is:

$$N(R) \, dR \, n(a) \, (v_t(R) - v_g(a)) \, dt \, \pi \, (R+a)^2 \, \eta \, E \qquad (4.32)$$

Finally, the decrease in number of particles during dt is found by adding the collection by drops of all sizes:

$$dn = -n \, dt \int_0^\infty N \, (v_t - v_g) \, \pi \, (R+a)^2 \, \eta \, E \, dR \qquad (4.33)$$

Consequently, the scavenging rate is given by:

$$\Psi = \int_0^\infty (v_t - v_g)\ \pi\ (R+a)^2\ \eta\ E\ dR \qquad (4.34)$$

As mentioned above, the collection efficiency E' is the product of the collision efficiency and the retention efficiency η. For particles larger than 10 μm (Slinn, 1982), bounce-off can be significant and a retention efficiency other than 1 should be taken into account. The collision efficiency contains contributions from the Brownian diffusion, interception and impaction.

Field measurements and theoretical calculations for the collection efficiency differ up to a factor of three (Slinn 1983) (Figure 4.10).

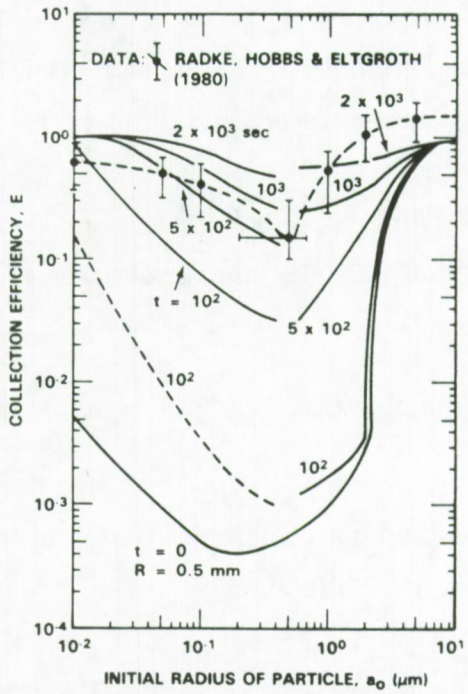

Figure 4.10: Experimental versus theoretical collection efficiencies (Slinn, 1983)

Equation 4.34 can be simplified according to Slinn (1983). Usually $a << R$ and $v_g << v_t$. Therefore:

$$\Psi = \int_0^\infty N \pi R^2 v_t \eta E \, dR \tag{4.35}$$

Since there are substantial uncertainties in the collection efficiency, E can be approximated by a single average $<E>$ for a single average drop radius $<R>$. This approximation should be quite good in the case of impaction, because the collision efficiency for impaction is essentially independent of R. Furthermore, impaction usually dominates when we want to know the total mass scavenged:

$$\Psi = \eta E(a,R) \int_0^\infty N \pi R^2 v_t \, dR \tag{4.36}$$

If we compare equation 4.36 with the expression for the rainfall intensity:

$$p = \int_0^\infty N \frac{4}{3} \pi R^3 v_t \, dR \tag{4.37}$$

we can see the small difference between the two integrands. Since the overall uncertainty in the entire formalism is quite high (Slinn, 1983), we can replace equation 4.36 by:

$$\Psi = \eta \frac{E}{R} \frac{3}{4} \int_0^\infty N \frac{4}{3} \pi R^3 v_t \, dR \tag{4.38}$$

and therefore:

$$\Psi = \frac{c E p}{R} \tag{4.39}$$

where c is a constant. The scavenging rate, averaged over a full year is given by:

$$\Psi_{year} = \frac{c\,E\,P}{R} \qquad (4.40)$$

The major problem remains in the definition of collection efficiencies. Shumann (1989) determined the below-cloud scavenging coefficients of particles in the diameter range 0.28-15 μm as a function of aerosol diameter. He concluded that compared with theoretical predictions particles below 2 μm are much more effectively scavenged: 10 to 100 times for 0.5 μm particles. Giant particles above 2 μm seem to be less efficiently scavenged than predicted by theory (Figure 4.11).

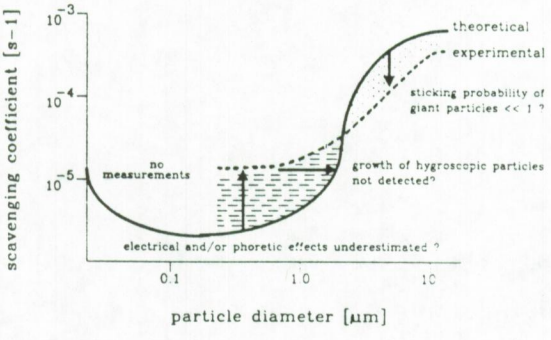

Figure 4.11: Experimental versus theoretical scavenging rates (Shumann, 1989)

Shumann (1989) postulates that state-of-the-art models are not able to represent the observed overall effects of the interaction between precipitation and aerosol particles correctly.

4.2.3.4 Relationship between scavenging ratios and scavenging rates

Scavenging ratios or washout factors can be understood in terms of scavenging rates. The flux can be written as:

$$F_w = \int_0^\infty \Psi \, C_a(z) \, dz \qquad (4.41)$$

$$F_w = C_a(0) \, W p$$

and thus:

$$\frac{F_w}{C_a(0)} = W p = \int_0^\infty \Psi \, \frac{C_a(z)}{C_a(0)} \, dz \qquad (4.42)$$

Assuming no vertical concentration gradient and the particle concentration above the mixing height H = 0, we can write:

$$W p = \Psi \, H = \frac{c \, E \, p \, H}{R} \qquad (4.43)$$

4.3 Comparsion of our dry and wet trace metal deposition fluxes with literature data on experimental results.

4.3.1 Calculation of dry and wet deposition

The dry deposition of Cd, Cu, Pb and Zn was calculated from size-differentiated atmospheric concentrations as a function of wind direction and dry deposition velocities obatined with the model of Slinn and Slinn (1980). In calculating the dry deposition velocity, following parameters are taken into account: meteorological variables such as the aerodynamic roughness height, the friction velocity, atmospheric stability, humidity gradients and particle properties such as hyddrophobic or hygroscopic qualities (Williams, 1982; Slinn, 1983; Rojas et al., 1991). The fraction

of the aerosol that is hygroscopic is calculated from size-differentiated Laser microprobe mass spectrometry results of analysis of North Sea aerosol particles assuming that sulphate-containing particles are hygroscopic.

The wet flux is calculated using equation 4.31 and 4.40 assuming $c = 0.5$, a rain drop radius as given by Mason (1971) and the collection efficiency as given by Slinn (1983). The precipitation rate as a function of wind sector is calculated by using data from the Deutscher Wetterdienst and data from Hohn (1973) for the southern part of the North Sea. Table 4.1 lists the dry and wet fluxes in $kg.km^{-2}.yr^{-1}$ for the Southern Bight of the North Sea as a function of wind sector.

In order to estimate the deposition flux to the total North Sea, we assume that the values obtained for the Southern Bight of the North Sea are two times higher than the average deposition flux to the whole North Sea. This assumption is based on the deposition flux gradient as predicted by the model of Van Jaarsveld et al. (1986). Table 4.2 lists the average yearly dry, wet and total deposition in $ton.yr^{-1}$ for the whole North Sea. It is clear that our estimates indicate that wet deposition is about two times higher than dry deposition.

A complete detailed overview of the followed calculation procedure and the computer programs that were developed can be found in the work of Rojas (1991).

4.3.2 Experimental measurements of dry deposition of trace elements to the North Sea

Only a few experimentalists have tried to measure the dry deposition of trace elements to the North Sea. Cambray et al. (1975) used a Whatman 541 cellulose filter, which was placed horizontally 12 cm under a protective screen. The collectors were placed at 1.5 m height for the coastal stations Leiston (Suffolk), Gresham (Norfolk), Collafirth

Table 4.1
Dry and wet fluxes of Cd, Cu, Pb and Zn into the Southern Bight of the North Sea as a function of wind sector ($kg.km^{-2}.yr^{-1}$)

Wet deposition	Cd	Cu	Pb	Zn
Southwest-west	0.165	1.13	1.26	3.01
Northwest-north	0.016	0.11	0.76	0.12
Northeast-east	0.083	0.20	2.95	6.27
Southeast-south	0.122	0.23	2.56	5.84
Local	0.044	1.79	1.14	4.52
Total wet flux	0.430	3.45	8.68	19.70
Dry deposition	**Cd**	**Cu**	**Pb**	**Zn**
Southwest-west	0.159	1.01	1.38	2.99
Northwest-north	0.004	0.02	0.16	0.03
Northeast-east	0.023	0.06	0.85	1.70
Southeast-south	0.080	0.17	1.60	4.55
Local	0.012	0.64	0.24	1.05
Total dry flux	0.280	1.90	4.23	10.30

Table 4.2
Dry and wet flux of Cd, Cu, Pb and Zn into the total North Sea ($ton.yr^{-1}$)

	Cd	Cu	Pb	Zn
Dry flux	73	500	1110	2710
Wet flux	113	910	2280	5190
Total flux	186	1410	3390	7900

(Shetland), Petten (North-Holland) and Lerwick (Shetland) and at 25 m height on a gas platform (position 53°5'N, 2°11'E). Samples were collected on a monthly basis.

For the gas platform, much higher deposition values were found than for the coastal stations. A possible explanation given by the authors is the contamination of the samples by resuspended seawater (enriched in trace metals) or by the platform itself.

Dedeurwaerder et al. (1988) used vasilinated plexi glass plates to collect dry deposition during 14 day intervals. Samples were taken from the Westhinder lightvessel (position 51°23'30''N, 2°21'30''), the R/V Mechelen and the R/V Belgica during several cruises on the North Sea. The collector plates were used both horizontally and vertically. In order to validate their results, a comparison was made between experimentally obtained deposition fluxes and fluxes calculated from size fractionated air samples and dry deposition values obtained with the model of Slinn and Slinn (1980). A surprisingly good agreement was found between the theoretical predictions and the experimental results obtained with the vertically placed dry deposition collectors (Dedeurwaerder, 1988).

In Table 4.3 our results are compared with those of Cambray et al. (1975) and those of Dedeurwaerder (1988).

4.3.3 Experimental measurements of wet deposition

Dedeurwaerder (1988) collected 31 individual rain events between 1981 and 1984. Samples were collected from the Westhinder lightvessel, from the R/V Mechelen positioned at the Bassurelle station (position 50°33'24''N, 0°54'E), from the R/V Alkaid and from the R/V Belgica during different cruises in the Southern Bight of the North Sea. Average elemental concentrations in rainwater are listed in Table 4.4.

The wet flux was calculated in two ways according to eq. 4.25 and eq. 4.27 as explained before (see also Table 4.4). An estimate of the

Table 4.3
Dry deposition of trace metals into the North Sea ($kg.km^{-2}.yr^{-1}$). Comparison with experimental dry deposition measurements.

	Cd	Cu	Pb	Zn
Cambray et al., 1975				
Leiston		4	8	5
Gresham		5	10	12
Collafirth		30	8	24
Petten		20	18	33
Lerwick		15	11	21
Gas platform		30	24	420
Dedeurwaerder, 1988				
measured	0.19	3.4	7.5	12.6
calculated	0.24	1.9	1.7	3.6
This work				
Southern Bight	0.28	1.9	4.2	10.3

rainfall rate over the North Sea was made by installing a calibrated rain gauge at the Westhinder and at a 22 km landinward location in Belgium. The average rain fall ratio North Sea/coast was found to be 0.72. For his calculations, Dedeurwaerder (1988) used an average precipitation rate of 430 $mm.year^{-1}$ for the Southern Bight of the North Sea, based on measurements between February 1985 and January 1987. The number of rain events was estimated by multiplying 177 days per year with at least one rain event with a factor of 1.5 (average rain events per rainy day).

Balls (1989) reported on the measurement of trace metals in 32 rainfall events collected at Aberdeen (Scotland) between June 1987 and July 1988. The volume weighted trace metal concentrations are listed in Table 4.4. The highest concentrations were found in events with the

smallest precipitation volume. Indeed, also Dedeurwaerder (1988) found a hyperbolic relationship between the trace metal concentration and the precipitation volume. For flux calculations, the greater volume of rain tends to compensate for the lower concentration and the highest depositions are generally observed with the larger events. From the volume weighted concentrations and rain fall data, wet fluxes were calculated (Table 4.4).

Results of wet deposition measurements, performed by Ross (1987) at the coast of southern Sweden, are also included in Table 4.4.

In June 1989, the Secretariat of the Paris Commision (PARCOM, 1989a) reported on a pilot project for monitoring the atmospheric input of pollutants to Paris Convention waters. Although it was encouraged to use wet-only samplers for rain water collection, most data are to be regarded as total deposition data, since dry deposition was collected simultaneously. Only at two locations (Brugge, Belgium and Torry, UK) wet-only samplers were used. Measured rainwater concentrations are given in Table 4.4.

4.3.4 Experimental measurements of total deposition

An important number of "rain water" measurements has to be regarded as total deposition measurements, since they basically consist of a sampling method whereby a rain sampler is used continuously during and in between rain events. It is obvious that there is no information on whether a rain collector is also a good dry deposition collector. Therefore, results from total deposition measurements should be regarded as indicative estimates, rather than as analytical measurements.

In Table 4.5, the results of experimentally obtained total deposition values for the North Sea obtained by Cambray et al. (1975) and as reported by the Paris Commission (PARCOM, 1989a) are compared with our estimates for the total deposition to the North Sea.

Table 4.4
Wet deposition of trace metals into the North Sea ($kg.km^{-2}.yr^{-1}$). Comparison with experimental wet deposition measurements.

	Cd	Cu	Pb	Zn
Balls, 1989				
Aberdeen	0.39	0.13	0.23	0.76
Ross, 1987				
Southern Sweden	0.09	0.80	0.51	0.93
Dedeurwaerder, 1988				
eq. 4.25	4.1	3.3	1.2	21.3
eq. 4.28 (N=177)	3.0	2.4	0.6	16.8
eq. 4.28 (N=266)	3.0	2.5	0.7	17.3
PARCOM, 1989a				
Brugge (B)			0.5	
Torry (UK)	0.24		1.1	4.5
This work				
Southern Bight	0.43	2.5	8.8	19.7

Table 4.5

Total deposition of trace metals into the North Sea ($kg.km^{-2}.yr^{-1}$). Comparison with experimental total deposition measurements

	Cd	Cu	Pb	Zn
Cambray et al., 1975				
Leiston (UK)		12	17	110
Gresham (UK)		13	17	100
Collafirth (UK)		36	17	46
Petten (NL)		21	27	76
Lerwick (UK)		28	34	130
Gas platform		21	49	530
Average		13	16	71
PARCOM, 1989a				
Brugge (B)	0.46		7.3	54.8
Bredene (B)	0.49		11.3	71.8
Koksijde (B)	0.49		6.8	74.9
Leduin (NL)	0.11	4.61	9.1	10.4
Birkenes (N)	0.19		5.5	14.1
Karvatn (N)	0.04		1.6	3.5
Svartedalen (N)	0.08	1.20	2.0	6.7
East Ruston (IK)	0.22	1.48	7.2	6.0
Staxton Wold (UK)	0.42	4.30	18.2	35.2
Banchory (UK)	0.25	4.36	9.2	10.5
Average	0.28	3.19	7.8	28.8
This work				
Southern Bight	0.71	5.36	12.9	30.2
Total North Sea	0.35	2.68	6.5	15.1

4.4 Comparison with model calculations

4.4.1 The model of Krell and Roeckner (1988)

Krell and Roeckner (1988) developed a model to estimate the dry and wet deposition of Pb and Cd into the North Sea. They start from the emission estimates by Pacyna (1985). With a three dimensional stochastic transport model, the long range transport over Europe is simulated. Meteorological variables included are based on analysis by the European Center for Medium-range Weather Forecast (ECMWF) for the wind field data and the precipitation statistics and on analysis of the Norwegian Weather Service for mixing height information.

The deposition close to the surface is characterized by a dry deposition velocity = 0.2 $cm.s^{-1}$ and a washout factor = 500,000 for Pb and 300,000 for Cd. A yearly precipitation rate of 558 $mm.year^{-1}$ is taken into account. Only the major size range of Pb and Cd, containing aerosols between 0.2 and 1.0 μm, is considered.

Their results suggest that the North Sea pollution takes place predominantly in the vicinity of the emission sources, i.e. the southern and the western parts of the North Sea.

For Pb, the total (wet and dry) deposition flux to the Southern Bight of the North Sea is estimated to be 3.8 to 15.3 $kg.km^{-2}.yr^{-1}$. For Cd a corresponding value of 0.038 to 0.153 $kg.km^{-2}.yr^{-1}$ is found.

4.4.2 The model of Van Jaarsveld et al. (1986)

Van Jaarsveld et al. (1986) use a long range version of the Gaussian plume model in which dry and wet deposition are described as a function of particle size and meteorological variables.

Meteorological data on atmospheric stability, wind speed, friction velocity, mixing height and rainfall statistics are determined from 1977 to

1985 data for the Netherlands. The rainfall intensity above the North Sea is taken to be 25% less than over the Netherlands. Dry and wet deposition parameters were calculated for five separated size classes. Information on the size distribution was obtained from measurements in the Netherlands.

The dry deposition velocity was calculated with the model of Sehmel and Hodgson (1978). A representative value of 0.22 $cm.s^{-1}$ was found for most trace elements. This initial value decreases to 0.12-0.13 $cm.s^{-1}$ during transport since larger particles are removed preferentially.

Scavenging ratios were determined from atmospheric particle concentrations and rainwater concentrations. Values between 90,000 and 410,000 were found. A representative value of 150,000 is used.

For all elements considered, the calculated concentration and deposition patterns show maximum values in the Southern Bight of the North Sea and rather strong gradients from the coast.

Table 4.6 compares model estimates of trace metal input into the North Sea with our results. The data, recently reported by Warmenhoven et al. (1990) are also included in Table 4.6.

For Cd, Cu and Zn, our total deposition estimates are about a factor of 10 higher than estimates from model calculations. For Pb, the discrepancy is less, but this is probably due to the fact that most model estimates use Pb emission data from a number of years ago when the Pb emission was significantly higher because the use of unleaded gasoline was not yet widely spread.

If we consider only the particle size fraction below 8 μm from our impactor measurements, our results agree much better with the model calculations. This confirms the enormous importance of large particles in deposition estimates. It is not at all clear how different models that start from different particle size ranges finally end up with similar deposition estimates. Krell and Roeckner (1988) considered only particles between 0.2 and 1 μm, while Van Jaarsveld et al. (1986) used five size classes,

the lowest <0.95 μm, the highest 20 μm.

Table 4.6 also includes results of model calculations by Grassl et al. (1989) and by Warmenhoven et al. (1990) who used an elaborated version of the models developed by Krell and Roeckner (1988) and by Van Jaarsveld et al., respectively.

Table 4.6
Total deposition of trace metals into the North Sea (ton.yr^{-1}).
Comparsion with model calculations

	Cd	Cu	Pb	Zn
Van Jaarsveld et al. (1986)	14		2600	
Krell and Roeckner (1988)	14		1531	
Grassl et al. (1989)			2300	
Warmenhoven et al. (1990)	15	110	1900	930
This work				
Complete size range	186	1410	3390	7900
Particles < 8 μm	24	110	440	1300
Particles > 8 μm	162	1300	2950	6600

4.5 Comparison with other marine areas.

In Table 4.7, the total fluxes of trace elements into different marine regions are listed. The data were obtained from recent compilations of flux measurements and calculations (GESAMP, 1985; Soudine, 1989; GESAMP, 1989).

It is clear that the flux of trace metals to the sea surface decreases by 2 and 3 orders of magnitude from coastal areas to the remote regions

Table 4.7
Atmospheric flux of trace elements to different marine areas ($kg.km^{-2}.yr^{-1}$)

	Reference	Cd	Cu	Pb	Zn
New York Bight	1	0.30		39.0	14.0
Baltic Sea	2	0.16		11.0	
Baltic Sea	3	0.14	2.90	2.4	11.0
W Meditteranean	4	0.13	0.96	10.5	10.8
NW Meditteranean	5	1.00	4.20	29.0	34.0
Bermuda	6	0.045	0.30	1.00	0.75
Bermuda	7	0.09	1.01	1.18	1.76
North Atlantic	8	0.05	0.20	3.10	1.30
North Atlantic	3			1.03	
South Atlantic	3			0.08	
North Pacific	9	0.0035	0.089	0.07	0.67
North Pacific	3			0.20	
South Pacific	3			0.02	
North Indian	3			0.33	
South Indian	3			0.05	
This work:					
Southern Bight		0.71	5.35	12.9	30.1

References: 1: Duce et al., 1976a; 2: GESAMP, 1985;
3: GESAMP, 1989; 4: Arnold et al., 1982; 5: Bergametti et al., 1989;
6: Duce et al., 1976b; 7: Jickells et al., 1984;
8: Buat-Menard and Chesselet, 1979; 9: Arimoto et al., 1985

of the different oceans. The total atmospheric flux of Pb into marine environments varies from 39 $kg.km^{-2}.yr^{-1}$ for the New York Bight to 0.02 $kg.km^{-2}.yr^{-1}$ in the south Pacific Ocean. The Pb flux to the North Sea is comparable with the Pb flux to the Baltic Sea and the Meditterranean Sea.

For Cd, Cu and Zn, our flux values agree fairly well with values reported by Bergametti et al. (1989) for the northwestern Meditterranean Sea.

Guerzoni et al. (1989) reported on atmospheric trace metal concentrations and calculation of the dry deposition flux into the Meditterranean Sea, the Adriatic Sea and the Ionic Sea.

The Cd flux for the Southern Blght of the North Sea (Table 4.8) is much higher than the values reported by Guerzoni et al; (1989). The Pb and the Zn flux to the Southern Bight of the North Sea is comparable to the flux into the Meditterranean Sea.

Table 4.8
Dry deposition fluxes ($kg.km^{-2}.yr^{-1}$) to the North Sea the Meditterranean Sea, the Adriatic Sea and the Ionic Sea.

	Cd	Cu	Pb	Zn
Guerzoni et al. (1989)				
Meditterranean	0.018		6.2	6.0
Adriatic	0.060		1.2	1.9
Ionic	0.013		0.9	2.9
This work				
Southern Bight	0.28	1.90	4.2	10.3

4.6 Evaluation of the relative contribution of the atmosphere as an individual input source of the total load of heavy metals into the North Sea.

Trace elements reach the North Sea through a number of different routes. They are transported by rivers and canals, both in solution and as suspended particulate material. Direct discharges at the coast of industrial waste and sewage is a second input source of contaminants. Dumping of toxic materials by ships is another cause of North Sea pollution. Incineration at sea of industrial waste results in a release of noxious substances, albeit indirectly through the atmosphere. Furthermore, operational discharges at the coast and on the sea by ships and offshore oil and gas industry have to be taken into account. Finally, trace elements reach the North Sea from the atmosphere through different physical processes as discussed in section 4.2.

In evaluating the relative contribution of the atmosphere as an individual input source of trace elements into the North Sea, one must consider the accuracy and reliability of the available data for the other input sources. Most input estimates are subject to considerable uncertainty arising from analytical variation and sampling problems. For heavy metals however, the data set is the most complete.

The quantity of pollutants entering the North Sea will vary from year to year, depending on a number of factors, such as:

- natural variations in river flows and water exchange with adjacent sea areas
- economic variations: industrial expansion and reorganization, large strikes
- changing legislation: emission and dumping restrictions
- atmospheric conditions: wind flow patterns, rainfall intensity
- unforeseen circumstances: accidents

4.6.1 Riverine input of trace elements into the North Sea

As mentioned above, riverine input of trace elements into the North Sea will be subjected to variations from year to year because of the variation in the natural flow regime and the water exchange with adjacent sea areas. Industrial discharges in the various rivers are a function of economic expansion and can be influenced by environmental legislation, i.e. waste dumping criteria.

Since heavy metals may adhere to suspended particles as a function of salinity, they can be deposited in estuaries and harbours (Forstner and Salomons, 1988). As a result of dredging activities and dumping on land, part of the heavy metals does not reach the sea. One should be very careful in estimating the riverine input from concentrations at a certain point in the river and river flow rates in order to avoid double counting of dredged material.

Van Aalst el al. (1983) estimated the Rhine and Meuse to have the largest contribution to the riverine input of heavy metals into the North Sea (Table 4.9). The contribution of the English rivers at the east coast is about half that of the Rhine. In their report Van Aalst et al., (1983) estimated the overall uncertainty of their results to be less than a factor of 2.

Table 4.9

Riverine input of trace elements into the North Sea (ton.year^{-1}) as reported by Van Aalst et al., 1983

	Cd	Cu	Pb	Zn
Rhine/ Meuse	200	1300	1800	10000
Total	230	1600	2400	16500

In 1987, the Scientific and Technological Working Group of the Second International Conference on the Protection of the North Sea published a "Report on the Quality Status of the North Sea". In their report, they note that by no means all rivers entering the North Sea are covered. However it is clear that the data for the Southern Bight of the North Sea (below 54° N) are the most complete (Table 4.10). The riverine input for this area contributes 70-80% of the total riverine input for the North Sea.

Table 4.10

Riverine input of trace elements into the North Sea (ton.year^{-1}) as reported by the Scientific and Technological Working Group (1987)

	Cd	Cu	Pb	Zn
Ems	0.7	21.2	12.4	43.8
Weser	2.9	84	25.6	219
Elbe	8.4	183	219	1825
Western Scheldt	6.9	81	86	452
Eastern Scheldt	0.5	12	8.8	70
Rhine/ Meuse	13.8	442	248	2533
Yzer	0.1	1.4	1.0	7.0
Lys Bypass	0.2	3.5	1.9	21.0
Humber	4.0	117	124	358
Thames	1.8	25.3	40.9	58.5
Southern Bight	39.3	970	768	5587
Total North Sea	52.3	1332	977	7366

In 1989, the Secretariat of the Paris Commission published a "Report on Land-Based Inputs of Contaminants to the Waters of the Paris Convention". All numbers refer to 1987 data except for the Danish and the English data which refer to 1986. In Table 4.11 only data for the North Sea are included.

Table 4.11

Riverine input of trace elements into the North Sea (ton.year^{-1}) as reported by the Secretariat of the Paris Commission (PARCOM, 1989b)

	Cd	Cu	Pb	Zn
Belgium	6.1	190	61	510
Denmark	0.8	24	8.0	80
F.R.G.	16	460	360	3500
Netherlands	16	550	330	2900
Norway	-	-	-	-
Sweden	0.2	27	7.0	130
U.K.	14	280	200	1400
Total	53.1	1531	966	8060

Compared with the data of Van Aalst et al. (1983) the riverine input for Cd is now estimated to be 77% lower, the Pb input is 60% lower, the Zn input is 51% lower and the Cu input is nearly the same.

4.6.2 Direct land-based inputs

Direct inputs may originate from industrial sources, municipal sources (sewage and sewage sludge) and drainage activities (polders). For Belgium, only two sewage outlets at Depanne and between Koksijde and

Oostduinkerke are operational. For these input routes, much less complete data are available. The most recent estimates indicate that 65% to 85% of the direct heavy metal input is due to discharges located in the UK. Table 4.12 lists the most recent estimates for input by direct discharges.

Table 4.12: Input of trace metals into the North Sea by direct discharges (ton.year^{-1}).

	Cd	Cu	Pb	Zn
Scientific and Technological Working Group, 1987				
Belgium	0.3			2.0
Denmark	0.0	2.9	1.0	9.1
F.R.G.	0.6	1.7	0.4	9.2
Netherlands	2.5	29.3	25.7	78.4
Norway	0.9	63.9	4.9	77.0
Sweden		3.0	1.3	9.0
U.K.	15.8	214.8	132.6	986.1
total	20	315	170	1170
PARCOM, 1989b				
Belgium				
Denmark	0.3	3.0	1.3	20
F.R.G.	0.2	3.3	4.0	15.9
Netherlands	1.6	40	20	220
Norway	0.8	25	2.2	71
Sweden	0.2	1.2	0.6	6.2
U.K.	14	200	120	940
total	17	270	144	1260

4.6.3 Input by dumping

Data regarding dumping are considered to be quite accurate, since the exact amounts of dumped material are known. A summary of dumping data reported by Van Aalst et al. (1983) are listed in Table 4.13.

The most recent data on sea disposal were obtained from the Scientific and Technological Working Group (1987). The values reported refer to the year 1985. During 1985, 2.1×10^6 tons of liquid waste, mostly from the TiO_2 industry, were dumped into the North Sea. The UK dumped 1.7×10^6 tons of solid industrial waste consisting mainly of colliery wastes and fly ash. 25% of all sludge arising was dumped into the North Sea. Dredge spoil material was dumped by countries with major North Sea ports: Belgium, the Netherlands and the United Kingdom. During 1985, approximately 77×10^6 tonnes of sediment material were dredged.

It is important to notify that a large proportion of trace elements measured in dredge material, colliery waste and fly ash are bound to the mineral matrix and are therefore unavailable for the food chain. Analytical data therefore represent an overestimate of what is available. Much dregded material merely represents a relocation of seabed material.

4.6.4 Incineration at sea

In 1985, approximately 100,000 tons of waste were incinerated by the Vulcanus II and Vesta. This technique was especially designed for destruction of liquid organochlorine wastes with a maximum chlorine content of 70% w/w (Compaan, 1988). The heavy metal amount emitted is listed in Table 4.14 as reported by the Scientific and Technological Working Group (1987).

It is obvious that the amounts of trace metals emitted during waste incineration at sea are insignificant compared with riverine input, direct discharges and dumping.

Table 4.13

Input of trace elements into the North Sea trough dumping activities (ton.year^{-1})

Data from : Van Aalst et al., 1983

	Cd	Cu	Pb	Zn
Industry	42	2020	1950	4400
Sewage	43	180	250	1300
Total	87	2200	2200	5700

Data from : The Scientific and Technological Working Group, 1987

Type	Total quantity	Cd	Cu	Pb	Zn
Liquid	2.13×10^6	0.078	2.25	2.5	44
Solid	1.66×10^6	0.21	160	206	396
Sewage	5.01×10^6	2.5	103	99	219
Dredging	6.52×10^7	20	1000	2100	8100
Total	7.40×10^7	25	1300	2400	8800

4.6.5 Other non-atmospheric input routes

Inputs from offshore oil and gas activities consist mainly of oil components. They are released by accident (2%), as produced water and as storage displacement water (6-9%) and during drilling operations (90%). The use of toxic diesel based mud has been prohibited since 1987. The amount of trace metals released during drilling activities is relatively very small compared with other trace element input sources.

Legal and illegal discharges of oil components from shipping do not contribute significantly to the total trace metal input in the North Sea.

Table 4.14

Trace metal amount emitted during waste incineration on the North Sea (kg.year^{-1}) (The Scientific and Technological Working Group, 1987)

Country	Total amount	Cd	Cu	Pb	Zn
Belgium	1.28×10^7	92	2647	1456	6941
F.R.G.	5.82×10^7	48	407	469	4055
France	1.00×10^7	-	-	-	-
Netherlands	2.76×10^6	2.5	93	200	880
Norway	3.11×10^6	0.3	-	0.6	0.6
Sweden	0.00	-	-	-	-
U.K.	2.24×10^6	1	1	1	1
Other	1.66×10^7	-	-	-	-
Total	1.06×10^8	140	3100	2100	12000

4.6.6 Comparison of different input routes

In Table 4.15 the different input routes (riverine, direct discharges, dumping and atmospheric) of trace metals to the North Sea are compared. The atmosphere is clearly a main input source of trace elements into the North Sea. Some 66% of all Cd entering the North Sea comes from the atmosphere. Although the atmospheric source-strenght for Pb is 49%, this number will be reduced in the following years thanks to the growing use of unleaded gasoline for motor vehicles. The different Cu and Zn contributions are very similar: riverine input, dumping and atmospheric

input are each responsible for about 1/3 of the total input.

It must be emphasized again that the accuracy of the estimate of the relative contribution of the atmosphere to the total input of trace elements into the North Sea is basically limited by two factors: the accuracy of the size-differentiated concentration measurements, and the accuracy of the estimates for the other input routes.

The next, necessary step in this field of environmental research would be the study of the fraction of heavy metals that is available to living species and can be taken up into the biological food chain. It is therefore important to find out which part of the atmospheric trace metal input into the North Sea will be dissolved in the sea water and which fraction will stay in a chemically inert form.

Table 4.15a

Total input (ton.year^{-1}) of trace elements into the North Sea through different routes.

	Cd	Cu	Pb	Zn
Rivers (1)	53	1530	970	8100
Discharges (1)	17	270	144	1260
Dumping (2)	25	1300	2400	8800
Atmosphere (3)	186	1410	3390	7900
Total	281	4510	6900	26100

Table 4.15b

Relative contribution (%) of the different input routes of trace elements into the North Sea.

	Cd	Cu	Pb	Zn
Rivers (1)	19	34	14	31
Discharges (1)	6	6	2	5
Dumping (2)	9	29	35	34
Atmosphere (3)	66	31	49	30

References: (1): PARCOM, 1989b, (2): Scientific and Technological Working Group, 1987, (3): This work

4.7 References

Arimoto R., Duce R.A., Ray B.J. and Unni C.K. (1985): *Atmospheric trace elements at Enewetak Atoll: 2. Transport to the ocean by wet and dry deposition.* J. Geophys. Res. 90, 2391-2408.

Arnold M., Seghaier A., Martin D, Buat-Menard P. and Chesselet R. (1982): *Geochemie de l'aerosol au-dessus de la Meditterranee occidentale.* Workshop on Pollution of the Meditterranean. Cannes, France, December 1982, pp. 27-37.

Balls P.W. (1989): *Trace metal and major ion composition of precipitation at a North Sea coastal site.* Atmos. Environ. 23, 2751-2759.

Bergametti G., Dutot A.L., Buat-Menard P., Losno R. and Remoudaki E. (1989): *Seasonal variability of the elemental composition of atmopsheric aerosol particles over the northwestern Meditterranean.* Tellus 41B, 353-361.

Buat-Menard P. (1986): *The ocean as a sink for atmospheric particles.* In: The Role of Air-Sea Exchange in Geochemical Cycling. Buat-Menard P. (Ed), Reidel, Dordrecht, pp 165-184.

Buat-Menard P. and Chesselet R. (1979): *Variable influence of the atmospheric flux on trace metal chemistry of oceanic suspended matter.* Earth Planet. Sc. Lett. 42, 339-411.

Buat-Menard P., Ezat U. and Gaudichet A. (1983): *Size distribution and mineralogy of alumino-silicate dust particles in tropical Pacific air and rain.* In: Precipitation Scavenging, Dry Deposition and Resuspension. Pruppacher H.R., Semonin G. and Slinn W.G.N. (Eds.), Elsevier, New York.

Cambray R.S., Jefferies D.F. and Topping G. (1975): *An estimate of the input of atmospheric trace elements into the North Sea and the Clyde Sea (1972-3).* AERE-Report 7733.

Compaan H. (1988). *Waste incineration at sea.* In: Pollution of the North Sea. An Assessment. Salomons W., Bayne B.L., Duursma E.K. and Forstner U. (Eds.), pp. 257-274.

Dedeurwaerder H.L. (1988): *Study of the dynamic transport and the fall-out of some ecotoxicological heavy metals in the troposphere of the Southern Bight of the North Sea.* Ph.D. thesis, University of Brussels (VUB), Belgium.

Duce R.A., Wallace G.T. and Ray B.J. (1976a): *Atmospheric trace metals over the New York Bight.* NOAA Technical Report. ERL 361-MESA 4.

Duce R.A., Hoffman G.L., Ray B.J., Fletcher I.S., Wallace G.T., Fashing G.L., Piotrowicz S.R., Walsh P.R., Hoffman E.J., Miller J.M. and Heffter J.L. (1976b): *Trace Metals in the Marine Atmosphere: Sources and Fluxes.* In: Marine Pollutant Transfer. Windom H. and Duce R. (Eds.), Heath and Co., Lexington, Massashusets, pp.77-117.

Friedlander S.K., Turner J.R. and Hering S.V. (1986): *A new method for estimating dry deposition velocities for atmospheric aerosols.* Atmos. Environ. 17, 240-244.

Fitzgerald J.W. (1975): *Approximate formulas for the equilibrium size of an aerosol particle as a function of its dry size and composition and the ambient relative humidity.* J. Appl. Met. 14, 1044-1049.

Forstner U. and Salomons W. (1988): *Dredged materials.* In: Pollution of the North Sea An Assessment. Salomons W., Bayne B.L., Duursma E.K. and Forstner U. (Eds.), Springer-Verlag, Berlin, pp. 225-245.

GESAMP - IMO/FAO/UNESCO/WMO/WHO/IAEA/UN/UNEP Joint Group of Experts on the Scientific Aspects of Marine Pollution (1985): *Interchange of pollutants between the atmosphere and the oceans.* Reports and Studies GESAMP-WMO 23.

GESAMP - IMO/FAO/UNESCO/WMO/WHO/IAEA/UN/UNEP Joint Group of Experts on the Scientific Aspects of Marine Pollution (1989): *The atmospheric input of trace specis to the world ocean.* Reports and Studies GESAMP-WMO 38.

Gillette D.A. (1972): *Aerosol profile measurements in the surface layer.* J. Appl. Met. 19, 1977-1985.

Guerzoni S., Lenaz R. and Quarantotto G. (1989): *Trace metals characterization of airborne particles from different Meditterranean areas.* In: Airborne Pollution of the Meditterranean Sea. Meditterranean Action Plan- Tecnical Report.

Grassl H., Eppel D., Pettersen G., Schneider B., Weber H., Gandrass J.G., Reihardt K.H., Wodarg D. and Fliess J. (1989): *Stofeintrag in Nord- und Ostsee über die Atmosphäre.* GKSS Report 89/E/8.

Harms U. and Kerkhoff M.A.T. (1988): *Accumulation by fish.* In: Pollution of the North Sea. An Assessment. Salomons W., Bayne B.L., Duursma E.K. and Forstner U. (Eds.). Springer-Verlag, Berlin, pp. 567-578.

Hohn R. (1973). *On the climatology of the North Sea.* In: North Sea science. Goldberg E.D. (Ed.), pp. .

Jickells T.D., Knap A.H. and Church T.M. (1984): *Trace metals in Bermuda rainwater.* J. Geophys. Res. 73, 8827-8836.

Krell U. and Roeckner E. (1988): *Model simulation of the atmospheric input of lead and cadmium into the North Sea.* Atmos. Environ. 22, 375-381.

Lodge J.P. (1978): *An estimate of deposition velocities over water.* Atmos. Environ. 12, 973-974.

Main H.H. and Friedlander S.K. (1990): *Dry deposition of atmospheric aerosols by dual tracer method- I. Area source.* Atmos. Environ. 24A, 103-108.

Mason B.J. (1971): *The Physics of Clouds.* Clarendon Press, Oxford.

Moller U. and Schumann G. (1970): *Mechanisms of transport from the atmosphere to the arth's surface.* J. Geophys. Res., 75, 3013-3019.

Pacyna J.M. (1985): *Spatial distributions of As, Cd, Cu, Pb, V and Zn emissions in Europe within a 1.5 grid net.* Nilu Report 60/85.

PARCOM, Secretariat of the Paris Commission (1989b): *Report on land-based inputs of contaminants to the waters of the Paris Convention in 1987.* PARCOM 11/6/1-E.

PARCOM, Secretariat of the Paris Commission (1989a): *Results of atmospheric maesurements made at coastal stations in 1987.* PARCOM 11/6/2 REV.1-E.

Radke L.F., Eltgroth M.W. and Hobbs P.V. (1980): *Precipitation scavenging of aerosol particles.* J. Appl. Meteorol. 19, 715-722.

Ranz W.E. and Wong J.B. (1952): *Impaction of dust and smoke particles on surface and body collectors.* Indust. Engin. Chem. 44, 1371-1381.

Ross H.B. (1987): *Trace metals in prcipitation in Sweden.* Wat. Air Soil Pollut. 36, 349-363.

Rojas C. (1991). Ph. D. thesis, University of Antwerp (UIA), in preparation.

Shumann T. (1989): *Theoretical and field-determed scavenging coefficients.* J. Aerosol Sci. 20, 1158-1162.

Scientific and Technological Working Group of the Department of the Environment of the European Community (1987). *Quality status of the North Sea.* Second International Conference on the Protection of the North Sea, London, September 1987.

Sehmel G.A. (1980). *Particle and gas dry deposition: a review.* Atmos. Environ. 14, 983-1011.

Sehmel G.A. and Hodgson W.J. (1978): *A Model for Predicting Dry Deposition of Particles and Gases to Environmental Surfaces.* PNL-SA-6721, Battelle, Pacific Northwest Laboratory, Richland, Washington.

Sehmel G.A. and Sutter S.L. (1974). *Particle deposition rates on a water surface as a function of particle diameter and air velocity.* J. Rechs. Atmos. 3, 911-918.

Sievering H. (1981): *Profile measurements of particle mass transfer at the air-water interface.* Atmos. Environ. 15, 123-129.

Slinn W.G.N. (1982): *Predictions for particle deposition to vegetative canopies.* Atmos. Environ. 16, 1785-1794.

Slinn W.G.N. (1983): *Air-to-sea transfer of particles.* In: Air-sea Exchange of Gases and Particles. Liss P.S. and Slinn W.G.N. (Eds.), D. Reidel, Dordrecht, pp. 299-405.

Slinn S.A. and Slinn W.G.N. (1980): *Predictions for particle deposition on natural waters.* Atmos. Environ. 14, 1013-1016.

Soudine A. (1989): *Airborne pollution of the Meditteranean Sea.* The fourth Interntional Conference on Environmental Quality and Ecoystem Stability. Jerusalem, Israel, June 1989.

Van Aalst R.M., Van Ardenne R.A.M., De Kreuk J.F. and Lems Th. (1983). *Pollution of the North Sea from the atmosphere.* TNO-Report CL 82/152.

Van Jaarsveld J.A., Van Aalst R.M. and Onderlinden D. (1986): *Deposition of metals from the atmosphere into the North Sea.* RIVM-Report 842015002.

Warmenhoven J.P., Duiser J.A., de Leu L.Th. and Veldt C. (1989): *The contribution of the input from the atmosphere to the contamination of the North Sea and the Dutch Wadden Sea.* TNO-Report R89/349A.

Williams R.M. (1982): *A model for the dry deposition of particles to natural water surfaces.* Atmos. Environ. 16, 1933-1938.

Wu J. (1979): *Oceanic whitecaps an sea state.* J. phys Oceanogr. 9, 1064-1068.

Chapter 5

SO_2 and O_3 concentrations in the lower troposphere above the Southern Bight of the North Sea

5.1 Introduction

Cities located in areas with cold climates, where electric power and domestic heating are major sources of gaseous and particulate pollutant emissions, are often confronted with air pollution consisting mainly of primary sulphur dioxide and secondary sulphate particles. This has been the first type of air pollution widely recognized and is often referred to as 'London smog' (Finlayson-Pitts and Pitts, 1986).

Sulphur dioxide may affect atmospheric properties, materials, vegetation and human health. Concentrations of air pollutants, mainly SO_2, can reach on occasion very high levels, which has resulted in the past in a number of pollution episodes with sometimes high excess deaths. The most striking example took place in London in 1952 where 4000 fatalities occurred.

The U.S.A. National Ambient Air Quality Standard, based on the results of epidemiological studies, for sulphur dioxide is 140 ppb for a maximum exposure of 24 hours and 30 ppb for an annual arithmetic mean. The World Health Organization (1978-1979) recommends a value of 15 to 23 ppb as a maximum for an annual arithmetic mean SO_2 concentration.

Gas to particle conversion of SO_2 leads to formation of sulphuric acid and sulphate containing aerosol particles. These aerosols have important effects on atmospheric visibility and fog and cloud formation processes. Twomey (1972) observed that atmospheric condensation nuclei consist mainly of ammonium sulphate.

Ozone is an essential atmospheric trace substance. Since it absorbs UV light, it plays an important role in the global radiation budget. It also protects living species from harmful UV radiation. This process regards mainly stratospheric ozone.

In the troposphere, ozone is regarded as a pollutant rather than as an essential compound. Ozone is involved in photochemical air pollution.

The main primary pollutants in photochemical smog are nitric oxide and hydrocarbons which are rapidly converted to secondary pollutants such as ozone, oxidized hydrocarbons and organic nitrates. This type of air pollution results from the widespread use of gasoline as motor fuel. It has been recognized for the first time in the mid-1940's in Los Angeles and is often referred to as 'Los Angeles smog' (Finlayson-Pitts and Pitts, 1986).

The effects of long-term exposure to ozone levels of 100 to 200 ppb (typical urban levels) has not been clearly established so far.

In section 5.2 the sources, both natural and anthropogenic, of sulphur compounds are discussed. Next ambient concentrations in continental and marine, polluted and unpolluted air are described. Special attention is paid to trends in sulphur dioxide concentrations in the Flanders region specifically. Finally, sinks of sulphur dioxide, homogeneous and heterogeneous oxidation reactions and physical removal processes such as dry and wet deposition, are evaluated.

In section 5.3 the formation and destruction processes of stratospheric ozone are briefly described. Next, the role of ozone in photochemical smog formation is explained.

Analytical equipment used for in situ measurements of sulphur dioxide and ozone are described in section 5.4. In the next section, vertical temperature, SO_2 and O_3 profiles measured in the lower troposphere above the Southern Bight of the North Sea are discussed. Finally, in section 5.6, an evaluation is made of the relation between trace metal concentrations and sulphur dioxide levels above the Southern Bight.

5.2 Sources, concentrations and sinks of sulphur dioxide

5.2.1 Sources of sulphur compounds

5.2.1.1 Natural sources of sulphur compounds

The natural emission of sulphur compounds is related to volcanic activity, the production of sea salt particles from the sea surface and decomposition of biological material, both on land and in in the ocean.

The available data for the sulphur content in volcanic eruptions show large variations. Kellogg et al. (1972) estimated that 1.5 Tg $S.yr^{-1}$ is globally emitted as volcanic sulphur. Friend (1973) proposed a value of 2 Tg $S.yr^{-1}$, Granat et al. (1976) a value of 3 Tg $S.yr^{-1}$. Berresheim and Jaeschke (1982) estimated the SO_2 emission by volcanoes to be 7 Tg $S.yr^{-1}$ besides 1 Tg $S.yr^{-1}$ as H_2S and 1 Tg to 3 Tg $S.yr^{-1}$ as sulphate. Varhelyi and Gravenhorst (1981) reported much higher emission rates from volcanoes: 15 Tg to 30 Tg $S.yr^{-1}$.

The sulphur mass in sea salt particles formed at the sea surface of the oceans is estimated at 44 Tg to 47 Tg $S.yr^{-1}$ (Seinfeld, 1986).

Emission of sulphur compounds through decay of biological matter takes place in the form of chemically reduced sulphur gases: H_2S, DMS (dimethyl sulphide), DMDS (dimethyl disulphide), CS_2 and COS. The global flux produced by microbiota is not well known. Erickson (1960, 1963) estimated the global biogenic emission to be 280 Tg $S.yr^{-1}$. Robinson and Robbins (1968, 1970) proposed a value of 98 Tg $S.yr^{-1}$ which is comparable to the value of Friend (1973): 106 Tg $S.yr^{-1}$. Granat et al. (1976) calculated the biogenic sulphur emission to be 32 Tg $S.yr^{-1}$. More recent calculations by Varheyli and Gravenhorst (1981), as reported by Georgii (1982), are listed in Table 5.1. The high discrepancy between minimum and maximum values are the result of extrapolation from small scale region data to the global scale.

Table 5.1

Global biogenic sulphur emission (Tg $S.yr^{-1}$) as reported by Varhelyi and Gravenhorst (1981)

Compound	Min	Max
H_2S	0.1	1.8
DMS	3.0	31.6
CS_2	0.2	1.8
COS	0.1	0.3
Total	3.3	35.5

5.2.1.2 Anthropogenic sources of sulphur compounds

Anthropogenic sulphur is primarily (95%) emitted as SO_2. The huge quantity of yearly emitted SO_2 is mainly due to combustion processes by fossil fuel containing sulphur. The global estimates for anthropogenic sulphur emission also vary over a large range. Different estimates, compiled by by Seinfield (1986) are listed in Table 5.2.

Table 5.2

Global anthropogenic sulphur emission (Tg $S.yr^{-1}$) (Seinfield, 1986)

Author	Amount
Erickson, 1960; 1963	40
Robinson and Robbins, 1968; 1970	70
Kellogg et al., 1972	50
Friend, 1973	65
Granat et al., 1976	65

The present estimates of emissions (see Table 5.3) of anthropogenic sulphur makes clear that in the northern hemisphere the total man-made sulphur emission exceeds the total natural sulphur emission, while in the southern hemisphere the natural emission exceeds the anthropogenic sulphur production by far (Cullis and Hirschel, 1980).

Table 5.3

Sulphur emissions in the northern and southern hemisphere (Tg $S.yr^{-1}$)
(Cullis and Hirschel, 1980)

	northern	southern
natural	80	66
anthropogenic	88	6
total	168	72

2/3 of the anthropogenic emissions of sulphur components take place within about 5% of the earth's surface, 38% in Europe on 2% of the global area (Georgii, 1982).

5.2.2 Concentrations of sulphur dioxide

5.2.2.1 General

Since the tropospheric residence time of SO_2 is only in the order of days, large variations of the concentrations are observed. Generally speaking, the SO_2 concentration over the continents is higher than over the oceans resulting in a horizontal gradient of SO_2 from land to sea. Maximum values are found in densely inhabited areas and industrial regions. The production of SO_2 near the ground with sinks and dispersion in the troposphere leads to a strong decrease of SO_2 concentration with

altitude above the continents. At about 3 to 5 km altitude a background concentration of approximately 0.5 $\mu g.m^{-3}$ is reached (Georgii, 1978).

The compilation of SO_2 data gained over the Atlantic Ocean as reviewed by Meszaros (1981) is presented in Figure 5.1. A maximum in the sulphur dioxide concentrations is found at the northern mid-latitudes.

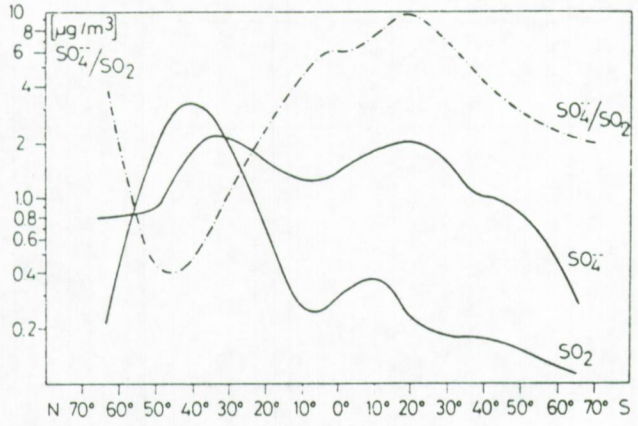

Figure 5.1: Latitudonal SO_2 and SO_4^{2-} concentration distribution (Meszaros, 1981).

Ockelman et al. (1981) measured the SO_2 concentration over the Atlantic during several cruises with the research vessel Meteor. Mixing ratios range from 30 pptv over the open Arctic Ocean to values near the detection limit over ice-covered polar sea. 30 to 300 ppt were found over the Atlantic Ocean. During all cruises large variations of the mixing ratio could be detected with characteristic periods of the order of days. It can be assumed that enhanced SO_2 concentrations were due to long range transport from the continents. Besides that, the transformation of ocean produced organic sulphur compounds is responsible for the marine SO_2 distribution.

Meszaros (1981) proposed model background concentrations for Europe: 0.35 $\mu g.m^{-3}$ (SO_2 as S) for clean northern areas, 1.0 for Southern

Europe, 3.5 for areas with low concentrations (Sweden), 4.5 for moderately polluted areas and 7.5 for areas with high concentrations (western Europe).

5.2.2.2 Trends in SO_2 concentrations.

The SO_2 emissions doubled between 1950 and 1970 mainly by the increase of use of fossil fuel. However, the concentrations in industrialized areas have decreased. It is believed (Salmon et al., 1978) that this is the result of the use of higher stacks. In unpolluted areas however such a decrease is not observed, although a clear increase is also not observed.

Also in the Flanders region in Belgium, a clear trend can be observed. The air quality in Flanders is controlled by several measurement networks (Kelchtermans, 1989). Since 1968, the daily average SO_2 concentration is measured at 92 semi-automatic stations. A full automatic network of 44 stations is operational since 1978 and collects data on half-hour averages of SO_2 concentrations.

Between 1980 and 1987 the total SO_2 emission in Flanders has decreased with 54% from 533000 to 245000 ton.year^{-1}. The SO_2 emission from motor vehicles has increased in that period with 15% from 6810 to 8360 ton.year^{-1}. This is clearly due to the increased use of diesel powered motor vehicles. The SO_2 emission from residence heating installations has decreased in Flanders between 1980 and 1987 with 62% from 84400 to 31900 ton.year^{-1}. This is the result of the increase in use of natural gas and sulphur poor oil.

The total industrial emission of SO_2 in Flanders decreased from 442000 to 205000 ton.year^{-1}, i.e. a 54% reduction in 7 years. The main reason for this decrease is the spectacular reduction of SO_2 emission in the electricity sector: 68% (Table 5.4).

Table 5.4

SO_2 emission in Flanders: 1980 versus 1987 ($ton.yr^{-1}$) (Kelchtermans, 1989)

Source	1980	1987
Electricity	266000	85000
Refines	87000	45000
Metal industry	42000	34000
Other industry	16000	9000

The highest SO_2 concentrations are found in the agglomeration of Ghent and Antwerp. In Ghent the average SO_2 concentration went down from 175 $\mu g.m^{-3}$ to 50 $\mu g.m^{-3}$ between 1969 and 1985 and in Antwerp from 160 to 65 $\mu g.m^{-3}$ between 1969 and 1981.

5.2.3 Sinks of SO_2.

Sulphur dioxide can be removed from the atmosphere by oxidation reactions, both homogeneous and heterogeneous. Dry deposition to the oceans, to vegetation and other surfaces is a second removal process. Finally SO_2 can be removed from the atmosphere by rainout and washout processes. The residence time of sulphur dioxide is limited to a few days.

Five oxidation processes can be differentiated for SO_2 according to Wilson (1978). These are listed in Figure 5.2 (Georgii, 1982).

Because of the limited quantum-yield by sunlight, the sulphur dioxide oxidation by direct absorption of sunlight is severely restricted. This mechanism is insignificant with regard to the total SO_2 oxidation.

Mechanisms	reaction	dominant factors
1. Direct Photooxidation	$SO_2 \longrightarrow H_2SO_4$	SO_2-concentration Intensity of sunlight
2. Indirect Photooxidation	$SO_2 \xrightarrow[OH,\ HO_2,\ RO_2]{} H_2SO_4$	SO_2-concentration, Oxidants, OH, NO_x, HO_2, RO_2
3. Heterogeneous oxidation in droplets	$SO_2 \xrightarrow{\text{liquid water}} H_2SO_3$ $NH_3 + H_2SO_3 \longrightarrow NH_4^+ + SO_4^=$	pH of liquid water NH_3-concentration
4. Heterogeneous catalytic oxidation in droplets	$SO_2 \xrightarrow[\text{heavy metal ions}]{\text{liquid water}} SO_4^=$	Concentration of heavy metals (Fe, Mn, V)
5. Heterogeneous catalytic oxidation in aerosols	$SO_2 \xrightarrow[\text{heavy metal ions}]{\text{liquid film}} SO_4^=$	surface area of particles heavy metal aerosols (Fe, Mn, V)

Figure 5.2: Oxidation mechanisms for SO_2 (Georgii, 1982).

The homogeneous oxidation mechanism that involves OH radicals is thought to be of dominant importance. Experimental results show that the HSO_3 radical, produced by the reaction of sulphur dioxide with OH radicals, is quickly transformed in sulphuric acid.

Georgii (1982) states that in our climates, at least in the winter time, heterogeneous oxidation processes (reaction 3 to 5 in Figure 5.2) are of greater relevance. Heterogeneous oxidation occurs in cloud and fog droplets. The rate determining factor is the oxidation step and not the transport to or within the droplet (Beilke, 1980).

In the absence of catalysts, the oxidation process is highly pH dependent and leads to relevant oxidation rates only when the pH of the droplet is higher than 6. Since the pH of cloud and fog droplets is

generally between 3 and 5, this mechanism is not an important one. A special type of heterogeneous oxidation in the absence of catalysts is oxidation in the presence of ammonia. The effect of ammonia is to keep the pH high when sulphur dioxide is oxidized to sulphate. In acidic droplets however, ammonia can not enhance this oxidation process.

Catalytic oxidation occurs mainly in the presence of transition metals such as Mn, Fe and V. On the basis of experiments carried out by Barrie and Georgii (1976) it can be concluded that catalytic oxidation of sulphur dioxide can be significant in clouds and fogs of polluted regions.

Experiments by Runca-Koberich and Georgii (1978) have pointed out that the rate of sulphate formation after absorption of sulphur dioxide on aerosol particles depends on the relative humidity and the chemical behaviour of the particles and the catalysts. If the particles are covered with a liquid film at higher humidities, they act as droplets do.

Sulphur dioxide can be removed from the atmosphere by dry deposition to all kinds of surfaces. Many factors such as seasonal effects, diurnal effects (sunlight, atmospheric stability) and meteorological effects (temperature, humidity and wind speed) can influence dry deposition of gases, resulting in a wide range of experimentally determined dry deposition velocities for SO_2. A value of 1 $cm.s^{-1}$ seems a good overall estimate for sulphur dioxide.

Finally, sulphur dioxide can be removed from the atmosphere by absorption in rain and cloud droplets and subsequent rainfall.

5.3 Sources, concentrations and sinks of ozone

5.3.1 Stratospheric ozone

Ozone is an essential atmospheric trace substance. It absorbs UV radiation in the wavelength region 240 to 320 nm and is therefore responsible for protection of the living species on earth from harmful UV

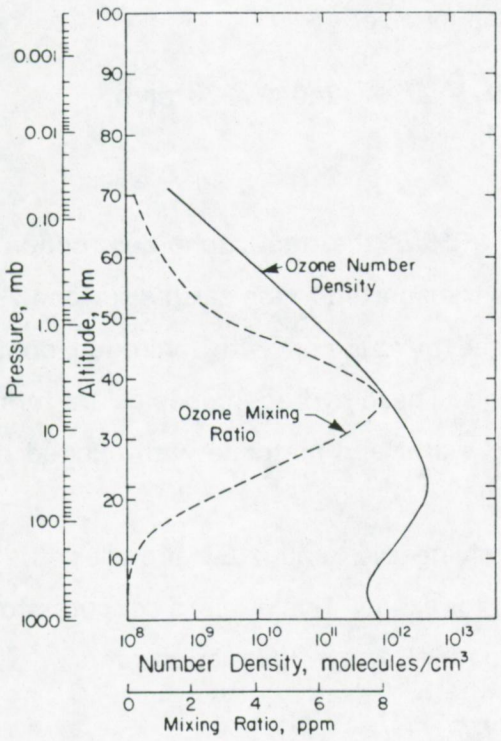

Figure 5.3: Vertical ozone profile (Seinfield, 1986)

radiation. Figure 5.3 shows the vertical profile of ozone in terms of molecules.cm^{-3} and ppm. The maximum concentration can be found at 23 km altitude.

The amount of ozone in the atmosphere is maintained as a result of a dynamic balance between formation and destruction processes. Formation occurs predominantly at altitudes above 30 km by photodissociation of O_2:

$$\begin{aligned} O_2 + h\nu &\rightarrow O + O \quad (\lambda < 242\ nm) \\ O_2 + O + M &\rightarrow O_3 + M \end{aligned} \tag{5.1}$$

where M is an atmospheric molecule.
Destruction processes of ozone involve:

$$\begin{aligned} O_3 + h\,\nu &\rightarrow O_2 + O \qquad (240<\lambda<320\ nm) \\ O_3 + O &\rightarrow O_2 + O_2 \end{aligned} \tag{5.2}$$

These processes account for 20% of the total ozone destruction in the stratosphere. Another 0.5% is transported to the earth's surface. 10% of the formed ozone is destructed by reaction with hydrogen containing species: H, OH and HO_2 radicals. These hydrogen species are formed by reaction of naturally occurring water and methane with excited oxygen atoms.

A catalytic cycle involving NO and NO_2 provides the most important destruction process for ozone. This process accounts for most of the remaining 70% of the natural ozone destruction rate:

$$\begin{aligned} O + NO_2 &\rightarrow NO + O_2 \\ NO + O_3 &\rightarrow NO_2 + O_2 \end{aligned} \tag{5.3}$$

$$O + O_3 \rightarrow O_2 + O_2$$

Atomic Cl and Br and their oxides ClO and BrO can catalyze the destruction of ozone. The key species from the viewpoint of stratospheric effects are the chloro-fluoro-carbons $CFCl_3$ and CF_2Cl_2. Within a few years after release, these compounds are well distributed throughout the troposphere. They rise slowly into the atmosphere. In the stratosphere, at altitudes between 25 and 50 km, they are decomposed by UV light of wavelengths around 200 nm, with production of Cl atoms. The Cl atoms participate in the ClO_x catalytic cycle:

$$O + ClO \rightarrow Cl + O_2$$
$$O_3 + Cl \rightarrow ClO + O_2 \qquad (5.4)$$
$$O + O_3 \rightarrow O_2 + O_2$$

The importance of stratospheric ozone destruction by this mechanism has been recognized by Rowland and Molina, 1975.

5.3.2 Stratospheric ozone as a source for tropospheric ozone

Stratospheric ozone is transported in poleward direction by atmospheric motions. This circulation is particularly strong in winter and spring months when stratospheric air moves downward over polar regions. At the same time the lower stratosphere is characterized by a light updraft (Meszaros, 1981). During the late spring and summer, the stratospheric ozone reaches the troposphere first of all trough the tropopause gaps.

The ozone molecules formed in the stratosphere reach the troposphere where they move downward by turbulent diffusion. The latitude of the three ozone maxima (Figure 5.4) is related to the presence of tropopause discontinuities. The contact of two air masses with different thermal structure produces a tropopause gap through which the mass exchange between stratosphere and troposphere becomes very intensive.

The annual variation of the total ozone can be approximated by a sine curve at mid latitudes. The tropospheric ozone level shows similar variations with a delay of 1 to 2 months. On the basis of this findings, Junge (1963) estimates the residence time of tropospheric ozone to be 2 months.

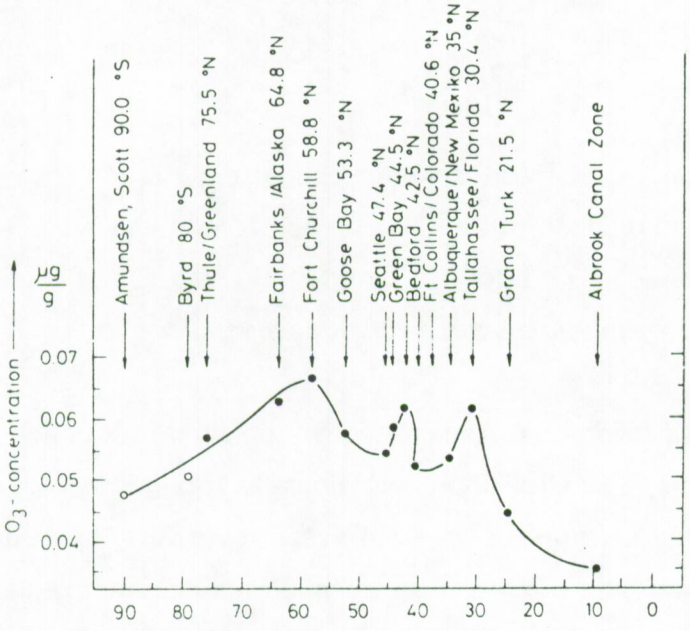

Figure 5.4: Tropospheric ozone concentration as a function of latitude (Meszaros, 1981).

5.3.3 Ozone and photochemical smog formation

Ozone is naturally present in the clean, background troposphere at concentrations ranging from 20 to 80 ppb. The natural variability is due to combinations of tropospheric chemistry and ozone transport in the troposphere from the stratosphere. Additions to the concentration of natural ozone come from local ozone synthesis by chemical processes and transport from urban centre originated ozone.

In polluted atmospheres, the ozone concentration can rise as it is produced as a secondary pollutant in photochemical smog formation. The prime ingredients for photochemical smog formation are hydrocarbons and nitrogen oxides exhausted mainly by automobiles. The atmosphere initially contains dilute concentrations of gaseous organic molecules and NO_x (NO + NO_2). The energy of solar radiation triggers an initial reaction in NO_2:

$$NO_2 + h\nu \rightarrow NO + O \qquad (5.5)$$

The resulting oxygen quickly combines with molecular oxygen to form ozone:

$$O + O_2 + M \rightarrow O_3 + M \qquad (5.6)$$

Ozone from this reaction rapidly oxidizes NO:

$$NO + O_3 \rightarrow NO_2 + O_2 \qquad (5.7)$$

These three reactions form a complete closed sequence so that they would proceed until an equilibrium is established. Calculations for expected ozone concentrations fail however to account for the large concentrations measured in photochemical smog. Therefore the NO_x - O_3 cycle itself is not sufficient to explain the formation of photochemical smog (Figure 5.5).

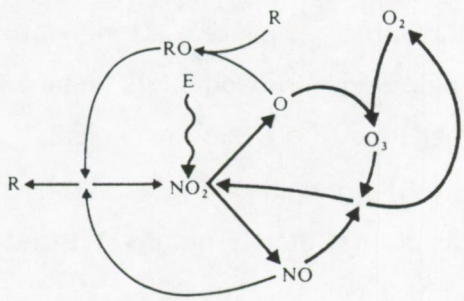

Figure 5.5: Photochemical smog formation: main reactions (Williamson, 1973).

In fact, these fast reactions are supplemented by a second process involving the participation of organic molecules, mostly hydrocarbons. Hydrocarbons compete for the free oxygen released by photo-dissociation of NO_2. The resulting oxidized hydrocarbons compete with ozone for the NO and the reaction yields NO_2 as an end product:

$$\begin{aligned} R + O &\rightarrow RO \\ RO + NO &\rightarrow R + NO_2 \end{aligned} \qquad (5.8)$$

Both ozone and NO_2 concentrations will increase at the expense of NO. Figure 5.6 shows the diurnal formation of smog species in Los Angeles. Early in the morning ambient concentrations of NO and hydrocarbons begin to rise. After sunrise, NO_2 is photo-dissociated. The atomic oxygen produced in this way leads to ozone and oxygenated hydrocarbon formation. The ozone concentration keeps pace with the increasing NO concentration. The slow increase of RO then becomes apparent and it starts to combine with NO to accelerate NO_2 build up. The higher NO_2 concentration and the more intense sunlight accelerate atomic oxygen and ozone production.

When NO is substantially depleted, ozone concentrations rise quickly. The strongly oxidizing atmosphere is meanwhile converting hydrocarbons into another type of organic molecules.

Hydrocarbons and NO_2 are finally removed by side reactions which yield other secondary pollutants, mainly organic nitrates in the form of aerosols.

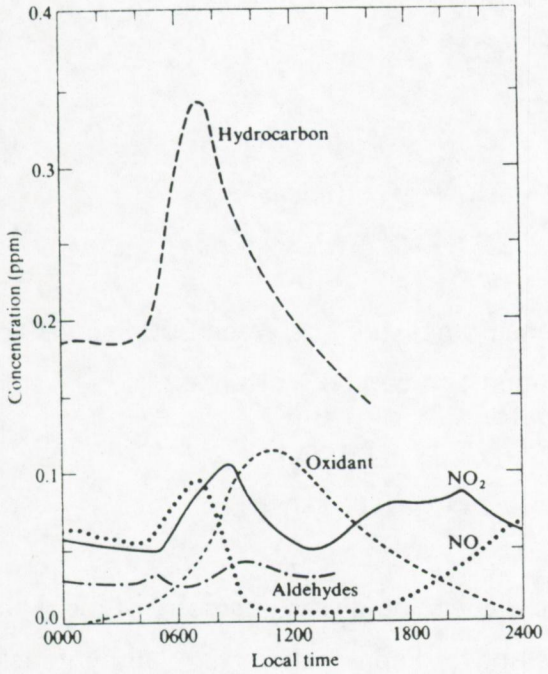

Figure 5.6: Diurnal variation of smog species in Los Angeles (Finlayson-Pitts and Pitts, 1986).

5.4 Analytical equipment

5.4.1 Sulphur dioxide monitor

For in situ measurements of sulphur dioxide concentrations a Thermo Electron pulsed fluorescence SO_2-analyzer, model 43A is used. Data acquisition is established by use of a BBC recorder, model SE430 with three input/output channels.

5.4.1.1 Principle

UV radiation of 220 nm wavelength is used for excitation of SO_2 molecules in the gas phase. The following reactions occur when SO_2 is irradiated with UV light:

$$SO_2 + h\nu_1 \rightarrow SO_2^*$$

$$\begin{aligned} SO_2^* &\rightarrow SO_2 + h\nu_2 \quad (fluorescence) \\ SO_2^* + M &\rightarrow SO_2 + M \quad (quenching) \\ SO_2^* &\rightarrow SO^\circ + O^\circ \quad (dissociation) \end{aligned} \qquad (5.9)$$

The fluorescence intensity measured between 300 and 400 nm is related to the SO_2 concentration and can be written as:

$$F = \frac{G\, k_f\, I_0\, a\, x\, [SO_2]}{k_f + k_d + k_q\, [M]} \qquad (5.10)$$

where G = geometrical factor depending on the geometry of the reaction chamber, k_f = reaction constant for fluorescence, I_0 = lamp intensity, a = absorption factor for SO_2, x = length of the reaction chamber, k_d = dissociation reaction constant and k_q = quenching reaction constant.

5.4.1.2 Gas flow through the monitor

The gas flow enters the monitor through the sample port (Figure 5.7) where aerosol particles with diameter > 1 μm are removed by a filter. Next, the gas stream is led trough a hydrocarbon-kicker for removal of gaseous hydrocarbons. After the hydrocarbon kicker, the gas stream enters the reaction chamber, goes through the flow meter and then trough the critical capillary. Subsequently, the gas stream is led through the hydrocarbon kicker once again, but in opposite direction, and leaves then the monitor trough the exhaust.

5.4.1.3 Hydrocarbon kicker

Because hydrocarbons can absorb UV light and interfere with the measurement of sulphur dioxide in the monitor, they have to be removed. A so-called hydrocarbon kicker consists of a double concentric tube. The inner tube is made of a silicon rubber substance. The entering gas stream

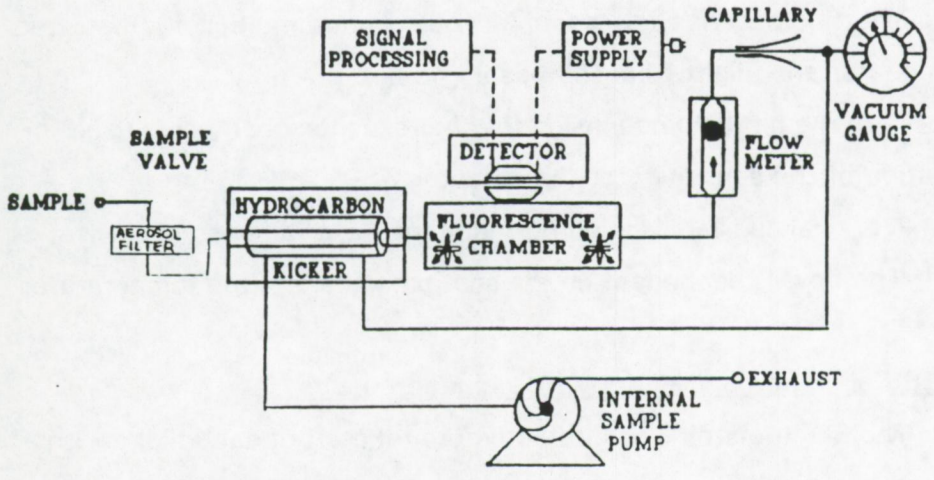

Figure 5.7: SO_2 monitor: schematic view.

flows through the inner tube, while the exiting gas stream flows in opposite direction through the outer tube. Because of the pressure difference between the inner and the outer tube, gas molecules will diffuse trough the inner tube. Since only organic compounds can dissolve in the silicon rubber, only these components will be removed from the gas stream flowing through the inner tube. For effective removal of gaseous hydrocarbons, a pressure difference of at least 0.3 bar is needed.

5.4.1.4 Fluorescence chamber

UV light is generated in the fluorescence chamber with a frequency of 10 Hz. Through a series of lenses and mirrors, the required UV wavelength (220 nm) is obtained. Opposite of the flashing tube a photo detector is installed to enable correction of fluctuations in the flashing intensity.

5.4.1.5 Detector and critical capillary

The fluorescence is measured with a photomultiplier tube after filtering interfering light from the flashing tube.

A light emitting diode inside the fluorescence chamber is used for calibration of the sensitivity of the detector.

A critical capillary is used for maintenance of a constant flow of 2 $l.min^{-1}$. The flow is dependent on the inlet pressure and the temperature.

5.4.1.6 Calibration and performance characteristics

The SO_2 monitor is calibrated before take-off of each flight with a standard gas mixture of sulphur dioxide and clean air.

Some optical, electronical and sampling modifications were carried out by the KEMA company (Arnhem, The Netherlands) in order to increase the response time.

5.4.2 Ozone monitor

5.4.2.1 Principle

For in situ measurements of ambient ozone concentrations a Bendix, model 8002 ozone monitor is used. The operation of this instruments is based on the photometric detection of chemiluminescence that occurs through a gas-phase reaction of ethylene with ozone.

5.4.2.2 Operational mode

The instrument can be used in three different modes. In the zero mode, ozone-free air is led into the reaction chamber together with ethylene. In the span mode an ozone generator is used for producing a known concentration of ozone. In the ambient mode, ambient air is led into the reaction chamber through a Teflon filter that removes all particles with a diameter > 10 μm.

5.4.2.3 Ozone generator

The ozone generator is made up of a ultra-violet lamp and a quartz tube. Dried ozone-free air, which was passed through a chemical filter consisting of molecular sieves, silicagel and active coal, is passed trough the quartz tube where ozone is generated by UV light.

5.4.2.4 Detector cell

The detector cell in the ozone analyzer exists of a photomultiplier. Inside the detector thermo-electrical coders are used to maintain the temperature at 5 °C. This increases the lifetime of the detector and reduces the background noise.

5.4.2.5 Reaction chamber

In the reaction chamber, the sampled atmosphere is mixed with ethylene. Between the reaction chamber and the photomultiplier, a window is placed for protective purposes.

5.4.2.6 Calibration and performance characteristics

Calibration is performed with ozone-free air and with a standard gas mixture with known ozone concentration. This calibration is performed before take-off of each flight.

The detection limit is 1 ppb, while a response time of 10 s is achieved.

5.5 Vertical profiles of sulphur dioxide and ozone concentrations above the Southern Bight of the North Sea

5.5.1 Meteorological aspects of air pollution

5.5.1.1 Dispersion of pollutants

The atmospheric layer into which pollutants are emitted seems to be a gigantic reservoir of about 5×10^{18} m^3. However, most of the pollution is emitted into relatively small air parcels over urban and industrial areas. Episodic air pollution disasters have shown that at certain periods of stagnating air masses, the limit of the dispersive power of the atmosphere has been reached.

The energy for all meteorological processes like material dispersion, diluting, scavenging and removal processes, is supplied by the sun. Part of the solar radiation does not reach the earth's surface but is rather attenuated and scattered back into space. The remaining part of the solar radiation is absorbed by the earth's surface and re-emitted as longwave or heat radiation. The air layers closest to the earth's surface are heated and start to rise as convectional air streams. The air motion produced in this way will disperse and dilute air pollutants.

Differential solar heating of the earth's surface produces pressure and temperature differences and hence air motion. Wind speed and turbulence are proportional to the transport and dispersion of pollutants. Mechanical turbulence is produced by passing air over a rough surface, and thermal turbulence is induced by thermal heating and convectional vertical airflow.

5.5.1.2 Environmental lapse rate and atmospheric stability

By heating the ground surface and the air adjacent to it, solar radiation produces changes in temperature with height, defined as the

environmental lapse rate. In well-mixed, dry air the dry adiabatic lapse rate is 1 °C per 100 m, which means that for each increase of 100 m in altitude, the temperature decreases with 1 °C. When the temperature decreases with height, as it usually does, the lapse rate is said to be positive.

When a warm air parcel (warmer than the surrounding ambient air) rises in an atmosphere with a lapse rate that exceeds the adiabatic lapse rate (i.e. the temperature decreases more rapidly than 1 °C/100 m), it will cool off at an adiabatic lapse rate of 1 °C/100 m (Figure 5.8). The temperature difference between the rising air parcel and the surrounding ambient air will increase with altitude and further vertical rising of the air parcel will continue.

An air parcel which is colder than its surrounding temperature will descend and warm up adiabatically in that same atmosphere. The temperature of the surrounding air increases faster and the downward motion of the air parcel continues.

A type of atmosphere where vertical motion is encouraged in both directions is said to be unstable. The lapse rate for such instability is called superadiabatic.

If, on the other hand, the environmental lapse rate is less than the adiabatic lapse rate, the atmosphere is stable and does not allow vertical mixing of pollutants. A rising warm air parcel will cool-off more rapidly than the surrounding air. A point is reached where the temperature of the rising air parcels equals the ambient air temperature. Any further upward motion would be opposed by a negative buoyancy force since the parcel would become slightly cooler than its surrounding atmosphere and thus would descend again.

Some of the most severe episodes of air pollution occur in stable air, or in air above which for some reason there is a stable layer of air.

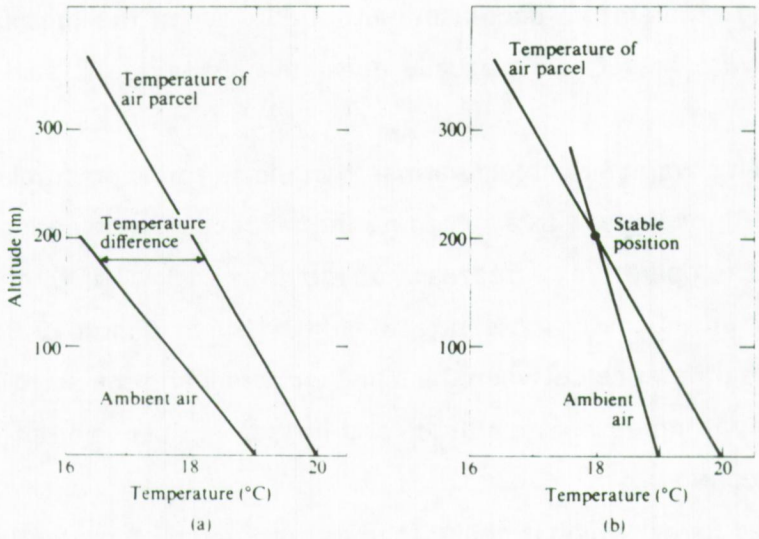

Figure 5.8: Unstable (a) and stable (b) atmospheres (Williamson, 1973).

5.5.1.3 Inversions

Extreme cases of atmospheric stability are characterized by a negative lapse rate, where the temperature increases with altitude. The region where the lapse rate is negative is called the temperature inversion layer.

Solar heating in a cloud-free atmosphere can result in high ground temperatures during the late morning and the afternoon. However, at night, radiation to the cold sky causes cooling at the ground. Consequently a radiative temperature inversion is formed at night and disappears again during the morning. The radiative inversion is suppressed in the case of clouds. Strong winds will also smooth out temperature gradients by mechanical turbulence.

Subsidence inversions (Figure 5.9) occur at altitudes between 300 and 1000 m generally. They are formed by the subsiding air that descends

slowly at a rate of 1000 m/day in an anticyclone. As the air sinks to lower altitudes and higher pressures, it is compressed and its temperature rises above the temperature of the air underneath. Thus the subsiding air establishes a temperature inversion with respect to the low-lying air.

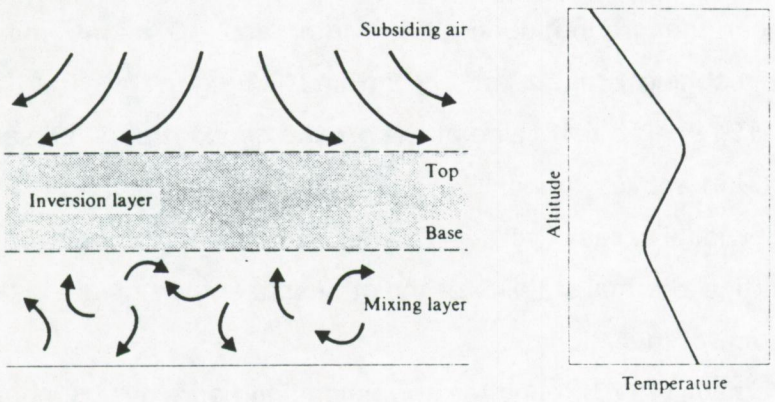

Figure 5.9: Subsidence inversion layer (Williamson, 1973).

Generally the base of the inversion does not touch the ground during the day. Heat radiation from the earth's surface allows upward convection and erodes the underside of the inversion. At night, the inversion layer may descend close to the ground, severely restricting the volume of the underlying mixing layer. Subsidence inversions may exist for several days.

Frontal inversions arise in conjunction with the interface between two air masses of quite different temperature, humidity and pressure.

One type of advective inversion is formed when warm air moves over a cold surface. Convective cooling of the lowest layer then leads to formation of a ground-based inversion. Another type of advective inversion is formed when warm air is forced to move over the top of a cold layer by for instance a mountain range.

5.5.2 Vertical SO2 profiles as reported in literature

From vertical SO2 measurements reported by Georgii and Jost (1964) and Jost (1964) it is clear that over western Europe the average SO_2 concentrations in unpolluted air decrease with altitude from about 20 $\mu g.m^{-3}$ near the ground during the winter and 10 $\mu g.m^{-3}$ during the summer, reaching 5 $\mu g.m^{-3}$ at 2-3 km and 0.5 $\mu g.m^{-3}$ at 5 km altitude (Georgii, 1978). The half value of the ground concentration is reached at about 1.5 km above ground.

Individual cases of vertical SO_2 distributions are strongly influenced by the vertical thermal stability of the atmosphere, particulary in the case of formation of inversions.

Varheyli (1978) found the corresponding figure over Hungary to be about one order of magnitude smaller than the concentrations reported by Georgii and Jost (1964). In contrast, the results of aircraft flights, carried out by Gravenhorst (1975) over the Bay of Biscay, indicate much less SO_2 vertical decrease over the sea than over continental areas.

Stauff and Jaescke (1975) performed SO_2 measurements in the upper troposphere and the lower stratosphere. Within the troposphere up to an altitude of 5 km, the SO_2 concentration decreases sharply to values around 100 ppt. Above 5 km a constant value up to the tropopause is observed. A SO_2 concentration of 20 to 100 ppt seems typical for the layer above 6 km and can be considered a background value for the higher troposphere.

Above the oceans nearly constant SO_2 concentrations in the troposphere were observed during aircraft flights over the Atlantic. A background concentration of approximately 0.2 to 1.0 $\mu g.m^{-3}$ is suggested.

5.5.3 Vertical temperature, sulphur dioxide and ozone profiles measured above the Southern Bight of the North Sea.

5.5.3.1 Average sulphur dioxide and ozone profiles

The average sulphur dioxide and ozone concentrations for each track of all 18 flights were classified into 10 altitude classes (0-100m, 100-200m, 200-400m, 400-600m, 600-800m, 800-1000m, 1000-1200m, 1200-1400m, 1400-1800m and 1800-2800m) (Figure 5.10). The average ozone profile shows a clear increase in concentration with increasing altitude. At sea level, an average ozone concentration of 35 ppb was measured, while above 1000m average values of 60 to 70 ppb were obtained.

For sulphur dioxide, a reverse trend can be observed. Generally, SO_2 concentrations at lower levels are higher than at higher altitudes. The maximum average SO_2 was measured between 100 and 200 m (16 ppb), while at the sea level, an average value of 10 ppb was measured. This is in good agreement with the average trace metal profiles as discussed in Chapter 3: trace metal levels yield also maxima between 100 and 200 m.

In the next subsections some specific profiles of selected flights are discussed.

5.5.3.2 Flight 6

Figure 5.11 shows the temperature, SO_2 and O_3 profiles measured during flight 6. This flight was performed when the sampled air masses originated from northwestern direction. The measured concentration profiles can therefore be regarded as background profiles for the atmosphere above the Southern Bight of the North Sea.

A lapse rate of 0.92 °C/100 m is measured between 15 and 1970 m. At 1970 m altitude a sharp temperature inversion is located. The sulphur dioxide concentration below the temperature inversion layer was nearly constant and very low with an average of 2.8 ppb. The ozone

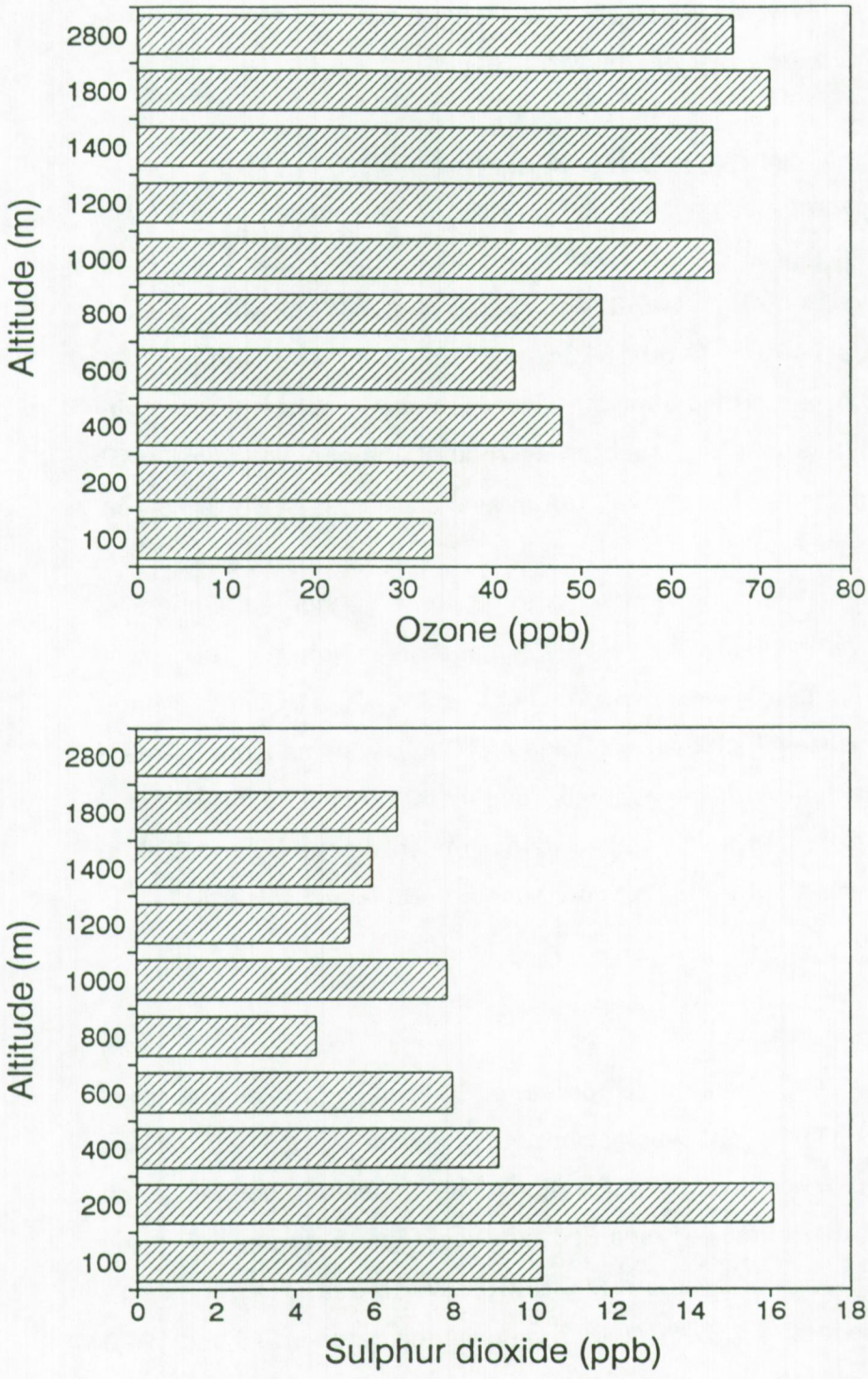

Figure 5.10: Average ozone and sulphur dioxide concentrations as a function of altitude above the Southern Bight of the North Sea.

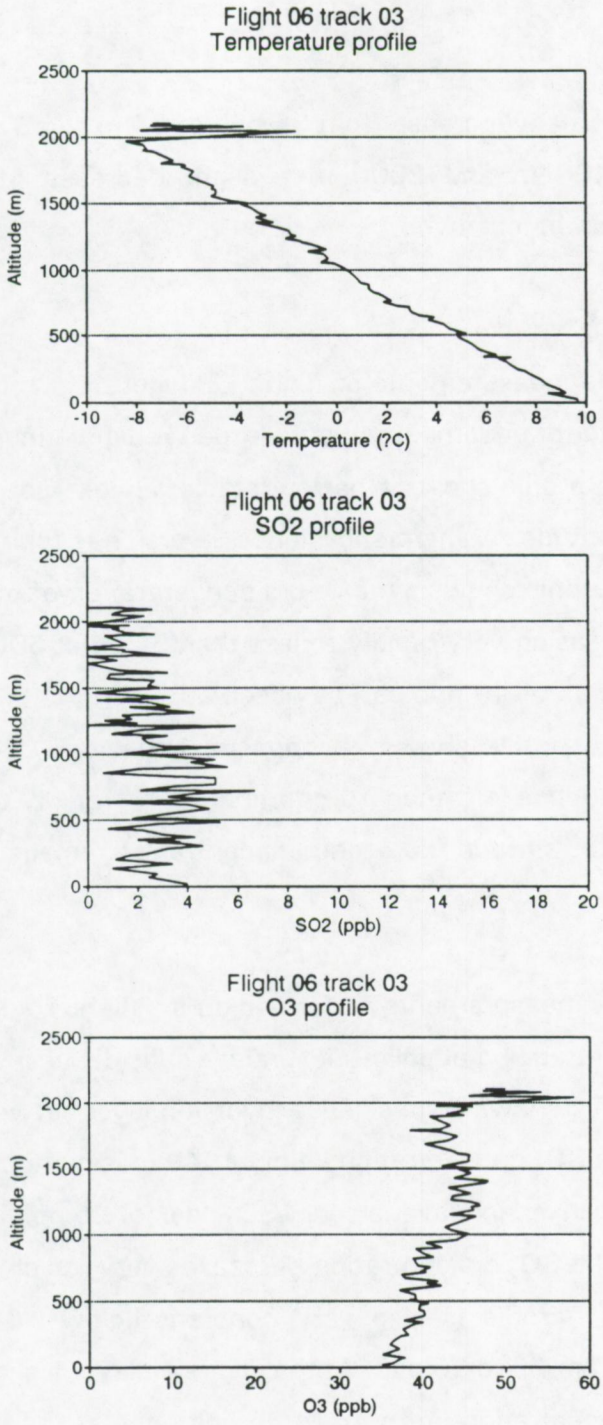

Figure 5.11: Flight 6 - T, SO_2 and O_3 profile.

profile shows a steady increase from 35 ppb at 15 m to 45 ppb at 1400 m. Between 1400 m and 2000 m a slight decrease of the ozone concentration can be observed.

5.5.3.3 Flight 12

The profile measurements of flight 12 (Figure 5.12) illustrate the capture of pollutants underneath a low altitude radiative inversion layer. The temperature profile shows a narrow stable, almost isothermal layer around 350 m altitude. A sharp subsidence inversion is found at 950 m.

The SO_2 profile shows a maximum concentration of 50 to 60 ppb at sea level decreasing very rapidly to less than 5 ppb at 500 m. At 350 m a small SO_2 peak of 40 ppb can be observed.

The ozone profile shows an opposite behaviour. The sea level ozone concentration is less then 10 ppb, increasing rapidly to 40 ppb at 500 m. Above this altitude the ozone concentration remains 40 ppb.

5.5.3.4 Flight 15

The profile measurements performed during flight 15 (Figure 5.13) are an example of trapping of pollutants under a subsidence inversion. The temperature profile shows a subsidence inversion layer between 1040 m and 1190 m. The SO_2 concentration below 1040 m is quite constant (15 to 17 ppb). In the inversion layer a sharp SO_2 peak of 26 ppb is observed. Above 1190 m the SO_2 concentration decreases very rapidly to 10 ppb.

The ozone profile is also very constant below 1040 m with concentrations from 25 to 30 ppb. At the inversion layer a sharp increase of the ozone concentration up to 45 to 50 ppb occurs.

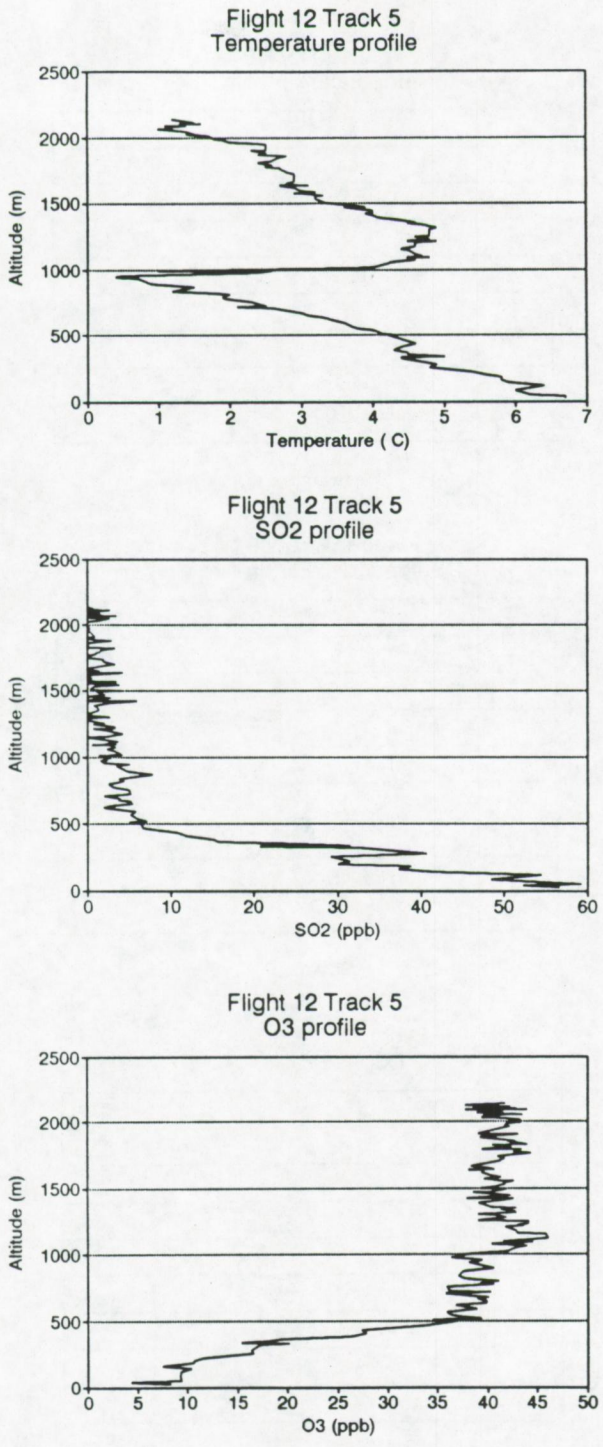

Figure 5.12: Flight 12 - T, SO_2 and O_3 profile.

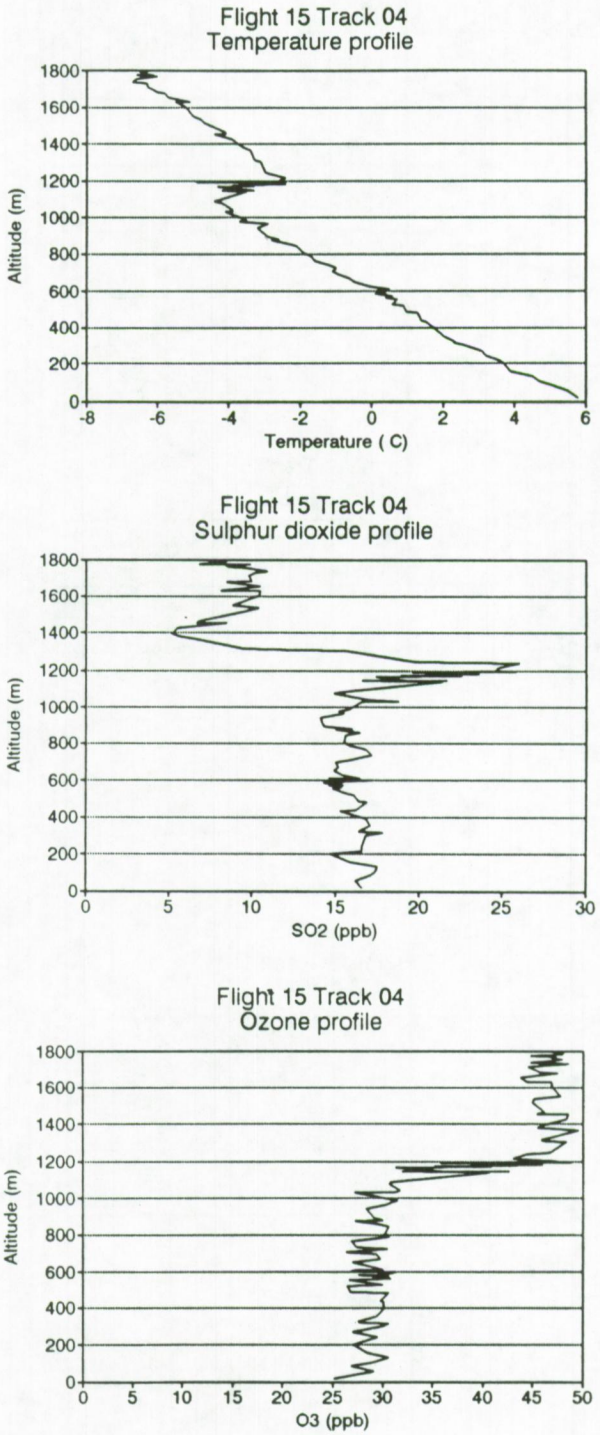

Figure 5.13: Flight 15 - T, SO_2 and O_3 profile.

5.5.3.5 Flight 16

Besides a radiative inversion layer between sea level and 450 m and a subsidence inversion layer between 2350 and 2450 m, the temperature profile of flight 16 yields a lapse rate of 0.86 °C per 100 m which results in a stable atmosphere that does not allow good mixing of pollutants (Figure 5.14).

The sulphur dioxide profile indicates a minimum level of 20 ppb between the two inversion layers. Superimposed on this minimum concentration, several high SO_2 peaks can be located: 60 ppb at 620 m, 115 ppb at 940 m and 95 ppb at 1140 m. The presence of several sharp sulphur dioxide peaks confirms the stability and low mixing ability of the atmosphere.

The fact that the sulphur dioxide concentration above the subsidence inversion layer and underneath the radiative inversion layer goes down rapidly from 20 ppb to 5 ppb illustrates that all pollutants are trapped between the two inversion layers.

The ozone profile of flight 16 shows a sharp increase in concentration from 35 ppb at sea level to 85 to 90 ppb at 450 m. Between 450 m and 1500 m a large gap at 940 m is present, corresponding to the high sulphur dioxide concentration at that level. Between 1500 m and 2350 m high ozone concentrations of 90 to 100 ppb are present. These high levels are probably due to photochemical reactions involving pollutants such as hydrocarbons and nitrogen oxides, since above the subsidence inversion layer ozone levels decrease again to about 75 ppb.

5.5.3.6 Flight 17

A low radiative inversion at 250 m and a subsidence inversion at 2200 m are illustrated in the temperature profile of flight 17.A sharp SO_2 peak of 24 ppb is present below the lower inversion, while SO_2 concentrations between the two inversion layers show a rather uniform

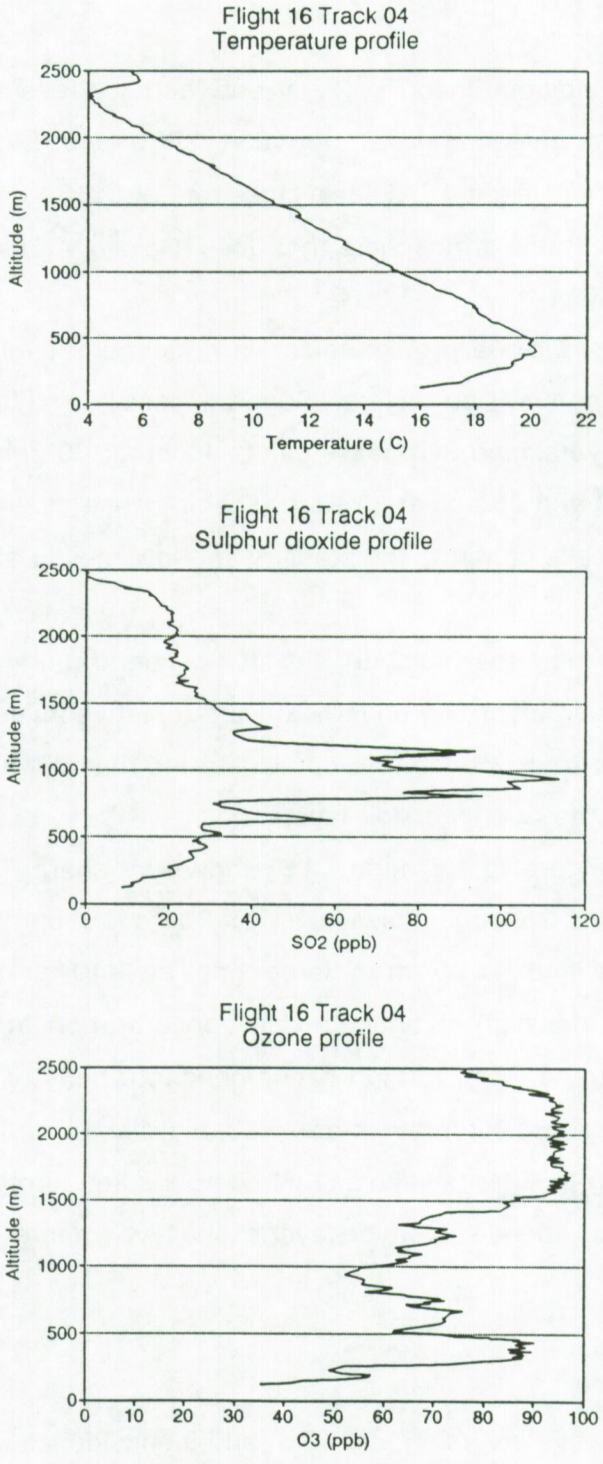

Figure 5.14: Flight 16 - T, SO_2 and O_3 profile.

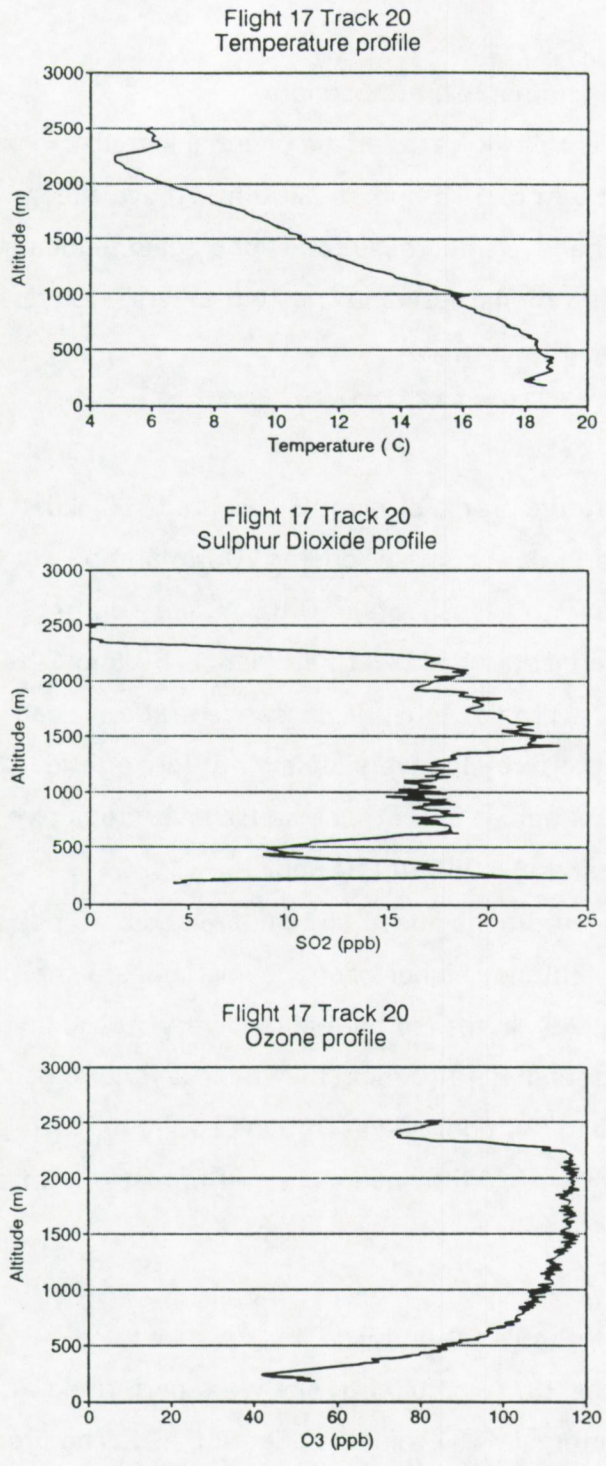

Figure 5.15: Flight 17 - T, SO_2 and O_3 profile.

profile, typical for un unstable atmosphere.

The ozone profile indicates an exponential increase in ozone levels from 40 ppb at 250 m to 115 ppb at 2200 m. Above the subsidence inversion, the ozone levels decrease to 80 ppb again, indicating that the high ozone concentrations between the two inversion layers is due to photochemical smog formation.

5.5.3.7 Flight 21

The temperature profile of flight 21 (Figure 5.16) illustrates a two-fold inversion layer at low altitude (one at 200 m and one at 370 m), a stable atmosphere with a lapse rate of 0.85 °C per 100 m between 430 and 1160 m and an isothermal layer between 1160 and 1480 m.

In the SO_2 profile two peak concentrations can be found corresponding to the twofold inversion layer at low altitude: 15 ppb at 150 to 210 m and 8 ppb at 350 m. The stable layer traps two SO_2 peaks at 810 m (9 ppb) and at 1050 m (10 ppb).

Ozone concentrations above 1550 m are about 40 ppb. In all three layers below this altitude, higher ozone levels indicate the presence of photochemical activity. In the isothermal (and very stable) layer an ozone peak of 56 ppb is found at 1420 m. In the stable layer two peak levels are measured at 1030 m (95 ppb) and at 860 m (100 ppb). Two other peaks are located at the two-fold low inversions: 74 ppb at 400 m and 68 ppb at 300 m.

5.5.3.8 Flight 23 - Profiles A and B

During flight 23, two spiral tracks were performed at a different location with an interval of 37 minutes (Figure 5.17). The first track was flown at 51°95'N 4°41'E and between 11.13 h and 11.18 h (October 17, 1989). The wind direction varied between 220° and 260°.

The second spiral flight was flown much more east at position 51°84'N 2°26'E and between 11.50 h and 11.56 h, on October 17,

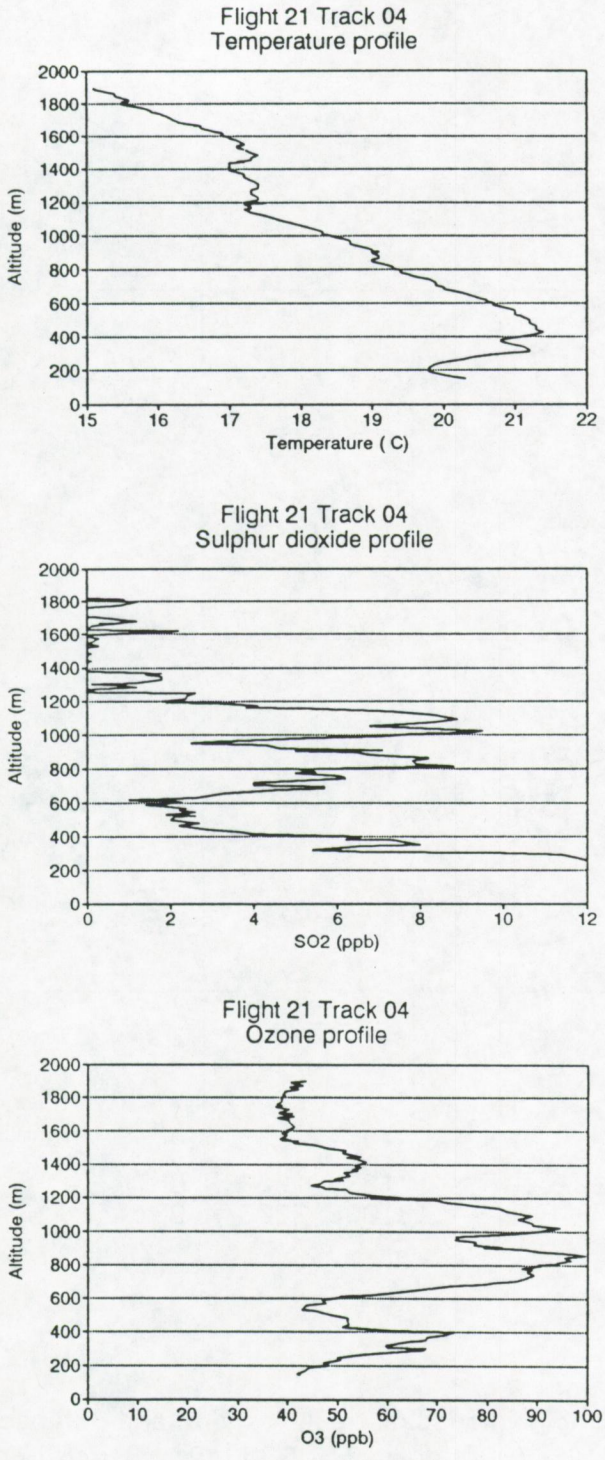

Figure 5.16: Flight 21 - T, SO_2 and O_3 profile.

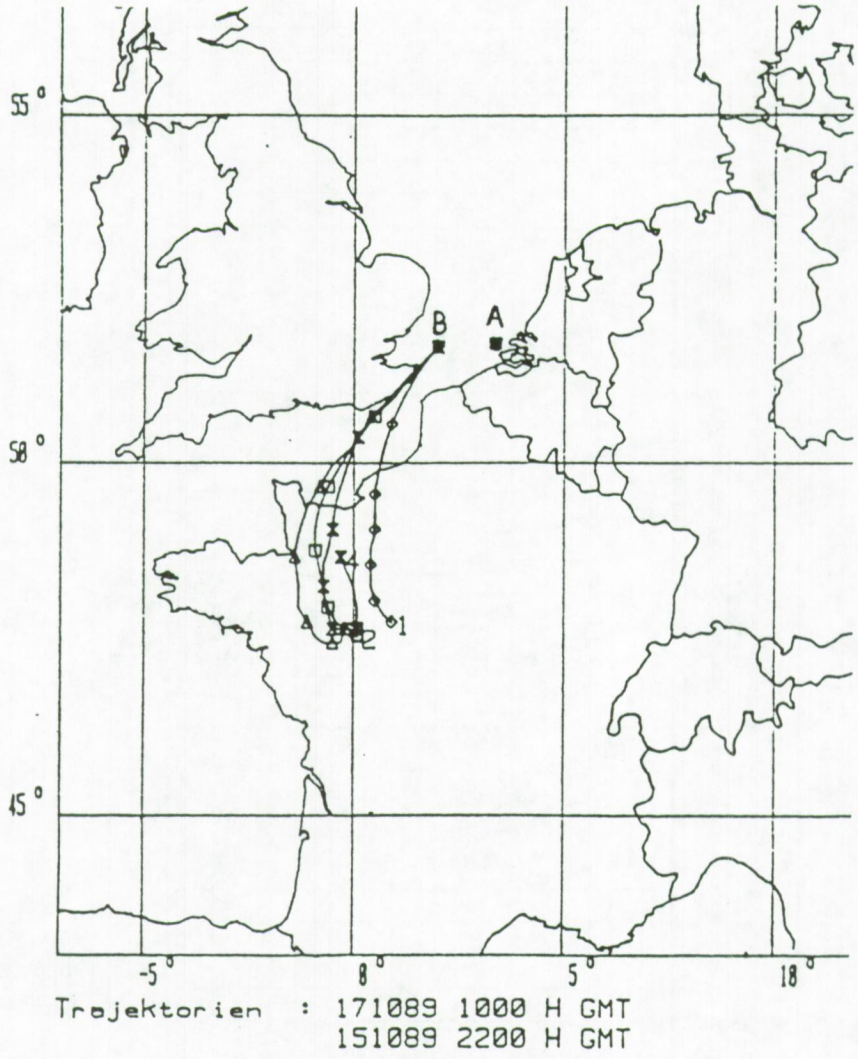

Figure 5.17: Sampling points (spiral track A and B) and 36h backward air mass trajectories (1 = 1000 mbar, 2 = 925 mbar, 3 = 850 mbar and 4 = 700 mbar) for flight 23.

1989. Doppler-radar measured wind directions varied between 200° and 235°.

If we compare both temperature profiles (Figure 5.18 and 5.19) we can see that during the first profile track, the temperature inversion layer is located between 590 and 900 m. In the second track, this inversion layer is located between 720 and 950 m and a second inversion has been formed between 340 and 440 m. This inversion layer could be a frontal inversion formed by the interaction of two air masses with different meteorological characteristics.

The sulphur dioxide profiles are quite different. The first profile shows an exponential decrease in SO_2 concentration with altitude, while the second profile shows a very sharp sulphur dioxide peak at 480 m (24 ppb). In the ozone profile, less variation is obvious.

5.6 Average sulphur dioxide and ozone concentrations under the temperature inversion layer

5.6.1 SO_2 and O_3 concentrations as a function of wind direction

Table 5.5 lists the average sulphur dioxide and ozone concentration for the different wind sectors as described in Chapter 3.

The average SO_2 concentration over all flights, below the temperature inversion layer, equals 10.0 ppb. For individual flights, the average SO_2 concentration varies from 1.9 ppb for flight 18 to 19.5 ppb for flight 13. Although important variations are observed within each wind sector, the average SO_2 concentration per windsector indicates that similar concentrations are found for the NE-E and the SW-W sector. The NW-N sector yields much lower concentrations, while the SE-S and the variable windsector show higher average SO_2 concentrations (Table 5.5).

The average ozone concentration below the temperature inversion layer, measured over 18 flights, equals 46 ppb. The lowest concentration

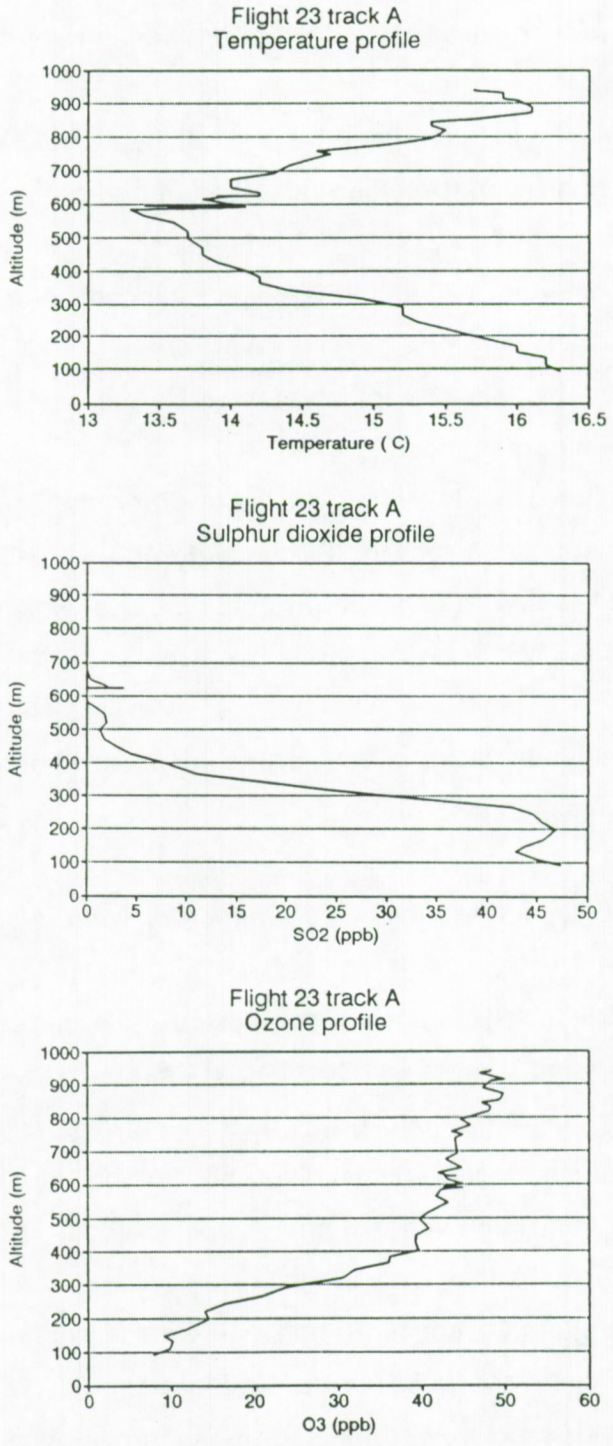

Figure 5.18: Fligt 23, spiral track A - T, SO_2 and O_3 profile.

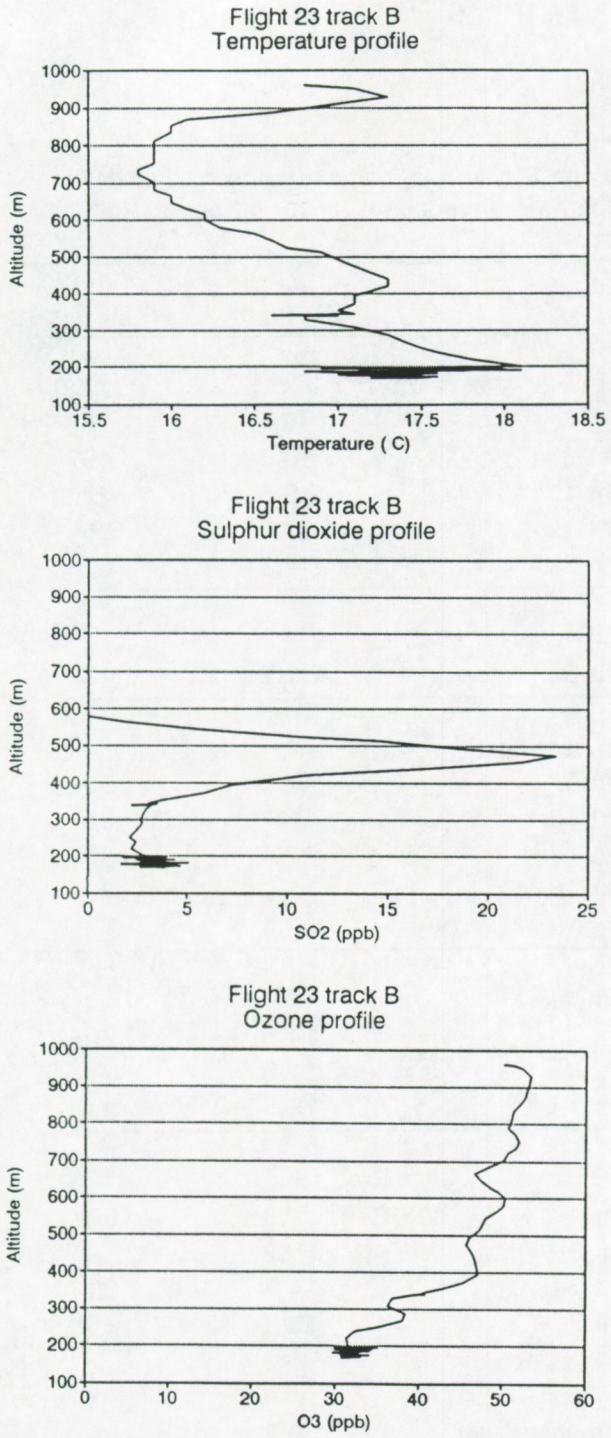

Figure 5.19: Flight 23, spiral track B - T, SO_2 and O_3 profile.

Table 5.5:
Average SO_2 and O_3 concentration below the temperature inversion layer for different wind sectors.

	SO_2 (ppb)	O_3 (ppb)
Southwest-West		
Flight 2	9.1	75
Flight 3	10.5	45
Flight 11	9.5	22
Flight 12	7.3	26
Flight 22	4.8	62
Northwest-North		
Flight 6	2.8	43
Northeast-East		
Flight 5	7.8	50
Flight 15	11.7	38
Flight 17	12.4	96
Flight 18	2.8	70
Flight 19	7.4	76
Southeast-South		
Flight 7	14.5	20
Flight 8	11.5	13
Flight 13	19.5	34
Variable		
Flight 4	1.9	50
Flight 9	15.2	8
Flight 14	14.7	35
Flight 21	16.3	66
Averages		
Southwest-West	8.2	46
Northwest-North	2.8	43
Northeast-East	8.4	66
Southeast-south	15.2	22
Variable	12.0	40
All sectors	10.0	46

(8 ppb) was measured during flight 9, while the highest concentration was observed during flight 17 (96 ppb).

Three windsectors (SW-W, NW-N and variable) yield similar ozone concentrations: 46, 43 and 40 ppb, respectively. For the SE-S sector, the average ozone concentration is a factor of 2 lower (22 ppb) while for the NE-E sector a relatively high ozone concentration of 66 ppb is observed.

5.6.2 Seasonal influence in SO_2 and O_3 concentrations

Figure 5.20 plots the average sulphur dioxide and ozone concentration below the temperature inversion layer as a function of flight number. Flights 2 to 6 were performed between September and October 1988, flights 7 to 15 between November 1988 and April 1989 and flights 17 to 22 between May 1989 and August 1989. The ozone concentration shows a clear seasonal dependence. All flights from 7 to 15 (winter period) yield ozone concentrations below 40 ppb, while all other flights (summer periods) yield ozone concentrations above 40 ppb.

Although the SO_2 concentration is generally anticorrelated with the ozone concentration, no obvious seasonal trend can be observed for SO_2. It seems that sulphur dioxide concentrations are primarily dependent on the wind direction and ozone concentrations are rather dependent on the season.

5.7 Relation between sulphur dioxide and trace metals

Figure 5.21 shows average sulphur dioxide concentrations and trace metal concentrations below the temperature inversion layer as a function of flight number. Generally speaking, similar trends can be found although some exceptions are obvious.

For Pb and Zn, concentrations during flight 21 are similar to those during flights 19 and 22 although the sulphur dioxide level is much higher

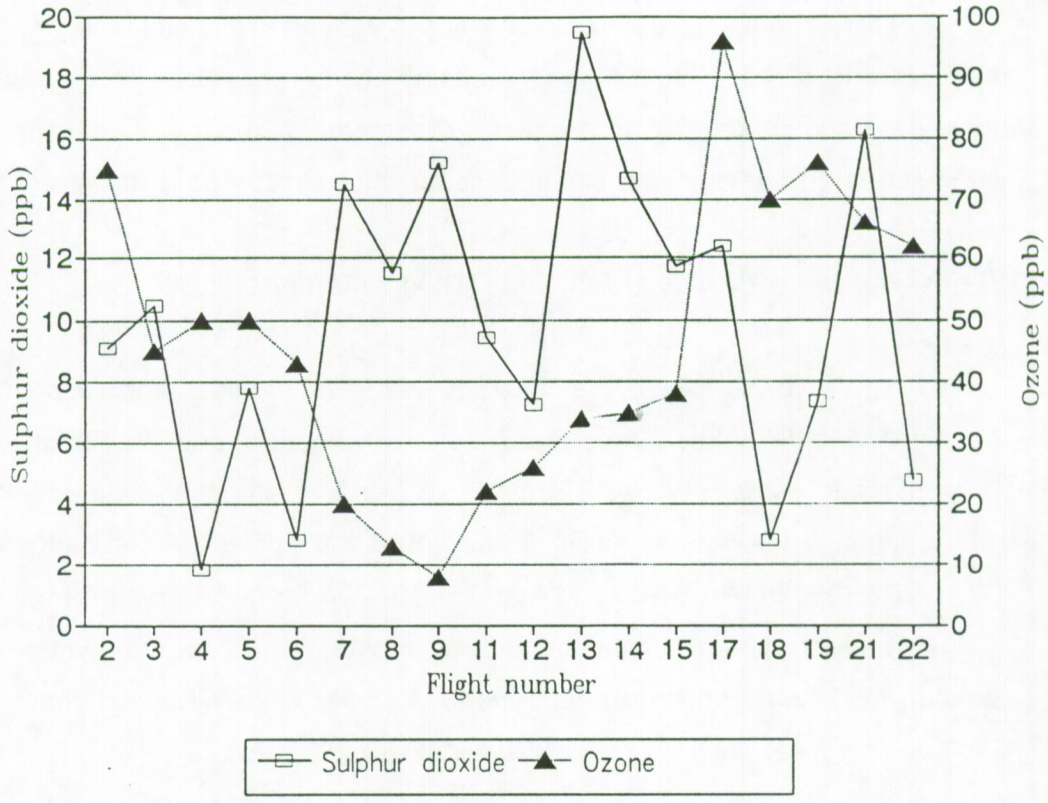

Figure 5.20: Average SO_2 and O_3 concentrations below the temperature inversion layer as a function of flight number.

during flight 21 (16.3 ppb) than during flight 19 (7.4 ppb) and 22 (4.8 ppb).

For Cu, an extremely high concentration is found for flight 22 (56 $ng.m^{-3}$ versus < 25 $ng.m^{-3}$ for all other flights).

Cd concentrations are also high for flight 22. Compared with flight 21, the Cd concentration increases by a factor of 5 in flight 22, while the sulphur dioxide concentration decreases by a factor of three from flight 21 to flight 22. Cd levels measured during flights 5 and 13 are relatively high compared with the corresponding sulphur dioxide concentration.

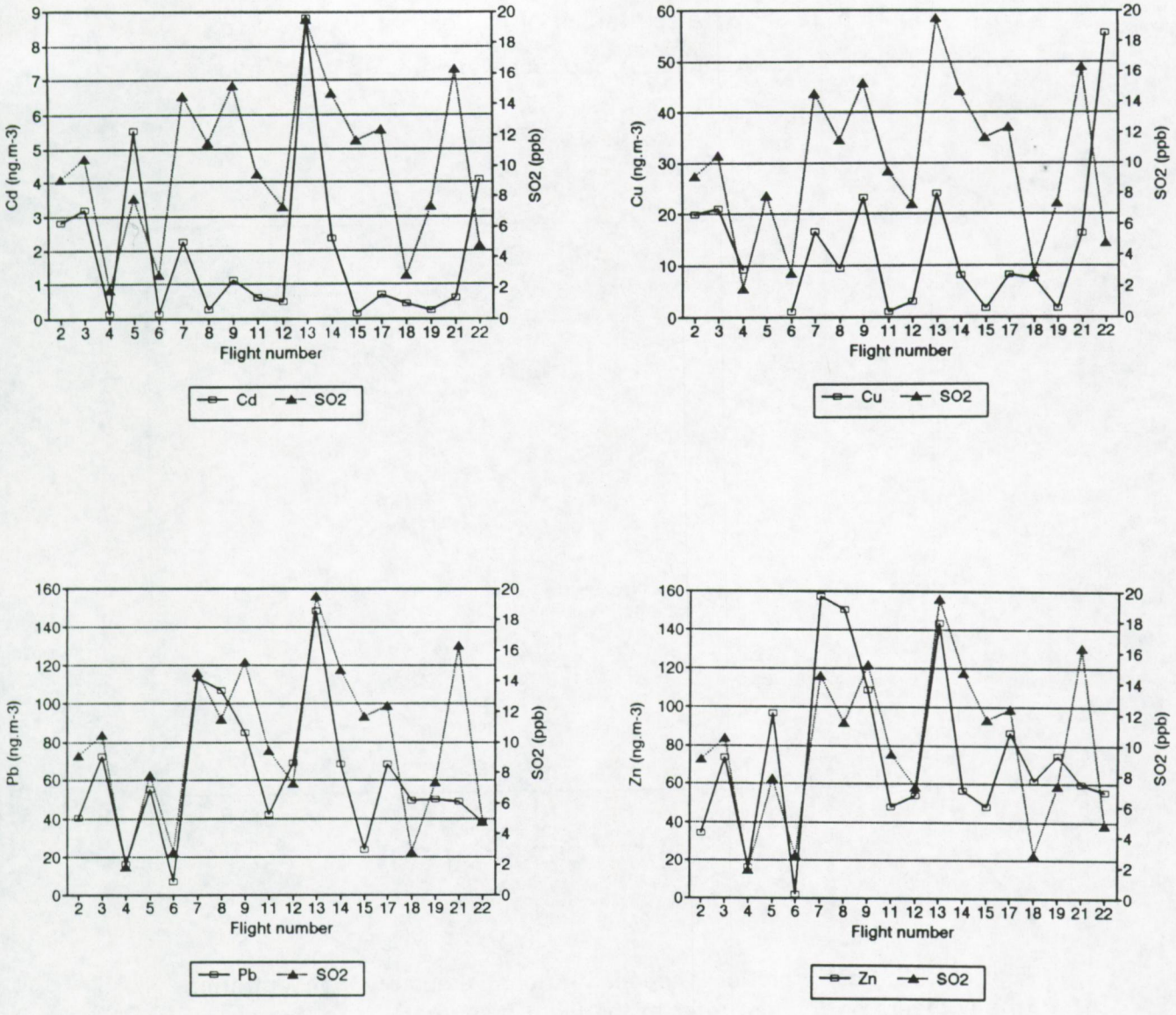

Figure 5.21: Cd, Cu, Pb and Zn concentration versus SO_2 concentration: average levels under the temperature inversion layer as a function of flight number.

Figure 5.22 shows a scatterplot of Pb concentrations versus sulphur dioxide concentrations. A poor correlation of 0.52 is found.

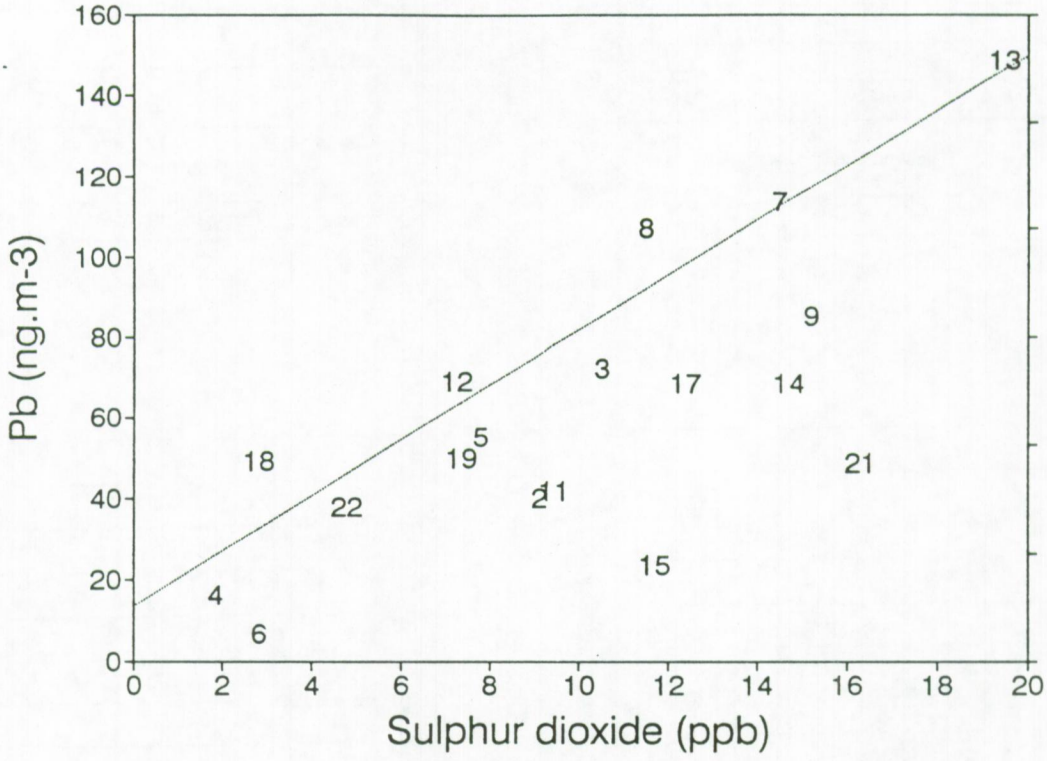

Figure 5.22: Scatterplot of Pb concentrations versus SO_2 concentrations (the numbers on the plot refer to the flight numbers).

5.8 Conclusion

During 18 sampling flights over the Southern Bight of the North Sea, sulphur dioxide and ozone concentrations were measured in the lower troposphere.

Average SO_2 concentrations below the temperature inversion layer ranged from 1.9 ppb during flight 18 to 19.5 ppb during flight 13. For the

NE-E and the SW-W wind sector, the average SO_2 concentrations are very similar: 8.4 and 8.2 ppb, respectively. The NW-N sector yields a much lower average concentration of 2.8 ppb SO_2 while the SE-S and the variable sector show higher average SO_2 concentrations of 15.2 and 12.0 ppb, respectively.

The average ozone concentration, measured over all flights, equals 46 ppb, ranging from 8 ppb (flight 9) to 96 ppb (flight 17). Low ozone concentrations illustrate ozone depletion through reaction with freshly emitted pollutants, while high ozone levels reflect photochemical activity due to automotive emissions. The SW-W, NW-N and variable wind sector show similar average ozone concentrations of 46, 43 and 40 ppb, respectively. For the SE-S sector, the average ozone concentration is two times lower (22 ppb), while the NE-E sector yields a high average of 66 ppb.

Ozone concentrations seem to be primarily dependent on seasonal influence, while SO_2 levels are more dictated by the history of the sampled air mass.

Although SO_2 and trace metal levels show similar trends, some differences are obvious. The correlation-coefficient between SO_2 and Pb concentrations is 0.52.

The highest SO_2 concentrations (just as the highest trace metal levels) are found between 100 and 200 m altitude. The average ozone profile shows an increase from 30-40 ppb at the sealevel to 60-70 ppb at altitudes above 1000 m.

Individual sulphur dioxide and ozone profile measurements clearly illustrate the high variability in vertical concentration distributions. The presence of SO_2 peaks at certain altitudes depends on the presence of radiative and subsidence inversion layers and on the atmospheric stability, i.e. the environmental laps rate.

5.9 References

Barrie L. and Georgii H.W. (1976): *An experimental investigation of the absorption of sulfur dioxide by water droplets containing heavy metal ions.* Atmos. Environ. 10, 743-749.

Beilke S. (1980): *Luftchemisches Verhalten von SO_2, Ergebnisse der VDI-Arbeitsgruppe "Luftchemie"*, 12-25.

Berresheim H. and Jaeschke W. (1982): *Sulfur emissions from volcanoes.* In Chemistry of the Unpolluted and Polluted Troposhere. Georgii H.W. and Jaeschke W. (Eds.), D. Riedel, Dordrecht, 325-337.

Cullis C.F. and Hirschler M.M. (1980): *Atmospheric sulphur: natural and man-made sources.* Atmos. Environ. 14, 1263-1278.

Erickson E. (1960): *The yearly circulation of chloride and sulfur in nature; meteorological, geochemical and pedological implications.* Tellus 11, 375-403.

Erickson E. (1963): *The yearly circulation of sulfur in nature.* J. Geophys. Res. 68, 4001-4008.

Finlayson-Pitts B.J. and Pitts Jr. J.N. (1986): *Atmospheric Chemistry: Fundamentals and Experimental Techniques.* John Wiley and Sons, New-York.

Friend J.P. (1973): *The global sulphur cycle.* In Chemistry of the Lower Atmosphere. Rasool S.I. (Ed.), Plenum, New York, 177-201.

Georgii H.W. (1978): *Large scale spatial and temporal distribution of sulfur compounds.* Atmos. Environ. 12, 681-691.

Georgii H.W. (1982): *The atmospheric sulfur budget.* In Chemistry of the Unpolluted and Polluted Troposhere, Georgii H.W. and Jaeschke W. (Eds.), D. Riedel, Dordrecht, 295-324.

Georgii H.W. and Jost D. (1964): *Untersuchungen über die Verteilung von Spurengasen in der freie Atmosphäre.* Pure and Apl. Geophys. 59, 217-224.

Granat L., Hallberg R.O. and Rodhe H. (1976): *The global sulphur cycle.* In Nitrogen, Phophorus and Sulfur - Global Cyles. Svensson B.H. and Soderlund R. (Eds.), SCOPE Report 7, Stockholm, Ecol. Bull. 22, 39-134.

Gravenhorst (1975): *Der Sulfatanteil in atmospharischen Aerosol uber den Nord Atlantic.* Berichte des Inst. Meteorol. Geophys. Universitat Frankfurt/Main, vol 30.

Jost D. (1974): *Aerological studies on the atmospheric sulphur budget.* Tellus 26, 206-213.

Junge C.E. (1963): *Air Chemistry and Radio-activity.* Academic Press, New York.

Kellogg W.W., Cadle R.D., Allen E.R., Lazrus A.L. and Martell E.A. (1972): *The sulphur cycle.* Science, 175, 587-596.

Kelchtermans T. (1989): *Mina-Plan 2000: analyse en voorstel voor een vernieuwd Vlaams milieu- en natuurbeleid.* Ministerie Vlaamse Gemeenschap, Brussel.

Meszaros E. (1981): *Atmopsheric Chemistry. Fundamental Aspects.* Elsevier, Amsterdam.

Ockelmann G., Meixner F. and Georgii H.W. (1981): *SO_2-measurements over the Artic and Atlantic Ocean.* IAMAP General Assembly, Hamburg.

Robinson E. and Robbins R.C. (1968): *Sources, abundance and fate of gaseous atmopsheric pollutants.* SRI Project Report PR-6755, prepared fro American Petroleum Institute, New York.

Robinson E. and Robbins R.C. (1970): *Gaseous sulfur pollutants from urban and natural sources.* J. Air Poll. Control Assoc. 20, 233-235.

Rowland F.S. and Molina M.J. (1975): *Chlorofluoromethanes in the environment.* Re. Geophys. Space Phys. 13, 1.

Runca-Koberich D. and Georgii H.W. (1978): *Surface recations of SO_2 on aerosol particles.* J. Aerosol Sci. 9, 238-240.

Salmon L., Atkins D.H.F., Fisher E.M.F. Healy C. and Law D.V. (1978): *Retrospective trend analysis of the content of U.K. particulate material 1957-1974.* Sci. Tot. Environ. 9, 161-200.

Seinfield J.H. (1986): *Atmospheric Chemistry and Physics of Air Pollution.* John Wiley and Sons, New York.

Stauff J. and Jaeschke W. (1975): *A chemiluminiscence technique for measuring atmospheric trace concentrations of sulfur dioxide.* Atmos. Environ. 9, 1038-1039.

Twomey S. (1972): *Measurements of the size of natural cloud nuclei by means of nuclepore filters.* J. Atmos. Sci. 29, 318-321.

Varhelyi G. (1978): *On the vertical distribution of sulphur compounds in the lower troposphere.* Tellus 30, 542-545.

Varhelyi G. and Gravenhorst G. (1981): *An attempt to estimate biogenic sulfur emissions into the atmosphere.* Idojaras 85, 126-134.

Williamson S.J. (1973): *Fundamentals of Air Pollution.* Addison-Wesley, Reading.

Wilson W.E. (1978): *Sulfates in the atmosphere.* Atmos. Environ. 12, 537-547.

World Health Organization (1978-1979): *Environmental health criteria: 8. Sulfur oxides and particulate matter.* WHO, Geneva.

SUMMARY

In this work, attention was focused on the lower troposphere above the North Sea. It is well known that the marine atmosphere acts as a source, a sink and a reaction reservoir for various chemical constituents. In the past 15 years it has become clear that the atmosphere above the North Sea can be an important source of pollutants for the sea.

In chapter 1, the sampling of marine aerosols with a cascade impactor was studied with regard to the possible interaction between particles collected on an impaction surface and reactive gaseous atmospheric components that are drawn through the impactor.

NaCl particles, generated by pneumatic nebulisation of a NaCl solution, were collected on an impaction plate of a cascade impactor. After passing through the impactor an air stream contaminated with nitric acid, the resulting particles were analyzed with laser microprobe mass spectrometry (LMMS). This technique allowed to confirm the importance of the reaction between NaCl aerosol particles and HNO_3 vapour, resulting in a central NaCl cube covered with a $NaNO_3$ layer. Both dry and wet NaCl particles were shown to react with nitric acid vapour during impactor sampling.

In order to avoid possible HNO_3-NaCl interaction, a NaF diffusion denuder can be placed in front of the cascade impactor to remove the gaseous HNO_3 quantitatively. An alternative procedure involves the use of extra-stages with high cut-off diameter. When loaded with at least a ten-fold excess of NaCl particles, relative to the amount of nitric acid expected to pass through the impactor during sampling, all gaseous HNO_3 will be removed. This setup has the obvious advantage of being more compact and less fragile and thus has some possibilities for use on the field, i.e. on the North Sea. Analogous sampling artifacts between sulphuric acid aerosols and ammonia were simulated in laboratory tests.

The LMMS technique was shown to be useful for the detection of

inorganic ammonium salts in single aerosol particles. It is one of the few techniques that can analyze thermally unstable compounds directly, without prior sample treatment, on the scale of one single particle. The high sensitivity of the LAMMA-500 instrument for Na^+, K^+ and some other cations, relative to the ammonium ion, limits the possibilities for detecting ammonium salts in ambient aerosol particles. Nevertheless, analysis of cascade-impactor collected aerosols from the North Sea atmosphere, sampled during easterly wind and under a low inversion height, showed the presence of high amounts of ammonium compounds in single particles. LMMS results of a few aerosol samples collected at the university campus during the winter of 1986-1987 indicated the presence of mixtures of ammonium chloride, ammonium nitrate and ammonium sulphate in single particles.

In chapter 2, the results of energy dispersive X-ray fluorescence (EDXRF) measurements on 71 aerosol samples, collected between 1984 and 1988 on the North Sea and the Channel, were presented. To our knowledge, this data set is the first one that covers not only an extensive period of time (5 years), but also the complete North Sea area.

Atmospheric concentrations of different elements in the lower troposphere above the North are highly variable as a function of place and time. Changes in wind direction and air mass history are reflected without delay in the composition of the North Sea aerosol. Except for Cl, all elements show a clear gradient from the southern to the northern part of the North Sea. Fe, Mn, Zn and Pb concentrations are 10 times lower on the average in the northern North Sea atmosphere, compared to the atmosphere above the Southern Bight of the North Sea. Atmospheric Si, S, K, Ca, Ti, Cr, V and Ni concentrations are 3 to 6 times higher above the Southern Bight compared to the northern North Sea atmosphere.

Factor analysis performed on all samples collected above the Southern Bight yielded the identification of three factors, that can be associated with: sea salt (Cl), residual oil burning (Ni and V) and mixed

anthropogenic aerosols (S, K, Ca, Fe, Cu, Zn and Pb).

Compared to coastal station measurements of atmospheric aerosols, relatively good agreement can be found. In some cases however, large discrepancies are noted for some elements. This is probably due to the possible contamination of coastal station collected air samples by local emission sources. It is clear that this can only be avoided by covering the complete North Sea during collection of aerosol samples, as we were able to do with the R/V Belgica.

For Pb, good agreement is found between our average Pb concentration for the 1984-1988 period and the model-predicted Pb-concentration for 1983.

In chapter 3, the lower troposphere of the Southern Bight of the North Sea was studied in a third dimension. 18 flights were performed in order to measure Cd, Cu, Pb and Zn concentrations, both total and size-differentiated, under different meteorological situations.

Air masses with southern and southeastern origin yielded the highest concentrations for all four elements. The lowest concentrations correspond to the northern and northeastern wind direction.

Above the temperature inversion layer, concentrations are much lower than below it. Inside this boundary layer, maximum concentrations generally occur at an altitude between 100 and 200 m. At higher altitudes and close to the sea surface, lower atmospheric trace metal concentrations are found.

Sampling tracks performed at very low altitude indicate that the sea is not an important source for trace metals in the atmosphere through production of seawater aerosols. We can conclude therefore, that the values discussed in chapter 2, are not biased by contamination through resuspension phenomena. Furthermore, very good agreement was found between the Cu, Pb and Zn concentrations obtained from the ship-based measurements between 1984 and 1988 and concentrations as obtained by aircraft sampling.

Size-differentiated measurements of Pb concentrations show highly variable size distributions. Both unimodal and bimodal distributions are observed. The average Pb distribution shows a maximum for particles between 0.25 and 0.5 μm and a second maximum for larger particles between 8 and 16 μm.

Chapter 4 focuses on deposition of trace metals into the Southern Bight of the North Sea. Atmospheric concentrations can be related to dry and wet deposition through the use of a dry deposition velocity (for dry deposition) and a scavenging ratio or scavenging rate (for wet deposition).

The dry flux of trace metals to the sea surface was calculated by using a dry deposition velocity obtained with the model of Slinn and Slinn (1980). Meteorological parameters such as the aerodynamic roughness height, the friction velocity, wind speed, the atmospheric stability and humidity gradients, and particle properties such as hydrophobic or hygroscopic qualities and particle diameter are taken into account (Rojas, 1991). The wet flux is calculated by using theoretically obtained scavenging rates and experimental data on the mixing height and rainfall statistics.

It is striking that the dry and wet fluxes of trace metals to the North Sea are largely dominated by the largest particle fraction. The uncertainty in deposition estimates can therefore be reduced to the uncertainty on atmospheric concentrations of large particles and thus ultimately on isokinetic sampling conditions.

The Pb flux to the North Sea is comparable to the Pb flux to the Baltic and the Mediterranean Sea. For Cd, Cu and Zn, the flux to the North Sea is comparable to the flux to the northwestern Mediterranean Sea.

The atmosphere is clearly a main input source of trace elements into the North Sea. Some 66% of all Cd entering the North Sea comes from the atmosphere. The atmospheric source-strength for Pb is 49%, but this number will be reduced in the following years thanks to the growing

use of unleaded gasoline for motor vehicles. The different Cu and Zn contributions are very similar: riverine input, dumping and atmospheric input are each responsible for about 1/3 of the total input.

In chapter 5, the results are discussed of continuous SO_2 and O_3 measurements performed during 18 flights over the Southern Bight of the North Sea. Average SO_2 below the temperature inversion layer ranged from 1.9 ppb to 19.5 ppb. The SE-E sector and the variable wind sector show the highest average SO_2 concentrations: 15.2 and 12.0 ppb, respectively.

The average ozone concentration ranged from 8 ppb to 96 ppb. Low ozone concentrations reflect ozone depletion through reaction with freshly emitted pollutants, while high ozone concentrations are an indication of photochemical activity.

Ozone concentrations seem to be primarily dependent on seasonal influence, while SO_2 levels are more dictated by the history of the sampled air mass.

Although SO_2 and trace metal levels show similar trends, some differences are obvious. The highest SO_2 concentrations are found between 100 and 200 m altitude. The average ozone profile shows an increase from 30-40 ppb at the sea level to 60-70 ppb at altitudes above 1000m.

Individual sulphur dioxide and ozone profile measurement clearly illustrate the high variability in vertical concentration distributions. The presence of SO_2 peaks at certain altitudes depends on the presence of radiative and subsidence inversion layers and on the atmospheric stability, i.e. the environmental lapse rate.

SAMENVATTING

Het centrale studie-object van dit werk is de atmosfeer boven de Noordzee. De mariene atmosfeer kan zowel een emissiebron, een immissieplaats en een reactievat zijn voor verschillende chemische componenten. Over de laatste 15 jaar is het duidelijk geworden dat de atmosfeer boven de Noordzee een bron belangrijke bron kan zijn van pollutie voor de zee.

In het eerste hoofdtsuk werd de bemonstering van marine aerosolen met een cascade-impactor bestudeerd met betrekking tot de mogelijke interactie tussen deeltjes die reeds gecollecteerd zijn op het impactie-oppervlak en reactieve gasvormige componenten in de luchtstroom die door de impactor wordt gezogen.

NaCl deeltjes, gegenereerd door pneumatische verstuiving van een NaCl oplossing, werden gecollecteerd op een impactie-oppervlak van een cascade-impactor. Nadat een met HNO_3 gecontamineerde luchtstroom doorheen de impactor werd geleid, werden de resulterende partikels geanalyzeerd met LMMS (laser microprobe massaspectrometrie). Dit toonde het belang aan van de reactie tussen NaCl deeltjes en HNO_3 in de gasfase, die uitmondt in de vorming van een centrale NaCl kubus met een laagje $NaNO_3$ er omheen. Zowel droge NaCl deeltjes als NaCl druppels reageren met gasvormig HNO_3 tijdens bemonstering van deeltjes met een cascade-impactor.

Om deze interactie tussen NaCl en HNO_3 te vermijden, kan een met NaF beklede diffusie-denuder voor de impactor geplaatst worden om het HNO_3 kwantitatief te verwijderen. Een alternative werkwijze bestaat uit het gebruik van extra trappen met een hoge cut-off diameter vóór de impactor. Wanneer een enkele extra trap wordt beladen met minimum een tien-voudige overmaat aan NaCl deeltjes ten opzichte van de hoeveelheid HNO_3 die men door de impactor zal zuigen tijdens de bemonstering, kan al het gasvormige HNO_3 verwijderd worden. Deze opstelling heeft het

voordeel kompakter en minder breekbaar te zijn, zodat ze ook geschikt is voor gebruik op een schip. Analoge interacties tussen zwavelzuur deeltjes en ammoniak werden eveneens uitgetest op laboratorium-schaal.

De LMMS techniek is geschikt om anorganische ammoniumzouten te detecteren in individuele partikels. Het is een van de weinige technieken die thermisch onstabiele verbindingen rechtstreeks kan analyseren, zonder monstervoorbereiding, op de schaal van individuele aerosol deeltjes. De hoge gevoeligheid van het LAMMA-500 instrument voor Na^+, K^+ en andere kationen, relatief ten overstaan van het ammonium ion, beperkt de mogelijkheden om ammoniumzouten te detecteren in atmosferische partikels. Nochtans werden hoge concentraties aan ammoniumzouten gemeten in individuele deeltjes, die gecollecteeerd waren op de Noordzee tijdens oostenwind en bij een lage temperatuursinversie-hoogte. LMMS resulaten van analyses op enkele monsters die tijdens de winterperiode van 1986-1987 werden gecollecteerd in de buurt van de campus van de UIA, toonden de aanwezigheid aan van zowel ammoniumchloride, ammoniumnitraat als ammoniumsulfaat in dezelfde individuele deeltjes.

In hoofdstuk 2, werden de resultaten besproken van EDXRF (energie-dispersieve X-stralen fluorescentie) metingen op 71 aerosol monsters, gecollecteerd tussen 1984 en 1988 op de Noordzee en het Kanaal. Voor zover ons bekend, is deze verzameling van gegevens de eerste die niet alleen een lange periode van 5 jaar, maar ook het volledige gebied van de Noordzee, bestrijkt.

Het blijkt dat atmosferische concentraties van verschillende elementen in de lagere troposfeer boven de Noordzee zeer variabel zijn in functie van plaats en tijd. Veranderingen in windrichting of in het traject dat de bemonsterde luchtmassa heeft afgelegd vóór bemonstering, worden zonder vertraging weerspiegeld in de atmosferische concentraties van verscheidene elementen. Voor alle elementen, behalve voor Cl, werd een duidelijk zuid-noord gradiënt in de concentratie waargenomen. Fe, Mn, Zn en Pb concentraties zijn gemiddeld een factor 10 lager boven het

noordelijke deel van de Noordzee in vergelijking met de atmosfeer boven het zuidelijke deel. Voor Si, S, K, Ca, Ti, Cr, V en Ni bedraagt deze verhouding 3 tot 6.

Door middel van factoranalyse, uitgevoerd op alle monsters gecollecteerd boven de Zuidelijke Bocht van de Noordzee, kunnen drie onafhankelijke aerosolbronnen geidentificeerd worden: zeezout (Cl), residu van olieverbranding (Ni en V) en gemengde pollutie-aerosoldeeltjes (S, K, Ca, Fe, Cu, Zn en Pb).

Over het algemeen is er een goede overeenkomst met de resultaten van metingen in kuststations. In sommige gevallen echter zijn er voor specifieke elementen grote verschillen. Dit is waarschijnlijk te wijten aan contaminatie van metingen in kuststations door de invloed van lokale emissiebronnen. Het is duidelijk dat dit enkel kan vermeden worden door monsters te collecteren, verspreid over de gehele Noordzee, zoals voor ons mogelijk was door gebruik te maken van de Belgica.

Voor Pb kan de goede overeenkomst opgemerkt worden tussen onze experimentele resultaten voor de periode 1984-1988 en modelberekeningen voor het jaar 1983.

De atmosfeer boven de Zuidelijke Bocht van de Noordzee werd in hoofdstuk 3 bestudeerd in een derde dimensie. Achttien vluchten werden uitgevoerd om metingen te verrichten van Cd, Cu, Pb en Zn concentraties, zowel totale concentraties als concentraties in functie van de deeltjesdiameter, en dit onder verschillende weersomstandigheden.

Luchtmassa's met zuidelijke en zuid-oostelijke oorsprong resulteren in de hoogste concentraties voor de vier bestudeerde elementen. de laagste concentraties werden gemeten tijdens noordelijke en noordwestelijke windrichting.

Boven de temperatuursinversiehoogte zijn de concentraties veel lager dan onder deze hoogte. Maximum concentraties werden in de regel gemeten op een hoogte tussen 100 en 200 m. Beneden 100 m en boven 200 m werden lagere concentraties gemeten.

De vlucht-trajecten die werden uitgevoerd op zeer lage hoogte geven aan dat de zee (in geval van de Noordzee) geen significante bijdrage levert, door produktie van zeewater-aerosolen, tot de atmosferische concentratie van zware metalen. We kunnen daarom besluiten dat de metingen uitgevoerd vanop de Belgica niet beinvloed zijn door contaminatie door geresuspendeerd zeewater. Daarenboven werd een zeer goede overeenkomst opgemerkt tussen de resultaten van onze metingen van de Belgica en de vliegtuigmetingen.

Atmosferische Pb concentraties in functie van de deeltjesdiameter zijn zeer variabel. Zowel unimodale als bimodale distributies werden gemeten. De gemiddelde Pb concentratieverdeling vertoont een maximum voor deeltjes met een diameter tussen 0.25 and 0.5 μm en een tweede maximum voor grotere deeltjes met een diameter tussen 8 en 16 μm.

In het vierde hoofdstuk werd de aandacht gevestigd op fluxen van zware metalen vanuit de atmosfeer naar de Noordzee toe. Atmosferische concentraties kunnen vertaald worden in fluxen door gebruik te maken van een droge valsnelheid (voor droge depositie) en van een uitwasverhouding ('washout ratio') of uitwas- en uitregen-coefficient.

De droge flux van zware metalen wordt berekend door gebruik te maken van een droge valsnelheid zoals die bepaald kan worden met het model van Slinn en Slinn (1980). Hierbij wordt rekening gehouden met meteorologische parameters zowel als met deeltjes-eigenschappen. De natte flux wordt berekend aan de hand van theoretisch uitwas- en uitregencoefficienten en experimentele gegevens over de menghoogte en neerslagstatistiek.

Het is opvallend hoe zowel de droge als de natte flux wordt gedomineerd door de grotere deeltjes. De onzekerheid bij het bepalen van fluxen kan dus herleid worden tot een onzekerheid op de deeltjesdistributie (vooral van de grotere deeltjes) en dus tot het probleem van isokinetische bemonstering.

In vergelijking met andrre mariene gebieden, is de depositie-flux

van Pb voor de Noordzee vergelijkbaar met die voor de Baltische en de Middellandse Zee. Voor Cd, Cu en Zn is de flux naar de Noordzee vergelijkbaar met deze naar de noordwestelijke Middellandse Zee.

Het is duidelijk dat de atmosfeer een belangrijke toevoerweg is voor zware metalen naar de Noordzee. 66% van alle Cd dat in de Noordzee terecht komt, bereikt de zee vanuit de atmosfeer. 49% van het Pb dat de Noordzee bereikt wordt aangevoerd via de atmosfeer. Deze hoeveelheid zal in de toekomst dalen door het toenemende gebruik van loodvrije brandstoffen. De toevoerwegen voor Cu en Zn nemen elk ongeveer 1/3 ven de totale fluxvoor hun rekening: rivieren, dumping en atmosferische toevoer.

In hoofdstuk 5 werden de resultaten besproken van SO_2 en O_3 metingen tijdens 18 vluchten boven de Noordzee. Gemiddelde SO_2 concentraties beneden de temperatuursinversiehoogte varieren van 1.9 tot 19.5 ppb. The ZO-O en de variabele sector vertonen de hoogste gemiddelde SO_2 concentraties: 15.2 en 12.0 ppb, respectievelijk.

De gemiddelde ozon concentratie varieert van 8 ppb tot 96 ppb. Lage ozon gehaltes duiden op ozon verbruik door reactie met recent geëmitteerde polluenten, terwijl verhoogde ozon niveau's op photochemische reacties duiden.

Ozon concentraties blijken vooral seizoensafhankelijk te zijn, terwijl SO_2 concentraties eerder terug te koppelen zijn naar de oorsprong van de gecollecteerde luchtmassa's.

Alhowel ozonconcentraties en concentraties aan zware metalen dezelfde trends vertonen, zijn er toch duidelijke verschillen in sommige gevallen. De hoogste SO_2 concentraties werden gemeten tussen een hoogte van 100 en 200 m. Het gemiddelde ozonprofiel vertoont een stijgende tendens van 30-40 ppb op zeeniveau to 60-70 ppb op 1000 m en hoger.

Individuele SO_2 en O_3 concentratie-profiel metingen illustreren de hoge variabiliteit van verticale concentratieverdelingen. Het voorkomen

van SO_2 pieken op bepaalde hoogten hangt af van de aanwezigheid van temperatuur-inversies en van de atmosferische stabiliteit, i.e. het temperatuursprofiel.

List of publications

Articles

Nitric acid interaction with marine aerosols sampled by impaction
Ph. Otten, F. Bruynseels and R. Van Grieken
Bull. Soc. Chim. Belg., 95 (1986), 447-453

Study of inorganic ammonium compounds in individual marine aerosol particles by laser microprobe mass spectrometry
Ph. Otten, F. Bruynseels and R. Van Grieken
Anal. Chim. Acta, 195 (1987), 117-124

Inorganic nitrogen speciation in single micrometer-size particles by laser microprobe mass analysis
F. Bruynseels, Ph. Otten and R. Van Grieken
J. Anal. Atomic Spect., 3 (1988), 237-240

Characterization of airborne particulate matter collected over the North Sea
C.M. Rojas, Ph.M. Otten and R. Van Grieken
J. of Aerosol Sci., 20 (1989), 1257-1260.

Chemical composition of atmospheric precipitation in Antwerp, Belgium
S. Rajsic, Ph. Otten and R. Van Grieken
Environmental Technology, submitted.

Micro-analysis of individual environmental particles.
R. Van Grieken, P. Artaxo, P. Bernard, L. Leysen, Ph. Otten, H. Storms, A. Van Put, L. Wouters and Ch. Xhoffer
Chemia Analityczna, in press.

Proceedings

Reaction of marine aerosols with HNO_3 vapour studied by single particle analysis.
Ph. Otten, F. Bruynseels and R. Van Grieken
Proceedings of the 1985 CEE Workshop on Aerosols and Acid Deposition, 67-71

LAMMA analysis of inorganic ammonium compounds in individual marine aerosol particles
Ph. Otten, F. Bruynseels and R. Van Grieken
Proceedings of the 3rd Laser Microprobe Mass Spectrometry Workshop, University of Antwerp, Antwerp (1986), 159-163

Detection of ammonia compounds at the single particle level
Ph. Otten, S. Rajsic and R. Van Grieken
Proceedings of the 1987 EURASAP Symposium on Ammonia and Acidification, W.A.H. Asman and H.S.M.A. Diederen, Eds., National Institute of Public Health and Environmental Hygiene, Bilthoven (1987), 83-85

Laser microprobe mass analysis : characteristics and applications
R. Van Grieken, A. Verbueken, F. Bruynseels, D. Vandeputte, C. Goossenaerts, L. Leysen, Ph. Otten and L. Wouters
in "Analytik-treffen 1986", Proceedings of the Conference of Analytical Atomic Spectroscopy, Karl-Marx Universiteit Leipzig, (1987), 208-222

Abstracts

Chemical composition, source identification and quantification of the atmospheric input into the North Sea
Ph. Otten, H. Storms, Ch. Xhoffer and R. Van Grieken
in "Progress in Belgian Oceanographic Research - 1989", G. Pichot, Ed., Prime Minister's Services of Science Policy, Office & Ministry of Public Health and Environment, Brussels (1989), 413-422.

Characterization of individual environmental particles
R. Van Grieken, P. Artaxo, P. Bernard, F. Bruynseels, Ph. Otten, H. Storms and Ch. Xhoffer
n "Chemistry for Protection of the Environment - 1987", L. Pawlowski, E. Mentasti, W.J. Lacy and C. Sarzanini, Eds., Elsevier, Amsterdam-Oxford-New York-Tokyo (1988), 307-316.

Study of local fog formation above the bridge of Beez by individual particle analysis
H. Storms, Ph. Otten and R. Van Grieken
Comptes-Rendus du Seminaire sur Brouillards denses localises et Charge local de l'Air en Noyaux de Condensation, FUL, Arlon (1989), 41-71.

Single particle analysis of particulate environmental samples
R. Van Grieken, P. Bernard, Ph. Otten, C. Rojas, A. Van Put, Ch. Xhoffer and L. Wouters
Proceedings of the 3rd Beijing Conference and Exhibition on Instrumental Analysis, BCEIA, Beijing A83-A84.

Atmospheric deposition of heavy metals over the North Sea
R. Van Grieken, Ph. Otten and Ch. Xhoffer
in "Environmental Quality and Ecosystem Stability", ISEEQS Publications, Jeruzalem (1989), Vol. IV., 87-88.